Vol. 268, No. 1, October 7, 1992 ISSN 0003-2670

ANALYTICA CHIMICA ACTA

An international journal devoted to all branches of analytical chemistry

ELSEVIER

ANALYTICA CHIMICA ACTA

Scope. *Analytica Chimica Acta* publishes original papers, preliminary communications and reviews dealing with every aspect of modern analytical chemistry. Reviews are normally written by invitation of the editors, who welcome suggestions for subjects. Preliminary communications of important urgent work can be printed within four months of submission, if the authors are prepared to forego proofs.

Submission of Papers

Americas

Prof. Harry L. Pardue
Department of Chemistry
1393 BRWN Bldg, Purdue University
West Lafayette, IN 47907–1393
USA
Tel:(+1-317) 494 5320
Fax:(+1-317) 496 1200

Computer Techniques

Prof. J.T. Clerc
Universität Bern
Pharmazeutisches Institut
Baltzerstrasse 5, CH-3012 Bern
Switzerland
Tel:(+41-31) 654171
Fax:(+41-31) 654198

Other Papers

Prof. Alan Townshend
Department of Chemistry
The University
Hull HU6 7RX
Great Britain

Tel:(+44-482) 465027
Fax:(+44-482) 466410

Prof. Willem E. van der Linden
Laboratory for Chemical Analysis
Department of Chemical Technology
Twente University of Technology
P.O. Box 217, 7500 AE Enschede
The Netherlands
Tel:(+31-53) 892629
Fax:(+31-53) 356024

Prof. Paul Worsfold
Dept. of Environmental Sciences
University of Plymouth
Plymouth PL4 8AA
Great Britain

Tel:(+44-752) 233006
Fax:(+44-752) 233009

Submission of an article is understood to imply that the article is original and unpublished and is not being considered for publication elsewhere. *Anal. Chim. Acta* accepts papers in English only. There are no page charges. Manuscripts should conform in layout and style to the papers published in this issue. See inside back cover for "Information for Authors".

Publication. *Analytica Chimica Acta* appears in 14 volumes in 1993. The subscription price for 1993 (Vols. 267–280) is Dfl. 4214.00 plus Dfl. 462.00 (p.p.h.) (total approx. US$ 2555.25). *Vibrational Spectroscopy* appears in 2 volumes in 1993. The subscription price for *Vibrational Spectroscopy* (Vols. 4 and 5) is Dfl. 700.00 plus Dfl. 66.00 (p.p.h.) (total approx. US$ 418.50). The price of a combined subscription (*Anal. Chim. Acta* and *Vibr. Spectrosc.*) is Dfl. 4592.00 plus Dfl. 528.00 (p.p.h.) (total approx. US$ 2797.75). All earlier volumes (Vols. 1–253) except Vols. 23 and 28 are available at Dfl. 259.50 (US$ 141.75), plus Dfl. 18.00 (US$ 9.75) p.p.h., per volume. The Dutch guilder price is definitive. The U.S. dollar price is subject to exchange-rate fluctuations and is given only as a guide. Subscriptions are accepted on a prepaid basis only, unless different terms have been previously agreed upon.
Our p.p.h. (postage, packing and handling) charge includes surface delivery of all issues, except to subscribers in the U.S.A., Canada, Australia, New Zealand, China, India, Israel, South Africa, Malaysia, Thailand, Singapore, South Korea, Taiwan, Pakistan, Hong Kong, Brazil, Argentina and Mexico, who receive all issues by air delivery (S.A.L.–Surface Air Lifted) at no extra cost. For Japan, air delivery requires 25% additional charge of the normal postage and handling charge; for all other countries airmail and S.A.L. charges are available upon request.

Subscription orders. Subscription orders can be entered only by calendar year and should be sent to: Elsevier Science Publishers B.V., Journals Department, P.O. Box 211, 1000 AE Amsterdam, The Netherlands. Tel: (+31-20) 5803 642, Telex: 18582, Telefax: (+31-20) 5803598, to which requests for sample copies can also be sent. Claims for issues not received should be made within three months of publication of the issues. If not they cannot be honoured free of charge. Readers in the U.S.A. and Canada can contact the following address: Elsevier Science Publishing Co. Inc., Journal Information Center, 655 Avenue of the Americas, New York, NY 10010, U.S.A. Tel: (+1-212) 6333750, Telefax: (+1-212) 6333990, for further information, or a free sample copy of this or any other Elsevier Science Publishers journal.
Advertisements. Advertisement rates are available from the publisher on request.

Detailed "Instructions to Authors" for *Analytica Chimica Acta* was published in Volume 256, No. 2, pp. 373–376. Free reprints of the "Instructions to Authors" of *Analytica Chimica Acta* and *Vibrational Spectroscopy* are available from the Editors or from: Elsevier Science Publishers B.V., P.O. Box 330, 1000 AH Amsterdam, The Netherlands. Telefax: (+31-20) 5862845.

US mailing notice – Analytica Chimica Acta (ISSN 0003-2670) is published biweekly by Elsevier Science Publishers (Molenwerf 1, Postbus 211, 1000 AE Amsterdam). Annual subscription price in the USA US$ 2555.25 (subject to change), including air speed delivery. Application to mail at second class postage rate is pending at Jamaica, NY 11431. *USA Postmasters*: Send address changes to Anal. Chim. Acta, Publications Expediting, Inc., 200 Meacham Av., Elmont, NY 11003. Airfreight and mailing in the USA by Publication Expediting.

ANALYTICA CHIMICA ACTA

An international journal devoted to all branches of analytical chemistry

(Full texts are incorporated in CJELSEVIER, a file in the Chemical Journals Online database available on STN International; Abstracted, indexed in: Aluminum Abstracts; Anal. Abstr.; Biol. Abstr.; BIOSIS; Chem. Abstr.; Curr. Contents Phys. Chem. Earth Sci.; Engineered Materials Abstracts; Excerpta Medica; Index Med.; Life Sci.; Mass Spectrom. Bull.; Material Business Alerts; Metals Abstracts; Sci. Citation Index)

VOL. 268 NO. 1 CONTENTS OCTOBER 7, 1992

(Continued overleaf)

Contents (continued)

ANALYTICA CHIMICA ACTA
VOL. 268 (1992)

ANALYTICA CHIMICA ACTA

An international journal devoted to all branches of analytical chemistry
Revue internationale consacrée à tous les domaines de la chimie analytique
Internationale Zeitschrift für alle Gebiete der analytischen Chemie

---

Anal. Chim. Acta, Vol. 268 (1992)

ELSEVIER, Amsterdam–London–New York–Tokyo

0003-2670/92/$05.00

Analytica Chimica Acta, 268 (1992) 1–6
Elsevier Science Publishers B.V., Amsterdam

Flow-injection analysis in the capillary format using electroosmotic pumping

Shaorong Liu and Purnendu K. Dasgupta

Department of Chemistry and Biochemistry, Texas Tech University, Lubbock, TX 79409-1061 (USA)

(Received 11th June 1992; revised manuscript received 17th July 1992)

Abstract

Electroosmotic flow induced by an electric field in a 75-μm bore fused-silica capillary is used as the pumping mechanism for flow-injection analysis (FIA). Injection of a sample into a reagent stream containing a carrier electrolyte or sequential injection of contiguous reagent, sample and reagent segments into a carrier electrolyte are accomplished hydrostatically. Colorimetric detection is performed by an optical absorbance detector using the diameter of the capillary as the optical path. Typical peak area precision is better than 3% in relative standard deviation for sample volumes $\leq$ 20 nl. The potential of capillary format electroosmotically driven FIA and related techniques is discussed.

Keywords: Flow injection; Electroosmotic pumping

Tissjen [1] was the first to calculate the consequences of downscaling the radius of a continuous flow analysis system from the millimeter to the micrometer regime and further point out the advantages. Hungerford [2] has subsequently examined in detail the consequences of such miniaturization for a short narrow and straight channel; Hirschfeldt is credited with the original concept [3]. Subsequently Van der Linden [4] enumerated on the theoretical limitations of ultraminiaturization. In their acclaimed treatise on flow-injection analysis (FIA) [3], Ruzicka and Hansen credit Olesik et al. [5] for the first "superminiaturized" FIA system. These authors used a 250-μm bore silica capillary and an infrared absorption detection of 2-μl volume in a medium of supercritical CO_2 as the carrier fluid. The system studied did not involve a sample–reagent reaction but rather the self conversion of the sample to a product with different spectral characteristics. This experiment merely used the capillary conduit as a conveyor for kinetic studies. Improvements in sample throughput, seen as an important advantage of miniaturization [3], was not investigated. In fact, the original publication of Stewart et al. [6] on FIA reports the use of conduits of comparable diameter (300 μm) but flow-rates, tubing lengths and detector cell volumes were all too large to take full advantage of the small bore. There was little improvement in reagent consumption, perceived to be an important advantage of miniaturization. The use of 300-μm bore conduits have become routine in our laboratories for continuous flow analysis and, although we have improved upon reagent consumption [7–9], the practice still suffers from the same drawbacks as in Ref. 6.

In their critical assessment, Ruzicka and Hansen [3] point out the major experimental difficulties towards attaining superminiaturized FIA

Correspondence to: P.K. Dasgupta, Department of Chemistry and Biochemistry, Texas Tech University, Lubbock, TX 79409-1061 (USA).

and realizing its benefits. These are likely to lie in achieving small enough detector volumes and stable enough flow-rates in the sub-μl min^{-1} domain. It is remarkable that in the few years since this opinion was expressed, on-column optical absorption detectors of sub-μl volume have become commercially available from a large number of vendors. Perhaps even more importantly, the technique of zone electrophoresis in a fused-silica capillary was introduced by Jorgenson and Lukacs [10] little more than a decade ago. In such a system, application of a high electric field (typically of the order of one hundred to several hundred V cm^{-1}) causes electroosmotic flow (EOF) of the bulk fluid. Because the stationary silanol groups are negatively charged over most of the pH range and the movements of the cations adjacent to the wall is responsible for the EOF, such flow typically occurs from the positive to the negative electrode.

The availability of a reliable pumping technology is perceived by many as a key development necessary to further the course of automated liquid phase analysis and such perceptions have led, for example, to the introduction of techniques such as sequential injection analysis [11] relying on a sinusoidal pump [12]. The utilization of EOF as a pumping means provides a new alternative to the practice of FIA. This effectively allows downscaling to capillaries < 50 μm in radius and to nanoliter volume scales. The cost of low current high voltage (HV) power supplies is lower than mechanical pumps. Switching (often referred to as DC to DC) HV power supplies can also be constructed very inexpensively [13]. The stored energy in such power supplies can be made sufficiently low to eliminate any major hazards from accidental electrical shocks. Such a pumping system has intrinsic high reliability since there are no moving parts. It has also been shown that the direction and magnitude of the EOF can be controlled by using a surfactant that attaches to the wall or by applying a second electric field from the radial direction of the capillary [14–16].

It was originally envisioned [3] that FIA systems of very small bore would not only use proportionately small flow-rates, the length of the conduit would also be relatively small (several cm). Typical reaction times would be attained within a small length and a further increase in length would be undesirable because that will only deteriorate sample throughput due to band broadening induced by laminar flow. EOF, however, is unique in that the flow originates at the wall. If the capillary is of small enough bore, the flow profile is essentially flat. In other words, EOF in a capillary represents the closest approach to true plug flow under nonturbulent conditions. Flow-induced dispersion is therefore essentially nonexistent. For the present context, this means that electroosmotically pumped flow can potentially endow FIA with one of the positive attributes of segmented flow analysis: limited dispersion despite long reaction times and continuous flow. In the present communication, we demonstrate the most basic of FIA applications in an electroosmotically pumped capillary system, the colorimetric estimation of an analyte by reaction of the sample with a single reagent.

EXPERIMENTAL

Equipment

The experimental arrangement is shown schematically in Fig. 1. A and B are rotatable turrets that can hold a number of 1.5-ml capacity microcentrifuge vials. Turret A vials contain the carrier electrolyte and turret B, located at a height of 10.5 cm above A contain the sample vials. Polyimide coated silica capillary C (60 cm $\times$ 75 μm i.d. $\times$375 μm o.d.; Polymicro Technologies, Phoenix, AZ) can be moved by means of two

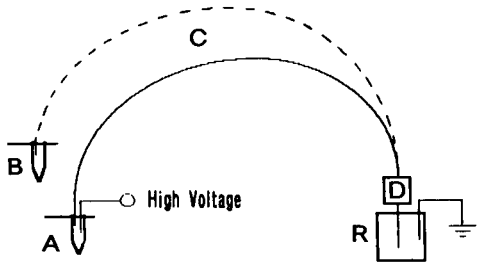

Fig. 1. Schematic diagram of the experimental system. (A) Turret containing carrier electrolyte vials; (B) turret containing sample vials; (C) capillary; (D) detector; (R) grounding electrolyte reservoir.

pneumatic actuators (one for dipping/lifting into/from individuals vials and one for sliding from station A to B). The HV electrode, a 0.25-mm dia Pt-wire, is affixed to the turret end of C. The polyimide coating is removed at a distance of ca. 55 cm from the turret end of C for a space of ca. 1 cm and constitutes the radial path detector cell for detector D equipped with ball lenses for the use of the capillary (206 PHD, Linear Instruments/Spectra Physics). The far end of the capillary goes to reservoir R, typically placed at the same height as A. R contains the carrier electrolyte solution as well. Various valves and liquid lines are attached to R (not shown) that allow washing, replenishment of reservoir liquid and backwashing capillary by pressurizing R. The HV power supply of adjustable range and polarity was built from Model 7977 and 7964 HV power modules (EMCO High Voltage, Sutter Creek, CA). All instrument functions, including sampling, were automated through a programmable microcontroller (LS-100, Minarik Electric, Los Angeles, CA). Vendor supplied software and a 80386 class PC was used to acquire data from the detector. A more detailed description of the instrument will be published elsewhere.

Protocol

The following steps are typically practiced for analysis: (a) transfer capillary to turret B, dip into sample vial for 10 s (except as stated otherwise; the measured sample introduction rate was 1.8 ± 0.2 nl s^{-1}); (b) lift capillary, transfer to turret A, dip into carrier electrolyte vial; (c) Apply HV (typ. +15 kV) for a desired period (typ. 10–20 s, to ensure that individual samples do not overlap) and then turn off HV and wait 5 s to allow any residual voltage to dissipate and (d) repeat step a to introduce new samples. This process may be repeated indefinitely, as peaks produced by the individual samples will be conveyed to and pass through the detector. More commonly, we repeated the above sequence until the capillary was loaded with as many samples as it can hold (typically the 60-cm capillary used in our work will accommodate > 30 samples) and then applied HV without further sample introduction until all loaded samples pass through the system.

Reagents

The colorimetric determination of Fe^{2+} with 1,10-phenanthroline was studied. 0–200 mg l^{-1} $FeSO_4 \cdot 7H_2O$ was used as sample, with or without hydrazine sulfate being added to prevent oxidation. The carrier electrolyte contained 10 mM tetrabutylammonium perchlorate and 20 mM 1,10-phenanthroline adjusted to pH 4.9 with dilute HCl. In another mode of operation, as specifically stated, the carrier electrolyte contained 5 mM 2-[bis(2-hydroxyethyl)aminoethane sulfonic acid] (BES) and 25 mM NBu_4ClO_4. One plug each of the 1,10-phenanthroline reagent were introduced on each side of a sample segment.

RESULTS AND DISCUSSION

Only uncharged moieties are subject solely to the EOF in a system such as that described above. If the detected species is charged, it is also subject to the existing electric field. If this charge is positive, the electrophoretic movement is in the same direction as the EOF in a bare silica capillary. Conversely, for a negatively charged species, the net velocity is given by the difference of the opposing electroosmotic and electrophoretic velocities, the former generally being greater in magnitude. When electrophoretic migration contributes significantly to the overall velocity, it is desirable that the speed of migration of the species of interest be comparable to that of the similarly charged primary charge carrier in the carrier electrolyte. Otherwise, peaks obtained can be badly fronting or tailing [17]. A relatively low mobility cation is therefore necessary to match the mobility of the large Fe(*o*-phen)$_3$ ion. Figure 2 shows two response peaks, using a carrier electrolyte of (a) 10 mM NBu_4ClO_4 and (b) 10 mM sodium phosphate, each adjusted to the same pH and containing the same concentration of 1,10-phenanthroline. The gross difference in peak shapes is readily apparent, in case b, the slow moving chelated metal ion simply cannot keep pace with the much faster sodium ion in the carrier electrolyte and the analyte peak tails badly as a result. If the number of plates (N) are calculated on the basis of $N = 5.54(t/w_{0.5})^2$

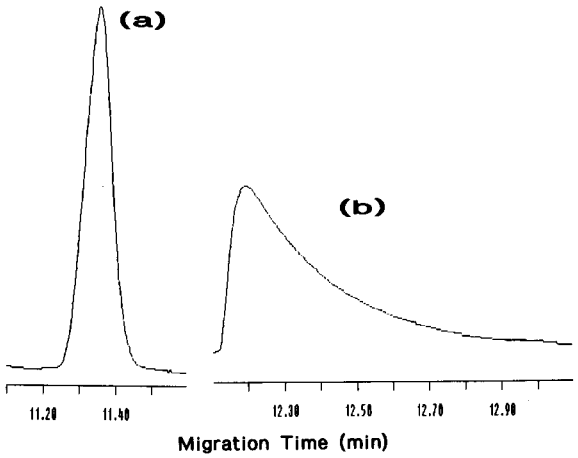

Fig. 2. Sample: 100 mg l^{-1} $FeSO_4 \cdot 7H_2O$ for 10 s, 15 kV applied, detection wavelength: 508 nm, carrier electrolyte: 20 mM 1,10-phenanthroline at pH 4.9 with (a) 10 mM tetrabutylammonium perchlorate and (b) 10 mM sodium phosphate.

(where t is the migration time and $w_{0.5}$ is the half width of the peak [18]), the number of plates in case a approaches 10^5 while that in b is an order of magnitude smaller. The importance of choosing an appropriate carrier electrolyte to maximize sample throughput rate and detection sensitivity must therefore be emphasized.

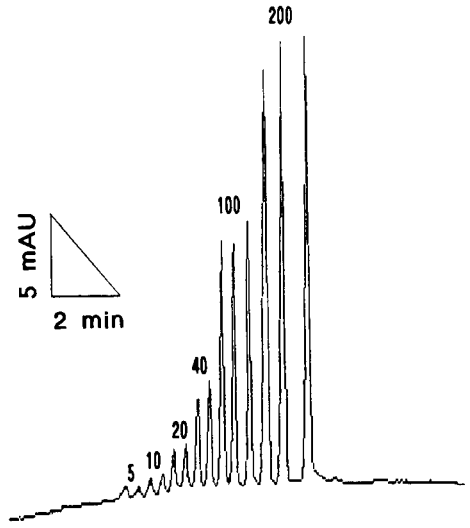

Fig. 3. Fiagram for 5–200 mg l^{-1} $FeSO_4 \cdot 7H_2O$, conditions as in Fig. 2a.

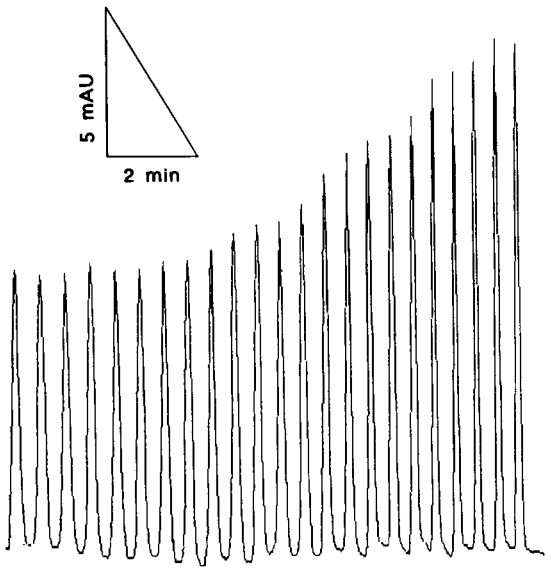

Fig. 4. A multiplicity of samples (100 mg l^{-1} $FeSO_4 \cdot 7H_2O$) are introduced into the capillary and then electroosmotically pumped out. Other conditions same as in Fig. 2a.

Figure 3 shows a traditional fiagram obtained with the present system. The transit time for the analyte from the beginning of the capillary to the detection point is 12 min. The Colorimetric reaction studied is essentially instantaneous relative to this time scale. Figure 4 shows a fiagram in which several samples are loaded in the capillary and then electroosmotically pumped out. Note that each time a sample is loaded by the hydrostatic pressure difference technique, the resulting flow is laminar and necessarily has flow-induced dispersion associated with it. Thus, as more and more samples are loaded, the previously loaded samples are subjected to this source of dispersion each time. Consequently, the peaks that elute first are shorter and wider than the ones to elute last. If peak area is considered for the 23 peaks shown in Fig. 4, the relative standard deviation is less than 2.9%. Even when the instrument is fully manually operated, reasonable results can be obtained. Figure 5 shows results from manually operated repeat injections using the reagent sandwiching approach.

The triangulated base width of the peak in Fig. 2a is 9 s. Based on this, a throughput rate of 400

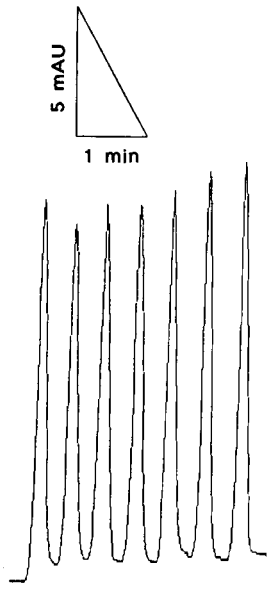

Fig. 5. Results from sandwiched reagent–sample–reagent introduction technique. 50 mM 1,10-phenanthroline introduced for 40 s, 100 mg l^{-1} $FeSO_4 \cdot 7H_2O$ for 10 s and 50 mM 1,10-phenanthroline reintroduced for 40 s. Timing was manually controlled. Carrier electrolyte 5 mM BES and 25 mM NBu_4ClO_4. Other conditions as in Fig. 2.

samples h^{-1} can be computed. However, the present system is limited to 120 samples/h because of the time invested in each hydrostatic injection. The above sampling rates cannot be reached until a more suitable sampling system

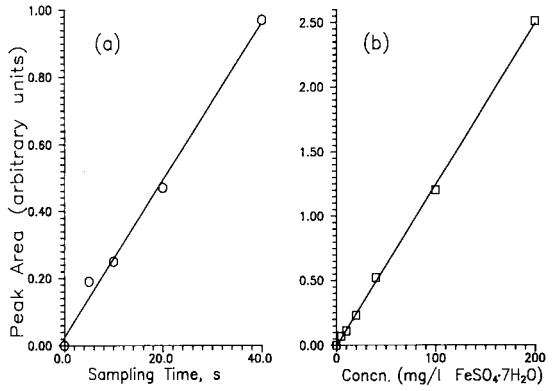

Fig. 6. (a) Sample introduction time vs. response. Conditions as in Fig. 5. (b) Sample concentration vs. response; sample introduction time 10 s, conditions as in Fig. 2a.

can be developed. We are at present fabricating a sample injection valve of the requisite size.

The amount of sample introduced varies linearly with the sample introduction time. Consequently, the peak area response increases linearly ($r^2 = 0.99934$) with sample introduction time (Fig. 6a). It is important to note that this means that even for the longest sample segment introduced (40 s introduction time, ca. 16 mm in length) the analyte fully reacts with the reagent. For a fixed sample introduction time of 10 s, the area response shows excellent linearity with the injected concentration: Area (arb. units) $= (1.249 \times 10^{-2} \pm 1.448 \times 10^{-4})c_{inj} - 6.505 \times 10^{-3} \pm 1.249 \times 10^{-2}$, $r^2 = 0.9993$.

Conclusions

Data presented in this paper clearly establish the practicality of electroosmotically pumped FIA. In preliminary experiments, we have observed that multianalyte determinations can be potentially performed in a number of ways. When Fe^{2+} and Cu^{2+} are both present in the sample, the resulting 1,10-phenanthroline complexes have different migration times. Because of the large number of plates in the system, a separation is feasible. Even when complete separation is not attained, a multiwavelength detector like the one used in the present studies can be readily used for monitoring a multitude of wavelengths and thus spectrally discriminate among the different species. (The particular example cited above is not especially attractive because of the low absorptivity of the Cu complex.)

It has also been found that a different reagent (e.g., 1,10-phenanthroline and ethylenediamine) can be used on either side of the sample plug to sandwich it. Thus two analytes (e.g., Fe^{2+} and Cu^{2+}), each with a preference for one reagent, can be individually determined. If the sample segment is sufficiently long, the response from each individual reagent can be completely separated. If greater interzone mixing than that allowed strictly by diffusion is desired (for example, to sequentially introduce and mix several reagents), it is possible to use a combination of electroosmotic pumping (which produces flow and allows very limited interzone mixing; alternating

the polarity of the applied voltage may have interesting consequences) and alternation of the hydrostatic head (which produces traditional laminar flow in alternate directions, thereby leading to significant zone mixing) to accomplish this. While all of the substrategies used in present day FIA may not be immediately applicable to the present system, a number of applications, including solvent extraction, can be envisioned. It is relevant to note that membrane introduction of samples in the capillary format has already been accomplished [19], it is obvious that reagents can also be introduced in this manner. We are therefore optimistic about the future of electroosmotically pumped FIA and related techniques.

This work would not have been possible without the machining expertise of Kavin Morris. This research was Supported by the Office of Basic Energy Sciences, U.S. Department of Energy, through DE-FG05-84ER-13281. However, this paper has not been reviewed by the DOE and no endorsements should be inferred.

REFERENCES

1 R. Tissjen, Anal. Chim. Acta, 114 (1980) 71.
2 J. Hungerford, Ph.D. Dissertation, University of Washington, Seattle, WA, 1986.
3 J. Ruzicka and E.H. Hansen, Flow Injection Analysis, Wiley, New York, 1988, 2nd edn., pp. 100–105.
4 W.E. van der Linden, Anal Chim. Acta, 180 (1986) 20.
5 S.V. Olesik, S.B. French and M. Novotny, Anal. Chem., 58 (1986) 2256.
6 K.K. Stewart, G.R. Beecher and P.E. Hare, Fed. Proc., 33 (1974) 1434.
7 Z. Genfa and P.K. Dasgupta, Anal. Chem., 61 (1989) 408.
8 Z. Genfa, P.K. Dasgupta and J.N. Marx, Anal. Chim. Acta, 243 (1991) 207.
9 Z. Genfa and P.K. Dasgupta, Anal. Chem., 64 (1992) 517.
10 J.W. Jorgenson and K.D. Lukacs, Anal. Chem., 53 (1981) 1298.
11 J. Ruzicka and G. Marshall, Anal. Chim. Acta, 237 (1990) 329.
12 J. Ruzicka, G. Marshall and G.D. Christian, Anal. Chem., 62 (1990) 1861.
13 P. Horowitz and W. Hill, The Art of Electronics, Cambridge University Press, Cambridge, 2nd edn., 1989, p. 368.
14 T. Tsuda, J. High Resolut. Chromatogr. Chromatogr. Commun., 10 (1987) 622.
15 C.S. Lee, W.C. Blanchard and C.-T. Wu, Anal. Chem., 62 (1990) 1550.
16 M.A. Hayes and A.G. Ewing, Anal. Chem., 64 (1992) 512.
17 F.E.P. Mikkers, F.M. Everaerts and Th.P.E.M. Verheggen, J. Chromatogr, 169 (1979) 11.
18 L.R. Snyder and J.J. Kirkland, Introduction to Modern Liquid Chromatography, Wiley, New York, 1979, 2nd edn., p. 31.
19 L. Bao and P.K. Dasgupta, Anal. Chem., 64 (1992) 991.

Analytica Chimica Acta, 268 (1992) 7–27
Elsevier Science Publishers B.V., Amsterdam

Mathematical modelling of a flow-injection system with a membrane separation module

Spas D. Kolev [1] and Willem E. van der Linden

Laboratory for Chemical Analysis, Department of Chemical Technology, University of Twente, P.O. Box 217, NL-7500 AE Enschede (Netherlands)

(Received 24th February 1992)

Abstract

A mathematical model for a flow-injection system with a membrane separation module based on the axially dispersed plug flow model was developed. It takes into account the geometrical dimensions and dispersion properties of the main sections of the manifold, the mass transfer in the channels of the separation module and the characteristics of the membrane (thickness and diffusion coefficient within it). The model was solved analytically in the Laplace domain. The inverse transformation was found to give satisfactory results for reactor Peclet numbers less than 120. Otherwise a numerical solution based on the implicit alternating-direction finite difference method was preferred. The adequacy of the model was confirmed experimentally on a flow-injection manifold with a parallel-plate dialysis module. The unknown flow and membrane parameters were determined by curve fitting. The membrane parameters were determined also by steady-state measurements. Fairly good agreement between the dynamic and steady-state results and with results given in the literature was observed, which, together with other experimental results, supported the validity of the model and showed that it can be used successfully for the mathematical description and optimization of flow-injection systems with membrane separation modules. In this connection, the influence of the reactor parameters and the sample volume on the performance of such a system were investigated and conclusions for improving its sensitivity and sample throughput were drawn. Other possible applications of the model are in membrane technology for characterizing of various membranes and in process engineering for investigating the mass transfer in different dialysers.

Keywords: Flow-injection; Optimization methods; Dialysis separation; Mathematical modelling; Membrane permeability

Flow-injection manifolds with modules for dialysis or gas diffusion have been shown to be very useful in dealing with samples containing macromolecules, particles or cells by separating them from the analyte prior to detection [1–4]. In this way, malfunctioning of the detector due to processes associated with the species mentioned above (e.g., clogging, light scattering) can be effectively prevented, thus securing accurate and reproducible results. This makes the flow-injection dialysis systems very advantageous in various fields (e.g., clinical analysis [3,4]) where, in addition to the accuracy and reproducibility of the analysis, a high sample throughput with minimum consumption of reagents is of crucial importance.

The mass-transfer process in the dialysis module of a flow-injection system is determined to a considerable extent by the properties of the membrane (i.e., its thickness and diffusivity). This allows experimental characterization of semi-permeable membranes using such systems [5].

Correspondence to: S.D. Kolev, Laboratory for Chemical Analysis, Department of Chemical Technology, University of Twente, P.O. Box 217, NL-7500 AE Enschede (Netherlands).
[1] Permanent address: Faculty of Chemistry, University of Sofia, Anton Ivanov Ave. 1, BG-1126 Sofia (Bulgaria).

For a better understanding of the processes taking place in a flow-injection manifold with a dialysis module, an adequate mathematical model is necessary. On the one hand, it will give possibilities for deriving guidelines for optimization of both the design and the operation of these manifolds, thus avoiding the costly and time-consuming "trial and error" approach. On the other hand, it will allow the separation of the contribution of the membrane to the overall mass transfer from that of the flow pattern in both channels of the dialysis module. This is necessary when the flow system is used for membrane characterization or for investigating the mass transfer in the channels.

Theoretical investigations of the mass-transfer process in dialysers based on fundamental physical laws (e.g., the Navier–Stokes equations and Fick's second law) have been limited mainly to the case of fully developed laminar flow in both channels and steady-state mass transfer. The reason for this situation is that industrial mass exchangers and haemodialysers used as artificial kidneys work under such conditions and the overall effect of the transient periods (e.g., start-up, shut-down, power surge and pump failure) is usually negligible. However, in flow-injection manifolds with dialysis separation, the transient mass transfer becomes the process governing the performance. The exact mathematical description must include the time dependence of the mass-transfer process, which greatly complicates the corresponding mathematical solution.

Bernhardsson et al. [6] used the approach mentioned above for the modelling of a flow-injection manifold assumed to consist of a dialysis module only and to operate under steady-state conditions. The latter assumption does not permit the calculation of the concentration profiles at the outlets of both channels under flow-injection conditions because they are the result of transient mass transfer. The model was successfully used for determining the membrane permeability [6,7].

The overall performance of a flow-injection manifold with a dialysis module depends on the processes taking place in all the separate sections (e.g., injection valve, reactor). Because of the complexity of the real hydrodynamic regime in the different sections, the development of a general mathematical model based on fundamental physical laws is exceedingly difficult and in most instances virtually impossible.

A possible approach for predicting the outlet concentration profiles of a given dialysis module is to find its impulse–response function under certain experimental conditions. This can be performed by deconvolution of the concentration profiles obtained under identical experimental conditions in a flow-injection manifold with and without the dialysis module [8,9]. However, it is difficult to relate the impulse–response function obtained in this way to the parameters that most affect the behaviour of the dialyser and to extend the results to other sets of parameters values.

The approach used in chemical engineering for the mathematical description of such complex flow systems is based on the application of the so-called hydraulic models (e.g., tanks-in-series, dispersion, combined and empirical models) [10,11]. In the modelling of flow-injection manifolds, the thanks-in-series and the dispersion models have been most frequently used [1,2]. For the mathematical description of flow-injection systems with membrane separation, the tanks-in-series model without back-mixing and with equal size of the tanks was used [12] and gave satisfactory qualitative agreement with the experimental results. However, most of the flow-through sections in a flow-injection manifold are tubular and for that reason the dispersion models appear to be closer to the real physical situation. Among them, the axially dispersed plug flow model [10] deserves special attention because it is simpler from a mathematical point of view and it has been already successfully utilized in the modelling of single-line flow-injection systems [13–17]. The flow pattern prevailing in these systems is laminar and another advantage offered by the axially dispersed plug flow model is the possibility of calculating the laminar Peclet number in both their tubular [18,19] and parallel-plate [20] sections. For parallel-plate dialysis modules, a theoretical relationship for determining the laminar flow mass-transfer coefficients in both channels has also been derived [21].

TABLE 1

Symbols and definitions [a]

a	Half of a channel height or radius of a tubular section (m)
A	Integrational constants (Appendix A)
B	Integrational constants (Appendix A)
c	Concentration (mol m^{-3})
c_0	Initial tracer concentration (mol m^{-3})
c_{av}	$= c_0 V_{inj}/V_t$. Average concentration (mol m^{-3})
C	$= c/c_{av}$ (under flow-injection conditions) or $= c/c_0$ (under steady-conditions). Dimensionless concentration
$\bar{C}$	Laplace transform of C
D	Molecular diffusion coefficient (m^2 s^{-1})
D_L	Axial dispersion coefficient (m^2 s^{-1})
e	Peak broadening (s)
E	$= ev_D/V_t$. Dimensionless peak broadening
f	Coefficient defined in Appendix A
F	$= c_m/c_{Dm}$ or c_m/c_{Am}. Distribution coefficients
g	Coefficient defined in Appendix A
h	Coefficient defined in Appendix A
H	$= ka_D/D_m$. Dimensionless group
k	Mass-transfer coefficient (m s^{-1})
K	$= kV_t/2av_D$. Dimensionless mass-transfer coefficient
K	Number of θ subintervals (Appendix B)
L	$= x_2$. Characteristic length (m)
M	Coefficients defined in Appendix A
M	Number of Y subintervals (Appendix B)
N	Number of X subintervals (Appendix B)
p	Laplace complex variable
P	$= \bar{u}L/D_L$. Peclet number
P_m	$= a_D^2 v_D/D_m V_t$. Dimensionless group
q	Coefficients defined in Appendix A
Q	Coefficient defined in Appendix A
r	Integrational constants (Appendix A)
s	Cross-sectional area of a flow section (m^2)
S	Coefficient defined in Appendix A
t	Time (s)
$\bar{u}$	Mean linear flow-rate (m s^{-1})
v	Volumetric flow-rate (m^3 s^{-1})
V	$= sL$. Volume (m^3)
V_{inj}	Injected volume of tracer (m^3)
V_t	$= \pi a_r^2 x_1 + 2a_D w(x_2 - x_1)$. Characteristic volume
w	Width of the channels of the membrane separation module (m)
x	Axial distance (m)
X	$= x/L$. Dimensionless axial distance
y	Transverse distance (m)
Y	$= y/a_D$. Dimensionless transverse distance
z	Roots of Eqn. A20

Greek letters

α	Coefficient defined in Appendix A
β	The only negative root of Eqn. C3
γ	$= V_t/V$. Coefficients
δ	Half-width of the membrane (m)
Δ	$= \delta/a_D$. Dimensionless half-width of the membrane
ΔX	X increment (Appendix B)
ΔY	Y increment (Appendix B)

TABLE 1 (continued)

Greek letters	
$\Delta\theta$	θ increment (Appendix B)
θ	$= tv_D/V_t$. Dimensionless time
μ	Statistical moment of the tracer response curve about the origin
σ^2	Variance of the tracer response curve
τ	$= Dx/(\bar{u}a^2)$. Fourier number
ϕ	Integrational variable
Ψ	Coefficients defined by Eqn. C4
ω	Coefficients defined by Eqn. C5

[a] Subscripts f, i, r and a refer to the fore-section, the injection section, the reactor and the after-section, respectively; D, A and m refer to the donor channel, the acceptor channel and the membrane, respectively; Dm and Am refer to the donor stream/membrane and the acceptor stream/membrane interfaces, respectively; max refers to maximum concentration. Superscript * refers to the acceptor line.

The aim of this paper is to outline a mathematical model of a flow-injection system with a membrane separation module based on the axially dispersed plug flow model, its experimental verification and the formulation of guidelines for improving its performance.

Among the various types of dialysers used in industry and medical practice and for analytical purposes (i.e., parallel-plate, tubular and spiral-plate dialysers), parallel-plate dialysers have been used most frequently in flow-injection manifolds. For this reason, the experimental verification of the model was performed on a flow-injection manifold with a parallel-plate dialysis module.

DEVELOPMENT AND SOLUTION OF THE MATHEMATICAL MODEL

Description of the model

A flow-injection manifold with a membrane separation module which may have arbitrary geometry can be presented schematically as consisting of one donor and one acceptor line (Fig. 1). The donor line includes the following flow-through sections connected in series: the fore-section, which connects the injection device with the reservoir of the carrier solution; the injection section (usually an injection valve); the reactor, which could be a straight, coiled, packed-bed, single-bead string or knitted tube; the donor channel inside the membrane separation module; and the after-section, which is the section of the flow system leading to waste. Similarly, the acceptor line consists of fore-section, acceptor channel and after-section. The measuring cell is assumed to be downstream of the acceptor channel. Its volume is usually negligible in comparison with the volume of the reactor and the two channels inside the membrane separation module. For this reason, it is not included as a separate element in the schematic representation of the acceptor line. The additional assumptions on which the model is built are the following: (i) the dispersion of the analyte in all sections of the manifold can be described by the axially dispersed plug flow model (Eqn. 1); (ii) the fore- and after-sections are tubular and infinitely long, so that the so-called "end effects" [22] can be neglected and Taylor's theory [18,19] can be used for calculating their Peclet

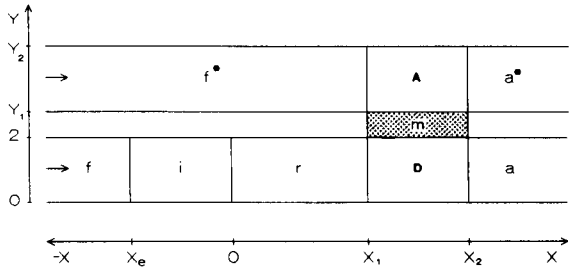

Fig. 1. Scheme of flow-injection manifold with membrane separation module. f, i, r and a refer to the fore-section, the injection section, the reactor and the after-section, respectively, D and A refer to the donor and the acceptor channels, respectively, and * refers to the acceptor line; $Y_1 = 2(1 + \Delta)$, $Y_2 = 2(1 + \Delta + a_A / a_D)$.

numbers (Eqn. 2); and the mass transport within the membrane is caused by transverse Fickian diffusion only. (All symbols are defined in Table 1).

$$\frac{\partial C}{\partial \theta} = \frac{1}{P}\frac{\partial^2 C}{\partial X^2} - \frac{\partial C}{\partial X} \tag{1}$$

$$P = 48DL/(\bar{u}a^2) \tag{2}$$

The flow system shown in Fig. 1 can be described by the following set of partial differential equations in dimensionless quantities and variables similar to Eqn. 1.

For the donor line:

$$\frac{\partial C_f}{\partial \theta} + \gamma_f \frac{\partial C_f}{\partial X} - \frac{\gamma_f}{P_f}\frac{\partial^2 C_f}{\partial X^2} = 0 \quad X \leqslant X_e \tag{3}$$

$$\frac{\partial C_i}{\partial \theta} + \gamma_i \frac{\partial C_i}{\partial X} - \frac{\gamma_i}{P_i}\frac{\partial^2 C_i}{\partial X^2} = 0 \quad X_e \leqslant X \leqslant 0 \tag{4}$$

$$\frac{\partial C_r}{\partial \theta} + \gamma_r \frac{\partial C_r}{\partial X} - \frac{\gamma_r}{P_r}\frac{\partial^2 C_r}{\partial X^2} = 0 \quad 0 \leqslant X \leqslant X_1 \tag{5}$$

$$\frac{\partial C_D}{\partial \theta} + \gamma_D \frac{\partial C_D}{\partial X} - \frac{\gamma_D}{P_D}\frac{\partial^2 C_D}{\partial X^2} + K_D(C_D - C_{Dm}) = 0 \quad X_1 \leqslant X \leqslant X_2 \tag{6}$$

$$\frac{\partial C_a}{\partial \theta} + \gamma_a \frac{\partial C_a}{\partial X} - \frac{\gamma_a}{P_a}\frac{\partial^2 C_a}{\partial X^2} = 0 \quad X \geqslant X_2 \tag{7}$$

For the membrane:

$$\frac{\partial C_m}{\partial \theta} - \frac{1}{P_m}\frac{\partial^2 C_m}{\partial Y^2} = 0 \quad 2 \leqslant Y \leqslant 2 + 2\Delta \tag{8}$$

For the acceptor line:

$$\frac{\partial C_f^*}{\partial \theta} + \gamma_f^* \frac{\partial C_f^*}{\partial X} - \frac{\gamma_f^*}{P_f^*}\frac{\partial^2 C_f^*}{\partial X^2} = 0 \quad X \leqslant X_1 \tag{9}$$

$$\frac{\partial C_A}{\partial \theta} + \gamma_A \frac{\partial C_A}{\partial X} - \frac{\gamma_A}{P_A}\frac{\partial^2 C_A}{\partial X^2} - K_A(C_{Am} - C_A) = 0 \quad X_1 \leqslant X \leqslant X_2 \tag{10}$$

$$\frac{\partial C_a^*}{\partial \theta} + \gamma_a^* \frac{\partial C_a^*}{\partial X} - \frac{\gamma_a^*}{P_a^*}\frac{\partial^2 C_a^*}{\partial X^2} = 0 \quad X \geqslant X_2 \tag{11}$$

The coefficients γ make it possible to use the equations given above for the description of flow systems consisting of sections with various cross-sections. When all cross-sections have equal diameters, the coefficients γ are unity.

The initial and boundary conditions are the following.

For the donor line:

$$C_f(X, 0) = C_r(X, 0) = C_D(X, 0) = C_a(X, 0) = 0;$$

$$C_i(X, 0) = V_t/V_{inj} \tag{12a}$$

$$C_f(X_e^-, \theta) = C_i(X_e^+, \theta) \tag{12b}$$

$$C_f(X_e^-, \theta) - \frac{1}{P_f}\frac{\partial C_f(X_e^-, \theta)}{\partial X} = C_i(X_e^+, \theta) - \frac{1}{P_i}\frac{\partial C_i(X_e^+, \theta)}{\partial X} \tag{12c}$$

$$C_i(0^-, \theta) = C_r(0^+, \theta) \tag{12d}$$

$$C_i(0^-, \theta) - \frac{1}{P_i}\frac{\partial C_i(0^-, \theta)}{\partial X} = C_r(0^+, \theta) - \frac{1}{P_r}\frac{\partial C_r(0^+, \theta)}{\partial X} \tag{12e}$$

$$C_r(X_1^-, \theta) = C_D(X_1^+, \theta) \tag{12f}$$

$$C_r(X_1^-, \theta) - \frac{1}{P_r}\frac{\partial C_r(X_1^-, \theta)}{\partial X} = C_D(X_1^+, \theta) - \frac{1}{P_D}\frac{\partial C_D(X_1^+, \theta)}{\partial X} \tag{12g}$$

$$C_D(X_2^-, \theta) = C_a(X_2^+, \theta) \tag{12h}$$

$$C_D(X_2^-, \theta) - \frac{1}{P_D}\frac{\partial C_D(X_2^-, \theta)}{\partial X} = C_a(X_2^+, \theta) - \frac{1}{P_a}\frac{\partial C_a(X_2^+, \theta)}{\partial X} \tag{12i}$$

$$C_f(-\infty, \theta) = \text{finite} \tag{12j}$$

$$C_a(\infty, \theta) = \text{finite} \tag{12k}$$

For the membrane:

$$C_m(Y, 0) = 0 \tag{13a}$$

$$\frac{\partial C_m(2, \theta)}{\partial Y} = -H_D[C_D(X, \theta) - C_{Dm}(X, \theta)] \tag{13b}$$

$$\frac{\partial C_m(2 + 2\Delta, \theta)}{\partial Y} = H_A[C_{Am}(X, \theta) - C_A(X, \theta)] \tag{13c}$$

For the acceptor line:

$$C_f^*(X, 0) = C_A(X, 0) = C_a^*(X, 0) = 0 \tag{14a}$$

$$C_f^*(X_1^-, \theta) = C_A(X_1^+, \theta) \tag{14b}$$

$$C_f^*(X_1^-, \theta) - \frac{1}{P_f^*}\frac{\partial C_f^*(X_1^-, \theta)}{\partial X} = C_A(X_1^+, \theta) - \frac{1}{P_A}\frac{\partial C_A(X_1^+, \theta)}{\partial X} \tag{14c}$$

$$C_A(X_2^-, \theta) = C_a^*(X_2^+, \theta) \tag{14d}$$

$$C_A(X_2^-, \theta) - \frac{1}{P_A}\frac{\partial C_A(X_2^-, \theta)}{\partial X} = C_a^*(X_2^+, \theta) - \frac{1}{P_a^*}\frac{\partial C_a^*(X_2^+, \theta)}{\partial X} \tag{14e}$$

$$C_f^*(-\infty, \theta) = \text{finite} \tag{14f}$$

$$C_a^*(\infty, \theta) = \text{finite} \tag{14g}$$

The superscripts − and + refer to the upstream and downstream side, respectively, of a given interface between two adjacent flow sections.

The empirical parameters of the model are the Peclet numbers of the different sections and the mass-transfer coefficients in both channels of the membrane separation module. The other parameters of the model are either fundamental constants (e.g., diffusion coefficient in the membrane) or physical parameters, some of which can be measured (e.g., geometrical dimensions, flow-rates). It should be pointed out that the membrane when contacting with solutions usually swells and its thickness under working conditions cannot be measured easily. There are theoretical and empirical relationships for calculating the laminar Peclet numbers of certain type of reactors (e.g., straight and coiled tubes), valid usually for the case of diffusion-controlled dispersion [16]. In most of the flow-injection systems an injection valve is used. In this instance the injection section includes the sample loop and the internal bores of the valve, thus having a rather complex geometry. Therefore, its Peclet number can be determined experimentally only. However, it has been found that if the volume of the injection section is considerably smaller than the reactor volume (e.g., less than 10% of it), which is frequently the case, the Peclet number of the injection section can be assumed to be equal to that of the reactor [17]. For volumes of the injection section of less than 3% a delta-function approximation can be used, which considerably simplifies the solution of the model [17]. Theoretical relationships have been derived for calculating the Peclet number and the mass-transfer coefficients in both channels of parallel-plate dialysers under laminar flow conditions [20,21].

Solution of the model

Equations 3–11 were solved by means of the Laplace transform technique:

$$\bar{C}(X, Y) = \int_0^\infty C(\theta, X) \exp[-p\theta]\, d\theta \tag{15}$$

In the Laplace domain these equations reduce to ordinary linear differential equations of the second order, which were solved analytically (Appendix A). Interesting points for monitoring the concentration are the inlet and outlet of the donor channel and the outlet of the acceptor channel in the case of both semi-permeable and impermeable membranes. The corresponding Laplace domain solutions of mass transfer in the membrane separation module are presented in Appendix A for three different cases: (i) overall transfer is governed by transfer in the channels and in the membrane; (ii) overall transfer is governed by transfer in the membrane only (i.e., infinitely high mass-transfer coefficients); and (iii) only transfer in the channels is of importance

(i.e., infinitely thin membrane or infinitely high diffusion coefficient within it). The time domain solutions were obtained by numerical inverse transformation of the corresponding Laplace domain solutions by expansion of the latter into Fourier sine series and subsequent analytical inverse transformation [23].

For high Peclet numbers of the reactor and the channels of the separation module (e.g., $P > 120$), the numerical technique described above does not give satisfactory results. The concentration curves are lower and exhibit oscillating fronts and tails. Taking into consideration that at high Peclet numbers the "end effects" are negligible [22], it can be assumed that the flow pattern in the membrane separation module does not affect the overall dispersion process in the reactor. This allows one to describe the concentration profile at the inlet of the donor channel as if the reactor is infinitely long. For a straight tube reactor in the case of diffusion-controlled dispersion (i.e., $\tau > 0.7$, Eqn. 2) and small sample volume, so that the injection section can be considered as part of the reactor, the corresponding analytical solution of Eqn. 5 will be the following [24]:

$$C(\theta, X_1) = \frac{1}{2}\left\{\mathrm{erf}\left[\frac{\gamma_r\theta - X_1}{2(\gamma_r\theta/P_r)^{1/2}}\right] + \mathrm{erf}\left[\frac{X_1 - X_e\gamma_r/\gamma_1 - \gamma_r\theta}{2(\gamma_r\theta/P_r)^{1/2}}\right]\right\} \quad (16)$$

where erf is the error function.

Equation 16 defines the input concentration profile for the membrane separation module. The equations describing the processes taking place in the two channels of the membrane separation module and in the membrane itself (i.e., Eqns. 6, 8 and 10) can be solved by the implicit alternating-direction finite-difference method [25]. The corresponding finite-difference equations are given in Appendix B. The concentration profiles monitored downstream of the outlet of the donor (Eqn. 17) and the acceptor (Eqn. 18) channels (Fig. 1) can be calculated on the basis of the convolution theorem:

$$C(\theta, X) = \left(\frac{P_a}{4\pi\gamma_a}\right)^{1/2} \int_0^\theta C_D(\theta, X_2)(\theta - \phi)^{-1/2} \times \exp\left[-P_a\frac{(X - X_2 - \gamma_a(\theta - \phi))^2}{4\gamma_a(\theta - \phi)}\right] d\phi \quad (17)$$

$$C(\theta, X) = \left(\frac{P_a^*}{4\pi\gamma_a^*}\right)^{1/2} \int_0^\theta C_A(\theta, X_2)(\theta - \phi)^{-1/2} \times \exp\left[-P_a^*\frac{(X - X_2 - \gamma_a^*(\theta - \phi))^2}{4\gamma_a^*(\theta - \phi)}\right] d\phi \quad (18)$$

where $C_D(\theta, X_2)$ and $C_A(\theta, X_2)$ are the numerical solutions of Eqns. 6, 8 and 10, and Eqn. 19 is the solution of the axially dispersed plug flow model in the case of an infinitely long tube and delta-function injection at $X = X_2$:

$$C(\theta, X) = \left(\frac{P}{4\pi\gamma\theta}\right)^{1/2} \times \exp\left[-P\frac{(X - X_2 - \gamma\theta)^2}{4\gamma\theta}\right] \quad (19)$$

EXPERIMENTAL

Flow-injection manifold

The main geometrical dimensions of the experimental flow system used in this work, and presented schematically in Fig. 2, are summarized in Table 2.

A constant flow-rate in both the donor and the acceptor lines was maintained by a low-pulsation computer-controlled peristaltic pump (Minipuls, Gilson). To reduce further the undesirable effects caused by pulsation and to remove the air bubbles from the donor and the acceptor streams, pulse dampers were installed downstream of the

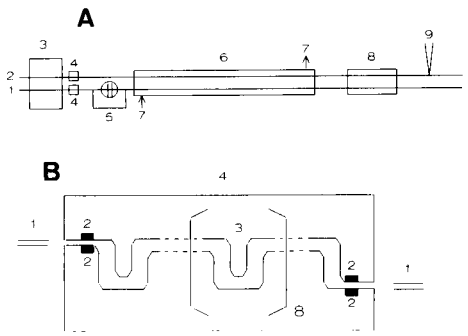

Fig. 2. (A) Scheme of the experimental manifold. 1 = Donor line; 2 = acceptor line; 3 = peristaltic pump; 4 = pulse dampers; 5 = injection valve; 6 = thermostating Perspex tube; 7 = thermostating water; 8 = dialysis module; 9 = thermocouple. (B) Scheme of one of the halves of the dialysis module. 1 = PTFE tubes; 2 = platinum electrodes; 3 = element of the channel, repeated eight consecutive times; 4 = Perspex body.

pump (Fig. 2). One of their walls consists of a gas-permeable membrane made by stretching a PTFE foil. The flow-rates in both lines were determined for each experiment by collecting and weighing their effluents over intervals of 5 min. The total lengths of the tubings of both lines were chosen to be almost equal to prevent a pressure difference between the two channels in the dialysers, which may cause deformation of the membrane, making the mass-transfer process more complicated. The flow-rates in the two lines of the manifold during all the experiments did not differ by more than 1%.

An automatic computer-controlled rotary injection valve (Universal, Anachem) with an external sample loop was used. The latter was a bent piece of PTFE tubing. It was assumed that the whole sample volume filling the external loop and some of the internal bores of the valve were situated in the external loop only. On this basis, the length of the external loop, which corresponds in this instance to the injection section in the model (Fig. 1), was recalculated (Table 2).

The fore-sections, the after-sections and the reactor were PTFE tubes. Their inside diameters were determined by the volume of doubly distilled water with which they can be filled. The reactor was a straight tube. The sections of the fore- and after-sections adjacent to the valve and the dialysis module were also straight tubes. Their lengths were chosen in such a way that the so-called "end effects" could be neglected [22].

A parallel-plate dialyser made of two Perspex halves with a meander-type rectangular groove (Fig. 2A) was used. The membrane was placed between the two halves before they were screwed together. The bottom of each groove was roughened by milling into small circles, thus creating turbulence promoters for intensifying the mass transfer in the channels. Short rectangular channels (5 μl each) connected the grooves of the dialyser with the PTFE tubes by ferrules and screws. Their volumes were considered in the calculations as parts of the corresponding adjacent flow sections (Fig. 1). Platinum plates (0.8 × 0.8 mm) were installed parallel to each other in the bores next to the grooves (Fig. 2a). They allowed the conductivity (PW9509 digital conductivity meter, Philips) of the influent and effluent of both the donor and the acceptor channels of the dialyser to be monitored.

Two types of hydrophilic membrane were used in the experiments, i.e., a PTFE membrane impermeable to potassium chloride and a permeable cellulose hydrate Cuprophan (Enka Glanzstoff) membrane.

The flow system was kept at 20.0 ± 0.1°C. The thermostating system consisted of a thermostat (P.M. Tamson) and a straight Perspex tube in which the reactor and the fore-section of the acceptor line were installed and through which water at the above temperature was constantly

TABLE 2

Geometrical dimensions of the manifold.

Section	Donor line		Acceptor line	
	Length (m)	Diameter (mm)	Length (m)	Diameter (mm)
Fore-section	0.500	0.5304	2.950	0.5304
Injection section	0.115	0.5304		
Reactor	2.487	0.5304		
Channel [a]	0.166	0.2405 [b]	0.166	0.2590 [b]
After-section	0.540	0.5304	0.450	0.5304

[a] The width of both channels is 0.0030 m. [b] Height of the channels.

circulating. The source bottles containing the carrier solutions for the donor and the acceptor lines were placed in the basin of the thermostat. The temperature of the acceptor stream was controlled by a platinum–platinum/rhodium thermocouple connected to a microvoltmeter (3478A Multimeter, Hewlett Packard) (Fig. 2).

The experimental manifold described above was operated by an Apple IIG computer. The software was written in Fysforth version 0.3. The data readings from the conductivity meter and the microvoltmeter were collected and transferred to an IBM-compatible PC for further processing.

Reagents

Standard solutions of potassium chloride in doubly distilled water with concentrations in the range 1.0×10^{-4}–1.0×10^{-2} M were used for injection, calibration and as carrier solutions in the steady-state experiments.

Procedure

The stimulus–response technique [10] was used for identification of the unknown parameters in the model outlined in this paper under flow-injection conditions. The tracer injected by the valve was a 1.0×10^{-2} M solution of potassium chloride. The carrier solutions in both lines, if not stated otherwise, were doubly distilled water.

Three series of experiments were performed as follows. In the first series, the membrane (PTFE foil) installed in the dialysis module was impermeable to the tracer (potassium chloride). The response curves at the inlet and outlet of the donor channel were monitored at four different flow-rates in the range 0.1–1.0 ml min^{-1}. For investigating the acceptor channel its position was interchanged with that of the donor channel, thus connecting it to the reactor. The same experimental procedure was performed again.

In the second series of experiments, the impermeable PTFE foil was replaced by Cuprophan membrane, permeable to the tracer. The response curves at the inlet and outlet of the donor channel and at the outlet of the acceptor channel were recorded at different flow-rates in the range 0.1–0.5 ml min^{-1}. For higher flow-rates the mass transfer under the working conditions used became negligible.

In the third series, doubly distilled water was maintained as the carrier solution in the acceptor line while the carrier solution in the donor line was 1.6×10^{-3} M potassium chloride solution. The steady-state concentrations at the outlets of both channels of the dialyser and at the inlet of the donor channel were measured at different flow-rates ranging from 0.1 to 0.5 ml min^{-1} as in the second series of experiments.

Calibration graphs for all four conductivity detectors were obtained on the basis of fourteen standard solutions of potassium chloride (0.0–2.2 $\times 10^{-3}$ M). The relationship between concentration and conductance was described by polynomial regression equations of the second power. It was found that the flow-rate had no effect on the calibration graphs.

Processing of the experimental response curves

The unknown parameters of the model are the Peclet numbers in all eight flow sections (Fig. 1), the mass-transfer coefficients of the donor and the acceptor channels, the diffusion coefficient and the thickness of the Cuprophan membrane. As already pointed out, the lengths of the fore- and after-sections were chosen such that their Peclet numbers (Eqn. 2) can be determined according to Taylor's theory [18,19]. The volume of the tracer injected in each experiment was less than 5% of the characteristic volume (V_t) (Table 2). In such a case the overall dispersion process should depend only slightly on the Peclet number of the injection section [17] and the latter can be assumed to be equal to that of the reactor. The flow-rates used in the experiments corresponded to Fourier numbers of the reactor (τ_r) well above 0.7, which made it possible to apply Eqn. 2 for the calculation of the Peclet number. On the basis of the above considerations, the eight unknown Peclet numbers could be reduced to three unknown parameters, i.e., the Peclet numbers of the donor and the acceptor channels and the diffusion coefficient of potassium chloride in doubly distilled water at 20°C. The last parameter was necessary for calculating the remainder of the Peclet numbers of the flow system according

to Eqn. 2. In fact, these three parameters are the only unknown parameters of the model under the assumptions made above in the case of an impermeable membrane (i.e., first series of experiments). From the response curves detected in the donor line before and after the donor or the acceptor channels, it was possible to determine the diffusion coefficient of the tracer in the liquid phase and the axial dispersion coefficients of both channels at different flow-rates. The other unknown parameters of the model, i.e., the mass transfer in the channels and within the membrane, were determined form the response curves monitored at the outlet of the donor and the acceptor channels in the second series of experiments (with the Cuprophan membrane). The results obtained were used to derive empirical relationships for the calculation of the mass-transfer and axial dispersion coefficients for both channels.

The values of the steady-state concentrations at the outlets of both channels measured at different flow-rates can be used for calculating the permeability of the Cuprophan membrane. The appropriate equations are given in Appendix C. For each flow-rate, the permeability of the membrane was determined as the average of the permeabilities based on the steady-state concentrations measured in donor and acceptor channels (Appendix C). In these calculations, the mass-transfer and axial dispersion coefficients (Peclet numbers) of the two channels of the dialyser were calculated by the relationships derived earlier. The proper functioning of the manifold was controlled by monitoring the tracer concentration at the inlet of the donor channel, which should be constant during all steady-state experiments.

Curve fitting was utilized to determine the unknown parameters when the tracer response curves were processed (i.e., in the first two series of experiments). A simplex optimization method based on the algorithm of Nelder and Mead [26] was used. The function minimized by this procedure was the square root of the mean squared error between experimental and theoretical response curves. Only those parts of the response curves where the concentration was greater than 5% of the maximum concentration were used in the calculations, thus saving computational time and excluding the less informative sections in the front and the tail of the experimental response curves. The zeroth and first statistical moments about the origin (Eqn. 20, $j = 0$ and $j = 1$) and the second moment about the mean (Eqn. 21) of the experimental response curves and of their best theoretical fits were calculated and compared.

$$\mu_j = \int_0^\infty C\theta^j \, \mathrm{d}\theta \tag{20}$$

$$\sigma^2 = \int_0^\infty C(\mu_1 - \theta)^2 \, \mathrm{d}\theta = \mu_2 - \mu_1^2 \tag{21}$$

It is possible to calculate the statistical moments directly from the Laplace domain solution of the model (Appendix A) without the necessity of performing its inverse transformation by the following relationship, proposed by Van der Laan [27]:

$$\mu_j = (-1)^{-j}\left(d^j\overline{C}/\mathrm{d}p^j\right)_{p\to 0} \tag{22}$$

The zeroth moments for the donor and the acceptor channels define the integral amount of tracer monitored in them. They are interrelated by the following equation:

$$\mu_{0_D} + (v_A/v_D)\mu_{0_A} = 1 \tag{23}$$

This relationship was used for controlling the manifold for malfunctioning during the experiments. The first moment about the origin (Eqn. 20, $j = 1$), known as the mean, defines the centre of gravity of the tracer response curve. The second moment about the mean, known as the variance, (Eqn. 21) characterizes the width of the tracer response curve and can be used for determining the sample throughput of the manifold.

Computer programs

The numerical procedures outlined above for processing of the tracer response curve and for solving the model were programmed in QuickC (Version 2, Microsoft) and the corresponding programs were run on an IBM-compatible PC.

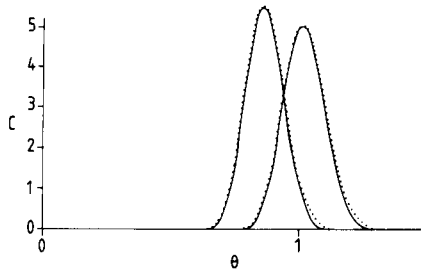

Fig. 3. Comparison of experimental tracer response curves (solid lines) measured at 0.133 ml min^{-1} before and after the donor channel and their best theoretical fits (dotted lines).

RESULTS AND DISCUSSION

Determination of the diffusion coefficient of the tracer in the flow system and its axial dispersion coefficients in the channels of the dialyser

Figure 3 illustrates the agreement between the experimental response curves from the first series of experiments (with the impermeable membrane) and their best theoretical fits.

The diffusion coefficient of potassium chloride obtained from the Peclet number of the reactor (Eqn. 2) by the curve-fitting procedure, outlined earlier was found to be 1.72×10^{-9} m^2 s^{-1}, which was fairly close to earlier results [15] and to literature data (1.77×10^{-9} m^2 s^{-1} at infinite dilution [28]). Very slight variations in this value (less than 3%) were observed for different flow-rates in the range 0.1–1.0 ml min^{-1}. Because the geometry of the dialyser channels is complicated, no theoretical relationships similar to Eqn. 2 for calculating the corresponding axial dispersion coefficients or Peclet numbers exist. It was found that the flow-rate dependence of the axial dispersion coefficients can be described successfully (Fig. 4) by the following empirical equations:

$$D_{L_D} = 1.531 \times 10^6 \, v_D^{1.2692} \quad (24)$$

$$D_{L_A} = 9.865 \times 10^4 \, v_A^{1.1414} \quad (25)$$

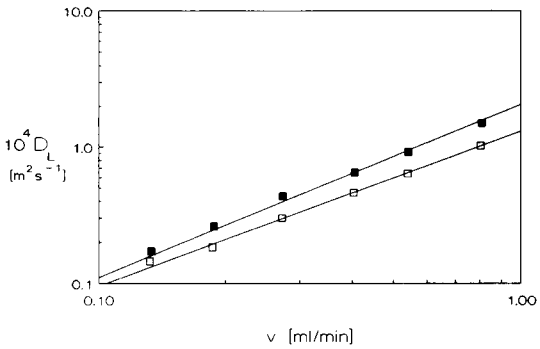

Fig. 4. Axial dispersion coefficient versus flow-rate in ml min^{-1} for the (■) donor and (□) acceptor channels.

Determination of the mass-transfer coefficients in the channels of the dialyser, the thickness of the membrane and the diffusion coefficient of the tracer within it

The tracer response curves obtained in the second series of experiments were processed by curve-fitting for determining the values of the following parameters of the model: K_D, K_A, P_m and Δ. From the last two parameters the thickness of the membrane and the effective diffusion coefficient of potassium chloride within it at 20°C can be easily calculated. In the calculations all the Peclet numbers in the model were calculated by using Eqn. 2 and Eqns. 24 and 25. In the second series of experiments, the flow-rate in both lines of the manifold was varied (0.1–0.5 ml min^{-1}), thus changing the hydrodynamimc conditions in both channels of the dialysis module. It can be expected that the corresponding mass-transfer coefficients will vary also with the flow-rate while the thickness of the membrane (2δ) and the diffusion coefficient of the tracer within it (D_m) should remain unchanged. The experimental results showed that 2δ and D_m obtained for four different flow-rates were within 3% of the their mean values (Table 3), i.e., 2.808×10^{-5} m and 7.915×10^{-11} m^2 s^{-1}, respectively. This result confirms the validity of the model. The

TABLE 3

Curve-fitting results for 2δ and D_m

v_D (ml min^{-1})	2δ (μm)	$10^{11} D_m$ (m^2 s^{-1})
0.1016	27.62	7.747
0.1917	28.08	8.141
0.2803	28.30	7.892
0.4153	28.32	7.880
Average	28.08	7.915

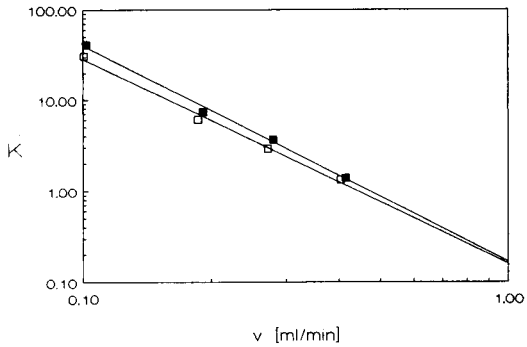

Fig. 5. Mass-transfer coefficient versus flow-rate in ml min^{-1} for the (■) donor and (□) acceptor channels.

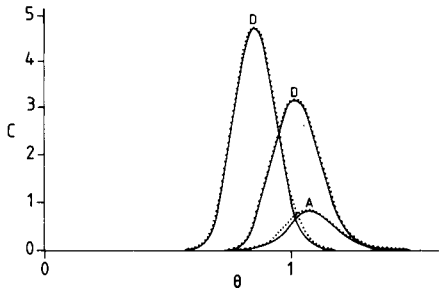

Fig. 6. Experimental tracer response curves (solid lines) measured at $v_D = 0.190$ ml min^{-1} and $v_A = 0.187$ ml min^{-1} before the donor channel and after the donor and the acceptor channels and their best model fits (dotted lines). D and A refer to the donor and acceptor lines, respectively.

thickness of the membrane (2δ) before contacting with water (normal state) is stated by the producer to be 1.3×10^{-5} m. Its increase during the transition from the normal to the wet state due to swelling is reported to amount to a factor of 1.9. This will result in a 2δ value of 2.48×10^{-5} m, which is close to the value obtained in the present investigation. This fact could be considered as further proof for the adequacy of the model outlined earlier. The values obtained for the mass-transfer coefficients of the channels for different flow-rates were found to obey fairly well the following relationships (Fig. 5):

$$K_D = 4.854 \times 10^{-20} v_D^{-2.382} \quad (26)$$

$$K_A = 3.465 \times 10^{-19} v_A^{-2.270} \quad (27)$$

The satisfactory agreement between the experimental response curves and their best theoretical fits is illustrated in Fig. 6.

Determination of the permeability of the membrane under steady-state conditions

The steady-state concentrations measured at the outlets of the donor and the acceptor channels for different flow-rates are presented in Fig. 7.

Under steady-state conditions, the thickness of the membrane and the diffusion coefficient of the tracer within it cannot be determined separately from each other, because only the ratio of these two parameters appears in the equations describing the steady-state mass transfer through the membrane (Appendix C). For this reason, the experimental results obtained in this series of experiments were used for determining the ratio $D_m/2\delta$, which is often referred to as the permeability of the membrane. The value of the permeability, averaged over the whole range of flow-rates, was found to be 2.35×10^{-6} m s^{-1}, which does not differ substantially from the corresponding value obtained under flow-injection conditions, i.e., 2.82×10^{-6} m s^{-1}. This result is further proof of the validity of the model. Permeability data for Cuprophan membranes with thickness 1.15×10^{-6} and 1.35×10^{-6} m, when a 0.01 M solution of sodium chloride at 20°C was used, were provided by the manufacturer. According to the manufacturer, the membrane used in the present experiment had a thickness of 1.27×10^{-6} m. For this membrane the perme-

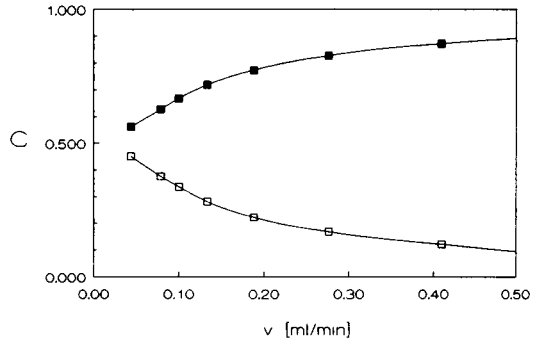

Fig. 7. Steady-state concentration versus flow-rate in ml min^{-1} measured downstream of the (■) donor and (□) acceptor channels.

ability was calculated by interpolation to be $(4.66 \pm 0.64) \times 10^{-6}$ m s^{-1}, which is at least of the same order of magnitude as the values obtained in the present study. Because the details of the experimental procedure for determining the permeability by the manufacturer are lacking and a different electrolyte at a different concentration is used, it is impossible to assess the causes of the discrepancy.

Influence of system parameters on sensitivity and sample throughput

After having proved the validity of the model, it is possible to investigate by numerical simulations the influence of the main design and operational parameters of a flow-injection system with a membrane separation module on the sensitivity and sample throughput of analysis. In this way costly and time-consuming experiments could be avoided. For convenience, the parameters of the experimental flow system outlined above could be used in the simulations. This will make it possible in some instances to compare simulated with experimental results. As the empirical flow-rate dependence of the axial dispersion and mass-transfer coefficients in the channels of the dialysis module was determined in the range 0–1.0 ml min^{-1} for the former and 0–0.5 ml min^{-1} for the latter coefficients, the simulations were confined to the narrower flow range. In an earlier study, the influence of the main parameters of a parallel-plate dialyser under laminar flow conditions was thoroughly investigated and conclusions for choosing their optimum values with respect to mass-transfer efficiency were drawn [21]. The calculations performed for a pulse concentration input were made under the assumption of zero length of the reactor and no dispersion in the injection section. Neither of these conditions holds in real flow-injection manifolds. For this reason, it is expedient to investigate how the dispersion processes in the flow sections upstream of the donor channel (i.e., fore-section, injection section and reactor) and the sample volume ($-X_e$) will influence the peak height (c_{max} or C_{max}) and the peak broadening (e or E) of the concentration profile monitored at the outlet of the acceptor channel. For flow systems with relatively small sample volumes, the dispersion of the analyte in the reactor is the process playing a major role in the formation of the concentration profile at the inlet of the donor channel [17]. This process can be characterized by the reactor Fourier number (τ_r):

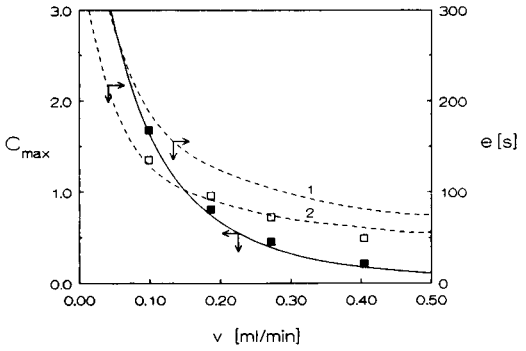

Fig. 8. Flow-rate dependence of the maximum concentration (C_{max}) in the acceptor channel (solid line) and the peak width (dotted lines) at (1) $0.01C_{max}$ and (2) $0.1C_{max}$. Experimental results for (■) C_{max} and (□) for the peak width at $0.1C_{max}$.

$$\tau_r = \pi D_r x_1 / v_D \quad (28)$$

From Eqn. 28, it follows that concentration profile at the inlet of the donor channel for a given analyte can be easily manipulated by varying the volumetric flow-rate or (and) the length of the reactor. The volumetric flow-rate in the acceptor channel was assumed to be equal to that in the donor line (as in the experimental manifold). The flow-rate v_D is an operational parameter affecting considerably the dispersion processes in all sections of the flow system (including the channels of the dialysis module) and the rate of mass transfer. Its effect on peak height and peak broadening is illustrated in Fig. 8. The peak broadening (e) is given in real dimensions (i.e., in seconds) to avoid confusion originating from the fact that on changing the flow-rate the mean residence time, which is the dimensionless time unit, also changes. The flow-rate dependences of C_{max} and e (at both 0.01 C_{max} and 0.1 C_{max}) are similar, showing that in choosing the flow-rate a compromise should be made between sensitivity and sample throughput. The comparison of the theoretically calculated relationships for the flow-rate dependence of the maximum C_A and

the peak width (at C_A equal to 10% of the maximum C_A) with experimental results shows a satisfactory agreement (Fig. 8). The agreement for e measured at 1% of the maximum C_A was poor because the signal monitored for such low concentrations (10^{-6}–10^{-5} M) was in the range of the noise of the conductivity meter used.

The influence of the reactor length (x_1) on c_{max} and e (at 1% of c_{max}) at a constant flow-rate (0.2 ml min^{-1}) is illustrated in Fig. 9. These results show that shorter reactors are more favourable for the optimum performance of the flow-injection manifolds considered in this study. However, it should be taken into consideration that a longer reactor can improve to a certain extent the reproducibility of analysis. The reason for this is that the greater the extent to which the dispersion process is diffusion controlled (i.e., high τ), the smaller is the influence or arbitrary disturbances in the flow (e.g., slight variation in the flow-rate, pulsations) on the detected signal.

The influence of the sample volume ($-X_e$) on the acceptor peak maximum ($c = -c_0/\gamma_i X_e C_{max}$, where c_0/γ_i is constant throughout the simulations) and on the peak width (at 1% of c_{max}) is presented in Fig. 10. For simplicity in the calculations, the axial dispersion coefficient in the injection section was assumed to be equal to that of the reactor even for relatively large sample volumes (i.e., $-X_e > 0.1$). As expected, an increase in the sample volume leads to a higher peak maximum and hence to a higher sensitivity of analysis. The dependence is almost linear for

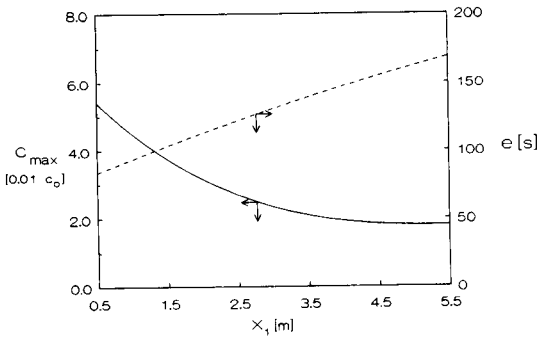

Fig. 9. Influence of the reactor length (x_1) on c_{max} (solid line) and e at $0.01c_{max}$ (dotted line). v_D = 0.2 ml min^{-1}.

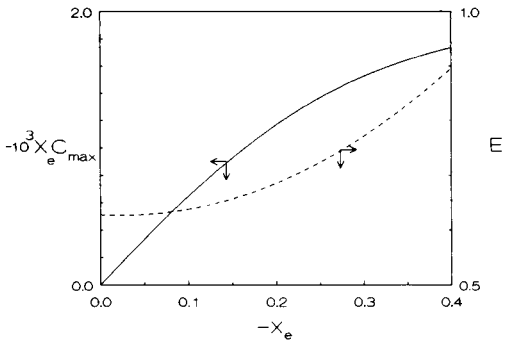

Fig. 10. Influence of the sample volume ($-X_e$) on c_{max} (solid line) and e at $0.01c_{max}$ (dotted line). V_D = 0.2 ml min^{-1}.

dimensionless sample volumes up to 0.2, above which the slope gradually decreases and C_A approaches asymptotically the steady-state acceptor concentration for volumes higher than 0.8 [21]. In the linear range mentioned above ($-X_e < 0.2$), the sample volume has virtually no influence on the sample throughput of the manifold. For larger sample volumes the baseline-to-baseline time increases with $-X_e$. These results show that choosing a sample volume in the upper part of the linear range (e.g., 0.1–0.2) seems to be appropriate with respect to both sensitivity and sample throughput.

Conclusions

A general mathematical model for a flow-injection system with a dialysis module based on the axially dispersed plug flow model was developed. It was solved by Laplace transforms for values of the reactor Peclet number of less than 120, whereas for higher values a numerical method using the implicit alternating-direction finite difference method was found to be more suitable.

The validity of the model was confirmed experimentally for a flow-injection manifold utilizing a parallel-plate dialysis model. This geometry of the dialyser does not limit the generality of the model, which can also be applied to other geometries of the membrane separation module (e.g., tubular) and other types of membranes (e.g., gas-diffusion).

The results obtained in this study show that the proposed model for a flow-injection manifold with a membrane separation module, together with the parameter identification procedure outlined above, can be used successfully for a better understanding of the processes taking place in such manifolds and for predicting the shape and magnitude of the analytical signal, for optimizing the performance of these manifolds with respect to sensitivity and sample throughput, for characterizing various membranes (i.e., determining their thickness and the diffusivity of different analytes in them) and for characterizing the mass-transfer properties of various geometries of the donor and the acceptor channels (i.e., determining their axial dispersion and mass-transfer coefficients). The last two possible applications of the model could be useful in membrane technology and in designing effective process, medical (for haemodialysis) or analytical flow-through dialysers.

The possibility provided by simulating the model to select the values of some construction and operational parameters of the flow-injection systems incorporating membrane separation modules which will ensure their optimum performance is illustrated on the experimental manifold used for verification of the model. On the basis of the simulation results, some more general conclusions concerning the selection of optimum sample volume and reactor length were drawn: the sample volume ($-X_e$) should be in the range 0.1–0.3 and the reactor length should not exceed the value necessary for obtaining a reproducible concentration profile at the inlet of the donor channel. The last condition is usually in effect for diffusion-controlled dispersion ($\tau_r > 0.7$). The guidelines for choosing optimum values for the parameters of the membrane separation module were formulated elsewhere [21].

The authors are grateful to Egbert Hoogendam for experimental help.

APPENDIX A

Laplace domain solution of Eqns. 3–11

The Laplace transforms of Eqns. 3–11 are the following.

For the donor line:

$$\frac{d^2\overline{C_f}}{dX^2} - P_f\frac{d\overline{C_f}}{dX} - \frac{pP_f}{\gamma_f}\overline{C_f} = 0 \qquad X \le X_e \tag{A1}$$

$$\frac{d^2\overline{C_i}}{dX^2} - P_i\frac{d\overline{C_i}}{dX} - \frac{pP_i}{\gamma_i}\overline{C_i} = -\frac{P_i}{\gamma_i} \qquad X_e \le X \le 0 \tag{A2}$$

$$\frac{d^2\overline{C_r}}{dX^2} - P_r\frac{d\overline{C_r}}{dX} - \frac{pP_r}{\gamma_r}\overline{C_r} = 0 \qquad 0 \le X \le X_1 \tag{A3}$$

$$\frac{d^2\overline{C_D}}{dX^2} - P_D\frac{d\overline{C_D}}{dX} - (p + K_D)\frac{P_D}{\gamma_D}\overline{C_D} + K_D\frac{P_D}{\gamma_D}\overline{C_{Dm}} = 0 \qquad X_1 \le X \le X_2 \tag{A4}$$

$$\frac{d^2\overline{C_a}}{dX^2} - P_a\frac{d\overline{C_a}}{dX} - \frac{pP_a}{\gamma_a}\overline{C_a} = 0 \qquad X \ge X_2 \tag{A5}$$

for the membrane:

$$\frac{d^2\overline{C_m}}{dY^2} - P_m p\overline{C_m} = 0 \qquad 2 \le Y \le 2 + 2\Delta \tag{A6}$$

For the acceptor line:

$$\frac{d^2\overline{C_f^*}}{dX^2} - P_f^* \frac{d\overline{C_f^*}}{dX} - \frac{pP_f^*}{\gamma_f^*}\overline{C_f^*} = 0 \qquad X \le X_1 \tag{A7}$$

$$\frac{d^2\overline{C_A}}{dX^2} - P_A \frac{d\overline{C_A}}{dX} - (p + K_A)\frac{P_A}{\gamma_A}\overline{C_A} + K_A \frac{P_A}{\gamma_A}\overline{C_{Am}} = 0 \qquad X_1 \le X \le X_2 \tag{A8}$$

$$\frac{d^2\overline{C_a^*}}{dX^2} - P_a^* \frac{d\overline{C_a^*}}{dX} - \frac{pP_a^*}{\gamma_a^*}\overline{C_a^*} = 0 \qquad X \ge X_2 \tag{A9}$$

The corresponding boundary conditions can be obtained from those of Eqns. 3–11 by simply replacing the concentrations with their Laplace transforms.

The Laplace domain solutions of Eqns. A1–A9 are the following.

$$\overline{C_f} = A_1 \exp[P_f(0.5 + q_f)(X - X_e)] \tag{A10}$$

$$\overline{C_i} = A_2 \exp[P_i(0.5 + q_i)X] + A_3 \exp[P_i(0.5 - q_i)X] + 1/p \tag{A11}$$

$$\overline{C_r} = A_4 \exp[P_r(0.5 + q_r)X] + A_5 \exp[P_r(0.5 - q_r)X] \tag{A12}$$

$$\overline{C_D} = \sum_{i=1}^{i=4} r_i \exp[z_i(X - X_1)] \tag{A13}$$

$$\overline{C_a} = A_6 \exp[P_a(0.5 - q_a)(X - X_2)] \tag{A14}$$

$$\overline{C_f^*} = B_1 \exp[P_f^*(0.5 + q_f^*)X] \tag{A15}$$

$$\overline{C_A} = \sum_{i=1}^{i=4} \alpha_i r_i \exp[z_i(X - X_1)] \tag{A16}$$

$$\overline{C_a^*} = B_2 \exp[P_a^*(0.5 - q_a^*)(X - X_2)] \tag{A17}$$

where

$$q_j = \left(\frac{p}{\gamma_j P_j} + 0.25\right)^{1/2} \tag{A18}$$

The coefficients A_1–A_6, $B1$, $B2$ and r_i are the unknown integrational constants which can be obtained from the boundary conditions of Eqns. A1–A5 and A7–A9. The coefficients α_i can be determined from solution of Eqn. A6 [21]:

$$\alpha_i = -\frac{z_i^2 - P_D z_i - [p + K_D(1 - f_D)]\dfrac{P_D}{\gamma_D}}{f_A K_D \dfrac{P_D}{\gamma_D}} \tag{A19}$$

where z_i are the roots of the following biquadratic equation [21]:

$$z^4 - (P_D + P_A)z^3 + \left(P_D P_A - [p + K_D(1-f_D)]\frac{P_D}{\gamma_D} - [p + K_A(1-g_A)]\frac{P_A}{\gamma_A} \right) z^2$$
$$+ P_D P_A \left(\frac{p + K_D(1-f_D)}{\gamma_D} + \frac{p + K_A(1-g_A)}{\gamma_A} \right) z$$
$$+ \frac{P_D}{\gamma_D}\frac{P_A}{\gamma_A}([p + K_D(1-f_D)][p + K_A(1-g_A)] - K_D K_A f_A g_D) = 0 \quad \text{(A20)}$$

In the general case when the overall mass-transfer process in the membrane separation module is governed by the transfer both in the channels and in the membrane, the coefficients f_D, f_A, g_D and g_A are defined as follows [21]:

$$f_D = \frac{H_D}{F_D Q}\{(q_m + H_A/F_A)\exp(2q_m\Delta) + (q_m - H_A/F_A)\exp(-2q_m\Delta)\}$$
$$f_A = (H_A/F_D Q)2q_m$$
$$g_D = (H_D/F_A Q)2q_m$$
$$g_A = (H_A/F_A Q)[(q_m + H_D/F_D)\exp(2q_m\Delta) + (q_m - H_D/F_D)\exp(-2q_m\Delta)]$$

where

$$Q = (q_m + H_D/F_D)(q_m + H_A/F_A)\exp(2q_m\Delta) - (q_m - H_D/F_D)(q_m - H_A/F_A)\exp(-2q_m\Delta)$$
$$q_m = (pP_m)^{1/2}$$

When the overall mass transfer is controlled only by the transfer in the channels of the membrane separation module, e.g., the resistance of the membrane is negligible because $\Delta \to 0$, the expressions for f_D, f_A, g_D and g_A can be considerably simplified:

$$f_D = \left(1 + \frac{F_D}{F_A}\frac{K_A}{k_D}\right)^{-1}$$
$$f_A = \left(\frac{F_D}{F_A} + \frac{k_D}{k_A}\right)^{-1}$$
$$g_D = \left(\frac{F_A}{F_D} + \frac{k_A}{k_D}\right)^{-1}$$
$$g_A = \left(1 + \frac{F_A}{F_D}\frac{k_D}{k_A}\right)^{-1}$$

Another extreme case is when the resistance of the membrane is much higher than that of the channels of the membrane separation module. It can be assumed that the mass-transfer coefficients of both channels are infinitely high, i.e., $k_D \to \infty$ and $k_A \to \infty$. The following relationships necessary for the solution of Eqn. A20 will hold:

$$K_D f_A = F_A q_m/[2P_m \sinh(2q_m\Delta)]$$
$$K_D(1-f_D) = F_D q_m/[2P_m \tanh(2q_m\Delta)]$$
$$K_A g_D = (a_D/a_A)F_D q_m/[2P_m \sinh(2q_m\Delta)]$$
$$K_A(1-g_A) = (a_D/a_A)F_A q_m/[2P_m \tanh(2q_m\Delta)]$$

The Laplace transforms of the concentration profiles in the flow sections situated upstream (i.e., reactor) and downstream (i.e., after-section of the donor line) of the donor channel and downstream of the acceptor channel (i.e., after-section of the acceptor line) are the following:

$$\overline{C_r} = \frac{1}{2q_r}\left\{\left[\sum_{i=1}^{i=4} r_i(0.5 + q_r - z_i/P_D)\right]\exp[P_r(0.5 - q_r)(X - X_1)]\right.$$
$$\left. - \left[\sum_{i=1}^{i=4} r_i(0.5 - q_r - z_i/P_D)\right]\exp[P_r(0.5 + q_r)(X - X_1)]\right\} \qquad 0 \le X \le X_1 \tag{A21}$$

$$\overline{C_a} = \left\{\sum_{i=1}^{i=4} r_i \exp[z_i(X_2 - X_1)]\right\}\exp[P_a(0.5 - q_a)(X - X_2)] \qquad X \ge X_2 \tag{A22}$$

$$\overline{C_a^*} = \left\{\sum_{i=1}^{i=4} \alpha_i r_i \exp[z_i(X_2 - X_1)]\right\}\exp[P_a^*(0.5 - q_a^*)(X - X_2)] \qquad X \ge X_2 \tag{A23}$$

where

$$r_1 = h - r_2 h_1^1 - r_3 h_2^1 - r_4 h_3^1$$

$$r_2 = \frac{h + r_3(h_2^2 - h_2^1) + r_4(h_3^2 h_3^1)}{h_1^1 - h_1^2}$$

$$r_3 = \frac{h(h_1^2 - h_1^4) + r_4[(h_1^2 - h_1^1)(h_3^4 - h_3^1) - (h_1^4 - h_1^1)(h_3^2 - h_3^1)]}{(h_1^4 - h_1^1)(h_2^2 - h_2^1) - (h_1^2 - h_1^1)(h_2^4 - h_2^1)}$$

$$r_4 = [h\{(h_1^2 - h_1^4)[(h_2^3 - h_2^1)(h_1^2 - h_1^1) - (h_1^3 - h_1^1)(h_2^2 - h_2^1)]$$
$$- (h_1^2 - h_1^3)[(h_1^2 - h_1^1)(h_2^4 - h_2^2) - (h_2^2 - h_2^1)(h_1^4 - h_1^1)]\}]$$
$$\times[[(h_3^3 - h_3^1)(h_1^2 - h_1^1) - (h_3^2 - h_3^1)(h_1^3 - h_1^1)][(h_1^2 - h_1^1)(h_2^4 - h_2^1) - (h_2^2 - h_2^1)(h_1^4 - h_1^1)]$$
$$- [(h_1^2 - h_1^1)(h_3^4 - h_3^1) - (h_3^2 - h_3^1)(h_1^4 - h_1^1)][(h_1^2 - h_1^1)(h_2^3 - h_2^1) - (h_2^2 - h_2^1)(h_1^3 - h_1^1)]]^{-1}$$

$$h = 2q_r M_3 \exp[P_r(0.5 + q_r)X_1]/S_1$$

$$h_j^1 = S_{j+1}/S_1$$

$$h_j^2 = [(0.5 - q_a - z_{j+1}/P_D)/(0.5 - q_a - z_1/P_D)]\exp[(z_{j+1} - z_1)(X_2 - X_1)]$$

$$h_j^3 = [\alpha_{j+1}(0.5 + q_f^* - z_{j+1}/P_A)]/[\alpha_1(0.5 + q_f^* - z_1/P_A)]$$

$$h_j^4 = [\alpha_{j+1}(0.5 - q_a^* - z_{j+1}/P_A)]/[\alpha_1(0.5 - q_a^* - z_1/P_A)]\exp[(z_{j+1} - z_1)(X_2 - X_1)]$$

where $j = 1, 2, 3$;

$$S_j = 2q_r M_1 + [M_2 \exp[2P_r q_r X_1] - M_1](0.5 + q_r - z_j/P_D)$$

where $j = 1, 2, 3, 4$;

$$M_1 = (q_r - q_i)(q_f + q_i)\exp[-2P_i q_i X_e] - (q_r + q_i)(q_f - q_i)$$

$$M_2 = (q_r - q_i)(q_f - q_i) - (q_f + q_i)(q_r + q_i)\exp[-2P_i q_i X_e]$$

$$M_3 = [(0.5 - q_i)(q_f - q_i) + 2q_i(0.5 + q_f)\exp[-P_i(0.5 + q_i)X_e]$$
$$- (0.5 + q_i)(q_f + q_i)\exp[-2P_i q_i X_e]]/p$$

If the membrane is impermeable to the analyte, the dispersion process in the donor channel will be described by Eqn. A24 instead of Eqn. A13:

$$\overline{C_D} = A_7 \exp[P_D(0.5+q_D)(X-X_1)] + A_8 \exp[P_D(0.5-q_D)(X-X_1)] \quad \text{(A24)}$$

The Laplace transform of the concentration profile monitored in the donor line downstream of the donor channel (i.e., in the after-section) will be given by Eqn. A14, where

$$\begin{aligned} A_6 = \frac{1}{p}\{&4q_r q_D \exp[P_r(0.5-q_r)X_1 + P_D(0.5-q_D)(X_2-X_1)] \\ &\times\{(0.5+q_i)(q_f+q_i) - (0.5-q_i)(q_f-q_i)\exp[2P_i q_i X_e] - 2q_i(0.5+q_f)\exp[-P_i(0.5-q_i)X_e]\}\} \\ &\times\{\{(q_a+q_D)(q_r+q_D) - (q_a-q_D)(q_r-q_D)\exp[-2P_D q_D(X_2-X_1)]\} \\ &\times\{(q_r+q_i)(q_f+q_i) - (q_f-q_i)(q_r-q_i)\exp[-2P_i q_i X_e]\} - \{(q_r-q_i)(q_f+q_i) - (q_r+q_i) \\ &\times(q_f-q_i)\exp[-2P_i q_i X_e]\} \\ &\times\{(q_a+q_D)(q_r-q_D) - (q_a-q_D)(q_r+q_D)\exp[-2P_D q_D(X_2-X_1)]\}\exp[-2P_r q_r X_1]\}^{-1} \end{aligned} \quad \text{(A25)}$$

APPENDIX B

Implicit finite-difference equations for the membrane separation module

The θ, X and Y regions of interest were divided into K, N and M sub-intervals, respectively, so that it can be written:

$\theta = k\ \Delta\theta \quad (k = 0, 1, 2, \ldots, K)$

$X = i\ \Delta X \quad (i = 0, 1, 2, \ldots, N)$

$Y = j\ \Delta Y \quad (j = 0, 1, 2, \ldots, M)$

X-implicit equations

$$-\frac{\gamma_D \Delta\theta}{4\Delta X}\left(1+\frac{1}{P_D \Delta X}\right)C_{D_{i-1,k+0.5}} + \left[1+\frac{\Delta\theta\gamma_D}{(\Delta X)^2 P_D}\right]C_{D_{i,k+0.5}} + \frac{\gamma_D\ \Delta\theta}{4\ \Delta X}\left(1-\frac{2}{P_D\ \Delta X}\right)C_{D_{i+1,k+0.5}}$$
$$= \left(1-\frac{K_D\ \Delta\theta}{2}\right)C_{D_{i,k}} + \frac{K_D\ \Delta\theta}{2F_D}C_{m_{i,0,k}} \quad \text{(B1)}$$

$$-\frac{\gamma_A\ \Delta\theta}{4\ \Delta X}\left(1+\frac{2}{P_A\ \Delta X}\right)C_{A_{i-1,k+0.5}} + \left[1+\frac{\Delta\theta\gamma_A}{(\Delta X)^2 P_A}\right]C_{A_{i,k+0.5}} + \frac{\gamma_A\ \Delta\theta}{4\ \Delta X}\left(1-\frac{2}{P_A\ \Delta X}\right)C_{A_{i+1,k+0.5}}$$
$$= \left(1-\frac{K_A\ \Delta\theta}{2}\right)C_{A_{i,k}} + \frac{K_A\Delta\theta}{2F_A}C_{m_{i,M,k}} \quad \text{(B2)}$$

$$C_{m_{i,0,k+0.5}} = \frac{1}{1+H_D\ \Delta Y/F_D}\left(C_{m_{i,1,k+0.5}} + H_D\ \Delta Y C_{D_{i,k+0.5}}\right) \quad \text{for } j=0 \quad \text{(B3)}$$

$$C_{m_{i,j,k+0.5}} = \left(1-\frac{\Delta\theta}{(\Delta Y)^2 P_m}\right)C_{m_{i,j,k}} + \frac{\Delta\theta}{2(\Delta Y)^2 P_m}\left(C_{m_{i,j+1,k}} + C_{m_{i,j-1,k}}\right) \quad \text{for } 0<j<M \quad \text{(B4)}$$

$$C_{m_{i,M,k+0.5}} = \frac{1}{1+H_A\ \Delta Y/F_A}\left(C_{m_{i,M-1,k+0.5}} + H_A\ \Delta Y C_{A_{i,k+0.5}}\right) \quad \text{for } j=M \quad \text{(B5)}$$

Y-implicit equations

$$C_{D_{i,k+1}} = \frac{\gamma_D \Delta\theta}{4\Delta X}\left(1 + \frac{2}{P_D \Delta X}\right) C_{D_{i-1,k+0.5}} + \left[1 - \frac{\Delta\theta\gamma_D}{(\Delta X)^2 P_D} - \frac{K_D\,\Delta\theta}{2}\right] C_{D_{i,k+0.5}}$$

$$- \frac{\gamma_D\,\Delta\theta}{4\,\Delta X}\left(1 - \frac{2}{P_D \Delta X}\right) C_{D_{i+1,k+0.5}} + \frac{K_D\,\Delta\theta}{2F_D} C_{m_{i,0,k+0.5}} \tag{B6}$$

$$C_{A_{i,k+1}} = \frac{\gamma_A \Delta\theta}{4\Delta X}\left(1 + \frac{2}{P_A \Delta X}\right) C_{A_{i-1,k+0.5}} + \left[1 - \frac{\Delta\theta\gamma_A}{(\Delta X)^2 P_A} - \frac{K_A\,\Delta\theta}{2}\right] C_{A_{i,k+0.5}}$$

$$- \frac{\gamma_A \Delta\theta}{4\Delta X}\left(1 - \frac{2}{P_A \Delta X}\right) C_{A_{i+1,k+0.5}} + \frac{K_A\,\Delta\theta}{2F_A} C_{m_{i,M,k+0.5}} \tag{B7}$$

$$\left(1 + \frac{H_D\,\Delta Y}{F_D}\right) C_{m_{i,0,k+1}} - C_{m_{i,1,k+1}} = H_D\,\Delta Y C_{D_{i,k+1}} \quad \text{for } j = 0 \tag{B8}$$

$$\frac{\Delta\theta}{2(\Delta Y)^2 P_m} C_{m_{i,j-1,k+1}} - \left[1 + \frac{\Delta\theta}{(\Delta Y)^2 P_m}\right] C_{m_{i,j,k+1}} + \frac{\Delta\theta}{2(\Delta Y)^2 P_m} C_{m_{i,j+1,k+1}} = -C_{m_{i,j,k+0.5}} \quad \text{for } 0 < j < M \tag{B9}$$

$$-C_{m_{i,M-1,k+1}} + \left(1 + \frac{H_A\,\Delta Y}{F_A}\right) C_{m_{i,M,k+1}} = H_A\,\Delta Y C_{A_{i,k+1}} \quad \text{for } j = M \tag{B10}$$

Both the sets of X-implicit and Y-implicit equations have a tridiagonal coefficient matrix and were solved in a straightforward way by the Gaussian elimination method [25].

APPENDIX C

Equations for calculating the steady-state membrane permeability

The concentrations at the outlets of the donor and the acceptor channels under steady-state conditions (i.e., $\partial C/\partial\theta = 0$) can be calculated by the following equations [29]:

$$C_D = \frac{\omega}{\omega - F_D/F_A}\left\{1 - \frac{F_D}{\omega F_A} \exp[\beta(X_2 - X_1)]\right\} \tag{C1}$$

$$C_A = \frac{\omega}{\omega F_A/F_D - 1}\{1 - \exp[\beta(X_2 - X_1)]\} \tag{C2}$$

The coefficient β is the only negative root of Eqn. C3 and can be calculated analytically by Cardan's equation [30]:

$$z^3 - (P_D + P_A) z^2 + \left[P_D P_A - \Psi\left(\frac{v_A}{v_D} F_D P_D + F_A P_A\right)\right] z + \Psi P_D P_A \left(\frac{v_A}{v_D} F_D + F_A\right) = 0 \tag{C3}$$

where

$$\Psi = \left[\frac{v_A}{v_D} \gamma_D \left(\frac{a_D}{a_A} \frac{F_A}{K_A} + \frac{F_D}{K_D} + 4P_m \Delta \right) \right]^{-1} \quad \text{(C4)}$$

Once determined, β can be used for calculating the coefficient ω in Eqns. C1 and C2:

$$\omega = \frac{v_D \beta}{v_A F_A \Psi} \left(1 - \frac{\beta}{P_D} \right) + \frac{F_D}{F_A} \quad \text{(C5)}$$

REFERENCES

1 J. Ruzicka and E.H. Hansen, Flow Injection Analysis, Wiley, New York, 2nd edn., 1988.
2 M. Valcárcel and M.D. Luque de Castro, Flow-Injection Analysis. Principles and Applications, Horwood, Chichester, 1987.
3 E.H. Hansen and J. Ruzicka, Anal. Chim. Acta, 87 (1976) 353.
4 L. Gorton and L. Ögren, Anal. Chim. Acta, 130 (1981) 45.
5 J.F. van Staden and A. van Rensburg, Analyst, 115 (1990) 1049.
6 B. Bernhardsson, E. Martins and G. Johansson, Anal. Chim. Acta, 167 (1985) 111.
7 L. Risinger, G. Johansson and T. Thorneman, Anal. Chim. Acta, 224 (1989) 13.
8 I.C. van Nugteren-Osinga, M. Bos and W.E. van der Linden, Anal. Chim. Acta, 214 (1988) 77.
9 I.C. van Nugteren-Osinga, PhD Thesis, Twente University, Enschede, 1991.
10 O. Levenspiel and K.B. Bischoff, Adv. Chem. Eng., 4 (1963) 95.
11 C.Y. Wen and L.T. Fan, Models for Flow Systems and Chemical Reactors, Dekker, New York, 1968.
12 W.E. van der Linden, Anal. Chim. Acta, 151 (1983) 359.
13 J.M. Reijn, W.E. van der Linden and H. Poppe, Anal. Chim. Acta, 114 (1980) 105.
14 J.M. Reijn, W.E. van der Linden and H. Poppe, Anal. Chim. Acta, 126 (1981) 1.
15 S.D. Kolev and E. Pungor, Anal. Chem., 60 (1988) 1700.
16 S.D. Kolev and E. Pungor, Anal. Chim. Acta, 208 (1988) 117.
17 S.D. Kolev and E. Pungor, Anal. Chim. Acta, 208 (1988) 133.
18 G. Taylor, Proc. R. Soc. London, Ser. A, 219 (1953) 186.
19 G. Taylor, Proc. R. Soc. London, Ser. A, 225 (1954) 231.
20 S.D. Kolev and W.E. van der Linden, Anal. Chim. Acta, 247 (1991) 51.
21 S.D. Kolev and W.E. van der Linden, Anal. Chim. Acta, 257 (1992) 331.
22 S.D. Kolev and E. Pungor, Talanta, 34 (1987) 1009.
23 S.D. Kolev and E. Pungor, Anal. Chim. Acta, 194 (1987) 61.
24 S.D. Kolev, G. Nagy and E. Pungor, Anal. Chim. Acta, 241 (1990) 43.
25 B. Carnahan, H.A. Luther and J.O. Wilkes, Applied Numerical Methods, Wiley, New York, 1969.
26 J.A. Nelder and R. Mead, Comput. J., 7 (1964) 308.
27 E.Th. Van der Laan, Chem. Eng. Sci., 7 (1958) 187.
28 A.M. Suhotina (Ed.), Handbook of Electrochemistry, Khimiya, Leningrad, 1st edn., 1981.
29 S.D. Kolev and W.E. van der Linden, Anal. Chim. Acta, 256 (1992) 301.
30 G.A. Korn and T.M. Korn, Mathematical Handbook, McGraw-Hill, New York, 1968.

Analytica Chimica Acta, 268 (1992) 29–38
Elsevier Science Publishers B.V., Amsterdam

Spectrophotometric measurement of pH gradients in continuous-flow systems

S. Sagrado Vives, M.J. Medina Hernández, J.L. Martín Herrera and G. Ramis Ramos

Departament de Química Analítica, Facultat de Química, Universitat de València, 46100 Burjassot, València (Spain)

(Received 30th August 1991; revised manuscript received 24th April 1992)

Abstract

In the presence of an acid–base indicator and using fast diode-array spectrophotometric scans, pH gradients in the spectrophotometric cell can be measured at the same time as any other colorimetric flow-injection (FI) determination is performed. The effects of refractive index changes, adsorption–desorption processes at the tube walls and association of the indicator species with the system to be investigated are considered. Effective correction for the first two effects is demonstrated. Indicators with different molecular structures and polarities gave similar pH gradients, suggesting adequate accuracy for most potential applications. Application to the detection and correction of systematic and random errors in pH-sensitive FI procedures is demonstrated using the *o*-phthalaldehyde–*N*-acetyl-L-cysteine method for bovine serum albumin.

Keywords: Flow injection; UV–Visible spectrophotometry; Gradient scanning; pH; Tristimulus colorimetry

Routine pH measurements are usually performed potentiometrically with a glass electrode. Also, new types of pH sensors based on modified optical fibres (optrodes) and semiconductor devices have been developed [1,2]. Spectrophotometry in the presence of acid–base indicators is not a usual means of measuring pH values; however, under optimum conditions, it can be as precise as potentiometry [3]. Moreover, it can be very useful when other devices cannot be used, such as in inaccessible sampling sites or in corrosive environments.

In addition, electrodes and other devices that rely on the establishment of an equilibrium at a surface or through interfaces are also limited in speed; thus, for instance, they cannot accurately measure the rapid pH changes that are found in many flow-injection (FI) situations. Instead, indicator acid–base reactions in solution are fast enough to follow closely any FI pH gradient, and the pH in the cell can be measured at the same time as any other spectrophotometric assay is performed.

The use of the dispersion coefficient of a dye in the presence of an acid–base buffer has been proposed as an indirect means of measuring pH gradients in FI systems [4]. This approach assumed the identity of the dispersion coefficients of the species involved, measurements being limited to the front and back parts of the bolus where the dye and the buffer systems undergo dispersion. Application to the determination of the pK' values of coloured substances was demonstrated.

In this work, pH gradients in FI experiments were directly and continuously measured using an acid–base indicator added to both sample and carrier solutions. The pH values are determined on the basis of the spectral changes of the indicator system. The effects of refractive index changes, adsorption–desorption processes at the tube walls and association of the indicator species with those

Correspondence to: G. Ramis Ramos, Departament de Química Analítica, Facultat de Química, Universitat de València, 46100 Burjassot, València (Spain).

of the system to be investigated were considered, and effective correction of the two former effects is demonstrated. In addition, spectrophotometric monitoring of the pH throughout an FI experiment is proposed as a means of revealing systematic or accidental errors in determinations and of correcting the value of the analyte signals, thus improving the reliability and accuracy of pH-sensitive determinations.

Many pH-sensitive procedures have been reported for FI systems. Thus, for instance, the fluorimetric and spectrophotometric *o*-phthalaldehyde–2-mercaptoethanol (OPA–ME) procedure to determine ammonium ion has been adapted to the FI methodology [5]; however, the recommended carrier pH of 6.8 is critical as a signal vs. pH plateau does not exist. Consequently, to analyse acid samples routinely, small sample volumes or large dilution factors should be used. The use of large buffer concentrations is not advisable owing to the systematic errors introduced by changes in the refractive index at the sample/carrier interfaces. Many other analytical procedures exhibit a short optimum pH range and a large dependence of the sensitivity on the pH outside that range.

In this work, the pH gradients and the FI peaks for bovine serum albumin (BSA) after derivatization with OPA–*N*-acetyl-L-cysteine (NAC) reagent [6] were simultaneously measured. Throughout an FI peak, many spectra of the indicator and the derivatized BSA were acquired using a diode-array spectrophotometer, the pH gradient being calculated from the indicator spectra. Finally, to increase the precision of the pH measurements, and to facilitate immediate application to all substances that exhibit colour changes within the visible region, complementary tristimulus colorimetry [7] was applied.

THEORY

In the presence of an acid–base indicator, the pH of the medium can be related to the absorbance of the solution by means of the equation

$$\mathrm{pH} = \mathrm{p}K' + \log\frac{A_1 - A}{A - A_0} \qquad (1)$$

where A is the absorbance of the indicator at a given pH and concentration, A_1 and A_0 are the absorbances given by solutions of the acid and base conjugated forms of the indicator at the same concentration, respectively, and $\mathrm{p}K'$ is the protonation constant of the indicator. As absorbances are related to concentrations rather than to activities, a conditional constant should be used.

Instead of using single absorbances, A, A_1 and A_0 can be replaced with a linear combination of absorbances, taken at two or more than two wavelengths, $A(\lambda)$, $A_1(\lambda)$ and $A_0(\lambda)$. This permits a substantial improvement in the precision of a determination. Precision is optimized by increasing the difference $A_1 - A_0$, which can be necessary in some instances, e.g., when the sensing system would exhibit a small spectral change. However, in most practical situations the judicious selection of a pair of single wavelengths, or a pair of different weighted sums of wavelengths, will give satisfactory precision.

Complementary tristimulus [7] provides a suitable general-purpose combination of absorbances which should give good precision when a chemical indicator that shows a colour change within the visible region is used as the pH-sensing system. In complementary tristimulus colorimetry, weights given to the absorbance values account for the different sensitivities of the human eye in relation to the three primary colours. The resulting three functions, X_c, Y_c and Z_c, are generically represented by R_c. Equation 1 can be written using an R_c function:

$$\mathrm{pH} = \mathrm{p}K' + \log\frac{R_{c1} - R_c}{R_c - R_{c0}} \qquad (2)$$

It should be emphasized that the use of the tristimulus functions is not necessary; however, using these functions the same software package can be immediately applied to a large number of sensing substances traditionally used as visual acid–base indicators without selecting wavelengths and without changing the weights assigned to the wavelengths. In most instances, the spectrophotometric determination of organic substances, including many drugs, is performed in

the UV region and the use of a pH indicator giving colour changes in the visible region is desirable. In these instances, tristimulus functions have the advantage of being universally applicable. Obviously, other functions should be implemented when sensing substances exhibiting spectral changes in the UV region are used. As stated above with Eqns. 1 and 2, the theory which follows is developed comparatively, using both generic and tristimulus functions.

A drawback of Eqns. 1 and 2 is that A or R_c must be measured at the same concentration at which the spectra of the acid and basic conjugated forms of the indicator were measured. This is a problem in FI determinations where the indicator concentration can be changed unpredictably by adsorption–desorption processes at the tube walls. To overcome this difficulty, the two following approaches can be used. First, if calibration and measurements are also done at a second wavelength, or using a different linear combination of absorbances, B, the following expression can be deduced:

$$\mathrm{pH} = \mathrm{p}K' + \log\frac{A_1 - (A/B)B_1}{(A/B)B_0 - A_0} \qquad (3)$$

In Eqn. 3, the spectra of the sample can be taken using any concentration, independent of the concentration at which the values of A_0, A_1, B_0 and B_1 were obtained. Equation 3 can also be expressed using a pair of tristimuli, or even a linear combination of tristimuli. Thus, for instance, one can write

$$\mathrm{pH} = \mathrm{p}K' + \log\frac{X_{c1} - X_c[(Y_{c1} + Z_{c1})/(Y_c + Z_c)]}{X_c[(Y_{c0} + Z_{c0})/(Y_c + Z_c)] - X_{c0}} \qquad (4)$$

which can be also expressed in relative terms, using the complementary chromatic coordinates, Q_x, Q_y and Q_z (generically, Q_r) and the optical concentration parameter, J. The expression proposed by Flaschka [8] results:

$$\mathrm{pH} = \mathrm{p}K' + \log\frac{J_1(Q_{r1} - Q_r)}{J_0(Q_r - Q_{r0})} \qquad (5)$$

where $Q_r = R_c/(X_c + Y_c + Z_c)$ and $J = k(X_c + Y_c + Z_c)$, k being a constant.

Alternatively, the value of A at the calibration concentration can be written as a function of two absorbances taken at different wavelengths, or as a function of two different linear combinations of absorbances, A^* and B^*, which can be measured at any other concentration, the same or different of that used to obtain A:

$$A = A^*\left[\frac{(A_1B_0 - A_0B_1)}{A^*(B_0 - A_1) - B^*(A_1 - B_0)}\right] \qquad (6)$$

Analogously, using a pair of tristimuli, such as X_c^* and Y_c^*,

$$X_c = X_c^*\left[\frac{(X_{c1}Y_{c0} - X_{c0}Y_{c1})}{X_c^*(Y_{c0} - X_{c1}) - Y_c^*(X_{c1} - X_{c0})}\right] \qquad (7)$$

Equation 6 or 7 can be used in combination with Eqn. 1 or 2, respectively, to establish the pH of a solution using measurements taken at any indicator concentration. Moreover, Eqn. 6 or 7 can be used to find the relative variation of the indicator concentration, $f = A^*/A = X_c^*/X_c$, where the calibration concentration at which A or X_c were measured is taken as the reference value.

EXPERIMENTAL

Apparatus and reagents

A pH meter (MicropH 2000, Crison, Barcelona) and a diode-array spectrophotometer (Model 8452A, Hewlett-Packard, Palo Alto, CA) connected to a Vectra computer via an HPIB protocol (Hewlett-Packard) were used. The FI assembly was built using a peristaltic pump (Model Minipuls 3, Gilson, Middleton, WI), an injection valve (Model 5020, Rheodyne, Berkeley, CA), a 18-μl flow-cell (Model 178012-QS, Hellma, Mülheim/Baden) and 0.5 mm i.d. PTFE tubes. The coil reactor used to evaluate pH gradients was constructed using a 50-cm PTFE tube, and a coil reactor built up with a 150-cm tube, followed by a 100-cm single-bead string reactor (SBSR), was used in the experiments done in the presence of BSA.

The following stock solutions were prepared: 0.04% bromothymol blue (BTB) (Riedel, Hannover), thymol blue (TB) (Probus, Barcelona), phenol red (PR) (Probus) and neutral red (NR) (Adlershof, Berlin) in water; 5×10^{-2} M OPA (analytical reagent grade; Serva, Heidelberg) prepared weekly in ethanol and stored in the dark; 5×10^{-2} M aqueous NAC (> 99%; Fluka, Buchs) prepared weekly and stored in a refrigerator; 1.25×10^{-4} M BSA (for microbiology; Fluka) in water; 0.1 M phosphate buffer solution; and boric acid–borate buffer solution, prepared from 6.2 g of orthoboric acid and 15 g of NaOH in 1 l of water. The OPA–NAC–buffer reagent consisted of 30 ml of the OPA and NAC solutions and 5 ml of the boric acid–borate buffer diluted to 500 ml. Distilled, deionized water (Barnstead deionizer; Sybron, Boston, MA) was used throughout.

Software

Data acquisition and control of the spectrophotometer were performed by the Hewlett-Packard MS-DOS UV–VIS package. The program PHSENSOR, written in QuickBASIC, was designed to make direct use of the *.WAV and *.TIM files generated by the MS-DOS UV–VIS package. The program should be provided with the pK' value of the indicator, its nominal concentration (optional), the *.WAV spectra of the acid and base conjugated forms of the indicator taken at the same arbitrary calibration concentration from which the R_{c1}, R_{c0}, Q_{r1} and Q_{r0} parameters of the indicator are to be calculated and a *.TIM file containing a series of spectra measured at different time values and at any indicator concentration during a single FI injection. If an FI acid–base pseudo-titration is performed, the entire colour transition of the indicator will be obtained from the information provided by the *.TIM file.

The program uses absorbance values within the 380–770 nm range to calculate tristimulus, chromatic coordinates and the J parameter, in addition to pH values on the basis of Eqns. 2 and 7 or, optionally, of Eqn. 5. When the program default option is used, the Q_r chromatic coordinate showing the largest range of values is selected to apply Eqn. 5. Similarly, to apply Eqn. 7, the program selects the combination of the two tristimuli showing the largest reversed correlation (*i.e.*, the closest to a correlation coefficient $r = -1$). In both instances, the proposed choice should lead to the most precise pH values.

The ASCII output matrix can be formatted to contain times, pH values, X_c, Y_c and Z_c tristimuli, the relative variations of the indicator concentration, f, and absorbances at any given wavelength. The appropriate columns of this matrix file can be plotted using general-purpose plotting software.

Evaluation of pK' values

The pK' values of the indicators used were evaluated by continuously pumping 1×10^{-5} M BTB, PR, NR or TB solutions through the flow cell. The spectra of the acid and base forms of the indicators were measured by pumping solutions of the indicators containing 1×10^{-3} M HCl and NaOH, respectively. The spectra of series of indicator solutions containing 1×10^{-3} M phosphate buffer of pH 7.30 were also measured. From Eqns. 2 and 7, and Eqn. 5, pK'(BTB) = 7.32 ± 0.01, pK'(PR) = 8.02 ± 0.04 and pK'(NR) = 6.78 ± 0.04 (six measurements).

For TB in the OPA–NAC–boric acid–borate buffer medium, p$K' = 9.15$, but when the determination was made in the presence of 2.5×10^{-5} M BSA, p$K' = 7.7$ was obtained. The spectra of the TB acid and base conjugated forms also showed changes in the presence of BSA. These changes were observed to be pH dependent, i.e., bathochromic shifts produced by the presence of BSA were larger in weakly acidic or weak basic solutions than in more basic and more acidic media. Spectral changes together with the apparent higher acidity of TB suggested that, within some pH range, BSA is bound to the indicator, the interaction being stronger with the anionic basic TB species than with the non-ionic acidic species.

Evaluation of pH gradients

The pH gradient measuring procedure was studied by injecting 1×10^{-3} M HCl or NaOH solutions containing 1×10^{-5} M of each indicator on a carrier containing the same indicator con-

centration and 1×10^{-3} M phosphate buffer of pH 7.30. Other FI conditions were flow-rate 1 ml min^{-1}, sample volume 150 μl and number of spectra taken per injection 80 (one spectrum per second).

BSA determinations

A carrier containing the OPA–NAC–boric acid–borate buffer of pH 9.5 was used. Injected samples contained 2.5×10^{-5} M BSA at several pH values. All these solutions were made 1×10^{-5} M in TB. Other FI conditions were flow-rate 1.9 ml min^{-1}, sample volume 180 μl and number of spectra taken by injection 100 (one spectrum per second).

RESULTS AND DISCUSSION

Study of the pH gradient measuring procedure

The colour transitions produced when acidic and basic BTB solutions were injected on a buffered carrier solution of pH 7.25 are shown in Fig. 1 using a Z_c vs. Y_c plot. The corresponding [Y_c(pH), Z_c(pH)] straight line theoretical transition, between the (Y_{c0}, Z_{c0}) and (Y_{c1}, Z_{c1}) points, is also given in Fig. 1. The experimental points showed a curved colour transition, indicating the presence of background drift due to refractive index changes and, probably, changes in the indicator concentration. These undesirable effects have been described elsewhere [9,10], and were also observed with the other indicators used.

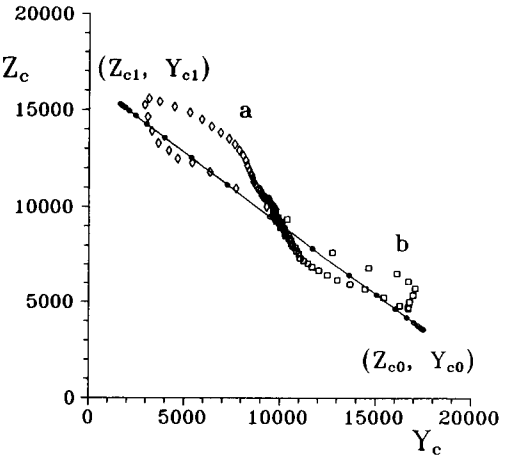

Fig. 1. Z_c vs. Y_c plot for BTB. ○ = Theoretical colour transition using points spaced every 0.25 pH units; ◇ = injection of an acidic solution into the buffered carrier of pH ≈ pK'; □ = injection of a basic solution into the same carrier.

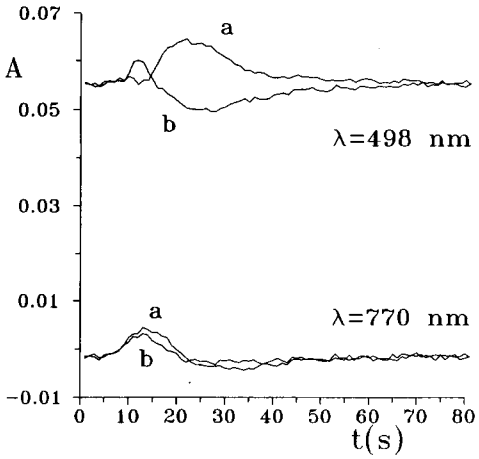

Fig. 2. Absorbance vs. time during the injection of (a) an acidic and (b) a basic sample. Absorbance was measured at 770 nm (baseline) and 498 nm (BTB isosbestic point).

Refractive index and concentration effects for BTB can be distinguished in Fig. 2, where the corresponding absorbances at two wavelengths, 770 and 498 nm, are plotted against time. The indicator did not absorb at 770 nm and, therefore, absorbance variations were attributed only to changes in refractive index. In addition, 498 nm is the isosbestic point of BTB and, consequently, absorbance changes at this wavelength were attributed to the sum of both refractive index and total indicator concentration changes.

It has been shown that the effects produced by refractive index changes are independent of wavelength, which makes the correction of refractive index changes possible by subtraction [11]. The corrected points, [$A(\lambda) - A(770)$, t], were used to calculate the (R_c^*, t) or (Q_r, t) data which are needed to establish the pH gradient using Eqns. 2 and 7, or Eqn. 5.

The pH gradients for the injections of acidic and basic solutions of BTB, calculated by means of Eqns. 2 and 7, and also Eqn. 5, using uncorrected [$A(\lambda)$, t] points, are given in Fig. 3. In the

absence of systematic error, the same series of (pH, t) points should be obtained. However, differences between the points obtained by the two methods can be observed in Fig. 3. These differences were higher when the injections were performed using more concentrated solutions. However, when the correction for refractive index changes was applied, Eqns. 2 and 7 and Eqn. 5 lead to exactly the same (pH, t) values.

Figure 4 shows the variation of the concentrations of several indicators in FI experiments, in which HCl or NaOH solutions containing an indicator at a given concentration were injected into a buffered carrier containing the same indicator concentration. These experiments were duplicated using independent solutions, the results being the same. After correction of the refractive index changes by subtraction, the relative variations of indicator concentration were calculated as $f = (R_c^*/R_c)$.

The indicators used here belong to different chemical families, and show large differences in hydrophobicity. Thus, BTB and PR are triphenylmethane derivatives, with two phenolic groups and a similar structure; however, the hydrophobicity is much larger for the non-ionic acid form of BTB than for the corresponding form of PR, owing to the additional bromine, methyl and isopropyl groups. In addition, BTB and PR have anionic base forms, whereas NR is a diphenyldiazine derivative with a protonated amino group as the cationic acid form.

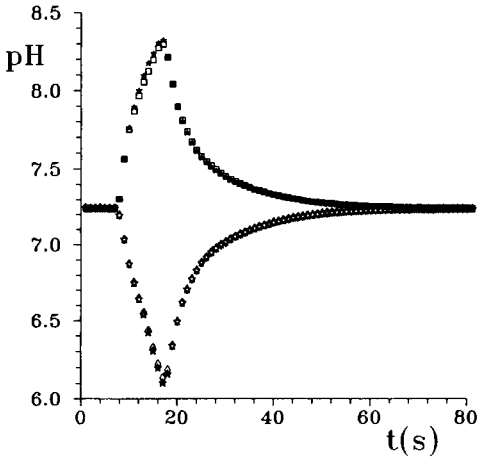

Fig. 3. Calculated pH gradients during the injection of acidic and basic samples. ◇, □ = Eqn. 5; ☆, ★ = Eqns. 2 and 7.

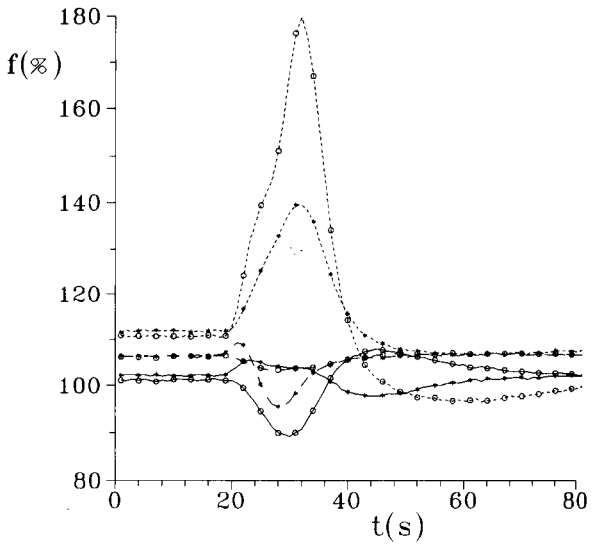

Fig. 4. Relative variation of the BTB (———), PR (— — —) and NR (- - - - -) concentration, $(R_c^*/R_c)\times 100 = f(\%)$, during the injection of (○) an acidic and (∗) a basic sample into a buffered carrier. All solutions contained the same indicator concentration.

When the basic BTB and PR solutions were injected, the indicator concentration increased at the bolus front and decreased at the back. The opposite behaviour was observed when the acidic BTB and PR solutions were injected. This can be rationalized in terms of the adsorption–desorption processes at the tube walls. It seems reasonable to assume that the non-ionic acidic forms of the indicators are more strongly adsorbed on the non-polar PTFE tube walls than the anionic basic forms [6]. Both conjugated forms of the indicators are present in significant concentrations at the pH of the carrier, which is close to the pK' values; therefore, any change in pH lead to large variations in the concentrations of the two species. When an acidic solution is injected, an increase in the concentration of the acid form leads to an increase of the amount of adsorbed indicator, and the indicator concentration in solution decreases. When the pH returns to its former carrier value, the indicator excess is desorbed and its

concentration in solution increases. The opposite can be argued for an injection of basic solution.

Rapid and small pH changes (less than 1 pH unit) should be enough to produce these reversible processes. In comparison with the PR, the larger adsorption–desorption effects observed in Fig. 4 for BTB can be attributed to the higher hydrophobicity of its acid form. Other differences between the BTB and PR curves can be attributed to the higher pK' value of PR. Differential migration effects through the liquid–liquid bolus/carrier interfaces could also be produced, probably being much smaller than the adsorption–desorption effects.

Concerning NR, the large concentration increase initially produced by the injection of acidic solution can be attributed to protonation of the amino group producing desorption. Adsorption of the indicator to restore equilibrium can explain the lower concentration observed after the bolus. No explanation was found for the concentration increase produced by the basic injection, which suggests that desorption is also produced. However, the use of Eqns. 2 and 7 or Eqn. 5 should filter out all concentration variations in the calculation of pH gradients.

Accuracy of the pH gradient measuring procedure

Finally, to establish an adequate procedure to evaluate the accuracy of the pH gradients obtained is not a simple matter. However, a comparison of the results obtained with different indicators can be an indirect means of evaluating the accuracy of the pH measurements. Such a comparison relies on the different physical and chemical behaviours of the indicators and, therefore, indicators of different chemical families, or with large differences in hydrophobicity, as occurs with BTB, PR and NR, should be used.

A comparison of results obtained with the three indicators is shown in Fig. 5. The pH gradients were obtained by injecting HCl and NaOH solutions into a buffered carrier, all solutions containing the same indicator system. Differences within the optimum sensing region of $pH = pK' \pm 1$ were below 0.2 pH units, which indicates the absence of large systematic errors. The accuracy

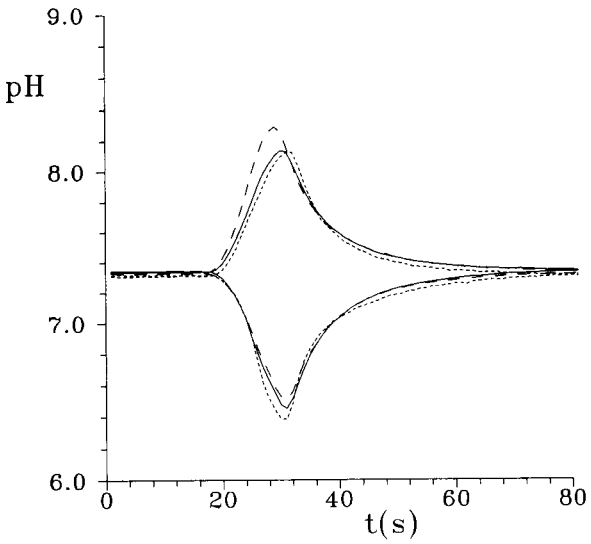

Fig. 5. pH gradients obtained with BTB (———), PR (— — —) and NR (- - - - -) by injecting HCl (pH decreases) and NaOH (pH increases) solutions into a buffered carrier.

of the pH gradients obtained should rely on both accurate calibration of the pK' and absorbance functions of the conjugated forms of the indicator and effective correction of refractive index changes and adsorption–desorption effects.

Application to the improvement of the reliability and accuracy of BSA determination

As shown above, BSA produces changes in the TB spectral and acid–base characteristics and, therefore, calibration of the TB parameters under the same experimental conditions at which the BSA determination is to be performed is not possible. An appropriate BSA calibration concentration does not exist for the following two reasons. First, the BSA concentration decreases as longitudinal mixing and diffusion progress along the FI experiment and, consequently, continuous-flow or batch experiments cannot adequately reproduce the FI injection conditions. Second, the BSA concentration will obviously change when different BSA standards and samples are used.

Calibration of TB parameters at two extreme situations was tried, i.e., absence of BSA and maximum BSA concentration to be used for the calibration graph. The TB calibration spectra and pK' values obtained in an OPA–NAC–boric acid–borate buffer medium in the absence of BSA and with 2.5×10^{-5} M BSA were used to calculate the pH gradients during a series of injections of 2.5×10^{-5} M BSA samples containing different amounts of HCl and NaOH. Injections were made into the OPA–NAC–boric acid–borate carrier of pH 9.5. The resulting derivatized BSA peaks, measured at the wavelength of maximum absorbance (336 nm), together with the corresponding pH gradients, are shown in Fig. 6. As can be observed in Fig. 6 (upper part), small changes in the pH gradient produced large changes in the height and shape of the derivatized BSA peaks.

The differences between the pH gradients calculated using both calibration conditions (middle and lower parts of Fig. 6) obey two independent factors: first, the different calibration pK' values which cause a shift of the ordinate scale, and second, the differences in the absorbance calibration functions used, which are due to the changes in the spectra of the indicator acid and base forms, and which determine the different shapes of the pH gradient curves.

Owing to the presence of different BSA concentrations, the pH gradients calculated using any set of calibration parameters are not accurate; however, both the middle and lower parts of Fig. 6 show sets of well separated (pH, t) curves, which suggests that both can be reliably used for qualitative purposes, to reveal an accidental change in the pH of a BSA sample. In addition, quantitative correction of systematic or accidental errors of the BSA concentration due to pH

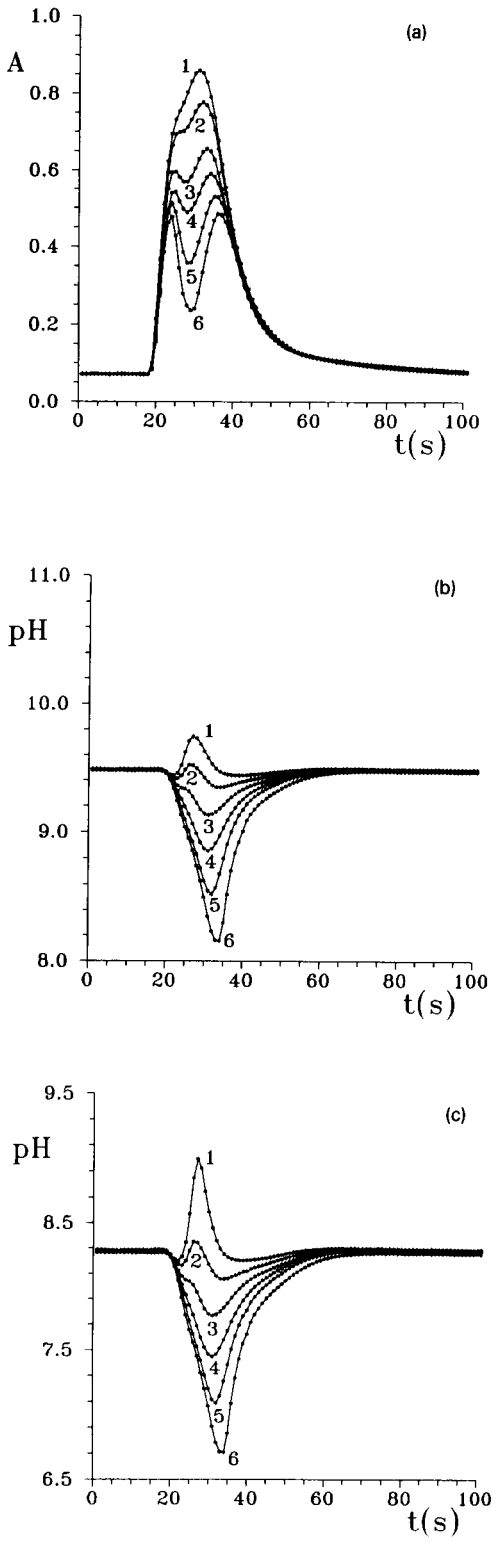

Fig. 6. Absorbance and pH gradients for injections of BSA solutions having various pH values into an OPA–NAC–boric acid–borate buffer carrier of pH 9.5. Samples were prepared in (1) 1×10^{-3} M NaOH, (2) 6×10^{-4} M NaOH, (3) water, (4) 2×10^{-5} M HCl, (5) 4×10^{-5} M HCl and (6) 6×10^{-5} M HCl. The pH gradients were calculated using the TB calibration parameters obtained in the absence of BSA (middle part) and in a 2.5×10^{-5} M BSA solution (lower part).

changes can be performed by applying second-order modelling of the BSA sensitivity–pH dependence. The proposed model is

$$A_c = \frac{A_e}{1 - k_1 S_{pH} - k_2 S_{pH}^2} \quad (8)$$

where A_c and A_e are corrected and experimental (uncorrected) functions of the absorbances at the BSA peak, respectively, S_{pH} is a function of the pH and k_1 and k_2 are constants. To establish k_1 and k_2 by linear least-squares, Eqn. 8 is rearranged as follows:

$$\frac{A_r - A_{e,i}}{A_r S_{pH,i}} = k_1 + k_2 S_{pH,i} \quad (9)$$

where an "optimum" or reference value of the signal, A_r, has been written instead of the corrected signal, A_c, and where $(A_{e,i}, S_{pH,i})$ represents the signal and the respective value of the pH function of the ith calibration standard.

Modelling using Eqns. 8 and 9 can be applied using absorbances and pH values measured at a given time (e.g., the time at which maximum absorbance of the reference solution is obtained) for the A and S_{pH} functions, respectively. The problem of choosing an adequate time value is avoided by using $A \times t$ and $pH \times t$ areas.

The latter approach was used to model the series of experiments in Fig. 6. The area between the $A(t)$ curve for injection 1 and the baseline was used as the reference value, A_r. Analogously, the $A \times t$ areas of the other curves were measured to provide the $A_{e,i}$ calibration values. The corresponding $S_{pH,i}$ values were obtained as the areas measured between the pH gradient curve of injection 1 (reference) and the other pH gradient curves. Using the TB calibration parameters obtained in the absence of BSA, the values $k_1 = 3.49 \times 10^{-2}$ and $k_2 = -6.5 \times 10^{-4}$ were calculated. In addition, using the TB parameters obtained in the presence of BSA, $k_1 = 1.77 \times 10^{-2}$ and $k_2 = -3.9 \times 10^{-5}$ were obtained.

The errors obtained by using these constants and Eqn. 8 to correct the BSA concentrations for the same series of injections, together with the errors obtained by using the corresponding "uncorrected" values of the signal, $A_{e,i}$, are plotted against S_{pH} in Fig. 7. It can be deduced that, independently of the experimental conditions used to obtain the TB parameters, application of the model permits satisfactory correction of the BSA concentrations, giving rise to average errors of about 1.5%.

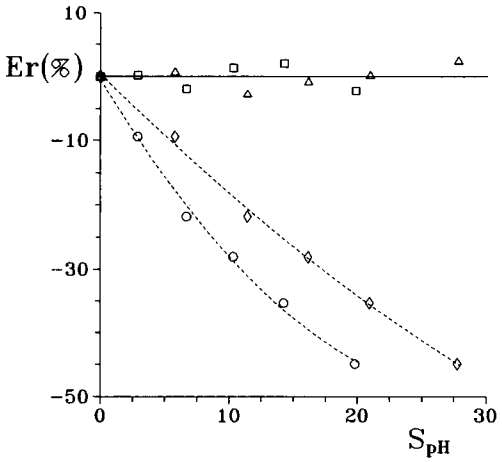

Fig. 7. Relative errors obtained for the series of injections in Fig. 6. Errors were calculated as (○, ◇) $100(A_r - A_e)/A_r$ and (□, △) $100(A_r - A_c)/A_r$ for the uncorrected and corrected values, respectively. Corrections were performed using TB calibration parameters obtained in an OPA–NAC–buffer solution in (○, □) the absence and (◇, △) the presence of 2.5×10^{-5} M BSA.

Conclusions

The FI gradient scanning technique described here permits effective monitoring of the pH inside the spectrophotometric cell at the same time as an FI determination is performed. The procedure is rapid and simple and gives reproducible results. Applications in detecting unexpected pH changes and in correcting the analyte signal, improving the reliability and accuracy of pH-sensitive determinations, have been demonstrated.

Accurate pH values can be obtained only within the range of 2–3 pH units where the indicator exhibits its spectral change; however, samples giving pH values outside the optimum sensing range can be reliably detected as outliers. A limitation is posed by the need to avoid chemical reaction between the species of the selected indicator and those of the sensed system; how-

ever, as it has been shown, this can be tolerated in some extent and, even in these instances, the analyte signal correction procedure proposed here can be applied successfully.

This work was partially supported by the CICYT, Project DEP89/429/C2.

REFERENCES

1 J. Janata and A. Bezegh, Anal. Chem., 60 (1988) 62R.
2 J. Janata, Anal. Chem., 62 (1990) 33R.
3 R.G. Bates, Determination of pH, Wiley, New York, 1973.
4 R.S. Vithanage and P.K. Dasgupta, Anal. Chem., 58 (1986) 326.
5 S.S. Goyal, D.W. Rains and R.C. Huffaker, Anal. Chem., 60 (1988) 175.
6 M.C. García Alvarez-Coque, M.J. Medina Hernández, R.M. Villanueva Camañas and C. Mongay Fernández, Anal. Biochem., 180 (1989) 172.
7 C.N. Reilley, H.A. Flaschka, S. Laurent and B. Laurent, Anal. Chem., 32 (1960) 1218.
8 H. Flaschka, Talanta, 8 (1961) 342.
9 B.A. Woods, J. Ruzicka and G.D. Christian, Anal. Chem., 59 (1987) 2767.
10 S. Sagrado Vives, M.J. Medina Hernández, J.L. Martín Herrera and G. Ramis Ramos, Anal. Chim. Acta, 252 (1991) 133.
11 E.A.G. Zagatto, M.A.Z. Arruda, A.O. Jacintho and I.L. Mattos, Anal. Chim. Acta, 234 (1990) 153.

Analytica Chimica Acta, 268 (1992) 39–47
Elsevier Science Publishers B.V., Amsterdam

Chiral recognition and enantiomeric separation of alanine β-naphthylamide by cyclodextrins

Yuko Yamashoji, Takahiro Ariga, Satoshi Asano and Minoru Tanaka

Department of Applied Chemistry, Faculty of Engineering, Osaka University, Yamada-oka, Suita, Osaka 565 (Japan)

(Received 13th March 1992; revised manuscript received 5th May 1992)

Abstract

The host–guest interaction of chemically unmodified and modified (methylated and acetylated) cyclodextrins (CDs) with alanine β-naphthylamide was studied by ^{1}H NMR spectrometry. The inclusion complex formation of the guest with CDs, except for α-CD, was evaluated on the basis of remarkable changes in their chemical shifts. The chiral recognition of DL-alanine β-naphthylamide by CDs was confirmed from duplication of its proton resonances. The enantiomeric separation ability of CDs was also investigated by capillary zone electrophoresis. Diacetylated β-CD and unmodified β- and γ-CDs exhibited high enantioselectivities. Moreover, the chemical modification produced a reverse in the migration order of the enantiomers.

Keywords: Electrophoresis; Nuclear magnetic resonance spectrometry; Alanine β-naphthylamide; Chiral recognition; Cyclodextrins; Enantiomeric separation

Cyclodextrins (CDs) have attracted much attention in various fields and have been increasingly used for enzyme models, drug and food formulations, separations and many other applications [1,2]. The functions of CDs are derived from the well known ability of CDs to encapsulate a variety of guest molecules into their hydrophobic cavities. Both primary and secondary hydroxyl groups crowning the narrower and wider rims of CDs, respectively, are considered to play an important role in the formation and stabilization of their inclusion complexes. Chemical modifications of CDs with various functional groups [3] have been extensively investigated to improve the complexing and catalytic abilities of CDs. It is well known that the chemical modifications of CDs bring about changes in the shape and size of their cavities, in hydrogen-bonding ability and in other physical properties. Recently, it was reported that the chemical modifications of β-CD result in enantioselectivity changes in separating racemates by liquid chromatography on a CD stationary phase [4] and by capillary zone electrophoresis (CZE) using CDs as chiral additives [5].

NMR spectrometry has widely been used to study the formation of CD inclusion complexes. In a previous paper [6], host–guest interactions of α-, β- and γ-CDs with DL- and L-alanine β-naphthylamide and distinct chiral recognition by β-CD in aqueous solution were briefly described. The number of applications of CZE has increased because of its rapid run time, high separation efficiencies, high levels of automation and low sample requirements. Unmodified and modified CDs have been successfully used as chiral additives in CZE [7–11]. CZE is also useful for estimating host–guest interactions.

Correspondence to: M. Tanaka, Department of Applied Chemistry, Faculty of Engineering, Osaka University, Yamada-oka, Suita, Osaka 565 (Japan).

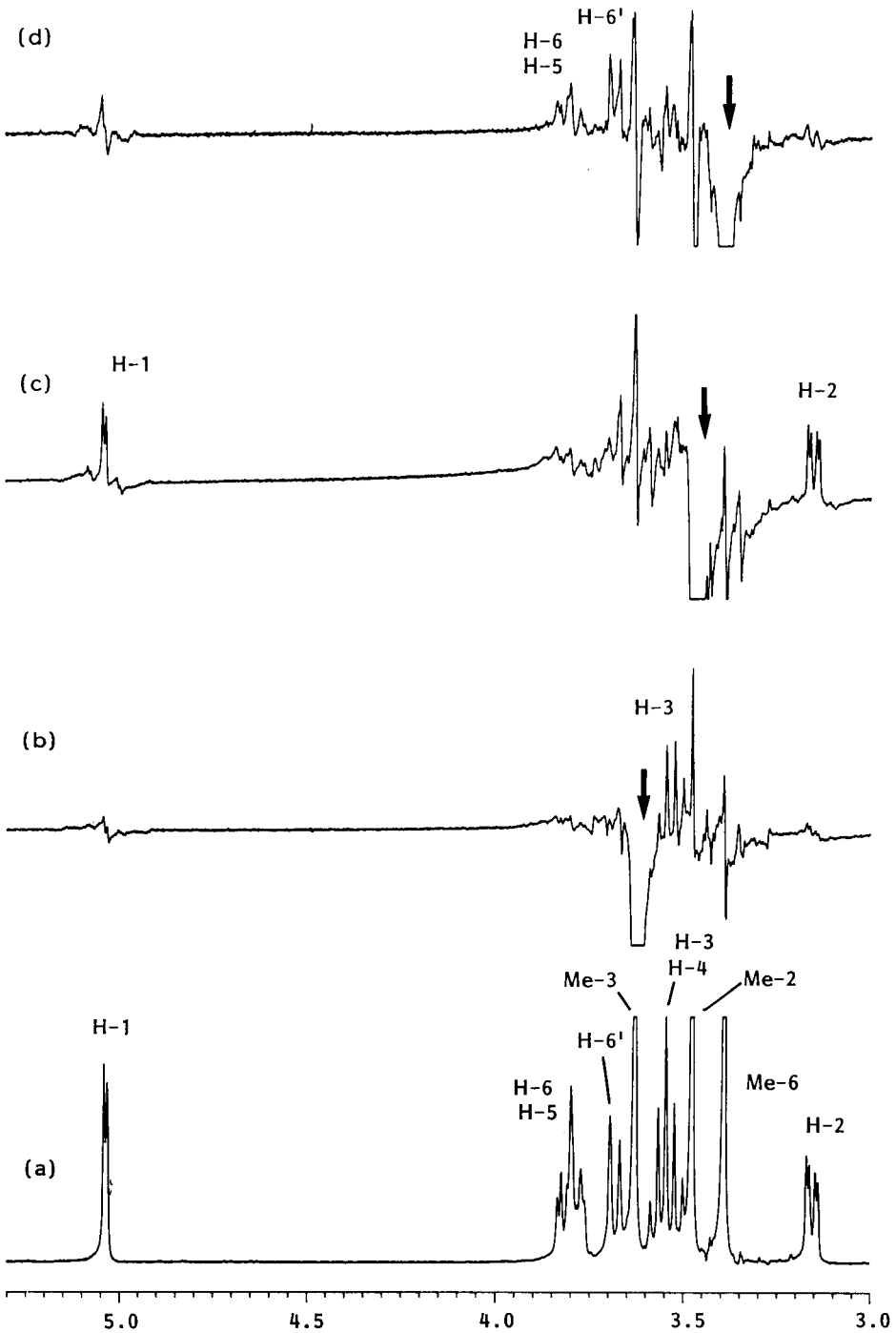

Fig. 1. ^{1}H NMR spectra of TM-α-CD in $CDCl_3$, (a) not irradiated, and irradiated at (b) 3.63, (c) 3.47 and (d) 3.39 ppm.

In this paper, host–guest interactions of chemically modified CDs (methylated and acetylated derivatives) with DL- and L-alanine β-naphthylamide by means of ^{1}H NMR in comparison with those of the unmodified CDs, and also enantiomeric separation of the guest by CZE in the presence of CDs as chiral additives are reported.

EXPERIMENTAL

Materials

Unmodified CDs (α-, β- and γ-CDs) were obtained from Wako (Osaka) and purified prior to use by repeated recrystallization from water. Hexakis(2,6-di-*O*-methyl)-α-CD (DM-α-CD), heptakis(2,6-di-*O*-methyl)-β-CD (DM-β-CD), hexakis(2,3,6-tri-*O*-methyl)-α-CD (TM-α-CD) and heptakis(2,3,6-tri-*O*-methyl)-β-CD (TM-β-CD) were prepared by well known methods [12,13]. Heptakis(2,3-di-*O*-acetyl)-β-CD (DA-β-CD) was also synthesized according to the literature [14]. DL-Alanine β-naphthylamide hydrochloride (DL-AN) and L-alanine β-naphthylamide hydrobromide (L-AN) were purchased from Sigma (St. Louis, MO) and used as received. D_2O (99.75%), NaOD (99%) and D_3PO_4 (99%) were obtained from Aldrich (Milwaukee, WI).

^{1}H NMR measurements

^{1}H NMR spectra were measured on a Bruker AM-600 spectrometer (600 MHz, Osaka University) at 25°C. ^{1}H chemical shifts (ppm) were determined relative to an external standard of sodium 2,3-dimethyl-2-silapentane-5-sulphonate (DSS) with an accuracy of ±0.0012 ppm. Concentrations of CDs and guest compounds were 2.0×10^{-3} M in D_3PO_4–NaOD buffer at pD 6.0 (ionic strength 0.05).

Determination of binding constants between L-AN and CDs

Fluorescence spectra were obtained with a Shimadzu RF-5000 spectrofluorimeter by excitation at 285 nm. Binding constants for the formation of 1:1 complexes between L-AN and CDs were determined using fluorescence intensity changes at 347 nm after addition of CDs. All measurements were made in 0.1 M sodium phosphate (pH 4.0). The concentration of L-AN was held constant at 1.0×10^{-6} M and the concentrations of CDs were varied in the range 5.0×10^{-5}–4.0×10^{-3} M. The data were treated on the basis of the Benesi–Hildebrand relationship [15].

CZE separation

An Applied Biosystems (Foster City, CA) Model 270A CZE system was used with a 50 μm i.d. × 72 cm (50 cm from inlet to detector) fused-silica capillary. On-column UV detection was at 220 nm. The temperature and applied voltage were held constant at 30°C and 30 kV, respectively, unless specified otherwise. Sample solutions (0.2 mM) were injected by the vacuum technique (5 inHg pressure difference for 0.5 s) after introducing methanol as a neutral marker to estimate the osmotic flow. Before each run, the capillary was rinsed successively with 1 M NaOH and separation buffer (0.05 M phosphoric acid–0.05 M NaOH, pH 2.0). Electropherograms were recorded with a Hitachi D-2500 Chromato-integrator.

RESULTS AND DISCUSSION

Proton resonance assignments for CDs and AN

Proton resonances of CDs and DL-AN in D_2O at pD 6.0 were assigned by ^{1}H–^{1}H homonuclear shift correlated spectroscopy (COSY) and *J* coupling resolved spectroscopy (2DJ). The assignments of the methoxy proton resonances of TM-α-CD were made by a nuclear Overhauser effect experiment. In this case, $CDCl_3$ was used as the solvent, because a distinct nuclear Overhauser effect was not observed in D_2O. Figure 1a shows a ^{1}H NMR spectrum of TM-α-CD in $CDCl_3$; chemical shifts (ppm): H-1 5.04, H-2 3.15, H-3 3.52, H-4 3.56, H-5 3.78, H-6 3.81, H-6′ 3.68; coupling constants (Hz): $J_{1-2} = 3.3$, $J_{2-3} = 9.5$, $J_{3-4} = 8.9$, $J_{4-5} = 9.3$, $J_{5-6} = 4.1$, $J_{5-6'} = 1.2$, $J_{6-6'} = 10.2$. In addition, three resonances due to the methoxy protons appeared at 3.63, 3.47 and 3.39 ppm. Signal enhancement of the H-3 proton was observed on irradiation of the methoxy protons at

3.63 ppm, as shown in Fig. 1b. This induced enhancement is ascribed to the energy transfer from the irradiated protons to the neighbouring protons located a short distance away via a dipole–dipole interaction. Therefore, the resonance at 3.63 ppm must originate from the methoxy group on C-3, i.e., Me-3. Similarly, irradiation of the 3.47 ppm signal induced enhancement of the H-2 and H-1 resonances (Fig. 1c), and irradiation of the 3.39 ppm signal enhanced the H-5, H-6 and H-6′ resonances (Fig. 1d). The assignments of the three methoxy resonances are in good agreement with those obtained by proton decoupled ^{13}C NMR measurements reported by Johnson et al. [16]. The assigned chemical shifts and coupling constants for CDs in D_2O are listed in Table 1 and those for DL-AN in Table 2.

Induced chemical shift changes caused by inclusion

Addition of α-CD to a D_2O solution of DL- or L-AN hardly affected the ^1H chemical shifts for the host or for the guest. On the other hand, when TM-α-CD, β-CD, TM-β-CD, DA-β-CD or γ-CD was added to a D_2O solution of L-AN, characteristic chemical shift changes were induced for both CD and L-AN, indicating the formation of inclusion complexes. In several subsequent figures, these chemical shift changes are plotted as a function of CD: L-AN molar ratio, where each CD was added to a fixed concentration of 0.04 M L-AN.

TABLE 1

Chemical shifts and coupling constants for CDs in D_2O

	TM-α-CD	β-CD	TM-β-CD	DA-β-CD	γ-CD
	Chemical shift (ppm)				
H-1	5.21	5.03	5.28	5.24	5.07
H-2	3.31	3.62	3.34	4.91	3.62
H-3	3.73	3.93	3.74	5.34	3.89
H-4	3.71	3.55	3.85	3.98	3.55
H-5	3.84	3.82	3.85	3.96	3.82
H-6	3.86	3.86	3.84	3.99	3.84
H-6′	3.71	3.84	3.64	3.91	3.83
Me-2	3.51		3.50		
Me-3	3.62		3.59		
Me-6	3.40		3.37		
CH_3CO				2.13	
CH_3CO				2.14	
	Coupling constant (Hz)				
J_{1-2}	3.4	3.8	3.6	3.6	3.8
J_{2-3}	9.8	10.1	9.5	9.8	10.0
J_{3-4}	8.9	9.0	8.5	8.7	9.1
J_{4-5}	9.6	9.2	8.3	8.9	9.2
$J_{6-6'}$	10.4	12.0	10.3	11.7	12.9

On addition of TM-α-CD to the guest, large upfield shifts were induced for its H-3 and Me-2 proton resonances, as seen in Fig. 2a. This is ascribed to the ring-current effect of the naphthyl group of the guest included in the host cavity. No upfield shift was observed for the H-5 proton, which is also located inside the cavity. This result strongly reflects shallow penetration of the naphthyl group of L-AN into the TM-α-CD cavity from the secondary hydroxyl side.

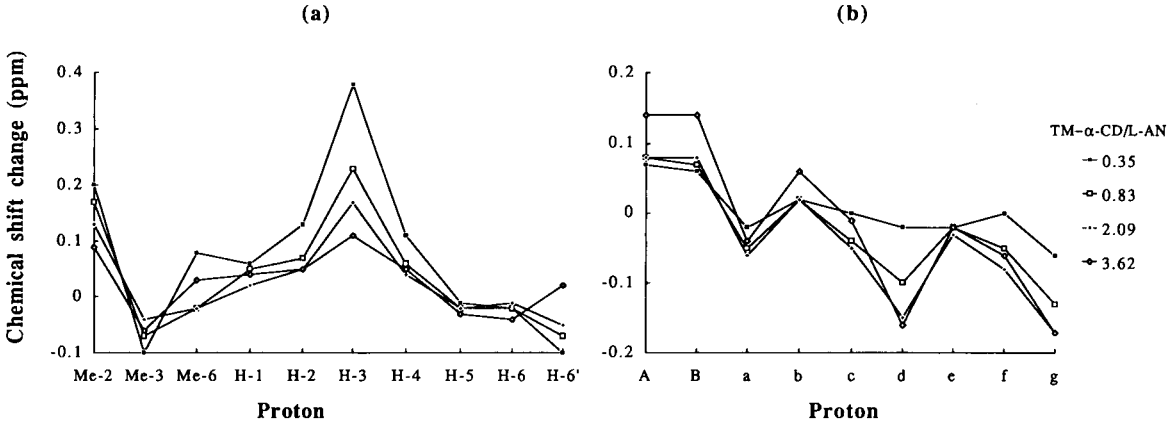

Fig. 2. ^1H chemical shift changes for (a) TM-α-CD and (b) L-AN on complexation. [TM-α-CD]:[L-AN]: ■ = 0.35; □ = 0.83, ● = 2.09; ◇ = 3.62.

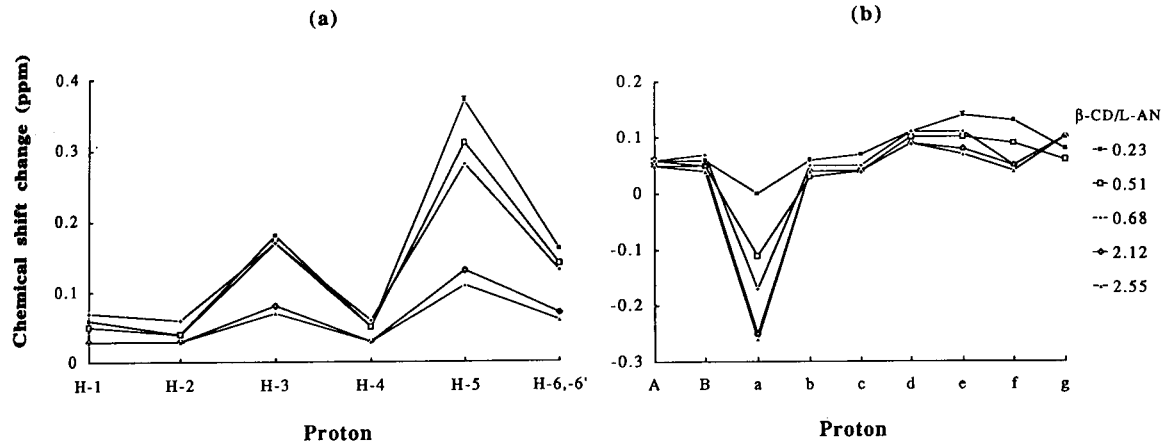

Fig. 3. ^{1}H chemical shift changes for (a) β-CD and (b) L-AN on complexation. [β-CD]:[L-AN]: ■ = 0.23; □ = 0.51; ● = 0.68, ◇ = 2.12; ▲ = 2.55.

Figure 3a shows large upfield shifts of both H-3 and H-5 proton resonances for β-CD, especially large for the latter. This reflects deep penetration of the naphthyl group of L-AN into the β-CD cavity. A large downfield shift of the H-a proton of L-AN was observed on addition of β-CD (Fig. 3b). With TM-α-CD, the H-a proton did not exhibit such a large downfield shift. This large downfield shift may come from a conformational change of L-AN due to deep penetration of its naphthyl moiety into the β-CD cavity, i.e., the H-a proton experiences a stronger unshielding effect by the carbonyl group in the guest itself after complexation. In order to explain this more convincingly, further work is needed.

The addition of TM-β-CD to L-AN resulted in smaller upfield shifts of all the protons except for H-4 of the host, and in a smaller downfield shift of H-a, compared with the β-CD addition in a nearly comparable amount. This suggests a weaker interaction of L-AN with TM-β-CD than with β-CD.

On addition of DA-β-CD, an upfield shift of H-3 was not observed, whereas large upfield shifts

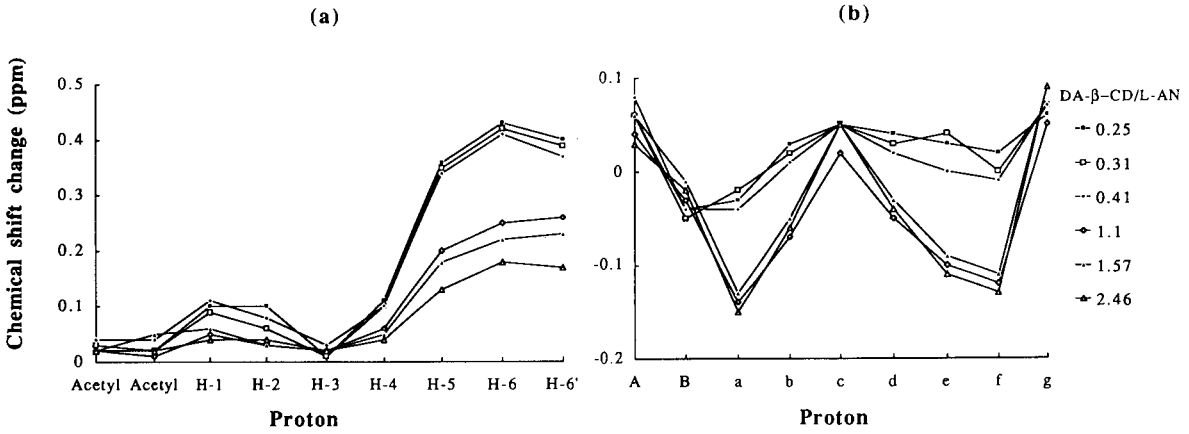

Fig. 4. ^{1}H chemical shift changes for (a) DA-β-CD and (b) L-AN on complexation. [DA-β-CD]:[L-AN]: ■ = 0.25; □ = 0.31; ● = 0.44; ◇ = 1.1; ▲ = 1.57; △ = 2.46.

were induced for the H-5, H-6 and H-6′ proton resonances (Fig. 4a). Downfield shifts of the H-e and H-f proton resonances and also the H-a resonance for the guest were observed (Fig. 4b). These results strongly suggest that L-AN penetrates shallowly into the narrower side of the DA-β-CD cavity, which is interesting. A typical ^{1}H NMR spectrum for the mixture of DA-β-CD and L-AN is shown in Fig. 5.

As shown in Fig. 6a, the induced shift pattern of the γ-CD proton resonances is similar to that of the β-CD proton resonances: the H-3 and H-5 protons located inside the cavity exhibit large upfield shifts. On the other hand, the induced shift pattern of L-AN observed after addition of γ-CD (Fig. 6b) is different from that after the addition of the other CDs. The addition of γ-CD caused larger upfield shifts of all the naphthyl proton resonances. The extents of the induced upfield shifts are larger at a [γ-CD]:[L-AN] molar ratio of 0.68 than those at a ratio of 1.67. This cannot be explained convincingly on the basis of exclusive formation of a 1:1 host–guest complex. It is suggested that those protons are strongly affected by a ring-current effect provided by the guest if two guest molecules are incorporated into the γ-CD cavity. Moreover, in the case of only 1:1 complex formation, the induced shifts are expected to increase with increasing [host]:[guest] ratio, as observed with the other CDs (Figs. 2b–4b).

In Fig. 7, for illustration, rough sketches of the

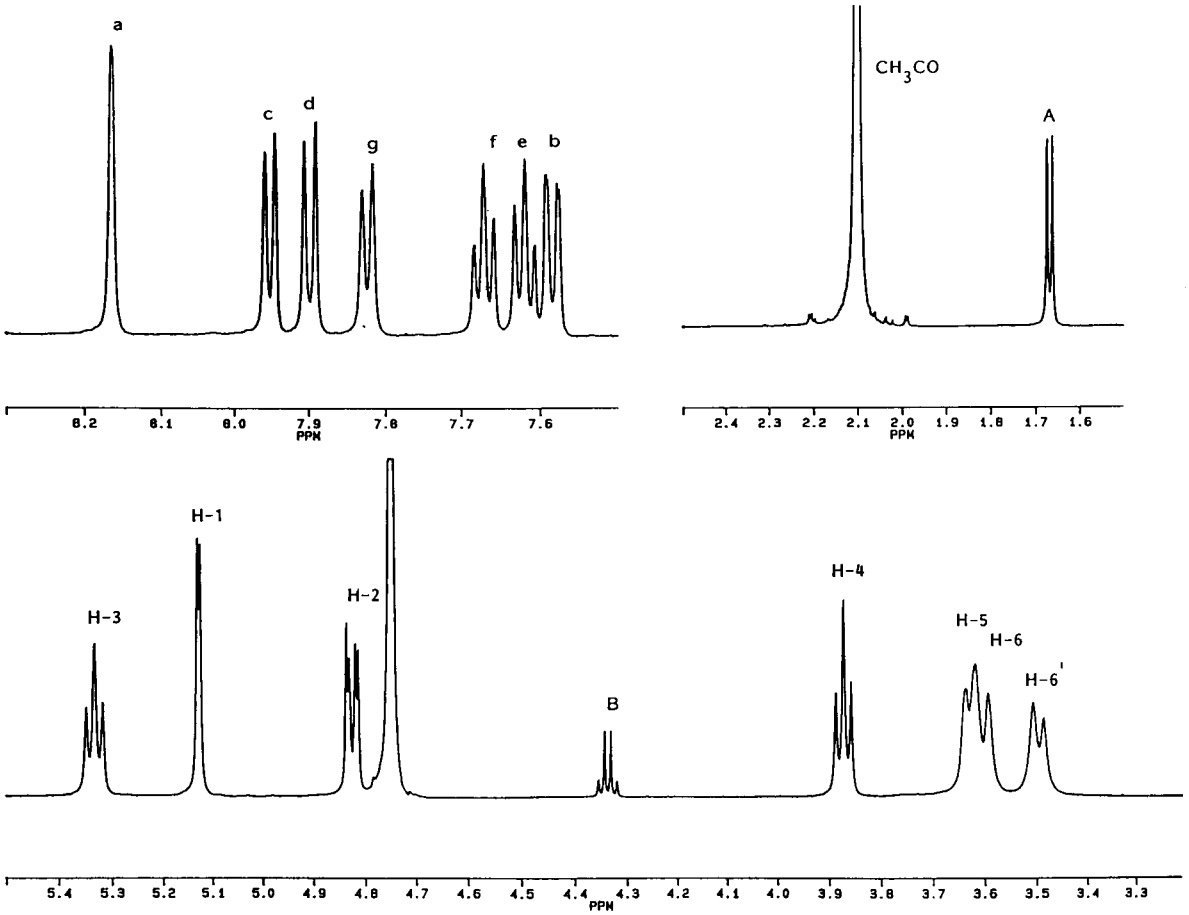

Fig. 5. ^{1}H NMR spectrum for a mixture of DA-β-CD and L-AN in D_2O ([DA-β-CD]:[L-AN] molar ratio = 0.7).

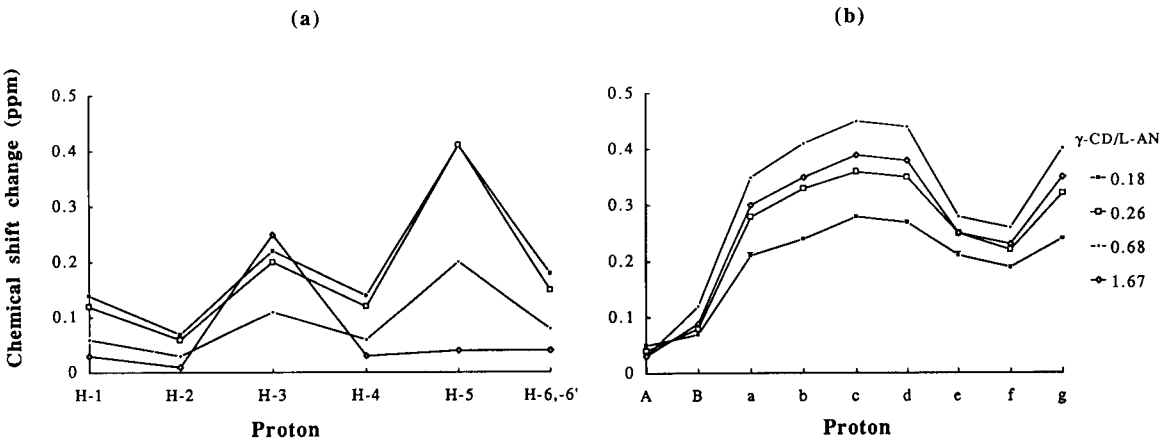

Fig. 6. ^{1}H chemical shift changes for (a) γ-CD and (b) L-AN on complexation. [γ-CD]:[L-AN]: ■ = 0.18; □ = 0.26; ● = 0.68; ◇ = 1.67.

host–guest complexes on the basis of the NMR results obtained are given for TM-α-CD, β-CD and DA-β-CD.

Chiral recognition and enantiomeric separation by CDs

The addition of unmodified, DM- or DA-β-CD to a solution of DL-AN brought about duplication of the proton resonances of the guest. The separations for H-a and H-B are given in Table 3, together with the [CD]:[DL-AN] molar ratio. Apparently, DA-β-CD or β-CD induced a relatively large separation for H-a, and DA-β-CD also for H-B. This indicates the strong chiral recognition of both the CDs, and the tighter fitting of the guest into the DA-β-CD cavity than the β-CD

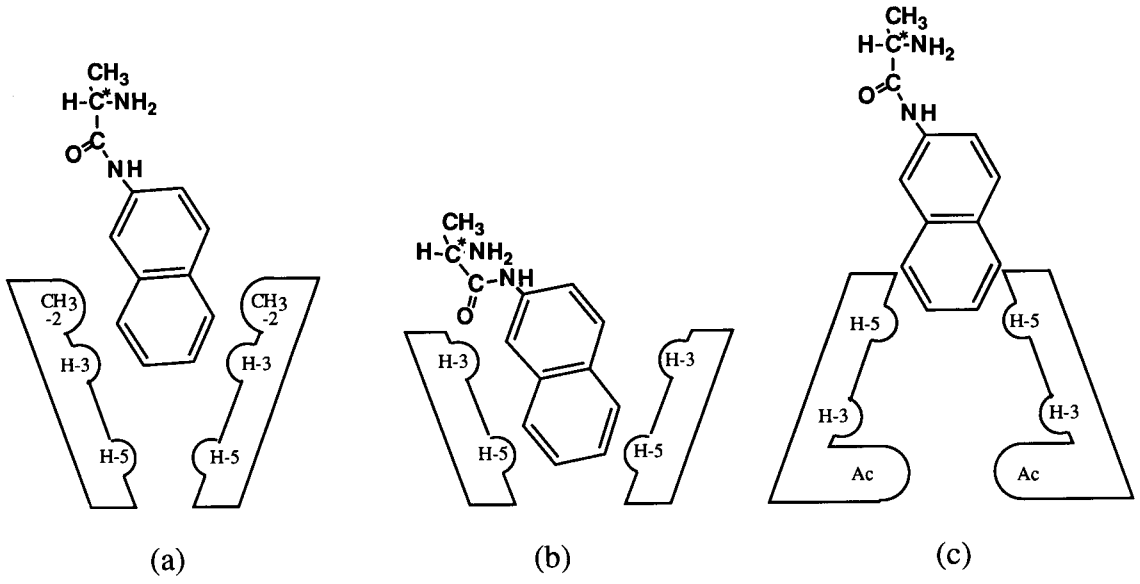

Fig. 7. Schematic illustrations of AN complexes with (a) TM-α-CD, (b) β-CD and (c) DA-β-CD.

TABLE 2

Chemical shifts and coupling constants for DL-AN in D_2O

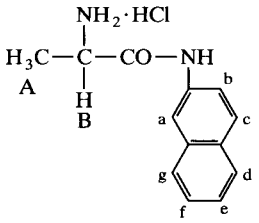

Proton	Chemical shift (ppm) [a]	Coupling constant (Hz)
A	1.73 (d)	$J_{A-B} = 7.12$
B	4.33 (q)	
a	8.06 (d)	$J_{a-b} = 2.21$, $J_{a-c} = J_{a-d} = J_{a-g} = 0.74$
b	7.55 (dd)	$J_{b-c} = 8.83$
c	7.96 (d)	$J_{c-d} = J_{c-g} = 0.74$
d	7.95 (d)	$J_{d-e} = 8.10$, $J_{d-f} = 1.48$, $J_{d-g} = 0.74$
e	7.58 (t)	$J_{e-f} = 6.9$, $J_{e-g} = 1.29$
f	7.61 (t)	$J_{f-g} = 8.07$
g	7.92 (d)	

[a] d, Doublet; dd, double doublet; t, triplet; q, quartet.

cavity. The duplication could not be observed at all with TM-α-CD or TM-β-CD. Only the H-A and H-b resonances were duplicated by adding

TABLE 3

Separation of H-a and H-B resonances of DL-AN on addition of CDs

CD	Separation (ppm)		[CD]:[DL-AN]
	H-a	H-B	
β-CD	0.0475	0.0082	1.4
DM-β-CD	0.0058	0.0115	0.91
DA-β-CD	0.0368	0.0325	1.2

γ-CD and their separations were ca. 0.005 and 0.025 ppm, respectively.

In order to optimize the CZE conditions for separating DL-AN, the applied voltage (15–30 kV) and pH (2.0–9.0) of the separation buffer (phosphate) solution containing 10 mM β-CD were investigated at 30°C. The enantiomers could not be separated at pH > 4.5. The best resolution was obtained at pH 2.0 and 30 kV. Under these CZE conditions, CDs are transported toward the negative electrode by electroosmotic flow. Each positively charged enantiomer migrates toward the negative electrode with the sum of the electrophoretic and the electroosmotic velocities, in the absence of CDs. When included in a CD cavity, the enantiomer is transported toward the negative electrode more slowly. Therefore, this

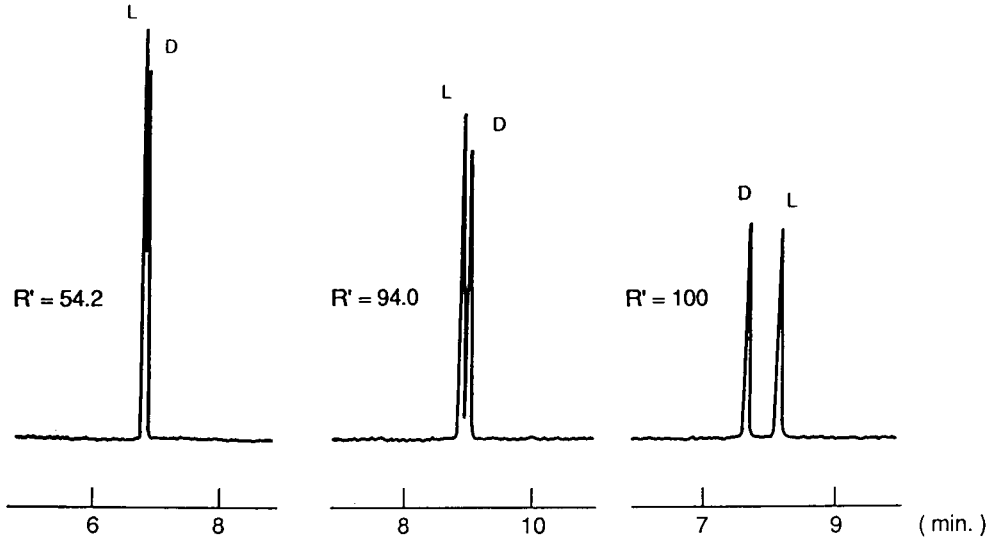

Fig. 8. Enantiomeric separations of DL-AN with (a) γ-CD, (b) β-CD and (c) DA-β-CD.

TABLE 4

Enantiomeric separation of DL-AN and binding constants between CDs and L-AN

CD	Migration time (min)	Resolution (R')	Binding constant ($l\ mol^{-1}$)
α-CD	6.73	–	–
DM-α-CD	7.37	–	–
TM-α-CD	8.69	–	203
β-CD	8.81 L	94.0	707
	8.92 D		
DM-β-CD	11.06	–	1233
TM-β-CD	7.44	–	234
DA-β-CD	7.62 D	100	228
	8.10 L		
γ-CD	6.73 L	54.2	–
	6.77 D		
None	5.54	–	–

means that a slower migrating enantiomer interacts more strongly than the other with the CD cavity.

Table 4 gives the results of the enantiomeric separation of DL-AN obtained under the optimum CZE conditions tested, together with binding constants between CDs and L-AN estimated from the fluorescence experiments. For a clear separation, the extent of separation of the two peaks is represented by $R' = 100(H - H')/H$, where H and H' are the height of the first peak and that of the valley between the two peaks, respectively. In this definition, the greater the R' value, the better is the resolution, and $R' = 100$ represents a baseline separation of the two peaks. The enantiomeric separation ability for DL-AN increased in the order γ-CD < β-CD < DA-β-CD. Typical electropherograms are shown in Fig. 8. DA-β-CD could bring about a complete baseline separation of the enantiomers. Moreover, the L-enantiomer migrated faster than the D-enantiomer in the presence of β-CD, indicating its stronger interaction with the D-enantiomer. The reverse migration order of the enantiomers was observed in the presence of DA-β-CD. The D-enantiomer exhibited a larger induced downfield shift for H-a than the L-enantiomer on addition of β-CD, and vice versa on the addition of DA-β-CD. As mentioned above, the guest penetrates into the β-CD cavity from the secondary hydroxyl side, but into the DA-β-CD cavity from the primary hydroxyl side. These selectivity changes are ascribed to the differences in the shape and size of the CD cavities and/or in their hydrogen-bonding abilities before and after acetylation.

In conclusion, the chemical modifications of β-CD brought about substantial changes in the enantioselectivity for DL-AN, and the high chiral recognition ability of DA-β-CD was demonstrated by both NMR and CZE. Considering the long migration time of 11.06 min and the large binding constant of 1233 $l\ mol^{-1}$ for DM-β-CD in Table 4, the interaction of DM-β-CD with the guest is the strongest among the CDs tested. An enantiomeric separation by CZE, however, cannot be obtained at all in this case.

The authors are grateful to Mrs. Y. Miyaji and T. Muneishi for obtaining NMR spectra on the Bruker AM-600 spectrometer.

REFERENCES

1 J. Szejtli, Cyclodextrins and Their Inclusion Complexes, Akadémiai Kiadó, Budapest, 1982.
2 J. Szejtli, Cyclodextrin Technology, Kluwer, Dordrecht, 1988.
3 A.P. Croft and R.A. Bartsch, Tetrahedron, 39 (1983) 1417.
4 M. Tanaka, T. Shono, D.-Q. Zhu and Y. Kawaguchi, J. Chromatogr., 469 (1989) 429.
5 M. Tanaka, S. Asano, M. Yoshinaga, Y. Kawaguchi, T. Tetsumi and T. Shono, Fresenius' J. Anal. Chem., 339 (1991) 63.
6 Y. Yamashoji, M. Tanaka and T. Shono, Chem. Lett., (1990) 945.
7 S. Terabe, H. Ozaki, K. Otsuka and T. Ando, J. Chromatogr., 322 (1985) 211.
8 S. Terabe, Trends Anal. Chem., 8 (1989) 129.
9 S. Fanali, J. Chromatogr., 474 (1989) 441.
10 J. Liu, K.A. Cobb and M. Novotny, J. Chromatogr., 519 (1990) 189.
11 A. Guttman, A. Paulus, A.S. Cohen, N. Grinberg and B.L. Karger, J. Chromatogr., 448 (1988) 41.
12 J. Boger, R.J. Corcoran and J.M. Lehn, Helv. Chim. Acta, 61 (1978) 2190.
13 J. Szejtli, A. Liptak, I. Jodal, P. Nanasi and A. Neszmelyi, Stärke, 32 (1980) 165.
14 K. Takeo, H. Mitoh and K. Uemura, Carbohydr. Res., 187 (1989) 203.
15 H.A. Benesi and J.H. Hildebrand, J. Am. Chem. Soc., 71 (1949) 2703.
16 J.R. Johnson, N. Shankland and I.H. Sadler, Tetrahedron, 41 (1985) 3147.

Analytica Chimica Acta, 268 (1992) 49–53
Elsevier Science Publishers B.V., Amsterdam

Liquid and gas chromatographic procedures for the simultaneous determination of copper, nickel and palladium using tetradentate Schiff bases as complexing agents

M.Y. Khuhawar and Altaf. I. Soomro

Institute of Chemistry, University of Sindh, Jamshoro (Pakistan)

(Received 11th September 1991; revised manuscript received 29th April 1992)

Abstract

The copper(II), nickel(II) and palladium(II) complexes of the tetradentate ligands *N,N'*-1,2-propylenebis(5,5-dimethyl-4-oxohexan-2-imine) and *N,N'*-1,2-propylenebis(6-methyl-4-oxoheptan-2-imine) (H_2IVA_2pn) were prepared and separated by gas chromatography and reversed-phase liquid chromatography (LC). The latter provides a good separation of copper, nickel and palladium from each other and from the excess of the reagent on a Nova-Pak C_{18} or Microsorb C_{18} column with an elution time of 5–14 min and UV detection. A liquid–liquid extraction procedure was used prior to the simultaneous determination of 0–100 μg copper and nickel by LC using H_2IVA_2pn. The detection limits for copper and nickel were 1 and 0.5 μg in a 1-cm^3 aliquot. A coin was analysed for copper and nickel.

Keywords: Gas chromatography; Liquid chromatography; Copper; Nickel; Palladium; Schiff bases

The use of gas chromatography (GC) for the separation and determination of metal chelates is limited by the thermal stability of the chelates. The common chelating ligands are different β-diketones, β-thioketones, bi- and tetradentate Schiff bases, dialkyldithiocarbamates, dialkyldithiophosphates and porphyrins [1,2]. Such complexing reagents have also proved promising for the determination of metals by liquid chromatography (LC) [3–5]. The tetradentate ketoamine Schiff bases are interesting for the determination of metal ions by GC and LC because of their selective reactions towards a limited number of metal ions, copper(II), nickel(II), palladium(II), oxovanadium(IV) and cobalt(II) [2,6–9]. In this work, the copper, nickel and palladium complexes of *N,N'*-1,2-propylenebis(5,5'-dimethyl-4-oxohexan-2-imine) (H_2APM_2pn) and *N,N'*-1,2-propylenebis(6-methyl-4-oxoheptan-2-imine) (H_2IVA_2pn) were prepared to examine their use as reagents for the GC and LC separation and determination of metal ions.

Dilli and Patsalides [10] have reported the GC of the oxovanadium complex of H_2APM_2pn, but the reagent H_2IVA_2pn appears to be reported here for the first time.

Correspondence to: M.Y. Khuhawar, Institute of Chemistry, University of Sindh, Jamshoro (Pakistan).

EXPERIMENTAL

Preparation of N,N'-1,2-propylenebis(6-methyl-4-oxoheptan-2-imine (H_2IVA_2pn)

To 6-methylheptane-2,4-dione (3.7 g, 0.025 mol) dissolved in ethanol (15 cm) was added

slowly 1,2-diaminopropane (1.02 cm^3, 0.012 mol). The mixture was warmed for 15 min and concentrated to about half the volume by distillation of the solvent. The remaining solvent was removed at room temperature in a vacuum desiccator. The product was dissolved in hexane (75 cm^3) and the solution was dried over anhydrous Na_2SO_4 and stored at −10°C. White crystals were obtained, which were recrystallized from hexane.

Preparation of N,N'-propylenebis(5,5-dimethyl-4-oxohexan-2-imine)(H_2APM_2pn).

To 5,5-dimethylhexane-2,4-dione (3.7 cm^3, 0.025 mol) dissolved in dry diethyl ether (30 cm^3) was added 1,2-diaminopropane (1.02 cm^3, 0.012 mol) dropwise with continuous stirring. The contents were stirred for a further 30 min and then allowed to stand at −10°C for 48 h. The oily mass obtained by evaporating the diethyl ether in a vacuum desiccator was extracted with portions of hexane. The combined hexane extract was dried over anhydrous Na_2SO_4, some of the solvent was evaporated under vacuum and the remainder was left at −10°C for 24 h. The white crystalline product obtained was recrystallized from hexane.

Preparation of copper(II) and nickel(II) chelates

A methanolic solution of copper(II) acetate or nickel(II) acetate (0.001 M, 20 cm^3) was added to a solution of H_2APM_2pn or H_2IVA_2pn (0.001 M, 10 cm^3) in ethanol. The mixture was refluxed for 30 min and concentrated to about half of the original volume by distillation of the solvent. The solution was left at −10°C overnight, then the precipitate was filtered off and recrystallized from ethanol–hexane (1:1, v/v). (The nickel complex of H_2IVA_2pn failed to crystallize and the oily mass obtained was used for further studies.)

Preparation of palladium(II) chelates

Palladium(II) chloride (0.09 g) was refluxed with 0.2 cm^3 of benzonitrile. The palladium–benzonitrile complex solution was diluted with benzene (5 cm^3). H_2APM_2pn or H_2IVApn (0.016 g) in benzene (5 cm^3) was added slowly and the mixture was refluxed for 12 h. Benzene was removed by distillation and the remaining solvent was removed in a vacuum desiccator. The palladium complex was dissolved in hexane (20 cm^3). The fine yellow crystals were recrystallized from hexane.

Equipment

Elemental microanalyses were carried out by Elemental Micro-Analysis, Okehampton, Devon. The mass spectrum of H_2IVA_2pn was recorded on a Finnigan MAT model 1125 spectrometer at the HEJ Research Institute of Chemistry, University of Karachi. Spectrophotometric studies were carried out on a Hitachi Model 220 instrument.

GC studies were done on a Hitachi Model 163 gas chromatograph fitted with a flame ionization detector and a Hitachi Model 056 chart recorder. Stainless-steel columns (2 m × 3 mm i.d. and 3 m × 3 mm i.d.) packed with 3% OV-101 on Chromosorb W HP (80–100 mesh) were used.

LC studies were done on Hitachi Model 655A chromatograph equipped with a variable-wavelength UV monitor, a Rheodyne Model 7125 injector and a Hitachi Model 561 recorder. A Nova-Pak C_{18} column (150 × 3.9 mm i.d.) with an ODS guard column (Waters) and Microsorb C_{18} column (150 × 4.6 mm i.d.) (Hewlett-Packard) were used.

Procedure for simultaneous determination of copper and nickel

A solution (1–2 cm^3) containing 0–100 μg each (20, 40, 60, 80 and 100 μg for calibration) of copper and (10, 20, 30, 40 and 50 μg for calibration) of nickel was transferred into a well stoppered test-tube, followed by sodium hydrogencarbonate buffer (pH 8) (1 cm^3) and H_2IVA_2pn solution [1% (w/v) in ethanol] (1.5 cm^3). The contents were warmed on a water-bath for 15 min at 70–80°C. The mixture was allowed to cool, cyclohexane (2 cm^3) was added and the contents were mixed thoroughly on a mechanical shaker for 15 min. The layers were allowed to separate and the organic extract (ca. 1 cm^3) was evaporated. The residue was dissolved in 1 cm^3 of methanol; 5 μl of this solution were injected on to the Microsorb C_{18} column and the complexes were eluted with 14% (v/v) water in methanol at 1 cm^3 min^{-1}. UV detection was at 300 mm.

Analysis for copper and nickel in a coin

A coin (5.63222 g) was placed in aqua regia (15 cm^3) and heated gently on hot-plate nearly to dryness. Hydrochloric acid (10 cm^3) was added and the mixture was heated nearly to dryness to expel most of the nitrogen oxides and free chlorine. The residue was dissolved in 250 cm^3 of water, 1 cm^3 of this solution was diluted to 100 cm^3 and from this solution 0.5 cm^3 was diluted to 1 cm^3 with water and extracted with H_2IVA_2pn reagent using the above procedure. The amount of copper and nickel was evaluated from the calibration graph.

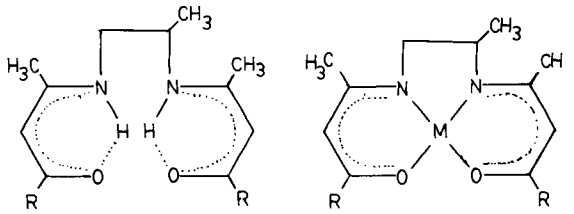

(I) $R=(CH_3)_2CH\cdot CH_2-$ M = Cu, Ni, Pd

(II) $R=(CH_3)_3C-$

Fig. 1. Structures of reagents and metal chelates.

RESULTS AND DISCUSSION

The results of elemental analysis (Table 1) agreed closely with the expected values. The mass spectrum of H_2IVA_2pn indicates a molecular ion peak M^+ at m/z (relative intensity) 322 (6.8). M^+ loses a fragment corresponding to an isobutyl group with a residual peak at m/z 265 (2.6), followed by a loss of C_4H_5NO to give a peak at m/z 182 (6.5). The reagent gives major ion peaks at m/z 168 (100) and 154 (9.8) due to the cleavage of the C–C bond at the bridge position (Fig. 1), and also peaks at m/z 85 (12) and 57 (21) corresponding to $(CH_3)_2CHCH_2CO$ and isobutyl groups, indicating that isobutyl groups are present near the carbonyl groups (Fig. 1).

When the copper(II), nickel(II) and palladium (II) chelates of H_2IVA_2pn and H_2APM_2pn were subjected to GC on a 2 m × 3 mm i.d. column packed with 3% OV-101 on Chromosorb W HP (80–100 mesh), the best separation of the three chelates with either ligand was achieved by injecting at a column temperature of 200°C, with programmed rise at 0.5°C min^{-1} to 230°C, with the injection port at 230°C and a nitrogen flow-rate of 30 cm^3 min^{-1}. Complete separation of palladium from copper and nickel but only a partial separation of copper and nickel was obtained. The resolution factor between copper and nickel chelates was calculated to be 0.75 and 1.29 for H_2IVA_2pn and H_2APM_2pn, respectively.

In order to improve the GC separation of the copper and nickel chelates, column (3 m × 3 mm i.d.) packed with the same stationary phase was tried. An improvement in the separation was observed (Fig. 2). The resolution factors calculated between copper and nickel were 1.14 and 2.0 for H_2IVA_2pn and H_2APM_2pn, respectively. Both reagents gave reasonable GC separations but a better separation was obtained with H_2APM_2pn.

TABLE 1

Results of elemental analysis

Compound	Molecular formula	M.p. (°C)	Expected (%)			Found (%)		
			C	H	N	C	H	N
H_2IVA_2pn	$C_{19}H_{34}N_2O_2$	85	70.80	10.50	8.69	70.73	10.89	8.71
IVA_2pnCu	$C_{19}H_{32}N_2O_2Cu$	83	59.4	8.34	7.29	58.81	8.14	7.14
IVA_2pnPd	$C_{19}H_{32}N_2O_2Pd$	107	53.52	7.51	6.57	53.77	7.89	6.62
H_2APM_2pn	$C_{19}H_{34}N_2O_2$	90	70.75	10.63	8.69	70.6	10.5	8.7
APM_2pnCu	$C_{19}H_{32}N_2O_2Cu$	130	59.42	8.34	7.29	60.2	8.7	7.4
APM_2pnNi	$C_{19}H_{32}N_2O_2Ni$	149	60.25	8.45	7.39	58.47	8.28	6.67
APM_2pnPd	$C_{19}H_{32}N_2O_2Pd$	219	53.52	7.51	6.57	53.77	7.89	6.62

The linear calibration ranges for the copper, nickel and palladium chelates of H_2IVA_2pn and H_2APM_2pn under the optimum separation conditions were obtained by plotting the average peak height ($n = 2$) versus the amount of complex injected, for 0.3–7.0 μg of complex, corresponding to 53–1860 ng of metal. The detection limits were determined by measuring each signal at least three times the background noise and were 40, 29 and 36 ng of copper, nickel and palladium chelates of H_2APM_2pn, corresponding to 6.6, 4.4 and 8.9 ng of copper, nickel and palladium, respectively.

GC gave adequate separation of the metal chelates, but required a long analysis time (up to 40 min). LC with UV spectrophotometric detection therefore was also examined for the separation of the metal chelates. The spectrophotometric studies of the reagents and their metal chelates were recorded in methanol. The results (Table 2) indicate that the metal chelates show a number of high absorbance bands due to intraligand π–π^* transitions, which could be used for spectrophotometric detection of the metal ions.

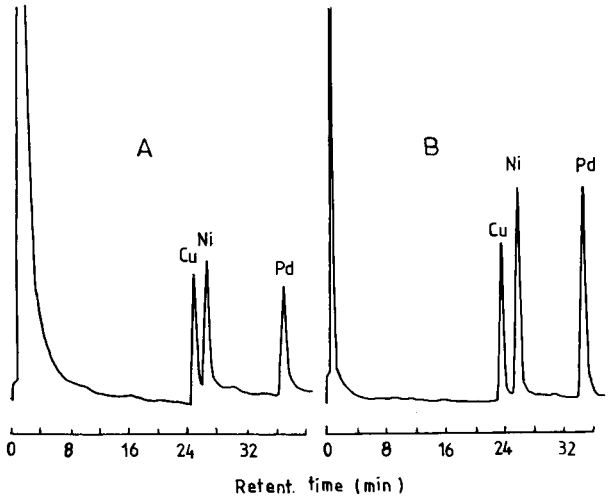

Fig. 2. GC separation of Cu, Ni and Pd chelates of (A) H_2IVA_2pn and (B) H_2APM_2pn. column, 3 m×3 mm i.d., packed with 3% OV-101 on Chromosorb W HP (80–100 mesh). Carrier gas (nitrogen) flow-rate, 30 cm^3 min^{-1}. Column temperature: (A) 210°C, increased at 1°C min^{-1} to 240°C; (B) 200°C, increased at 1°C min^{-1} to 240°C. Injection port temperature: (A) 240°C; (B) 250°C.

TABLE 2

Spectrophotometric data for the reagents and their metal chelates in methanol

Compound	λ_{max}(nm) (ϵ, l mol^{-1} cm^{-1})
H_2IVA_2pn	230(2960), 307(25600), 335(27800)
IVA_2pnCu	210(11300), 230.5(16300), 280(8080), 308(24000), 333(8840), 378(sh)(1130), 542(218)
APM_2pnCu	206(11800), 232(144500), 260(sh)(12300), 281(13900), 390(23000), 333(sh)(8300), 380(sh)(422), 543(235)
IVA_2pnNi	204(202600), 270(125000), 310(sh)(58300), 350(49400), 472(49800), 570(1855)
APM_2pnNi	233(67400), 272(45100), 310(sh)(14600), 355(14900), 372(15900), 464(233), 557(160)
IVA_2pnPd	211.5(57000), 236(9300), 275(17200), 300(22700), 326.5(28500), 347(19900)
APM_2pnPd	212.5(4330), 270(18400), 291(16300), 346(14100)

The separation of the metal complexes on a Nova Pak C_{18} column was examined. Complete separation between copper, nickel and palladium was achieved when the complexes were eluted with methanol–acetonitrile–water (80 + 10 + 10, v/v/v) and methanol–tetrahydrofuran–water (74 + 6 + 20, v/v/v) for the chelates of H_2APM_2pn and H_2IVA_2pn, respectively. The flow-rates were 0.5 and 0.6 cm^3 min^{-1}, using UV detection at 300 and 330 nm for the chelates of H_2APM_2pn and H_2IVA_2pn, respectively. The chromatograms were obtained within 15 min (Fig. 3).

In order to use the H_2IVA_2pn reagent for the determination of copper and nickel, the conditions for extraction were checked. A solution (1 cm^3) containing 50 μg of copper and nickel was taken and the effects of variation of the pH, solvent, reagent concentration and heating and shaking time were investigated. Sodium hydrogen-carbonate buffer (pH 8) gave the maximum extraction of copper and nickel. Hexane, cyclohexane, benzene and toluene were tried for the extraction of copper and nickel and cyclohexane gave the most reproducible results (R.S.D. = 2.5%, $n = 6$). A reagent concentration of 1% (w/v) (1.5 cm^3) proved adequate for the extrac-

tion of 0–100 μg of metal ions. A heating time of 15 min at 70–80°C and a shaking time of 15 min enabled copper and nickel to be extracted from the aqueous to the organic phase quantitatively and reproducibly.

Linear calibration graphs obtained under the optimum conditions for simultaneous determinations were obtained within the ranges 0–50 μg of nickel and 0–100 μg of copper in aqueous solution (Fig. 4). The detection limits measured as the signal three times the background noise, were 1 μg of copper and 0.5 μg of nickel in a 1-cm^3 aliquot (2 μl injected). This corresponds to detection limits of 1 ng of copper and 0.5 ng of nickel per injection. Test solutions containing copper and nickel in different ratios (1:1 to 1:5) were analysed and the relative error was found to be within the range ±0–6% and ±0–7% for nickel and copper respectively. Aluminium(III) and chromium(III) when added at 20 times the concentration of copper and nickel retarded the extraction of copper (46% and 69% respectively) and iron(II) decreased the extraction of nickel (57%). However, when these metal ions were present at concentrations similar to those of copper and nickel, they could be tolerated by increasing the reagent concentration to 1.5%. Cobalt(II)

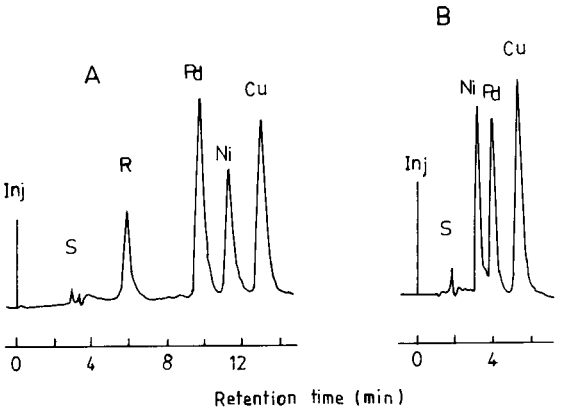

Fig. 3. LC separation of Cu, Ni and Pd chelates of (A) H_2IVA_2pn and (B) H_2APM_2pn. Column, 150×3.9 mm i.d. Nova-Pak C_{18} with ODS guard column. Eluent: (A) methanol–tetrahydrofuran–water (74+6+20, v/v/v), flow-rate 0.5 cm^3 min^{-1}, UV detection at 330 nm; (B) methanol–acetonitrile–water (80+10+10, v/v/v), flow-rate 0.5 cm^3 min^{-1}, UV detection at 300 nm.

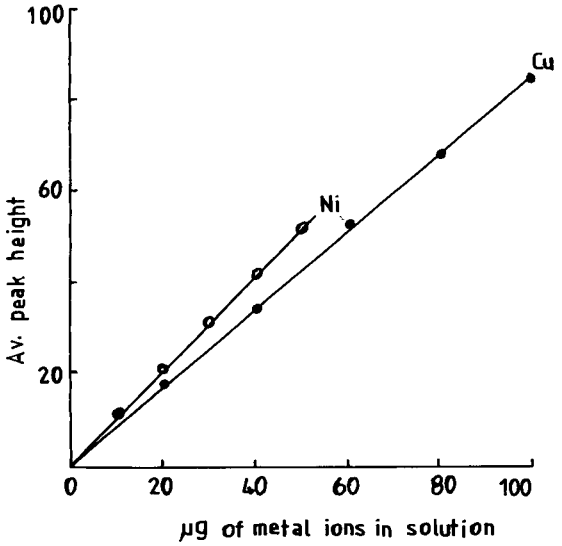

Fig. 4. Calibration graphs for Cu and Ni chelates after extraction with H_2IVA_2pn. Column, Microsorb C_{18} (150×4.6 mm i.d.); eluent, methanol–water (85+15, v/v); flow-rate, 1 cm^3 min^{-1}; UV detection at 300 nm.

forms a chelate with H_2IVA_2pn and is simultaneously extracted, resulting in an increase in the peak height of nickel.

A coin was analysed for copper and nickel and the results were 79.9 ± 1.0% and 22.6 ± 1.0% (mean ± 95% confidence limit, $n = 3$) for copper and nickel, respectively. The expected 80.0 and 20.0%, respectively.

REFERENCES

1 P.C. Uden and D.E. Henderson, Analyst, 102 (1977) 889.
2 P.C. Uden, J. Chromatogr., 313 (1984) 3.
3 G. Nickless, J. Chromatogr., 313 (1984) 129.
4 B.R. Willeford and H. Veening, J. Chromatogr., 25 (1982) 61.
5 M.Y. Khuhawar and A.G. Bhatti, Indian J. Chem., 26A (1987) 180.
6 M.Y. Khuhawar and A.G. Bhatti, J. Chem. Soc. Pak., 11 (1989) 246.
7 S. Dilli and E. Patsalides, Anal. Chim. Acta, 128 (1981) 109.
8 O. Lau and W.I. Stephen, Anal. Chim. Acta, 180 (1986) 417.
9 M.Y. Khuhawar, A.G.M. Vasandani and A.I. Soomro, J. Chem. Soc. Pak., 12 (1990) 119.
10 S. Dilli and E. Patsalides, J. Chromatogr., 130 (1977) 251.

Analytica Chimica Acta, 268 (1992) 55–65
Elsevier Science Publishers B.V., Amsterdam

Fully automated on-line liquid chromatographic separation system for polar pollutants in various types of water

J. Slobodnik and E.R. Brouwer

Department of Analytical Chemistry, Free University, De Boelelaan 1083, 1081 HV Amsterdam (Netherlands)

R.B. Geerdink and W.H. Mulder

Institute for Inland Water Management and Waste Water Treatment, P.O. Box 17, 8200 AA Lelystad (Netherlands)

H. Lingeman and U.A.Th. Brinkman

Department of Analytical Chemistry, Free University, De Boelaan 1083, 1081 HV Amsterdam (Netherlands)

(Received 17th January 1992; revised manuscript received 4th May 1992)

Abstract

A fully automated column liquid chromatographic separation system using on-line trace enrichment, gradient elution and diode-array detection for the trace-level determination of polar pollutants is described. Automation of the system was achieved by means of an automated cartridge-exchange system (PROSPEKT). Relevant parameters such as pH, volume and ionic strength of the sample, flow-rate during the enrichment step and wavelengths and band widths during detection were optimized for eighteen pollutants in various types of water at concentration levels below 5 $\mu g\ l^{-1}$. The determination limit for all test compounds in liquid chromatographic grade water was 0.1 $\mu g\ l^{-1}$, and identification, via diode-array spectra, could be performed at the same level. The mean relative standard deviations of the peak areas and the retention times for all the test compounds were 10% and 0.3%, respectively, at the 5 $\mu g\ l^{-1}$ level for river Rhine water.

Keywords: Liquid chromatography; Sample preparation; Pesticides; Polar pollutants; Waters

According to the Rhine Action Program of 1987, initiated after a disastrous fire at a pharmaceutical company in Basle (Switzerland), the AQUALARM environmental monitoring and alarm system for the major Dutch river systems, which monitors the presence of organic and inorganic micropollutants in the waters of the rivers Meuse and Rhine, and the branches of the river Rhine (Waal, IJsel), was developed and installed [1]. So far, no such system is available for the determination of polar pollutants. In the context of both the Rhine Action Program and the Rhine Basin Program [2,3], attention has been devoted to the development of a fully automated and robust early warning system for the determination of polar pollutants at trace levels (< 5 $\mu g\ l^{-1}$) with a procedure that simultaneously provides structural information of the analytes [3,4].

As a significant number of polar pollutants cannot be determined by gas chromatography (GC), column liquid chromatography (LC) is the separation technique of first choice [5]. Advan-

Correspondence to: H. Lingeman, Department of Analytical Chemistry, Free University, De Boelaan 1083, 1081 HV Amsterdam (Netherlands).

tages of LC over GC are the simplicity and robustness of the system. However, compared with GC, LC has some limitations with respect to selectivity and sensitivity. These disadvantages can be solved by using mass spectrometric or diode-array detection (DAD) in combination with on-line trace enrichment techniques based on small cartridges [2,3] or membrane extraction discs [6,7].

The development of a non-automated on-line trace enrichment gradient LC–diode-array detection (DAD) system for the determination of polar pollutants in river Rhine water, has been reported recently [3]. In this paper, a fully automated LC procedure using on-line trace enrichment and DAD for the identification and determination of eighteen polar pollutants, including carbamates, triazines, chloroanilines, phenylurea herbicides, aromatic chloroamines, hydroketolactones, chlorinated phenols and organophosphorus compounds, at trace levels is described. The main aim of this study was to investigate the various parameters that influence the sensitivity and the overall performance of such an automated system.

EXPERIMENTAL

Equipment

The LC analyses were performed with two Model 400 solvent-delivery systems (Applied Biosystems, Ramsey, NJ), a laboratory-made six-port injection valve (Free University, Amsterdam), equipped with a 30-μl injection loop, and a Model 1000 S diode-array detector (Applied Biosystems). For single-wavelength monitoring, the detector was set at 230 nm with a band width of 50 nm. During recording of the absorbance spectra the diode width was 2 nm and the spectra were recorded from 190 to 370 nm. Data from the detector were collected by a standard Model 80 286 microprocessor-based computer with 1 Mbyte of extended memory, and subsequently handled by the LabCalc software (Galactic Industries, Salem, NH). All experiments were done at ambient temperature.

Trace enrichment of the analytes was done on 10 mm × 2.0 mm i.d. disposable trace enrichment cartridges of the PROSPEKT (Spark Holland, Emmen, Netherlands) automated sample preparation unit. The cartridges contained styrene–divinylbenzene copolymer (15–25-μm PLRP-S; Polymer Laboratories, Church Stretton) with a pore size of 10 nm. The cartridges were conditioned via a solvent-delivery unit (SDU) (Spark Holland), and sampling was done with a Model 300 preparative pump (Gynkotek, Munich).

The PROSPEKT was used to condition the trace enrichment cartridges and to control the whole system.

Chemicals and reagents

The stainless-steel analytical columns were a 100 mm × 2.1 mm i.d. Hypersil C_{18} column (Hewlett-Packard, Waldbronn), a 150 mm × 4.6 mm i.d. LiChrosorb RP-18 column (Chrompack, Middelburg, Netherlands) and a 250 mm × 4.6 mm i.d. Chromspher Pesticides column (Chrompack). All columns were packed with 5-μm particles. A 250 mm × 4.6 mm i.d. PLRP-S column (Polymer Laboratories) packed with 5-μm particles was also tested.

LC gradient-grade acetonitrile, methanol and water were obtained from J.T. Baker (Deventer, Netherlands). Unless mentioned otherwise, LC-grade water was used. "Milli-Q water" was prepared by ultrafiltration using a Milli-Q system (Millipore, Bedford, MA). Disodium hydrogenphosphate, concentrated perchloric acid and phosphoric acid (85%) were supplied by J.T. Baker.

The various solutes were supplied by Hoechst (Frankfurt), Riedel-de Haen (Seelze), Promochem (Wesel), and Dr. S. Ehrenstorfer (Augsburg). They all were at least 95% pure. The eighteen pesticides used and the numbering used in this study are as follows: carbendazim (1), metamitron (2), chloridazon (3), aldicarb (4), bromacil (5), simazine (6), 2-chloroaniline (7), atrazine (8), diuron (9), monolinuron (10), warfarin (11), linuron (12), 3.3′-dichlorobenzidine (13), barban (14), dinoterb (15), dinoseb (16), pentachlorophenol (17) and phoxim (18).

River Rhine water was collected at Lobith and obtained from RIZA (Lelystad, Netherlands).

Prior to use, the samples were filtered over a 0.45-μm BA membrane filter (Schleicher & Schüll, Dassel).

Procedures

Stock standard solutions (1 mg in 5 ml) of the analytes in methanol were prepared every 6 weeks. Working standard solutions of the test compounds were prepared every 3 days by diluting the stock standard solutions with LC-grade, Milli-Q, tap or river Rhine water to a concentration of 0.01–5 μg l^{-1}. All stock and working standard solutions were stored at 4°C in the dark.

The gradient conditions for testing the analytical columns and using the LiChrosorb column (in the final procedure) were as follows: solvent A, acetonitrile–0.01 M phosphate buffer (pH 3) (90 + 10, v/v) and solvent B, acetonitrile–0.01 M phosphate buffer (pH 3) (5 + 95, v/v). The gradient profile was 0 min, 100% B, changed linearly to 100% A (55 min) and then linearly to 100% B (60 min). The flow-rate was 1.0 ml min^{-1}. Prior to use, all eluent components were degassed using a vacuum ultrasonic bath (5 min). Before starting the first gradient, the system was equilibrated daily for 15 min with solvent B (flow-rate 1 ml min^{-1}).

The trace enrichment cartridges were conditioned with 2 ml of methanol (flow-rate 2 ml min^{-1}) and then 2 ml of 0.001 M perchloric acid (1 ml min^{-1}) using the SDU of the PROSPEKT. Subsequently 100 ml, or in some instances 150 ml, of sample were enriched on the cartridge at a flow-rate of about 4 ml min^{-1}. Desorption of the cartridge was performed (with solvent A) by coupling the cartridge on-line with the analytical column and starting of the gradient (see above).

All steps of the procedure were automatically controlled by the PROSPEKT software. In Table 1 the sample preparation programme (SPP) for the overall procedure is given.

RESULTS AND DISCUSSION

Automation of the method

Automation of on-line trace enrichment systems can now be performed with commercially available systems. Both the OSP-2 (Merck) and the PROSPEKT (Spark Holland) systems are equipped with a disposable cartridge unit. As an additional unit, the PROSPEKT contains a solvent-delivery unit (SDU) for conditioning and washing of the trace enrichment cartridges. In this study, a preparative LC pump was used for loading the samples.

The time sequence of the automated procedure is given in Table 1. All steps of the sample

TABLE 1

Sample preparation programme of automated system [a]

Time (min:s)	Solvent	Valve 1	Valve 2	Flow-rate (ml min^{-1})	Aux 2	Aux 6	Other
00:00		PURGE	ELUTE				
00:01	1			2.0			CHC
02:00	3		PURGE	4.16	ON		
03:00	2		ELUTE	2.0	OFF		
05:00	2		PURGE	1.0			
07:00	3		ELUTE	0.0	ON		
31:02					OFF		
31:30	4	ELUTE	PURGE			ON	
31:31	1			2.0			
33:31	1			0.0		OFF	
65:00							END

[a] Solvents: 1, methanol; 2, 0.001 M perchloric acid; 3, sample; 4, eluent. Valves 1 and 2, positions according to Fig. 1. Aux 6, connection of PROSPEKT with 1000 S diode-array detector, positions ON/OFF; Aux 2, connection of PROSPEKT with LC pump, positions ON/OFF. CHC, change cartridge. END, end of analysis.

preparation programme (SPP) were programmed on, and automatically controlled by the PROSPEKT software. The total set-up of the system is shown in Fig. 1. The procedure starts by changing the trace enrichment cartridge (00 min:01s). After conditioning of the cartridge (00:01–31:02) the analysis is started by an auxiliary (Aux 6) signal to the detector (31:30). In detail, the following steps take place: 00:01, flushing of the system capillaries with methanol; 02:00, wetting of the cartridge with methanol and flushing of the sample capillaries with the sample; 03:00, flushing of the system capillaries with perchloric acid; 05:00, flushing of the cartridge with perchloric acid to displace the methanol; 07:00, start of the sampling; 31:02, end of the sampling; 31:30, desorption of the cartridge and start of the LC separation; 31:31, flushing of the system capillaries with methanol; 33:31, end of the flushing; 65:00, end of SPP.

This SPP can be used to perform a series of analyses in a fully automated manner. Therefore, at the end of the first run, the system immediately starts with conditioning and sampling of the second cartridge. The 60-min gradient programme starts at 31:30 of the first SPP and ends at 26:30 of the second run, which means that there are 5 min to flush the system with eluent B to prepare it for the next analysis at, again, 31:30. All data are automatically stored by the set option in the LabCalc software and are available at the end of the sequence.

The auxiliary (Aux 2) connects the PROSPEKT with the sample loading pump. As a result the exact flow-rate was 4.16 ml min^{-1} in this instance. The auxiliary (Aux 6) of the PROSPEKT is connected with the ground and event remote inputs of the detector. The SPP is defined in a specific RUNPROGRAM which is used to run a series of analyses in a fully automated manner. An analysis is started from the keyboard of the PROSPEKT by pressing START and typing the proper START and STOP RUNPROGRAM numbers.

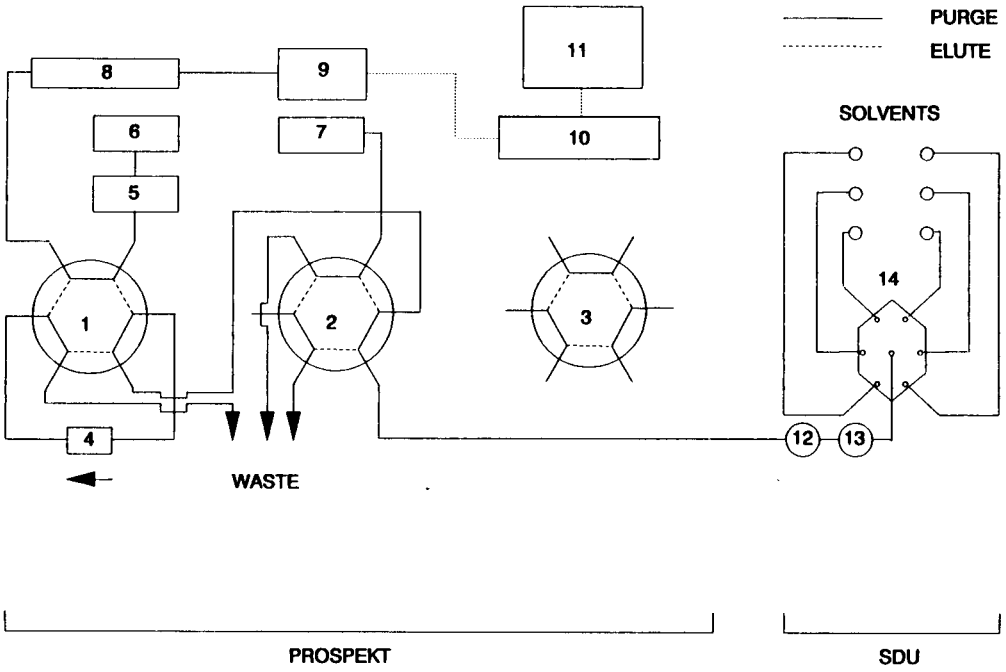

Fig. 1. Automated on-line trace enrichment system for water samples. 1, 2, 3 = High-pressure valves; 4 = trace enrichment cartridge; 5, 6 = high-pressure gradient pumps; 7 = preparative pump for sample loading; 8 = analytical column; 9 = detector; 10 = computer, 11 = printer; 12 = pulse damper; 13 = purge pump; 14 = solenoid valve.

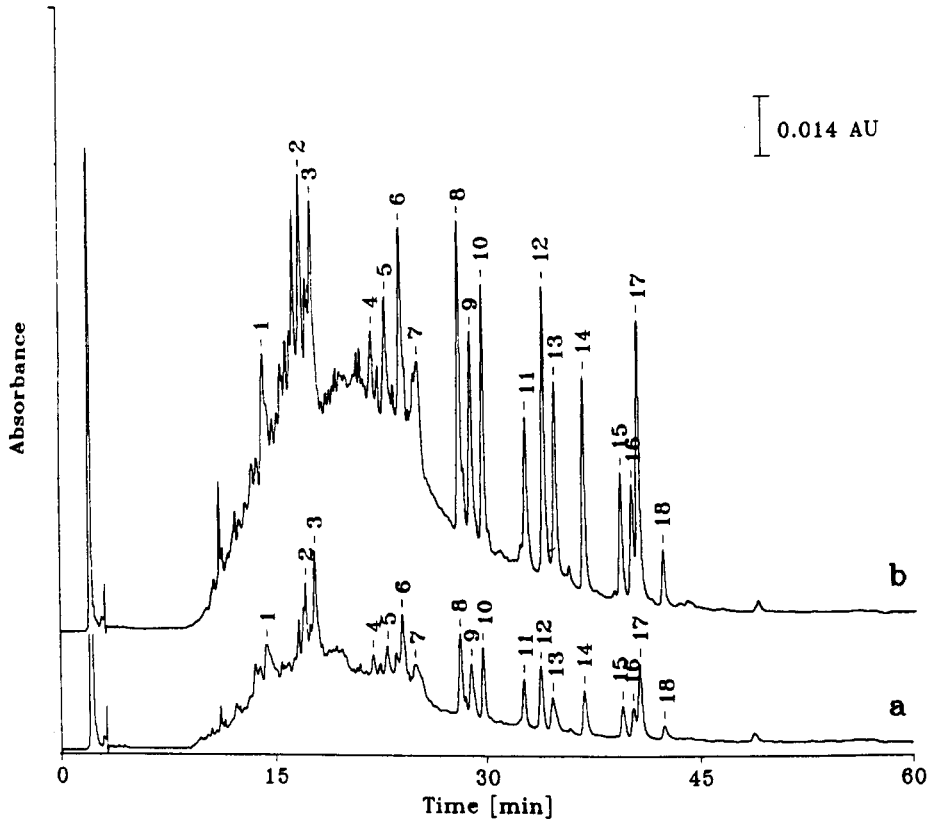

Fig. 2. Chromatograms of mixture of test compounds (5 $\mu g\ l^{-1}$) in river Rhine water. Enriched volume: (a) 30 ml and (b) 100 ml. For all other conditions, see text.

Optimization of the analytical system

Several parameters that can be expected to have profound influence on the detection sensitivity of the test pollutants and/or the robustness of the total analytical system were studied.

Analytical column. Four analytical columns were tested in combination with the 10 mm × 2.0 mm i.d. PLRP-S trace enrichment cartridges. As the sorbent of the analytical column should possess a hydrophobicity similar to that of the sorbent in the cartridge, three C_{18}-bonded silica columns and a polymer column were tested.

Analysis of the test mixture on the 5-μm Hypersil C_{18} column gave a hardly satisfactory resolution, although good resolution was obtained after loop injection of the same mixture. This slightly surprising behaviour was not investigated further. Completely satisfactory results were obtained with the 5-μm Chromspher Pesticides, 5-μm LiChrosorb RP-18 and 5-μm PLRP-S columns. As the overall separation efficiency of the LiChrosorb column was better than that of the Chromspher Pesticides column, and the 5-μm polymer material caused a higher back-pressure than the 5-μm C_{18}-bonded phases, the 150 mm × 4.6 mm i.d. LiChrosorb RP-18 column was used in all further work.

UV absorbance detection. In order to optimize the DAD, experiments were performed at various wavelength–bandwidth combinations. In each experiment, 100 ml of a text mixture in LC-grade water (analyte concentration 0.5 $\mu g\ l^{-1}$) were enriched and analysed under the conditions given under Experimental.

The chromatograms were recorded at 230 nm using a band width of 50 nm, a large band width

TABLE 2

Maximum absorbance wavelengths and breakthrough volumes of test compounds

No.	Compound	Maximum response wavelength (nm) [a]	Breakthrough volume (ml) [b]
1	Carbendazim	220	25
2	Metamitron	210	15
3	Chloridazon	220	15
4	Aldicarb	210	25
5	Bromacil	210	40
6	Simazine	220	50
7	2-Chloroaniline	210	20
8	Atrazine	220	90
9	Diuron	245	65
10	Monolinuron	210	75
11	Warfarin	210	> 100
12	Linuron	210	> 100
13	3,3'-Dichlorobenzidine	210	> 100
14	Barban	210	> 100
15	Dinoterb	210	> 100
16	Dinoseb	280	> 100
17	Pentachlorophenol	210	> 100
18	Phoxim	280	> 100

[a] Trace enrichment of 100 ml of LC-grade water at a concentration level of 0.5 $\mu g\ l^{-1}$ using a detection band width of 5 nm. [b] Breakthrough volumes on PLRP-S cartridge using the fraction collection method [3]. All other conditions are given in the text.

being advantageous only when a single wavelength has to be used for a wide variety of analytes. However, as most of the compounds tested possess absorbance maxima at mutually divergent wavelengths, the response can be improved significantly by using simultaneous detection at a number of carefully selected wavelengths. These turned out to be 210, 220, 245 and 280 nm [3,8,9], all at a band width of 5 nm as one is now working close to the absorbance maxima. For all analytes, at least one of the four wavelengths selected gave better results than the 230 nm–50 nm combination, with a 2.5-fold increase being observed for aldicarb, warfarin and pentachlorophenol. The wavelengths selected are given in Table 2.

Trace enrichment. The breakthrough volumes of the test compounds were determined in Milli-Q water at a spiking level of 2 $\mu g\ ml^{-1}$ by using the fraction collection method [3]. The results are included in Table 2. Actually, when using the overall analytical procedure, the UV response of all analytes showing early breakthrough increased on increasing the sample volume from 30 to 100 ml. This is illustrated in Fig. 2, where the LC–UV chromatograms obtained after trace enrichment of 30 and 100 ml of spiked river Rhine water are shown. For all pollutants, a 2–3-fold increase in the UV response is seen, which can be explained by the lower concentrations used than during the study of the breakthrough volumes [2].

Coquart and Hennion [10] carried out trace enrichment from sample volumes of up to 500 ml. Therefore, in this study, 100- and 500-ml tap water samples spiked with 0.5 $\mu g\ l^{-1}$ of all the test solutes except the early eluting carbendazim and metamitron were processed. As the time needed for trace enrichment should, ideally, be essentially the same as the time required for the LC separation, in this instance sample loading was performed at a flow-rate of 15 instead of 5 ml min^{-1}. This did not cause any problems, which is in agreement with early work in which flow-rates of up to 25 ml min^{-1} were used without adverse effects [11]. As regards trace enrichment, the UV response of all sixteen analytes was found to increase 2.5–5-fold on loading 500 instead of 100 or 150 ml of sample. Although it should be emphasized that these are only preliminary results, it is interesting that high-speed loading of large sample volumes is probably a viable approach in early warning procedures.

Sample treatment. Two further aspects of interest are the sample pH during trace enrichment, which may be a critical parameter for basic analytes, and the removal of matrix interferences.

In order to study the pH effect, spiked (1 $\mu g\ l^{-1}$) river Rhine water samples were adjusted to pH 3, 5.8, 6.8, 7.8 and 8.8 and 100-ml aliquots were analysed. For the present set of test compounds, the response over the whole pH range studied did not vary significantly. The matrix peak became slightly larger at lower pH values, but this did not affect the performance of the system. As the pH of river Rhine water (Lobith, Netherlands) varied between 6.2 and 8.2 in the period March 1990–June 1991, it will be possible to

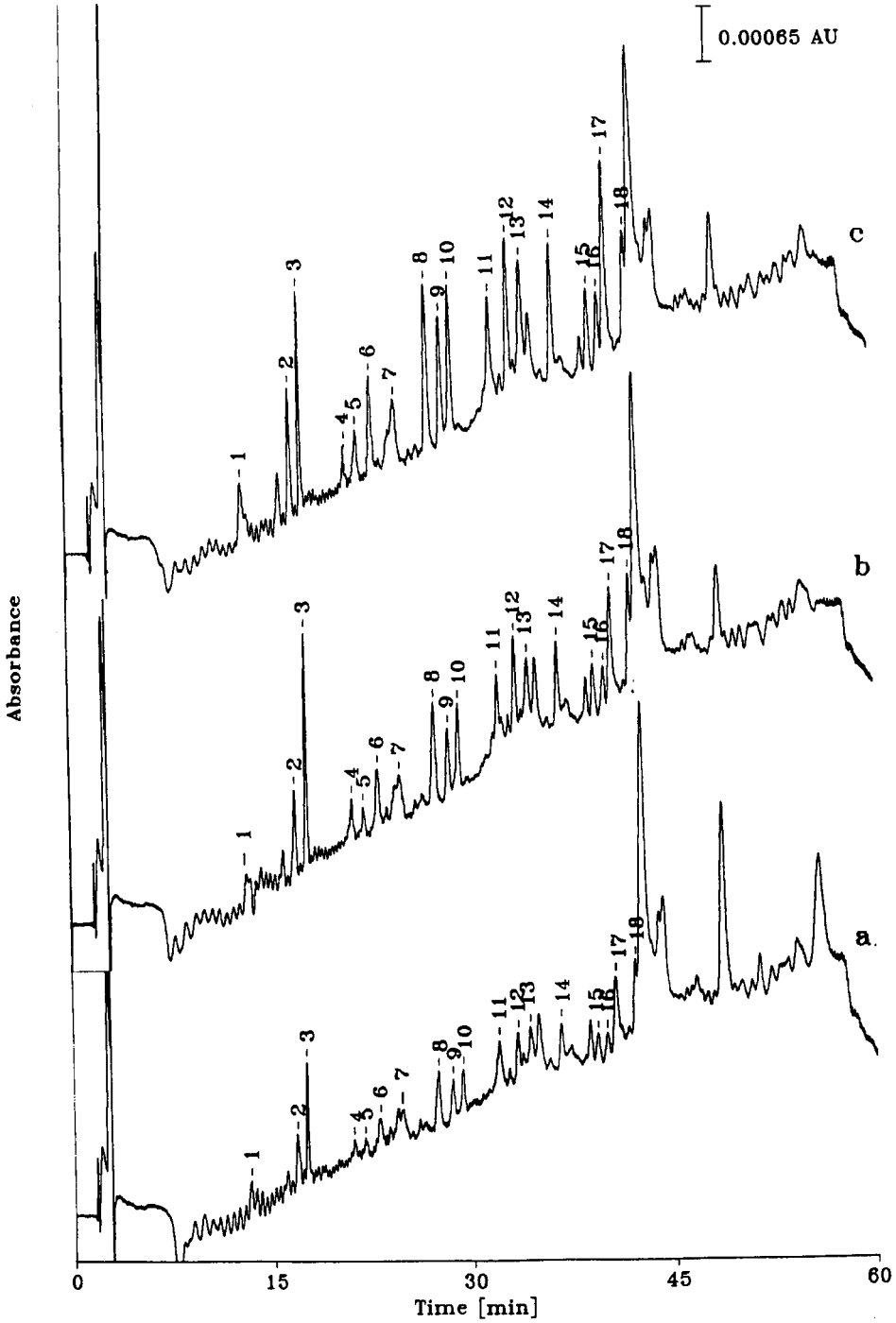

Fig. 3. Chromatograms of mixture of test compounds in LC-grade water. Concentrations of the compounds: (a) 30; (b) 50; (c) 100 ng l^{-1}. Enriched volume is 150 ml. For all other conditions, see text.

process unbuffered river Rhine water samples in the present automated system.

In a previous study, attempts to remove matrix interferences from the PLRP-S trace enrichment cartridge by washing with, e.g., acetonitrile–water (30 + 70, v/v) (pH 3) were not successful [12]. Because the humic and fulvic substances may be expected to be negatively charged at high pH, which should facilitate their removal, washing with 0.001–0.1 M sodium hydroxide solution was tested. However, even at pH 13 the matrix peak decreased by only ca. 30%. Moreover, the decrease tended to vary considerably between runs.

Finally, the addition of 0.1–0.5 mol l^{-1} of sodium chloride to river Rhine water samples, to test the influence of the ionic strength, did not have a positive effect on the response of the analytes as a result of a salting-out effect.

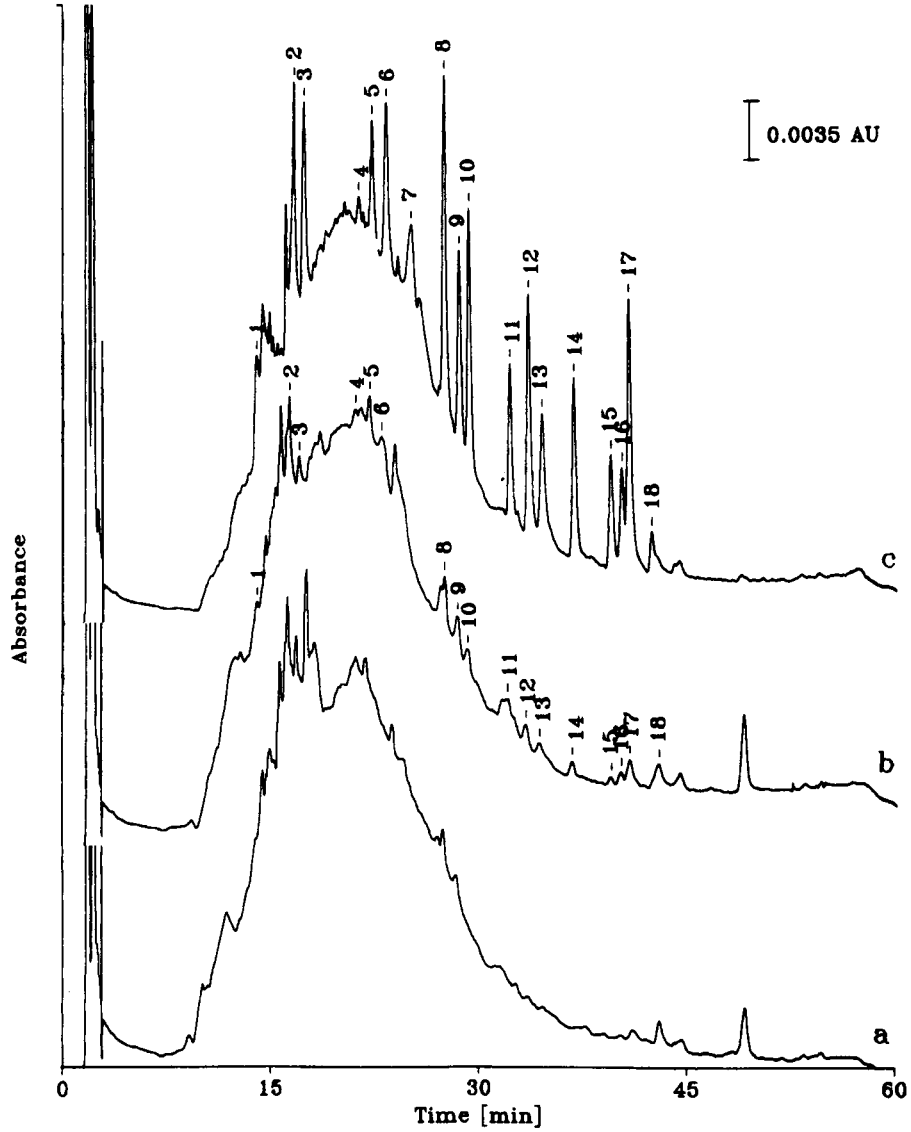

Fig. 4. Chromatograms of 150 ml of enriched tap water (a) and corresponding chromatograms after spiking with test compounds at the 0.1 $\mu g\ l^{-1}$ (b) and 1 $\mu g\ l^{-1}$ (c) level. For all other conditions, see text.

Performance of the total system

Using the optimized experimental conditions discussed in the previous sections, the detection limits of the eighteen pollutants in LC-grade water were determined by enrichment of 150-ml samples spiked at the 30–100 ng l^{-1} level. The chromatograms in Fig. 3 demonstrate that the detection limits are distinctly below 100 ng l^{-1}

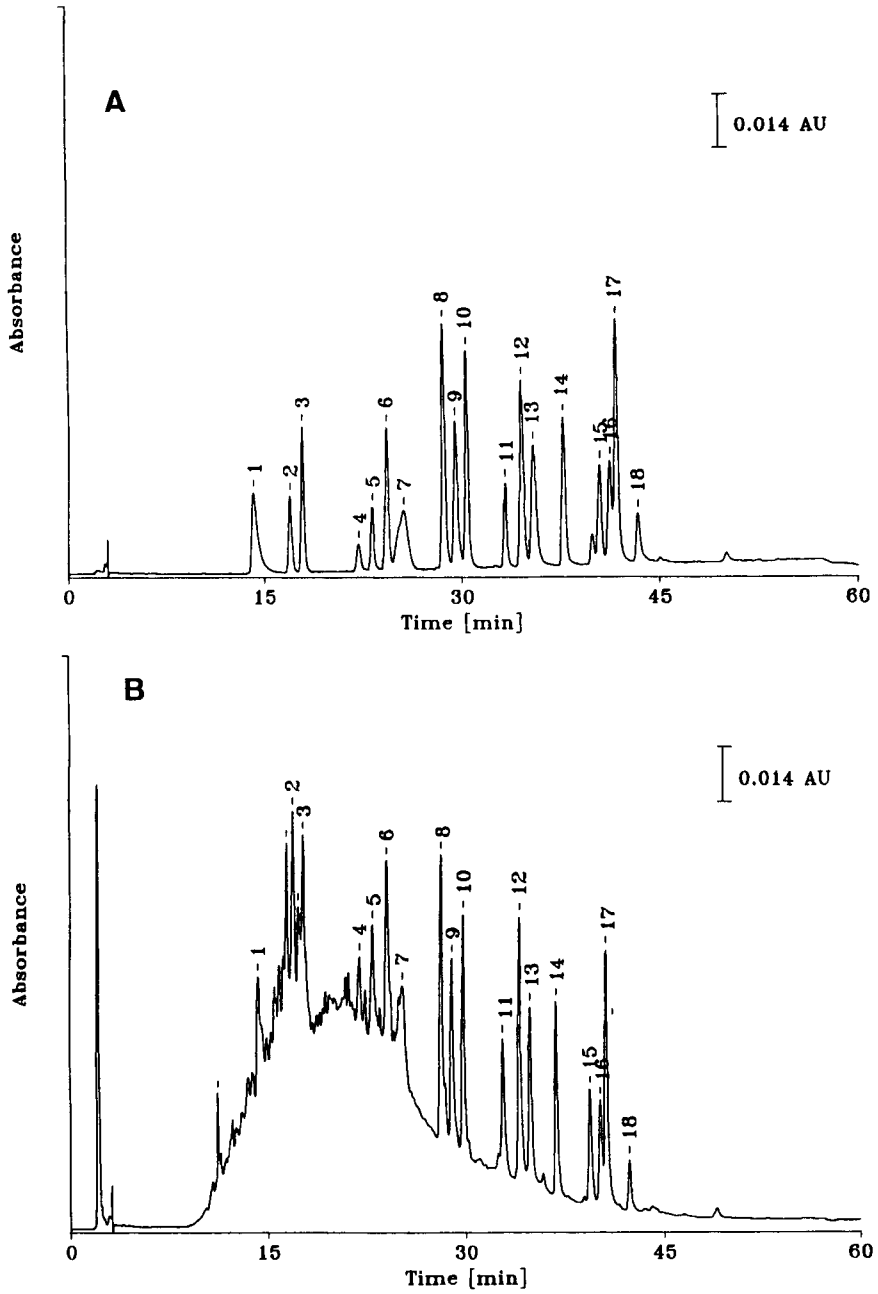

Fig. 5. Chromatograms of mixture of test compounds (5 $\mu g\ l^{-1}$) in (A) LC-grade water and (B) river Rhine water. Enriched volume is 100 ml. For all other conditions, see text.

for all compounds, even with single-wavelength (230 nm) detection. Reliable spectral recognition was possible in all instances at the 100 ng l^{-1} level.

As examples of real sample analyses, automated runs for blank and spiked (0.1 and 1 μg l^{-1}) tap water are shown in Fig. 4 and for spiked (5 μg l^{-1}) river Rhine water and, for comparison, LC-grade water in Fig. 5. It is interesting to add that, with river Rhine water, spectral recognition can easily be carried out at the 3 μg l^{-1} level, as is demonstrated for monolinuron in Fig. 6. The detection limits for the analyses in spiked surface water and tap water typically are about 1 and 0.3 μg l^{-1}, respectively.

Calibration graphs for all the test solutes were constructed using spiked river Rhine (100 ml; 0.5–5 μg l^{-1}) and Milli-Q (150 ml; 0.05–2 μg l^{-1}) water. For most analytes, the correlation coefficients are satisfactory (Table 3) and, with two exceptions (metamitron and 2-chloroaniline; matrix interference), they are essentially equal for both types of sample.

The repeatability of the automated system was tested several times by enriching a limited number of 100-ml spiked (5 μg l^{-1}) river Rhine and other water samples, using a fresh PLRP-S cartridge for each run. The results in Table 4 are satisfactory as far as the retention times are concerned. The peak-area data, with a relative standard deviation (R.S.D.) of less than 30% in all instances, are, by themselves, acceptable. By using peak-height data, however, similar results were obtained. The wide gap between a series of very low and a series of high R.S.D. values is not readily explained. Other series of runs typically gave similar results, as shown in Table 4.

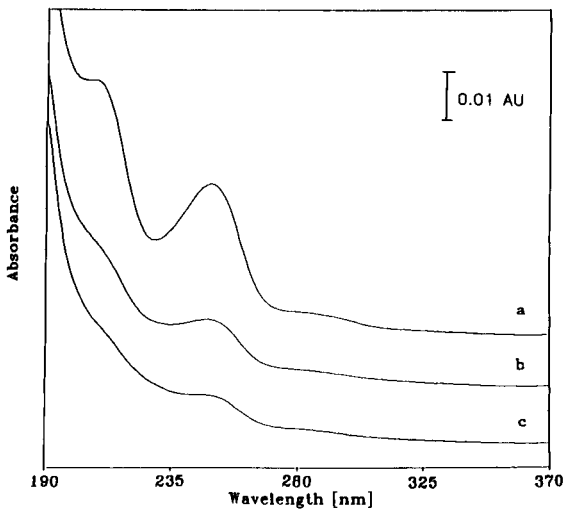

Fig. 6. Absorbance spectra of monolinuron in river Rhine water at concentrations of (a) 3, (b) 1 and (c) 0.5 μg l^{-1}.

TABLE 3

Correlation coefficients of test compounds after analysis in Milli-Q water and river Rhine water [a]

No.	Compound	r_{MW}	r_{RW}
1	Carbendazim	0.9898	0.9863
2	Metamitron	0.9946	– [b]
3	Chloridazon	0.9931	0.9929
4	Aldicarb	0.9801	0.9842
5	Bromacil	0.9998	0.9693
6	Simazine	0.9540	0.9999
7	2-Chloroaniline	0.9907	– [b]
8	Atrazine	0.9919	0.9991
9	Diuron	0.9849	0.9971
10	Monolinuron	0.9917	0.9994
11	Warfarin	0.9967	0.9992
12	Linuron	0.9988	0.9983
13	3,3'-Dichlorobenzidine	0.9631	0.9964
14	Barban	0.9832	0.9923
15	Dinoterb	0.9961	0.9976
16	Dinoseb	0.9998	0.9979
17	Pentachlorophenol	0.9944	0.9995
18	Phoxim	– [b]	0.9912

[a] r_{MW}, analyses in Milli-Q water (0.05–2 μg l^{-1}), enriched volume 150 ml; r_{RW}, analyses in river Rhine water (0.5–5 μg l^{-1}), enriched volume 100 ml. Each calibration graph was calculated from six data points, which were measured in triplicate. For all other conditions, see text. [b] Correlation coefficient < 0.9 owing to mobile phase or matrix interferences.

Conclusions

A fully automated system for the trace-level determination of polar pollutants in surface and tap water is described. The system consists of an automated cartridge-exchange module (PROSPEKT) containing small cartridges loaded with PLRP-S polymer packing material, and a reversed-phase LC–DAD system. All steps of the analytical procedure are controlled by the PROSPEKT software.

TABLE 4

Retention times and peak areas of test compounds (5 $\mu g\ l^{-1}$) in river Rhine water after a single use of four trace enrichment cartridges [a]

No.	Compound	RT_{RW} (R.S.D.)	PA_{RW} (R.S.D.)
1	Carbendazim	14.3 (0.1)	7.7 (27)
2	Metamitron	16.6 (0.4)	5.1 (20)
3	Chloridazon	17.8 (0.1)	5.3 (28)
4	Aldicarb	22.0 (0.1)	3.5 (2.4)
5	Bromacil	23.0 (0.2)	8.7 (28)
6	Simazine	24.0 (0.1)	11.3 (0.4)
7	2-Chloroaniline	25.2 (0.2)	3.3 (22)
8	Atrazine	28.2 (0.1)	16.1 (27)
9	Diuron	29.0 (0.1)	11.8 (0.3)
10	Monolinuron	29.8 (0.1)	13.9 (0.4)
11	Warfarin	32.8 (0.3)	7.2 (0.3)
12	Linuron	34.0 (0.4)	14.5 (3.4)
13	3,3'-Dichlorobenzidine	34.9 (0.1)	10.6 (0.4)
14	Barban	37.0 (0.4)	11.5 (1.5)
15	Dinoterb	39.6 (0.5)	7.1 (0.1)
16	Dinoseb	40.3 (0.5)	4.0 (11)
17	Pentachlorophenol	40.8 (0.4)	11.2 (4.9)
18	Phoxim	42.5 (0.4)	3.2 (1.3)

[a] RT_{RW}, retention time (min) in river Rhine water; PA_{RW}, peak area (arbitrary units) in river Rhine water; R.S.D., relative standard deviation (%). For other conditions, see text.

The various parts of the system have been optimized using eighteen polar pesticides as test solutes. The automated system has been used to analyse 30–150-ml blank and spiked, surface and tap water samples. Detection limits in units of concentration vary between about 0.1 and 1 $\mu g\ l^{-1}$, depending on the sample type and the characteristics of the analyte. Spectral resolution is generally possible at three fold higher concentrations. The linearity and precision are acceptable even at the low $\mu g\ l^{-1}$ spiking level. The present, admittedly still limited, experience indicates that unattended operation of the total system does not encounter special problems. With a slightly different fully automated system, in which only the ABI gradient and DAD system was replaced with the HP 1090 system, over 50 samples could be run unattended.

The analytical performance of the system essentially meets the prerequisites of the *I*-list of the Dutch National Policy Document on Water Management [1], which states that it should be possible to detect 3 $\mu g\ l^{-1}$ of a pesticide in surface water and 0.1 $\mu g\ l^{-1}$ in tap water.

This work was supported by the Institute for Inland Water Management and Waste Water Treatment (RIZA) (Lelystad, Netherlands) as part of the Rhine Action Program. Part of this research will be incorporated in the Rhine Basin Program (Amsterdam/Waldbronn).

REFERENCES

1 Water in the Netherlands: a Time for Action, National Policy Document on Water Management, House of Commons, Meeting period 1988–89, The Hague, No. 21250 (1–2).
2 E.R. Brouwer, I. Liska, R.B. Geerdink, P.C.M. Frintrop, W.H. Mulder, H. Lingeman and U.A.Th. Brinkman, Chromatographia, 32 (1991) 445.
3 I. Liska, E.R. Brouwer, A.G.L. Ostheimer, H. Lingeman, U.A.Th. Brinkman, R.B. Geerdink and W.H. Mulder, Int. J. Environ. Anal. Chem., 47 (1992) 267.
4 EEC Drinking Water Guideline, 80/779/EEC, EEC No. L229/11–29, EEC, Brussels, 30th August, 1980.
5 M.W.F. Nielen, R.W. Frei and U.A.Th. Brinkman, in R.W. Frei and K. Zech (Eds.), Selective Sample Handling and Detection in Liquid Chromatography, Part A, Elsevier, Amsterdam, 1988, Ch. 1.
6 E.R. Brouwer, H. Lingeman and U.A.Th. Brinkman, Chromatographia, 29 (1990) 415.
7 E.R. Brouwer, D.J. van Iperen, I. Liska, H. Lingeman and U.A.Th. Brinkman, Int. J. Environ. Anal. Chem., 47 (1992) 257.
8 R. Reupert and E. Plöger, HPLC Determination of 29 Controlled Herbicides in Water Supplies, Hewlett-Packard Application Note, Hewlett-Packard, Avondale, PA, 1990.
9 R. Reupert, R. Zube and E. Plöger, GIT Fachz. Lab., 11 (1991) 106.
10 V. Coquart and M.-C. Hennion, J. Chromatogr., 585 (1991) 67.
11 R.W. Frei and U.A.Th. Brinkman, Trends Anal. Chem., 1–2 (1981) 45.
12 R.B. Geerdink, A.M.B.C. Graumans and J. Viveen, Internal Report: Determination of Phenoxyacid Herbicides In Water, Institute for Inland Water Management and Waste Water Treatment, Lelystad, Netherlands, 1990.

Analytica Chimica Acta, 268 (1992) 67–71
Elsevier Science Publishers B.V., Amsterdam

Optimization of parameters for the gas chromatographic determination of polycyclic aromatic hydrocarbons

W.R. Trevelin, L.H. Vidal, M.D. Landgraf, I.C.E. Silva and M.O.O. Rezende

Universidade de São Paulo, Instituto de Física e Química de São Carlos, Departamento de Química e Física Molecular, Av. Dr. Carlos Botelho 1465, Cx.P. 369, 13560 São Carlos SP (Brazil)

(Received 5th February 1992; revised manuscript received 2nd April 1992)

Abstract

The optimization of conditions for the gas chromatographic determination of sixteen polycyclic aromatic hydrocarbons (PAHs) using the splitless injection mode is described. Parameters optimized were the type and amount of solvent, the temperature of the injection port and the column and the purge time. A factorial design was used initially to identify the most important parameters. Based on this initial study, xylene was chosen as the solvent and 100°C was chosen as the best value for temperature of the column. The other parameters were optimized by using a simplex method. The optimum conditions found were 3 μl of solvent, 280°C for the injection port and a purge time of 30 s. With these conditions, relative standard deviations for five replicate determinations of 2-ng amounts of PAHs were 3.2–10.8%.

Keywords: Gas chromatography; Optimization methods; Factorial design; Polycyclic aromatic hydrocarbons; Simplex optimization

Polycyclic aromatic hydrocarbons (PAHs) represent a class of organic compounds identified as "unambiguous priority pollutants" by the US Environmental Protection Agency (EPA) [1]. This class of compounds has been shown to contain several potent carcinogens [2]. The occurrence and potential hazards of these compounds have stimulated research related to the determination of PAHs in the environment.

Given the low concentrations of these species, it is important to use conditions that optimize the separation efficiency and detection limits in environmental samples. Grob and Grob [3,4] identified the solvent effect as one of the most important factors for alkanes such as heptane, octane and nonane determined using gas chromatography (GC) with the splitless injection mode. Cold trapping was originally described as the mechanism operating in the splitless injection mode. Subsequent studies [4,5] showed that the solvent effect is important for both splitless and on-column injection. Based on Grob and Grob's studies, Jennings et al. [6] described the theoretical basis of the solvent effect. Cold trapping and the solvent effect were described as the two functions that led to the reconcentration of elutes on the top of the column.

The factors affecting splitless injection are numerous, e.g., injection speed, liner size, matrix composition, presence of a liner plug [7], column temperature, volatility of the solvent, amount of solvent and time of vaporization [8].

Univariate studies, although useful, are seldom completely satisfactory for complex processes such as in GC that depend on multiple variables. The

Correspondence to: M.O.O. Rezende, Universidade de São Paulo, Instituto de Física e Química de São Carlos, Departamento de Química e Física Molecular, Av. Dr. Carlos Botelho 1465, Cx.P. 369, 13560 São Carlos SP (Brazil).

best conditions are usually obtained by multivariate studies such as factorial design and simplex methods such as the sequential simplex method introduced by Spendley et al. [9] and improved by Nelder and Mead [10]. In this study, a factorial design was used to identify the most important variables in GC to increase the sensitivity of sixteen PAHs and a simplex method was used to identify the optimum values for the most important parameters, namely the volume of solvent, the temperature of the injection port and the purge time.

EXPERIMENTAL

Reagents and standards

All solvents were glass distilled through a 150-cm column. The compounds studied were naphthalene, acenaphthene, acenaphthylene, fluorene, phenanthrene, anthracene, fluoranthene, pyrene, benz[*a*]anthracene, chrysene, benzo[*b*]fluoranthene, benzo[*k*]fluoranthene, benzo[*a*]pyrene, dibenzo[*a*,*h*]anthracene, benzo[*ghi*]perylene and indeno[1,2,3-*cd*]pyrene (Supelco, Bellefonte, PA). A stock solution was prepared in a mixed benzene–methylene chroride (1 + 1, v/v) solvent containg a nominal concentration of 2 mg ml^{-1} of each PAH. Further dilutions were made with benzene and xylene to give a final concentration of 2 μg ml^{-1} of each PAH.

Aliquots of the stock solution were measured using a 100-μl Type 701 RN syringe (Hamilton, Reno, NV).

Chromatographic conditions

All experiments were done using a Model 5890 high-resolution gas chromatograph (Hewlett Packard, Palo Alto, CA) equipped with a flame ionization detector (FID). The output of the FID was connected to an integrator (HP-3393). A fused-silica capillary column coated with cross-linked Ultra-1 methylsilicone (Hewlett-Packard) as the stationary phase (25 m × 0.32 mm i.d., film thickness 0.17 μm) was used with splitless injection. Some experimental conditions, including solvent, temperature of the injection port, initial temperature of the column, amount of solvent and purge time, were varied during the process. Other parameters, including flow-rate of the carrier gas (40 cm s^{-1}), heating rate (5°C min^{-1}) and final temperature (280°C), were the same in all experiments. Peak areas for all PAHs were added and normalized for each chromatogram.

TABLE 1

Parameters used in factorial design

Variable	Maximum level (+)	Minimum level (−)
S = solvent	Benzene	Xylene
P = time of purging	0.5 min	1.0 min
V = amount of solvent	1.0 μl	3.0 μl
T = initial column temperature	100°C	120°C
I = injection port temperature	270°C	290°C

Factorial design

Values of the parameters used in the factorial design are listed in Table 1. The combinations of these minimum and maximum levels are shown in Table 2.

TABLE 2

Combinations among the minimum and maximum levels of the parameters listed in Table 1

Experiment No.	Variable					Total area (%) [a]
	S	P	V	T	I	
E_1	+	−	+	−	+	75.5
E_2	−	+	−	+	+	25.4
E_3	−	−	−	−	+	29.4
E_4	−	−	+	−	−	81.2
E_5	+	−	+	+	−	100.0
E_6	−	+	+	+	−	73.1
E_7	−	−	−	+	−	27.4
E_8	−	+	−	−	−	32.0
E_9	+	+	−	−	+	45.4
E_{10}	+	+	−	+	−	41.8
E_{11}	−	+	+	−	+	78.6
E_{12}	−	−	+	+	+	75.0
E_{13}	+	−	−	−	−	43.2
E_{14}	+	−	−	+	+	31.8
E_{15}	+	+	+	−	−	98.9
E_{16}	+	+	+	+	+	82.9

[a] The total area for the sixteen PAHs was obtained by adding and normalizing for each chromatogram.

RESULTS AND DISCUSSION

Factorial design

Relative values of areas for the several combinations in the factorial design are included in Table 2. It is noted that the total area for experiments E_1, E_4–E_6, E_{11}, E_{12}, E_{15} and E_{16} are all greater than 50%, whereas the values for all other experiments are all less than 50%. Accordingly, the former represent the most significant combinations.

Table 3 shows estimates of the factorial analysis from factorial design. The order of relevance among the variables which can be observed is $V > S > SVT > SP > VT > P > ST > SV > TI > PV > T > VI > PT > SI > I$. By comparing the results experiment for E_{15} and E_{16} it is observed that lower values of T (effect = −0.4625) and I (effect = −0.9225) give a higher response. Combining results for E_6 with these results, it is concluded that a lower value of S (effect = 1.67) results in a significantly smaller value for the relative area. Therefore, it is concluded that larger values of S increase the sensitivity whereas smaller values of T and I give better sensitivity.

The factorial design shows that S, V and T are the most significant variables. Further, the variable T was minimized and kept constant and the variable S was maximized and also kept constant.

TABLE 3

Factorial analysis estimate

Variable or interaction	Effect
S	1.67
P	0.245
SP	0.3875
V	6.6875
SV	0.02
PV	−0.19
SPV	-7.5×10^{-3}
T	−0.4625
ST	0.24
PT	−0.63
SPT	−0.4975
VT	0.3475
SVT	0.46
PVT	−0.735
I	−0.9225

TABLE 4

Initial conditions for simplex optimization

Constants		Variables		
S	*T* (°C)	*V* (μl)	*P* (min)	*I* (°C)
Xylene	100	1.0–3.0	0.5–1.0	270–290

The maximum of the parameter V and the minimum value of the parameter I, their own interactions and their interactions with other parameters can be obtained from factorial design.

Simplex optimization

The initial conditions for simplex optimization are listed in Table 4. Based on these, the chromatographic conditions to obtain the maximum sensitivity using Nelder and Mead's algorithm [10] were investigated.

Table 5 shows the progress of the simplex and Fig. 1 shows some chromatograms which represent the importance of the simplex optimization of the injection mode with more dilute samples.

The initial simplex with vertices V_1, V_2, V_3 and V_4 was based on the indication supplied by factorial design. Following the algorithm, vertex V_4 was rejected as it gave the worst response (66.6%), and vertex V_5 was obtained by reflection of V_1 through the experiments containing the vertices V_1, V_2, V_3 and V_5. However, in vertex V_6 the variable V attains an unreal value which lies outside the optimized surface. So this vertex was contracted, obtaining a new system of vertices with V_1, V_2, V_5 and V_7, thus generating an area value equal to 75.0%. The algorithm continued to V_{15}, because the best response was obtained with V_2.

V_1 and V_4 indicate a small increase in the response only due to the purge time, but when compared with V_2 and V_{10} both responses are similar, considering the analytical error, which demonstrates that the purge time is not a very important variable.

Conclusions

The largest contribution was due to the amount of solvent, as expected. Xylene increases the area values mainly of the late-eluting peaks. Another

TABLE 5

Progress of the simplex

Vertex No.	Variables			Retained vertices	Response (%)
	V (μl)	P (min)	I (°C)		
V_1	2.0	0.70	280	–	71.8
V_2	3.0	0.50	280	–	100.0
V_3	2.0	0.50	285	–	66.9
V_4	2.0	0.50	280	1, 2, 3, 4	66.6
V_5	2.7	0.67	283	1, 2, 3, 5	88.6
V_6 [a]	3.1	0.72	277	– [a]	– [a]
V_7	2.3	0.55	283	1, 2, 5, 7	75.0
V_8 [a]	3.3	0.42	284	– [a]	– [a]
V_9	2.3	0.63	281	2, 5, 7, 9	79.3
V_{10}	3.0	0.62	280	2, 5, 9, 10	97.1
V_{11}	3.4	0.54	281	– [a]	– [a]
V_{12}	2.6	0.61	281	2, 5, 10, 12	82.2
V_{13}	3.2	0.56	281	– [a]	– [a]
V_{14}	2.8	0.60	281	2, 5, 10, 14	88.2
V_{15}	3.1	0.57	281	– [a]	– [a]

[a] The variable V attains an unreal value.

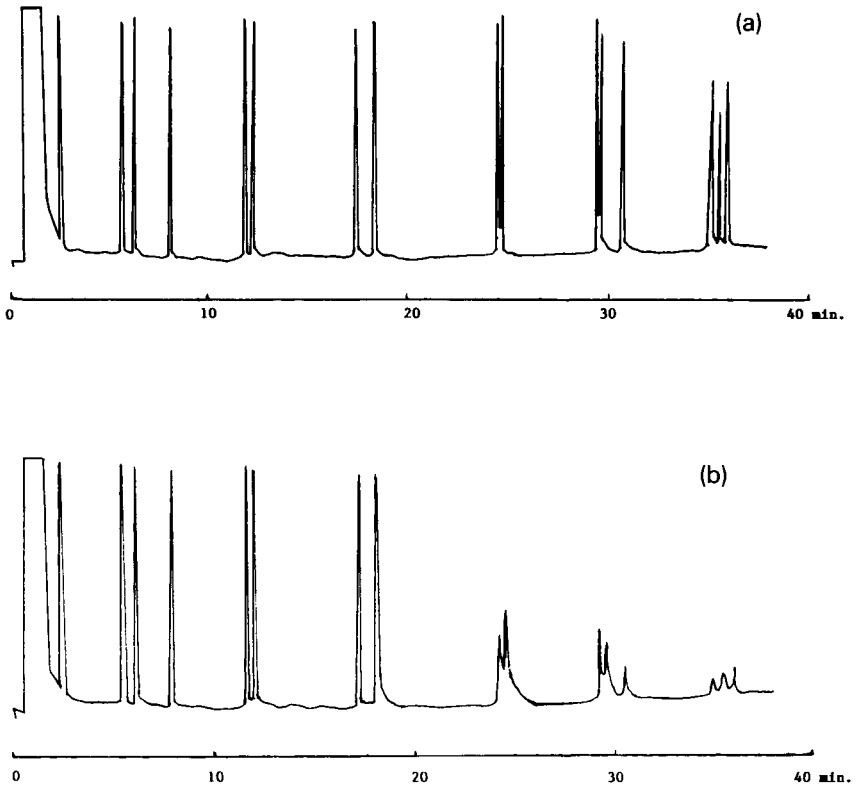

Fig. 1. Gas chromatogram of the sixteen PAHs: (a) after the best optimization (V_2 condition); (b) under the V_1 condition.

important parameter is the initial column temperature, whereas the purge time and injection port temperature are less significant.

These results show that the sensitivity is strongly increased by adopting the optimum chromatographic conditions. To determine trace constituents in a sample it is essential to establish the best conditions for analysis, for which chemometrics is a useful tool.

The authors thank FINEP/PADCT for financial support and Wagner R. Trevelin thanks CAPES for grants. The authors are also grateful to Dr. Horatio A. Mottola for reading and correcting the manuscript.

REFERENCES

1 Sampling and Analysis Procedures for Screening of Industrial Effluents for Priority Pollutants, US Environmental Protection Agency, Environmental Monitoring and Support Laboratory, Cincinnati, OH, 1977.
2 M.J. Shear, Am. J. Cancer, 26 (1936) 322.
3 K. Grob and K. Grob, Jr., J. Chromatogr. Sci., 7 (1969) 584.
4 K. Grob and K. Grob, Jr., J. Chromatogr., 94 (1974) 53.
5 K. Grob and K. Grob, Jr., J. High Resolut. Chromatogr. Chromatogr. Commun., 1 (1978) 57.
6 W.G. Jennings, R.R. Freemann and T.A. Rooney, J. High Resolut. Chromatogr. Chromatogr. Commun., 1 (1978) 275.
7 R.D. De Veaux and M. Szelewski, J. Chromatogr. Sci., 27 (1989) 513.
8 K. Grob, Classical Split and Splitless Injection in Capillary Gas Chromatography, Hüthig, Heidelberg, 1986.
9 W. Spendley, G.R. Hext and F.R. Himsworth, Technometrics, 4 (1962) 441.
10 J.A. Nelder and R. Mead, Comput. J., 7 (1965) 308.

Analytica Chimica Acta, 268 (1992) 73–80
Elsevier Science Publishers B.V., Amsterdam

Determination of theophylline and paraxanthine in urine samples by liquid chromatography using the H-point standard additions method

Pilar Campíns-Falcó, Francisco Bosch-Reig, Rosa Herráez-Hernández and Adela Sevillano-Cabeza

Departamento de Química Analítica, Facultad de Química, Universidad de València, 46100 Burjassot, València (Spain)

(Received 27th February 1992; revised manuscript received 21st April 1992)

Abstract

The simultaneous determination of theophylline and paraxanthine in urine samples by the H-point standard additions method (HPSAM) is described. Samples are extracted with C_{18} solid-phase extraction cartridges and chromatographed using a Hypersil C_{18}-ODS column and a mobile phase consisting of acetonitrile–phosphate buffer in the gradient elution mode. Under these conditions theophylline and paraxanthine are eluted with short retention times. Although their chromatographic peaks are overlapped and their spectra are very similar, the H-point standard additions method provides excellent results in the determination of both xanthines at therapeutic levels.

Keywords: Liquid chromatography; H-point standard addition method; Paraxanthine; Theophylline; Xanthines

Numerous liquid chromatographic (LC) methods for the determination of theophylline in biological fluids have been proposed. Although theophylline is easily detected when it is present at therapeutic concentrations (1–20 μg ml^{-1}), it has been reported that many exogenous and endogenous compounds interfere [1]. The inability to separate theophylline from some of its metabolites in a reasonable time has been a typical problem in most of the LC procedures [2–7]. The presence of the pharmacologically active dietary methylxanthines caffeine, theobromine and paraxanthine (1,7-dimethylxanthine) may influence patient compliance and may also complicate the evaluation and interpretation of theophylline therapeutic drug monitoring. The separation of theophylline from paraxanthine, the main metabolite of caffeine, remains the most serious interference in any LC assay.

Correspondence to: P. Campíns-Falcó, Departamento de Química Analítica, Facultad de Química, Universidad de València, 46100 Burjassot, València (Spain).

Although normal-phase conditions are reported to give a suitable separation between these two xanthines [8,9], this mode of chromatography is not routinely used in clinical laboratories owing to the difficulty of maintaining stable separations [1]. Likewise, in the reversed-phase mode under isocratic conditions, the resolution between theophylline and paraxanthine or other endogenous compounds takes a very long time or requires very high flow-rates [5,6]. Even when gradient elution conditions are used, the complete resolution of theophylline is slow [9].

To overcome the inadequate selectivity of the conventional reversed-phase procedures, the addition of an organic modifier such as *N*,*N*-dimethylformamide or tetrahydrofuran to the mobile phase has been reported. This modification, combined with flow-rates higher than 1.5 ml min^{-1}, provides an almost complete separation

between theophylline and paraxanthine in an acceptable time [7,10–13]. Leakey [14] described an LC procedure for the determination of several xanthines which utilizes a gradient elution programme with tetrahydrofuran in the mobile phase and a flow-rate of 0.8 ml min^{-1}. Under these conditions, theophylline and paraxanthine are eluted at 15.2 and 15.4 min, respectively.

Ion-pairing reagents have also been used to improve chromatographic separations of theophylline. Muir et al. [15] first described an ion-pair liquid–liquid extraction followed by ion-pair gradient elution chromatography based on the utilization of tetrabutylammonium ion. This procedure is lengthy but, owing to its advantages, has been extensively used, and several modifications have been proposed to increase the selectivity and reproducibility [1,7]. However, the experimental conditions (pH, ionic strength, temperature) must be strictly controlled if reproducible results are to be obtained. Rapid degeneration of the column packing due to the ion-pairing reagents, is also a problem [7,16].

We have previously established the fundamentals of the H-point standard additions method [17,18] for LC [19], which permits the simultaneous analysis of binary mixtures with overlapped chromatographic peaks, with known spectral features. This paper demonstrates the possibilities of such a method for the simultaneous determination of theophylline and paraxanthine, using the chromatographic conditions applied for the determination of acetazolamide in a previous study [20]. This diuretic has been reported to interfere in many chromatographic determinations of methylxanthines, as they have similar polarities and tend to co-elute under reversed-phase conditions [21,22]. With the proposed elution profile, the resolution between acetazolamide and the main xanthines is complete and interference is avoided.

EXPERIMENTAL

Reagents

All the reagents were of analytical-regent grade except methanol and acetonitrile, which were of LC grade (Scharlau). Water was distilled, deionized and filtered through nylon membranes (0.45 μm) (Teknokroma). Theophylline (Fluka), paraxanthine (Sigma), caffeine (Aldrich) and theobromine (Sigma) standard solutions were prepared by dissolving the pure compounds in methanol. The internal standard was β-hydroxymethyltheophylline (Sigma). Propylamine hydrochloride (Fluka), sodium dihydrogenphosphate monohydrate (Merck) and, phosphoric acid (Probus) were also used.

Standard solutions

Standard solutions of theophylline, paraxanthine, caffeine and theobromine were prepared by dissolving 50 mg of the pure compound in 25 ml of methanol (2000 μg ml^{-1}). Working solutions were prepared daily by dilution of these stock solutions with the appropriate volumes of methanol. The internal standard was prepared by dissolving 25 mg of the pure compound in 500 ml of methanol (50 μg ml^{-1}). All the solutions were stored in the dark at 2°C.

Apparatus

A Hewlett-Packard Model 1040A liquid chromatograph, equipped with a diode-array detector linked to a data system (Hewlett-Packard Chem Station), was used for data acquisition and storage. The system was coupled to a quaternary pump (Hewlett-Packard, 1050 Series) with a 25-μl sample loop injector.

The column was HP-Hypersil ODS-C_{18} (5 μm; 250 mm × 4 mm i.d.). The detector was set to collect a spectrum every 640 ms (over the range 200–400 nm) and all the assays were done at ambient temperature.

Mobile phase

A phosphate buffer–acetonitrile gradient, with increasing acetonitrile content from 12% at time zero to 15% at 3 min and 40% at 5 min, was used. After 5 min the acetonitrile content was kept constant. The phosphate buffer was prepared by dissolving 3.45 g of sodium dihydrogenphosphate monohydrate in 500 ml of distilled, deionized water, after the addition of 0.7 ml of propylamine hydrochloride. The pH was adjusted

to 3 by adding the minimum amount of concentrated phosphoric acid. The solution was prepared daily, filtered through a nylon membrane (0.45 μm) (Teknokroma) and degassed with helium before use. The flow-rate was set at 1 ml min^{-1}. The chromatographic signal was monitored at 275 nm.

Sample treatment

Solid-phase extraction columns (Extra-Sep C_{18}, 200 mg, 3 ml) for sample treatment were previously conditioned by drawing through 1.0 ml of methanol, followed by 0.5 ml of distilled water. Urine samples (2.0 ml) were drawn through the columns, followed by washing with 0.5 ml of distilled water to eliminate the biological matrix. Xanthines were then eluted from the column with 1.0 ml of methanol and the extracts were evaporated to dryness with a stream of nitrogen. The residues were reconstituted with 300 μl of the internal standard solution. The resulting solutions were finally filtered through nylon filters (15 mm, 0.45 μm) (Teknokroma) and 5-μl volumes were injected into the column.

Recovery studies

Xanthine-free urine samples of 2.0 ml were spiked with theophylline or paraxanthine standard solutions, producing different concentrations in the therapeutic range. These samples were subjected to the previously described extraction procedure. The percentage of drug recovered for a particular extraction was calculated by comparing the peak areas obtained for the xanthine in the spiked samples (referred to the internal standard), with the peak areas obtained for a direct injection of 5 μl of methanolic solutions containing an equivalent amount of drug. Each concentration was assayed in duplicate.

H-point standard additions method

Volumes of 300 μl of methanolic standard solutions of the analyte were added to 2.0 ml of urine containing known amounts of theophylline and paraxanthine, producing concentrations in the therapeutic range. The resulting solutions were treated and chromatographed as described above.

A sample obtained 3 h after a single administration of 200 mg of theophylline, from a subject who had previously consumed caffeine was also analysed.

RESULTS AND DISCUSSION

The basis of the H-point standard additions method (HPSAM) for the treatment of chromatographic data [19] requires fixing two wavelengths λ_1 and λ_2, at which the interferent species should have the same absorbance. Because an additional variable, time, is involved in the chromatographic process, this must also be considered. The best time value will be the retention time of the analyte because it provides better sensitivity. Peak height (absorbance values), registered at the retention time of the analyte, is the chromatographic variable used to apply the HPSAM method.

Application of the HPSAM method at the two wavelengths will yield two straight lines:

$$A_{\lambda_1} = b + b_0 + M_{\lambda_1} C_i \quad (1)$$

$$A_{\lambda_2} = A' + A_0 + M_{\lambda_2} C_i \quad (2)$$

which intersect at point H $(-C_H, A_H) = (-C_X, A_Y)$, where b_0 and A_0 being the absorbances of the analyte at λ_1 and λ_2, measured at the retention time of the analyte for the solution containing sample alone ($i = 0$), respectively, b and A' are the absorbances of the species Y at the same wavelengths ($b = A'$), C_H is the existing concentration of the analyte in the sample (C_X) and A_H, the ordinate of the H point, is the analytical signal due to the interferent (A_Y) corresponding to λ_1 and λ_2, as the two wavelengths were chosen in such a way that the latter species have the same absorbance at both. This value makes possible the determination of the interferent from a calibration graph or even from the calibration method with a single standard.

Subsequently, the HPSAM method was applied to the simultaneous determination of theophylline and paraxanthine. Figure 1 shows chromatograms obtained for a methanolic standard solution of (1a), theophylline, (1b) paraxanthine

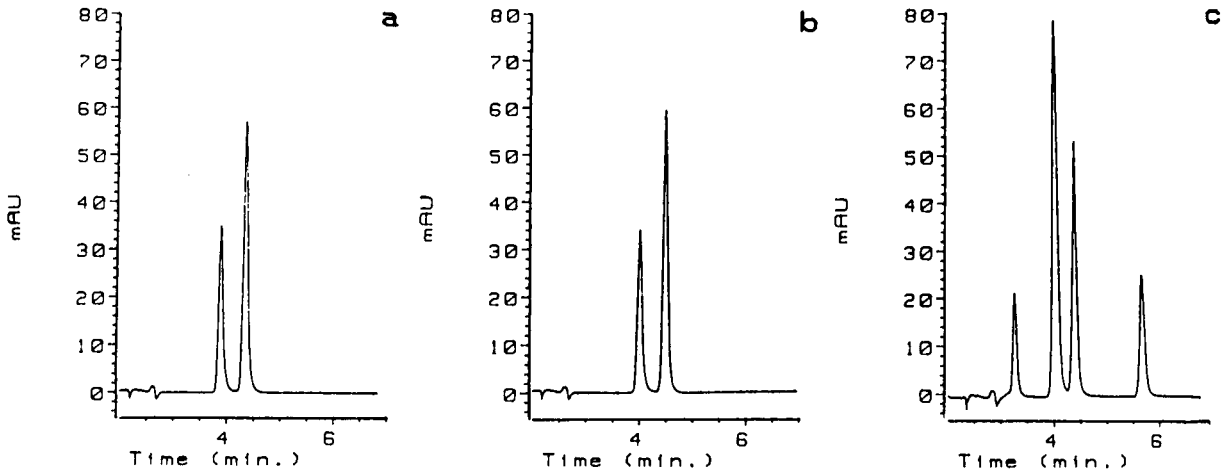

Fig. 1. Chromatograms at 275 nm of xanthines in methanol: (a) theophylline, $t_R = 4.0$ min; (b) paraxanthine, $t_R = 4.0$ min; (c) mixture of theobromine, $t_R = 3.3$ min, theophylline, paraxanthine and caffeine, $t_R = 5.8$ min. The concentration of each xanthine was 25 μg ml^{-1}. The peak at 4.5 min corresponds to the internal standard.

and (1c) a mixture of the main xanthines derived from caffeine.

With the sample treatment used, the determination is free from interferences from other endogenous compounds, as can be seen in Fig. 2, which shows the chromatogram of a blank urine sample. The percentages of drug recovered for both theophylline and paraxanthine at the different concentrations tested are given in Table 1. Significative differences between the different concentrations are not observed, and the mean recoveries obtained are 73 ± 5 and $75 \pm 4\%$ for theophylline and paraxanthine, respectively. These values are similar to those reported previously for urine samples [11,12].

The spectra of theophylline and paraxanthine are shown in Fig. 3 and are very similar. Therefore, the resolution of their chromatographic peaks is very difficult because the overlap is total.

Three pairs of wavelengths where, according to the HPSAM, the absorbance of the interferent is the same, were previously selected in order to test for the best pair. The selected wavelength pairs were 242–286, 254–282 and 258–278 nm for the determination of theophylline as analyte and 242–290, 254–286 and 258–282 nm for the determination of paraxanthine as analyte. The two compounds are determined with each other (exclusively) as interferent. Subsequently, the ab-

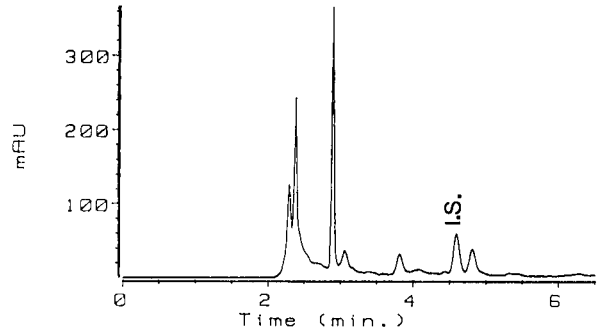

Fig. 2. Chromatograms at 275 nm of blank urine samples. I.S. = internal standard, $t_R = 4.5$ min.

TABLE 1

Recoveries of theophylline and paraxanthine at the different concentrations tested

Concentration (μg ml^{-1})	Recovery (%)	
	Theophylline	Paraxanthine
0.75	79	78
3.75	74	71
7.50	69	80
11.25	67	75
15.00	76	72
Mean	73 ± 5	75 ± 4

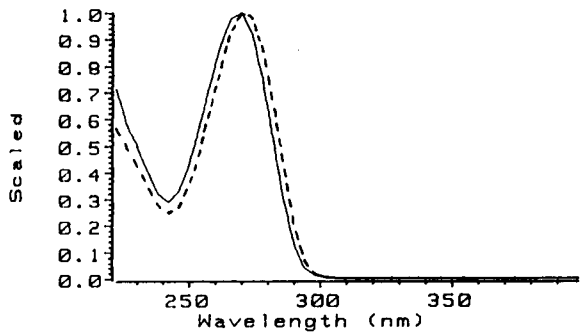

Fig. 3. Normalized adsorption spectra of (dashed line) theophylline and (solid line) paraxanthine.

sorbances at these wavelengths measured at t_R of the mixtures were utilized to construct the HPSAM plots.

Standard methanolic mixtures of theophylline and paraxanthine were initially tested to validate the applicability of the wavelengths chosen. The tested concentrations of both compounds, and the concentrations of analyte, were added so as to produce concentrations of urinary samples in the therapeutic range, after sample pretreatment.

Table 2 summarizes the different mixtures assayed and the concentrations of analyte and interferent found. The concentration of interferent was calculated in each sample by the calibration method with a single standard.

As can be seen from Table 2, when theophylline concentration is calculated as the analyte (samples 1–4), it is well determined at the three pairs of wavelengths tested if this concentration is similar to or higher than the concentration of paraxanthine. Even when the concentration of the interferent is ten times higher than the concentration of the analyte (sample 2), the results obtained are acceptable. When paraxanthine is determined in these samples as interferent, similar results are obtained. At low levels of paraxanthine (samples 1 and 3), the HPSAM method provides accurate results for a theophylline: paraxanthine concentration ratio of 5, but for a ratio of 50 the determination as interferent could be biased. The concentrations of paraxanthine obtained in samples 2 and 4 are good.

When paraxanthine is determined as analyte (samples 5 and 6), the method also provides ac-

TABLE 2

Concentrations of theophylline and paraxanthine for the different mixtures in methanol tested

Sample No.	Sample concentration (μg ml^{-1})		Concentration found (μg ml^{-1})					
	Analyte theophylline	Interferent paraxanthine	Analyte			Interferent		
			242–286 nm	254–282 nm	258–278 nm	242–286 nm	254–282 nm	258–278 nm
1	5	1	5.7 ± 0.4	6 ± 1	4.9 ± 0.7	1.6 [a]	0.7	1.1 ± 0.7
						0.43 [b]	0.64	0.9 ± 0.6
2	5	50	5.1 ± 0.3	5.3 ± 0.5	7.5	49 ± 2	46 ± 4	45 ± 3
						48.0 ± 0.4	50 ± 4	43 ± 3
3	50	1	53 ± 4	50 ± 2	50.7 ± 1.2	–	1	–
						–	0.9	–
4	50	50	52 ± 1	44 ± 7	46 ± 5	42	52 ± 6	44
						41	56 ± 6	43
	Analyte paraxanthine	Interferent theophylline	242–290 nm	254–286 nm	258–282 nm	242–290 nm	254–286 nm	258–282 nm
5	1	5	1.5 ± 0.5	1.8 ± 1.3	0.8	3.8 ± 0.1	3.9 ± 0.1	4.3 ± 0.7
						3.8 ± 0.1	4.1 ± 0.1	4.0 ± 0.5
6	50	50	53 ± 4	53 ± 2	46 ± 6	43 ± 4	39 ± 3	63 ± 2
						51 ± 5	43 ± 3	59 ± 2

[a,b] Values obtained at the two wavelengths of each pair of wavelengths used in the HPSAM and from the calibration method with a single standard.

ceptable results. Moreover, sample 5 is better resolved for both compounds using theophylline as analyte.

Figure 4 shows the HPSAM plots for samples (a) 1 and (b) 5. The sensitivity is better at 258–278 or 258–282 nm when theophylline or paraxanthine is added, respectively, as the absorbance for each analyte is higher at these wavelengths.

In Table 3 are summarized the concentration found for free urine samples spiked with different amounts of theophylline and paraxanthine. When low therapeutic levels of these xanthines are present (samples 1 and 2), the determination is only suitable at 258–278 or 258–282 nm when either theophylline or paraxanthine is used as the analyte because, as has been indicated previously, at these wavelengths the sensitivity is higher. The results obtained for both compounds are generally acceptable when they are determined as interferents.

The slopes for the calibration graphs obtained with urine samples are statistically equivalent to those obtained with standards in methanol if the mean percentage recovery is considered, hence the matrix of the sample does not modify the slope of the calibration graph obtained with standards. Thus, the results obtained for an unknown sample containing theophylline or paraxanthine will be unbiased.

The proposed HPSAM procedure was applied to the determination on theophylline in the presence of paraxanthine in a sample obtained from a subject 3 h after a single administration of theophylline (200 mg). The chromatogram obtained for this sample is shown in Fig. 5. The concentrations of theophylline and paraxanthine were obtained by constructing two H-point standard addition graphs. In each instance, the analyte concentration was calculated directly from the method, which also provides $A_H = A_Y$. The interferent concentration was calculated from that value and from the calibration method with a single standard. The values obtained at the two pairs of wavelengths which proportionate suitable measurements of the analytical signal for the application of the method are given in Table 4. The results obtained are similar when determining theophylline either as analyte (when this compound is added) or as interferent (from the A_H value obtained when paraxanthine is added). The same conclusions can be derived for paraxanthine. The concentration found is the existing

TABLE 3

Concentrations of theophylline and paraxanthine for the different spiked urine samples tested

Sample No.	Sample concentration (μg ml^{-1})		Concentration found (μg ml^{-1})					
	Analyte theophylline	Interferent paraxanthine	Analyte			Interferent		
			242–286 nm	254–282 nm	258–278 nm	242–286 nm	254–282 nm	258–278 nm
1	4	8	–	3.1	3.7	–	6.1 [a]	5.3
						–	6.9 [b]	5.4
2	8	4	–	7.4	8.3	–	3.0	3.0
						–	3.5	3.7
3	15	5	13.4	12.5	16.0	6.0	5.5	4.1
						5.8	6.1	4.0
	Analyte paraxanthine	Interferent theophylline	242–290 nm	254–286 nm	258–282 nm	242–290 nm	254–286 nm	258–282 nm
1	8	4	–	9.9	7.8	–	2.7	3.6
						–	2.3	3.4
2	4	8	–	5.9	4.4	–	6.5	8.1
						–	7.7	7.9
3	5	15	–	–	4.5	–	–	12.2
								11.9

[a,b] Values obtained at the two wavelengths of each pair of wavelengths used in the HPSAM and from the calibration method with a single standard.

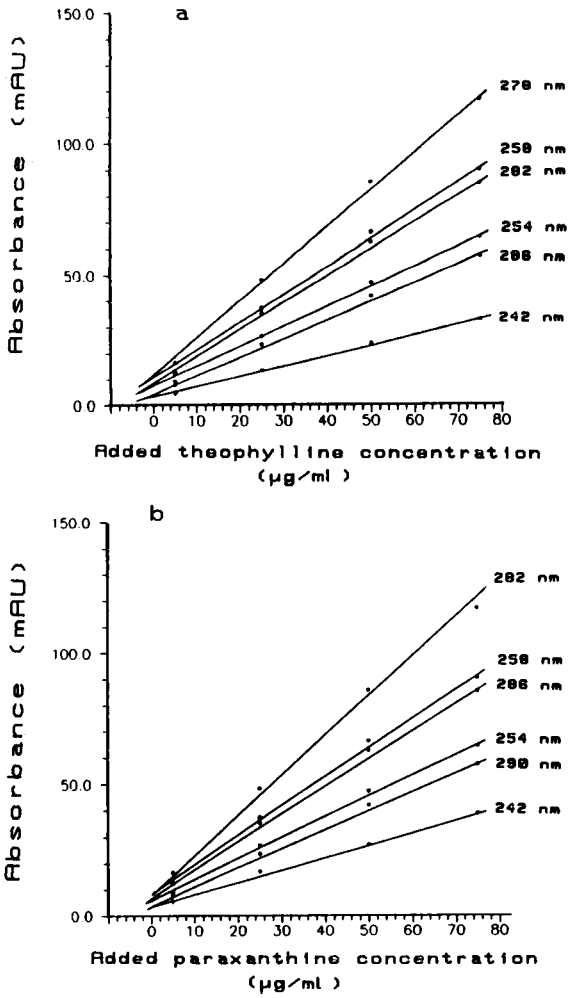

Fig. 4. HPSAM plots for (a) theophylline in sample 1 and (b) paraxanthine in sample 5.

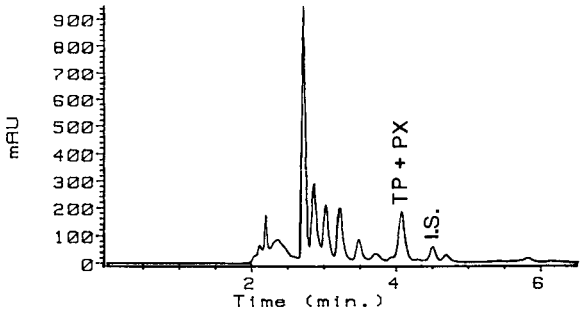

Fig. 5. Chromatogram at 275 nm of a sample obtained from a subject 3 h after a single administration of theophylline (200 mg) Peaks: TP = theophylline; PX = paraxanthine; I.S. = internal standard.

TABLE 4

Concentrations of theophylline and paraxanthine for a urine sample 3 h after a single administration of theophylline

Compound	Concentration found (μg ml^{-1})	
	258–278 nm	258–282 nm
Theophylline	6.0	5.9, 5.6 [a]
Paraxanthine	8.3, 8.2 [a]	7.1

[a] Values obtained at the two wavelengths of each pair of wavelengths used in the HPSAM and from the calibration method with a single standard.

concentration of the analyte in the sample as the fundamentals of the H-point standard additions method demonstrate [17–19]. The theophylline concentration found is in agreement with previously published pharmacokinetic values.

Conclusions

The described procedure provides good results for the simultaneous determination of theophylline and paraxanthine in urine samples by conventional reversed-phase LC. As paraxanthine is pharmacologically active, its determination may be required in either theophylline or caffeine therapeutic drug monitoring [14].

Although the chromatographic peaks of these compounds are completely overlapped and their spectra are very similar, their concentrations can be determined with suitable accuracy and precision at therapeutic levels. The resolution of the samples, even when the concentration of one of the components is many times higher than that of the other, requires a unique set of experiments by applying the HPSAM method. At very low therapeutic levels, two H-point standard addition plots might be required if it is necessary to determine both compounds, owing to the small values of A_H. The total time of analysis is short owing to the rapid pretreatment of the samples and the short retention times involved.

The authors are grateful to the DGICYT for financial support received for the realization of Project PB 88-0495.

REFERENCES

1 J.J. Lauff, J. Chromatogr., 417 (1987) 99.
2 J. Fitzpatrick and M. McClelland, Ann. Clin. Biochem., 20 (1983) 123.
3 D.B. Haughey, R. Greenberg, S.F. Schaal and J.J. Lima, J. Chromatogr., 229 (1982) 229.
4 C.N. Ou and V.L. Frawley, Clin. Chem., 29 (1983) 1934.
5 R. Hartley, I.J. Smith and J. Cookman, J. Chromatogr., 342 (1985) 105.
6 J. Moncrieft, J. Chromatogr., 568 (1991) 177.
7 N. Grgurinovich, J. Chromatogr., 380 (1986) 431.
8 P. Van Aerde, E. Moerman, R. Van Seeveren and P. Braeckman, J. Chromatogr., 222 (1981) 467.
9 L. Ferron, J. Weber, J. Hébert and P. Bédard, Clin. Chem., 31 (1985) 1415.
10 R. Hartley, J.R. Cookman and I.J. Smith, J. Chromatogr., 306 (1984) 191.
11 E. Naline, B. Flouvat, C. Advenier and M. Pays, J. Chromatogr., 419 (1987) 177.
12 R. Chiou, R.J. Stubbs and W.F. Bayne, J. Chromatogr., 422 (1987) 281.
13 P. Parra, A. Limon, S. Ferre, T. Guix and F. Jane, J. Chromatogr., 570 (1991) 185.
14 T.E.B. Leakey, J. Chromatogr., 507 (1990) 199.
15 K.T. Muir, J.H.G. Jonkman, D.S. Tang, M. Kunitani and S. Riegelman, J. Chromatogr., 221 (1980) 85.
16 S.A. Hotchkiss and J. Caldwell, J. Chromatogr., 423 (1987) 179.
17 F. Bosch-Reig and P. Campíns-Falcó, Analyst, 113 (1988) 1011.
18 F. Bosch-Reig and P. Campíns-Falcó, Analyst, 115 (1990) 111.
19 P. Campíns-Falcó, F. Bosch-Reig, R. Herráez-Hernández and A. Sevillano-Cabeza, Anal. Chim. Acta, 257 (1992) 89.
20 P. Campíns-Falcó, R. Herráez-Hernández and A. Sevillano-Cabeza, J. Chromatogr., submitted for publication.
21 J. Gal, P.P. Ellis and M. Rendi, Curr. Eye Res., 1 (1981) 361.
22 R. Hartley, M. Lucock, M. Becker, I.J. Smith and I.W. Forsythe, J. Chromatogr., 377 (1986) 295.

Analytica Chimica Acta, 268 (1992) 81–94
Elsevier Science Publishers B.V., Amsterdam

Application of chemometrics for the selection of microwave digestion procedures

S. Kokot

School of Chemistry, Queensland University of Technology, Brisbane (Australia)

G. King

Government Chemical Laboratories, Kessels Rd., Cooper's Plains, Brisbane (Australia)

H.R. Keller and D.L. Massart

Farmaceutisch Instituut, Vrije Universiteit Brussel, Laarbeeklaan 103, Brussels (Belgium)

(Received 16th December 1991; revised manuscript received 7th May 1992)

Abstract

The application of four chemometrics procedures viz., principal components analysis, SIMCA, multicriteria decision-making routines PROMETHEE and GAIA, and fuzzy clustering, was investigated for the selection of a suitable microwave digestion method for sediment and rock samples. The NBS 2704 SRM and a secondary rock standard were acid digested by 15 different methods and the digests analysed for six metals, Cu, Pb, Ni, Cr, Co and Zn. The four chemometrics approaches produced consistent results and provided similar information about the data structure (outliers, groupings, trends). Only the PROMETHEE procedure gave the ranking information necessary for the selection of a suitable digestion method. This method was based on the HF–HNO_3 acid composition of the digest mixture.

Keywords: Chemometrics; Fuzzy clustering; Microwave digestion

Sample preparation is important in any analysis and should be performed so that the integrity of the starting material is preserved. Ideally the preparative procedures should be optimised with respect to analytical criteria (e.g., accuracy, precision) and practical considerations (e.g., quantities of reagents, digestion time). For analyses of soils and similar materials, microwave–acid digestion methods have been frequently used to dissolve the samples [1–9]. Digestion recipes often (i) vary in the type and proportions of reagents used, and (ii) have different recommendations for microwave oven settings and conditions. Attempts to provide guidelines for the selection of suitable methods have been sparse [10].

Recently Feinberg [11] has catalogued outlines of some 780 microwave digestion procedures for a variety of materials including a small number of rocks and soils (24 cases). This database was statistically analysed (box plots and correspondence factor analysis) and qualitative method selection guidelines were proposed on the basis of reagents and microwave digestion conditions most preferred by the users. Kokot et al. [12] have investigated the results of metal analyses of the NBS 2704 (Buffalo River Sediment) SRM, samples of which were microwave digested using 17

Correspondence to: S. Kokot, School of Chemistry, Queensland University of Technology, Brisbane (Australia).

different acid–additive combinations. In this study a systematic chemometrics approach based on the application of exploratory principal components analysis (PCA) and the multicriteria decision making (MDM) techniques, PROMETHEE (Preference Ranking Organization METHod for Enrichment Evaluation) and GAIA (Geometrical Analysis for Interactive Aid), demonstrated how it is possible to rank digestion methods according to a chosen set of criteria. The PCA analysis was used to polish the data set, to remove the outliers and reveal any clustering. The PROMETHEE and GAIA routines were then applied to rank the methods retained in the polished data set. The qualitative conclusions of the PCA and the MDM ranking results were found to be consistent.

There are many statistical approaches that can be used to assist with the selection of a method of digestion. In the present study we examine the application of several chemometrics procedures for the selection of a suitable method of digestion of sediment or rock samples. Apart from the exploratory PCA and the MDM approaches, the results of SIMCA (Soft Independent Modelling of Class Analogies) and fuzzy clustering (FC) are included for comparison. The last two methods are examples of classification procedures with SIMCA representing the supervised modelling methods, i.e., those for which a-priori information about sample classification is available, and FC, the unsupervised modelling approach. Both of these methods attempt to characterise data by subdividing it into classes consisting of members with similar properties. These approaches should provide information about the underlying features of the methods of digestion data structure. The consistency of conclusions for the selection of the most suitable method of digestion by the four chemometrics procedures viz., PCA, MDM, SIMCA and FC, are assessed. The problem under consideration is typical of many practical multivariate cases in analytical chemistry and some guidelines for the application of chemometrics are suggested.

The solid materials used in this work were the NBS 2704 Buffalo river sediment and a secondary rock standard (BSR) produced and frequently used for metal analysis calibration in the Queensland Government Chemical Laboratories. Thus the BSR material may be considered as a typical example of rock or soil samples processed in large multipurpose laboratories. The proposed

TABLE 1

Acid digest compositions and microwave oven settings

Method [a]	Acid	Mixture	Step 1		Step 2		Step 3		Total time (min)	H_3BO_3	Vent
			Power (%)	t (min)	Power (%)	t (min)	Power (%)	t (min)			
2A	$HF-HNO_3-HCl$	5:2:2	100	8	50	15	0	0	23	yes	–
2B	HNO_3	–	100	8	50	15	0	0	23	–	–
4A	$HF-HNO_3-HCl$	2:5:5	100	10	75	20	25	5	35	yes	–
4B	$HF-HNO_3$	2:5	100	10	75	20	25	5	35	yes	–
4C	HNO_3-HCl	1:3	100	10	75	20	25	5	35	–	–
6A	$HF-HNO_3-HCl$	1:1:1	100	10	65	20	30	5	35	yes	–
7A	HNO_3-HCl	1:3	100	10	70	20	25	5	35	–	–
8A	$HF-HNO_3-HCl$	5:2:2	100	15	0	0	0	0	15	–	yes
8B	$HF-HNO_3-HCl$	5:17:17	100	15	0	0	0	0	15	–	yes
8C	$HF-HNO_3-HCl$	5:9:27	100	15	0	0	0	0	15	–	yes
11A	$HNO_3-H_2O_2$	5:1	100	10	70	20	25	5	35	–	–
11B	$HNO_3-H_2O_2-HF$	5:1 + 4 ml	100	10	70	20	25	5	35	–	–
12	$HNO_3-H_2O_2-HF$	5:1 + 4 ml	100	10	70	20	25	5	35	yes	–
13	Acetic	10 ml	100	10	70	20	25	5	35	–	–

[a] The digestion methods for the NBS 2704 and BSR materials are the same. To denote a BSR method a 'b' is added to the label, e.g., 2Ab. The hot plate method of digestion is denoted by HP.

metal values for this material, although not strictly certified, may be regarded as a model set of well defined within laboratory data.

Analytical results for Cu, Pb, Ni, Cr, Co and Zn from different digests of both materials were used in this work.

EXPERIMENTAL

Details of instrumentation, experimental procedures, reagents and samples have been described elsewhere [12]. In this paper only the essential experimental aspects or new features are included.

Microwave oven procedure

A CEM MDS-81D microwave oven operating at a frequency of 2450 ± 13 MHz with an energy output of 0–630 ± 70 W was used for the acid digestions. The experiments were always carried out with a full complement of 12 low pressure (830 ± 70 kPa) screw-top PTFE digestion vessels.

Microwave digestion

For each digestion, 1 g of sample was accurately weighed into a PTFE digestion vessel, the

TABLE 2

Metal content (ppm) in NBS 2704 and BSR materials as determined from various acid digests

Sample type	No.	Method [a] label	Cu	Pb	Ni	Cr	Co	Zn
NBS	1	2A	96.2	147	35	115	18	448
2704	2	2B	103	155	36	104	12.6	441
	3	4A	99.5	166	35	134	15	432
	4	4B	91.4	159	35	131	16	433
	5	4C	106	162	36	111	13.6	425
	6	6A	103	145	14	137	13.7	432
	7	7A	96.8	155	37.6	104	12.8	425
	8	8A	90	47.5	33.4	121	11	271
	9	8B	98	159	39.4	132	13	421
	10	8C	99	164	39	129	13	435
	11	11A	96.6	159	39	105	12	422
	12	11B	88	150	36	112	15	422
	13	12	96.6	126	32	135	14	386
	14	13	49.3	97.6	9	56	4	258
	15	HP	98.5	149	27.9	100	4	413
BSR	16	2Ab	89.5	107.7	117.7	156.6	51.9	150
	17	2Ab	94.6	94.6	98.6	88.6	45.5	103
	18	4Ab	86.8	128	114	196	49.7	148
	19	4Bb	89.2	115	113	186	52.8	144
	20	4Cb	80.9	92.9	95.9	131	48.9	130
	21	6Ab	91.9	117	114	193	54.5	142
	22	7Ab	88	85	100	131	45	136
	23	8Ab	89	46	110	166	48	136
	24	8Bb	147	51	192	116	128	89
	25	8Cb	94.5	132	121	193	49	147
	26	11Ab	87	91	98	98	42	103
	27	11Bb	83	111	111	166	52	143
	28	12b	90	104	112	173	48	127
	29	13b	71	34	11	19	22	33.5
	30	HPb	92.6	80.7	105	135	44.4	123
Refs.	31	NBS 2704	98.6 ± 5	161 ± 17	44.0 ± 3	135 ± 5	14 ± 0.6	438 ± 12
	32	BSR	89 ± 7	104 ± 8	107 ± 7	189 ± 18	50 ± 6	138 ± 9

[a] See footnote to Table 1.

acids were added and the mixture processed. The digests were diluted to 100 ml with deionised water.

The details for the 14 microwave procedures used in this work are summarised in Table 1.

In general, 10 ml of an acid mixture was added to a sample, however, for vented samples (8A, 8B, and 8C) more acid was included to prevent evaporation to dryness.

Procedural variations

In the venting experiments the pressure was allowed to build up in the digestion vessel beyond the 830 kPa, thus causing the pressure relief valve to open.

When boric acid was used, it was added (40 ml 4% H_3BO_3 solution) after a sample was submitted to a particular microwave digestion procedure. The vessel was then further heated in the microwave oven. After cooling, digests were made up to 100 ml with deionised water.

For hot plate digestion a sample was accurately weighed (1 g) into a conical flask and digested with 10 ml of aqua regia for at least 1 h until complete dissolution. The digests were made up to 100 ml with deionised water.

Materials

BSR material is an in-house (Government Chemical Laboratory, Brisbane), secondary quality control rock standard. This rock sample (1 g) is usually acid digested (10 ml HF–HNO_3–HCl {5:2:2}) for 4 h at 90°C. Boric acid is added and the digest made up to 100 ml with deionised water. Such digests are analysed by atomic absorption spectroscopy. The proposed metal analysis values (Table 2) consist of the means and standard deviations obtained from at least 60 results for each metal.

Instrumentation

A Varian SpectrAA 300 and a VarianAA 400 Zeeman graphite tube atomizer were available for flame atomic absorption (FAA) analysis and graphite furnace analyses respectively.

Standards and sample analysis

Mixed metal standards were prepared from the spectroscopically pure 1000 mg l^{-1} stock solutions and were appropriately diluted. The composition and preparation of various standards is detailed elsewhere [12].

Generally Cu, Pb, Cr and Zn were determined using FAA with instrumental parameters being adjusted as suggested by the instrument manufacturer [13]. Co and Ni were determined using a Lvov platform and the instrumental parameters were consistent with common practice [14,15].

CHEMOMETRICS METHODS

In this paper only outlines of the four chemometrics approaches will be provided. Detailed mathematical treatments as well as applications tutorials may be found in the referenced literature.

PCA

PCA is a well known chemometrics technique for multivariate data investigations [16]. Examples of tutorials and applications are readily available [e.g., 17,18]. PCA effects multivariate data reduction by transforming the data into orthogonal components which are linear combinations of the original variables. Each component is characterised by scores and loadings. The former are the projections of objects onto a particular component and the latter reflect the contribution of each variable to a particular component.

Principal components (PCs) are computed in such a way that the first PC accounts for the largest amount of variation in the data set while subsequent components describe progressively decreasing amounts of the data variance.

PCA is an especially useful method for investigating clustering and outlier features in the data. This may be achieved efficiently using a biplot [19] which displays simultaneously, suitably scaled scores and loadings in a PC plane (usually PC1 vs. PC2).

SIMCA

SIMCA is a well known supervised data classification approach [16,20,21]. For this method, a selected set of objects characterised by data from a set of variables is called a class and is submitted

to PCA. A PC class model is then defined using for example, the cross-validation procedure [22]. The shape of a class will depend on the number of components used in the model, e.g., a cylinder (2 PCs) or a rectangular box (3 PCs). The data for each object in a class is partitioned into information that is explained by the class model and into residuals which describe the non-systematic variance. Residual standard deviations (R.S.D.) are computed for a class as a whole and for each object. The former measures the mean distance between the objects of a class and the class model; the latter measures the orthogonal distance between the object and the class model. This R.S.D. indicates how well the object is explained by the class. If the residuals are assumed to be normally distributed, a critical F ratio for a selected level of significance may be computed and this in turn will yield the critical distance ($R.S.D._{crit}$), which defines the class boundaries.

PROMETHEE and GAIA

PROMETHEE is a procedure which is designed to rank a number of actions (objects) in the context of constraints present in or imposed on the data. The ordering is performed according to a set of user supplied preference conditions which are applied to the criteria (variables).

PROMETHEE and GAIA have been described [23,24] and chemical applications have been recently reported [12,25]. The PROMETHEE procedure is summarized as follows: for each criterion all the entries in the data matrix are compared pairwise in all possible combinations by subtraction, resulting in a difference, d, for each comparison. A preference function is then used to allocate a preference value for each difference, thus producing a preference table. Global preference indices are computed by summing all the preferences for each action. The positive and negative outranking flows, $\phi+$ and $\phi-$ are calculated from the preference indices refining the preference structure. The $\phi+$ values indicate how each action outranks all the others, while the $\phi-$ values show how each action is outperformed by all the others. With the help of a set of simple rules [25], the outranking flows may be compared to produce a partial rank order according to 3 possible results:

(i) one action is preferred to another,
(ii) there is no difference between actions,
(iii) actions cannot be compared.

This procedure is called PROMETHEE I. Its results are best demonstrated by a flow chart such as Fig. 7. In an attempt to eliminate the indecisive result, (iii), and to produce a simple ranking scale, a net outranking flow value, ϕ, for each action may be computed by taking the difference between the associated positive and negative outranking flows. This procedure is termed PROMETHEE II. Although such a scale is convenient and intuitively desirable, it can produce results which are less reliable than those from PROMETHEE I.

GAIA is a method for investigating the PROMETHEE results. The net outranking flows, ϕ, are decomposed such that a data table suitable for PCA is formed. The results are presented on a biplot with properties similar to those already outlined. This display method facilitates the interpretation of the significance of the criteria; an additional feature is the inclusion of the decision axis, π, which provides some information about the degree of decision power and indicates the approximate location of the preferred actions.

Fuzzy clustering

Fuzzy clustering is a non hierarchical cluster method, i.e., clusters are not formed either by agglomerating small clusters into larger ones or conversely subdividing large clusters.

In conventional classification the location of a member of a data set is defined uniquely, i.e., a member is assigned to one class only. Its membership of any other class is zero. The fuzzy clustering approach [26,27] attempts to assign a degree of class membership for a given object over several classes. The classification is performed with the aid of a membership function which may be specified, e.g., $m(x) = 1 - c\,|\,x - a\,|^{\mathbf{p}}$, where a and c are constants and $\mathbf{p}$ is positive, or constructed with reference to the data. The result is a table in which a membership value for each class is assigned for each object. The sum of the membership values for each object is 1.

The main advantage of such a procedure is that it facilitates the distinction between objects that clearly belong to one cluster (membership value of 1 or close to 1) and those that are members of several clusters (membership value of 1/(no. of clusters)).

DATA TREATMENT

Data matrix

The analytical data matrix (Table 2) consists of 6 columns of determinations for the elements Cu, Pb, Ni, Cr, Co and Zn respectively and 32 rows; the first fifteen of these correspond to the different digestion methods for the NBS 2704 SRM and rows 16–30 for the BSR secondary standard; the last two rows (NBS 2704 and BSR) contain the certified [28] and the proposed values of the analytes together with their associated uncertainties.

As previously reported [12], this data was transformed into a table of residual values (Table 3) to facilitate comparisons.

$$R = |(A - C)/U| \quad (1)$$

where A = the analytical result of a selected metal from a particular digest; C = the corresponding certified or proposed value of the selected metal; U = the uncertainty for the selected metal as

TABLE 3

Residuals for the NBS 2704 and BSR materials

Sample type	No.	Method [a] label	Cu	Pb	Ni	Cr	Co	Zn
NBS	1	2A	0.480	0.824	3.033	4.000	6.667	0.833
2704	2	2B	0.880	0.353	2.700	6.200	2.333	0.250
	3	4A	0.180	0.294	3.033	0.200	1.667	0.500
	4	4B	1.440	0.118	3.033	0.800	3.333	0.417
	5	4C	1.480	0.059	2.700	4.800	0.667	1.083
	6	6A	0.880	0.941	10.033	0.400	0.500	0.500
	7	7A	0.360	0.353	2.167	6.200	2.000	1.083
	8	8A	1.720	6.676	3.567	2.800	5.000	13.917
	9	8B	0.120	0.118	1.567	0.600	1.667	1.417
	10	8C	0.080	0.176	1.700	1.200	1.667	0.250
	11	11A	0.400	0.118	1.700	6.000	3.333	1.333
	12	11B	2.120	0.647	2.700	4.600	1.667	1.333
	13	12	0.400	2.059	4.033	0.000	0.000	4.333
	14	13	9.860	3.729	11.700	15.800	16.667	15.000
	15	HP	0.020	0.706	5.400	7.000	16.667	2.083
BSR	16	2Ab	0.071	0.463	1.529	1.800	0.317	1.333
	17	2Bb	0.800	1.175	1.200	5.578	0.750	3.889
	18	4Ab	0.314	3.000	1.000	0.389	0.050	1.111
	19	4Bb	0.029	1.375	0.857	0.167	0.467	0.667
	20	4Cb	1.157	1.388	1.586	3.222	0.183	0.889
	21	6Ab	0.414	1.625	1.000	0.222	0.750	0.444
	22	7Ab	0.143	2.375	1.000	3.222	0.833	0.222
	23	8Ab	0.000	7.250	0.429	1.278	0.333	0.222
	24	8Bb	8.286	6.625	12.143	4.056	13.000	5.444
	25	8Cb	0.786	3.500	2.000	0.222	0.167	1.000
	26	11Ab	0.286	1.625	1.286	5.056	1.333	3.889
	27	11Bb	0.857	0.875	0.571	1.278	0.333	0.556
	28	12b	0.143	0.000	0.714	0.889	0.333	1.222
	29	13b	2.571	8.750	13.714	9.444	4.667	11.611
	30	HPb	0.514	2.913	0.286	3.000	0.933	1.667

[a] See footnote to Table 1.

given in the last two rows of Table 2; R = residual.

All data were processed using an IBM PS/2 model 55 computer. The analytical data matrix (Table 2) was manipulated using the Excel 3.0 spreadsheet from which the residuals data (Table 3) was exported to SIRIUS (PCA, SIMCA, FC) [29] and PROMCALC (PROMETHEE and GAIA) [30] for analysis.

PCA data pretreatment

It is generally recommended for PCA work to standardise the variables to unit variance. As previously indicated [12], in the present case the size of the variance reflects the analytical performance of the digestion methods. Consequently, the data was investigated without any pretreatment.

SIMCA class modelling

In general, for the classes constructed from the data matrices, 2 or 3 PCs were sufficient to account for approximately 95% of the variance. Therefore class models were constructed usually from 3 and occasionally from 2 PCs. The more commonly used cross-validation method for the selection of the significant PCs was unsuccessful.

PROMETHEE conditions

The 6 criteria representing the different metals were equally weighted and set to "minimise". The latter condition denotes that lower residual values indicate better performing methods of digestion and are to be preferred. The preference function selected was:

$$P = 1 \quad \text{for } d \leq z \tag{2}$$

$$P = d/z \quad \text{for } 0 < d < z \tag{3}$$

$$P = 0 \quad \text{for } d \geq 0 \tag{4}$$

where d is the difference for each pairwise comparison.

The threshold (z) was set to -1, i.e. equal to one uncertainty unit for the residuals. The negative sign indicates that in a comparison the smaller of the two residual values is preferred as required by the "minimise" condition.

Typical results are shown in a preference flow chart (Fig. 7). The general rules for interpreting such a flow chart are:

(i) actions that are comparable are joined by one or more arrows,

(ii) any comparable action to the left of another is preferred,

(iii) any actions that are incomparable remain unconnected.

Fuzzy clustering

In SIRIUS the cluster membership function is unknown, however, in order to find the best cluster subdivision it is possible to vary the value of the weighting exponent which affects the degree of fuzziness. The suggested exponent range is 1.5–3; values closer to 1 give harder clustering while higher values favour the membership of the fuzziest state. A value of 2.5 was used on all data sets investigated. It was chosen because it gave membership values that were distributed over the 0–1 membership scale, however, the clustering of the principal members of each class still remained clearly evident.

RESULTS AND DISCUSSION

Preliminary investigations

The NBS 2704 and BSR data sets were submitted separately for analysis by PCA, MDM and FC. SIMCA which required a-priori class information was used to test some of the findings of these analyses.

PCA biplots (PC1 vs. PC2) of the two data sets showed that in each case, the scores (digestion methods) were collected in a comparatively tight cluster but also several outliers were clearly distinguished. For example, Method 13 (acetic acid), which was included as a marker outlier because of its extractive rather than digestive qualities, was clearly an outlier on both biplots. On each of these the influence of the outliers on the data structure was reflected in the location of the loadings (the metals) between the one cluster and the outliers. In contrast, when the outliers were eliminated to produce the polished data sets, most of the metals were located in close proxim-

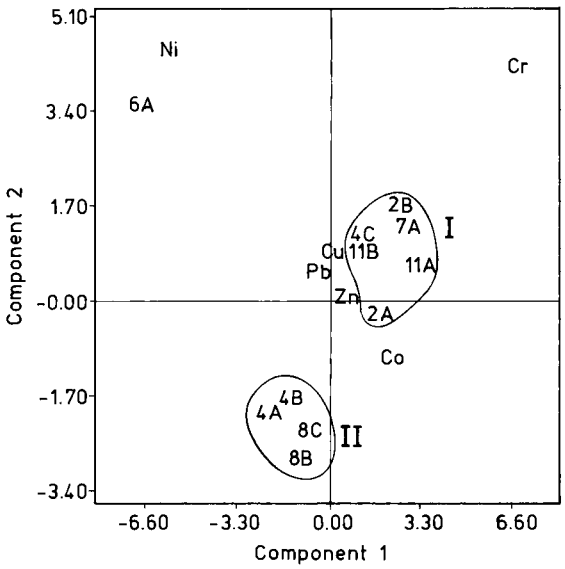

Fig. 1. Biplot for the polished data set from metal-analysis results of differently digested NBS 2704 SRM samples; objects are methods of digestion; variables are the metals. Method labels refer to Table 1.

ity to the objects (Figs. 1 and 2). The selected outlier methods of digestion are listed in Table 4 where they are compared with results from

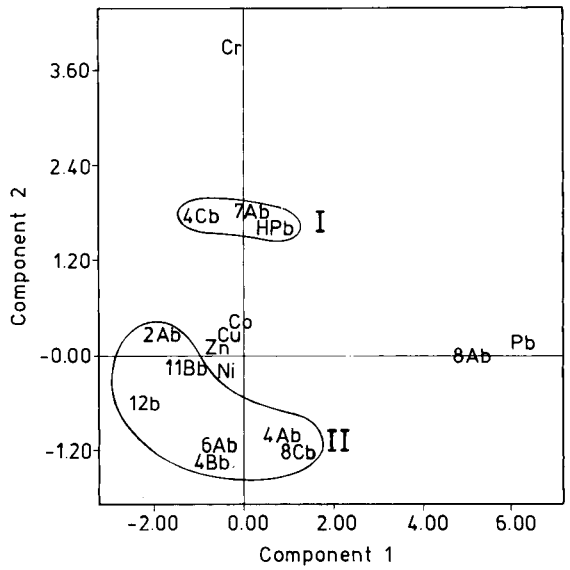

Fig. 2. Biplot for the polished data set from metal-analysis results of differently digested BSR secondary standard samples; objects are methods of digestion; variables are the metals. Method labels refer to Table 1.

TABLE 4

Comparison of outliers selected by the four chemometrics procedures

Sample type	PCA [a]	MDM [b]	FC [c]	SIMCA	
NBS	8A	Selected	Marginal	R.S.D. (crit)	8.41
2704	12	Selected	Not selected	= 0.91 [d]	2.36
	13	Selected	Selected		11.1
	HP	Selected	Selected		3.21
BSR	2Bb	Selected	Not selected	R.S.D. (crit)	1.7
	8Bb	Selected	Selected	= 0.70 [d]	11.2
	11Ab	Selected	Not selected		1.8
	13b	Selected	Selected		11

[a] See footnote to Table 1. [b] Worst performing digestion methods according to PROMETHEE II ranking and the GAIA biplots for each sample type. [c] These digestion methods were the principal members of one of the clusters in the 2 cluster model. [d] R.S.D. (crit) indicates the class boundaries of the training sets.

PROMETHEE II (Table 5) and from the two cluster model FC (Table 6). The last column in Table 4 shows the SIMCA results after the outliers indicated by the exploratory PCA were submitted for comparison with classes containing methods of digestion from the polished data sets. The results from three of the four chemometrics procedures are consistent and on this basis the outliers indicated by the exploratory PCA, were removed from the two data sets.

The outliers were also distinguished on the GAIA biplot as illustrated in Fig. 3 for the BSR results. In this and the NBS 2704 biplot, the 4 chosen outlier methods of digestion are located on the left of the graph, i.e, on the side opposite to the direction of the decision axis, π, and well removed from the location of the better performing digestion methods on the right. These observations suggest that the exploratory PCA may be unnecessary and that PROMETHEE results in conjunction with GAIA may be sufficient to indicate any atypical samples.

Data trends

Each of the PCA plots for the polished data sets (Figs 1 and 2) shows an atypical method of digestion, 6A and 8Ab respectively. Both digestion methods were members of the clusters char-

TABLE 5

PROMETHEE II ranking for complete NBS 2704, BSR and polished combined data.

Rank	Combined set (polished)		NBS 2704		BSR	
	Method [a] label	ϕ	Method [a] label	ϕ	Method [a] label	ϕ
1	12Bb	0.35	8C	0.52	4Bb	0.43
2	4Bb	0.34	8B	0.43	12b	0.42
3	6Ab	0.25	4A	0.40	11Bb	0.32
4	8Ab	0.25	6A	0.15	6Ab	0.31
5	11Bb	0.22	4C	0.13	8Ab	0.27
6	8C	0.21	7A	0.13	4Ab	0.23
7	4Ab	0.16	4B	0.12	2Ab	0.22
8	2Ab	0.14	11A	0.10	7Ab	0.12
9	4A	0.12	2B	0.08	8Cb	0.02
10	7Ab	0.10	12	0.03	4Cb	−0.02
11	8B	0.09	2A	−0.06	HPb	−0.05
12	6A	−0.01	11B	−0.10	2Bb	−0.22
13	8Cb	−0.02	HP	−0.40	11Ab	−0.26
14	4Cb	−0.11	8A	−0.54	8Bb	−0.83
15	HPb	−0.14	13	−0.96	13Bb	−0.95
16	4B	−0.16				
17	7A	−0.23				
18	4C	−0.23				
19	2B	−0.24				
20	11A	−0.25				
21	2A	−0.35				
22	11B	−0.49				

[a] See footnote to Table 1.

TABLE 6

Fuzzy clustering analysis of the complete NBS2704 and BSR data using the 2 cluster model.

NBS 2704			BSR		
Method [a] label	Membership values		Method [a] label	Membership values	
	Major Cluster	Outliers		Major Cluster	Outliers
2A	0.86	0.14	2Ab	0.96	0.04
2B	0.91	0.09	2Bb	0.85	0.15
4A	0.93	0.07	4Ab	0.95	0.05
4B	0.94	0.06	4Bb	0.95	0.05
4C	0.94	0.06	4Cb	0.96	0.04
6A	0.79	0.21	6Ab	0.95	0.05
7A	0.91	0.09	7Ab	0.96	0.04
8A	0.51	0.49 [b]	8Ab	0.84	0.16
8B	0.93	0.07	8Bb	0.20	0.80 [b]
8C	0.94	0.06	8Cb	0.93	0.07
11A	0.90	0.10	11Ab	0.86	0.14
11B	0.95	0.05	11Bb	0.96	0.04
12	0.86	0.14	12b	0.94	0.06
13	0.17	0.83 [b]	13	0.18	0.82 [b]
HP	0.45	0.55 [b]	HPb	0.96	0.04

[a] See footnote to Table 1. [b] Indicates the principal methods of a cluster.

acterising the two biplots of the complete data sets which included the outliers. Given this and the small size of the polished data sets, these two methods were retained. The other objects appear to cluster in at least two groups (I and II, Figs. 1 and 2). Reference to Table 1 indicates that clusters marked 'I' predominantly consist of digestion methods with acid mixtures that do not contain HF. This indicates a discrimination on the basis of the presence of HF in the acid mixture. This is consistent with our previous findings [12] which were obtained from a smaller set of data using a different metal suite, Cu, Pb, Co, Mn and Zn. Two digestion methods, 11B and 2A, present in cluster I, Fig. 1, are apparently atypical because HF was initially included in their acid mixtures. Both of these methods involved the addition of boric acid which is added to combine with any

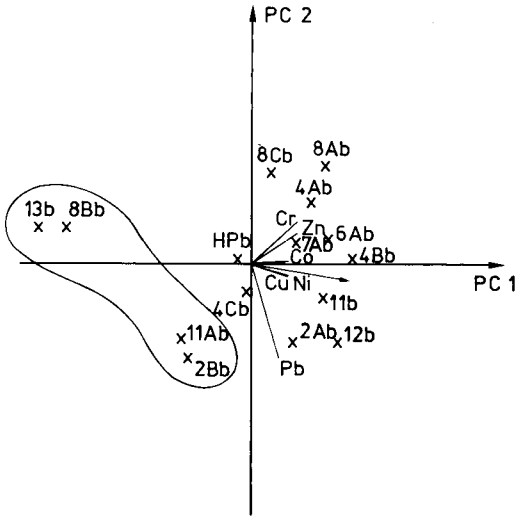

Fig. 3. GAIA plot for the BSR polished data set showing the separation of the outliers from the other methods. The decision axis (π) together with the six metal criteria vectors point away from the outlier cluster. Object (methods of digestion) labels refer to Table 1.

TABLE 7

SIMCA class membership of digestion methods without HF [a]

NBS 2704, R.S.D. (crit) = 1.0		BSR, R.S.D. (crit) = 0.70	
Method [b] label	R.S.D.	Method [b] label	R.S.D.
2B	1.1	4Cb	1.2
4C	0.53	7Ab	0.99
7A	1.2	HPb	1.0
11A	0.97		

[a] Training sets consisted of digestion methods which included HF in their acid mixtures. [b] See footnote to Table 1.

excess HF after digestion. This produces a digest solution that is effectively free of HF. Therefore it is not surprising to find these two methods close to those with a similar acid solution matrix. The two sister methods, 2Ab and 11Bb, from the BSR set are closely located on their PCA plot (Fig. 2) and are positioned roughly between cluster I and the remainder of the methods indicating a similar trend.

The above findings are reflected in the SIMCA and the FC results. For the former procedure (Table 7), the objects from the class of digestion methods without the HF, with the exception of 4C and possibly 11A, were excluded from membership of the training classes. The latter were constructed from methods of digestion characterised by the presence of HF. For the FC analysis (Table 8), the results for NBS 2704 on the basis of a 2 cluster model are consistent with exploratory PCA and the SIMCA findings; one cluster is dominated by the digestion methods without HF, while the opposite is observed with the second cluster. In the case of the BSR data,

TABLE 8

Fuzzy clustering analysis of polished NBS2704, BSR and combined data using various cluster models

Method [a] label	Membership values [b]						
	Combined set (2-cluster model)		NBS 2704 (2-cluster model)		BSR (3-cluster model)		
	HF Excluded	HF Included	HF Excluded	HF Included	HF Excluded	HF Included	Atypical Method
2A	0.62	0.38	0.56 **	0.44 **			
2B	0.80 *	0.20	0.89 *	0.11			
4A	0.29	0.71	0.09	0.91 *			
4B	0.45 **	0.55 **	0.19	0.81 *			
4C	0.77 *	0.23	0.76 *	0.24			
6A	0.50	0.50	0.42	0.58			
7A	0.80 *	0.20	0.88 *	0.12			
8B	0.25	0.75	0.21	0.79 *			
8C	0.27	0.73	0.21	0.79 *			
11A	0.76 *	0.24	0.82 *	0.18			
11B	0.82 *	0.18	0.78	0.22			
2Ab	0.25	0.75			0.39 **	0.53 **	0.08
4Ab	0.21	0.79			0.32	0.52 *	0.16
4Bb	0.14	0.86			0.12	0.84 *	0.04
4Cb	0.48 **	0.52 **			0.68 *	0.24	0.08
6Ab	0.12	0.88			0.15	0.80 *	0.05
7Ab	0.44 **	0.56 **			0.73 *	0.18	0.08
8Ab	0.41	0.59			0.02	0.01	0.97 *
8Cb	0.25	0.75			0.34	0.44 *	0.23
11Bb	0.19	0.81			0.27 *	0.67 *	0.06
12b	0.23	0.77			0.27	0.66 *	0.08
HPb	0.41 **	0.59 **			0.64 *	0.23	0.13

[a] See footnote to Table 1. [b] * Indicates important class members; ** Indicates the fuzziness of some important class members.

the two cluster model appears to be heavily influenced by the atypical method, 8Ab. However, in the three cluster model, this influence is removed by separating method 8Ab as a single member cluster. Good agreement is then obtained with the results from other chemometrics procedures. The methods of digestion without HF are isolated and the location of some of the members in the intermediate position e.g. 2A, is demonstrated. A two-dimensional visualisation of the clusters may be obtained using SIRIUS software by constructing a variable vs. variable plot on the basis of the two most discriminating variables. (A procedure for the selection of these is included in the software.) Such a plot for the three cluster model (BSR) is illustrated in Fig. 4 where Cr and Pb are the variables.

The two polished data sets were combined into a single matrix of 22 objects on the assumption that if the acid digestions were truly complete no discrimination on the basis of the origin of the solid sample should be evident, i.e., the dominant effect should be that of the acid mixture composition. The exploratory PCA biplot (PC1 vs. PC2) is shown in Fig. 5. Approximately 72% of the variance is explained by the first 2 PCs and 4 PCs are required to account for 97% of the variance. Cr and Ni are the most discriminating variables. It also appears that the methods without HF in their digest mixtures perform poorly on Co and Cr, while the methods with HF perform comparatively poorly in the analysis for Pb; most methods seem to perform well on Cu and Zn, but Ni results are particularly strongly influenced by the poor value with method 6A. These observations are supported by the residuals data (Table 3).

Figure 5 includes all the trends for the separate chemometric analyses of the NBS 2704 and the BSR samples with PC2 contributing strongly to the discrimination between methods with and without HF. In additon PC1 appears to distinguish between the two data sets on the basis of their sample origin with the majority of the BSR methods having positive scores. However, a number of NBS 2704 methods, viz. 4A, 8B and 8C,

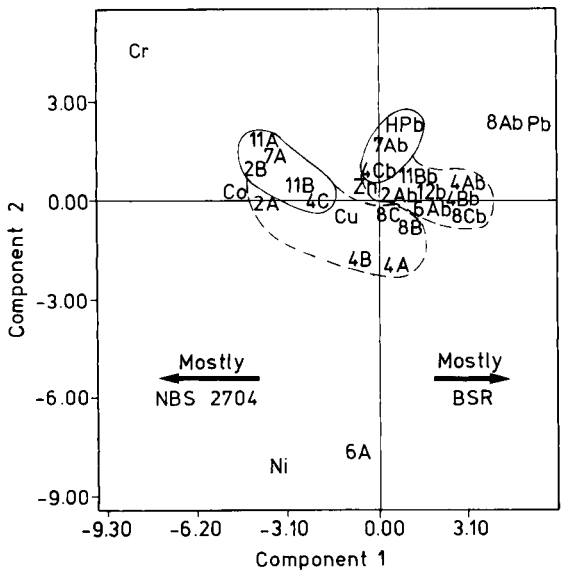

Fig. 5. Biplot for the combined polished data set showing the discrimination of the methods of digestion according to the acid digest composition (PC2) and the origin of the rock/soil sample (PC1). - - - - - -, clusters indicate discrimination on the basis of sample origin; ———, clusters include methods without HF in their digests. Object (methods of digestion) labels refer to Table 1.

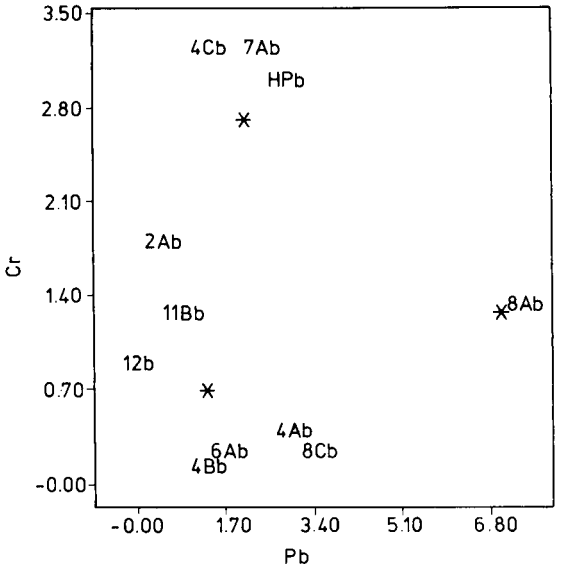

Fig. 4. Fuzzy clustering variable–variable plot for a 3-cluster model derived from the polished BSR data set. * refers to the cluster centres. Object (methods of digestion) labels refer to Table 1.

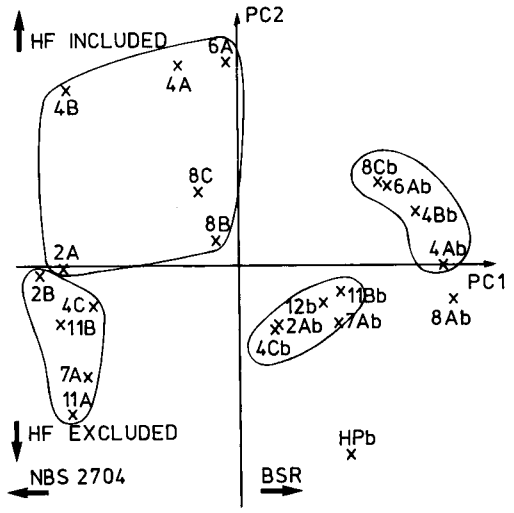

Fig. 6. GAIA biplot for the combined polished data set showing the discrimination of the methods of digestion according to the acid digest composition (PC2) and the origin of the rock/soil sample (PC1). Object (methods of digestion) labels refer to Table 1.

are also positive on PC1 which suggests that the sample origin effect is not as dominant as that of the acid digest composition.

SIMCA results support these findings. The polished BSR set has the lower R.S.D.$_{crit}$ value (0.70) in comparison to the NBS2704 data (0.91) and it was therefore used as the training set; only one NBS 2704 method of digestion was found to be a member of the BSR class. Similarly, when methods of digestion without HF from the two data sets (methods 2B, 4C, 7A, 11A, 2Bb, 4Cb, 7Ab, and HPb) were tested for membership of the training set containing digestion methods with HF, all but two methods (7Ab and HPb) were excluded; the two included methods had high R.S.D. values (1.1 and 0.98 respectively) in comparison with the R.S.D.$_{crit}$ of 1.3.

The results of fuzzy clustering analysis of the combined data using a two-cluster model (Table 8) appear to indicate a subdivision according to the acid composition of the methods. However, on this basis methods 4B, 4Cb, 7Ab and HPb should reflect their acid composition membership quite strongly. Their fuzziness with class membership values of approximately 0.4 to 0.5 suggests the presence of a less significant effect that is consistent with a class separation on the basis of sample origin.

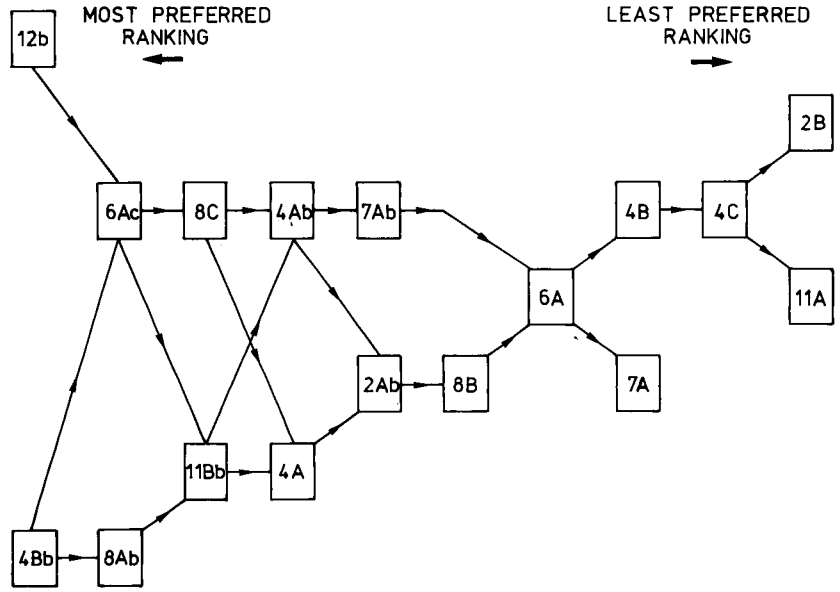

Fig. 7. PROMETHEE I partial preference flow chart showing the rank order of 17 of the digestion methods from the combined polished data set.

All of the above findings are particularly well displayed on the PC1 vs. PC2 GAIA plot (64% of variance described) in Fig. 6. PC1 discriminates the digestion methods on the basis of their origin, while PC2 distinguishes the two different acid composition groupings. The results are very similar to exploratory PCA, however, the cluster separation appears to be sharper.

Selection of the most suitable method of digestion

In any selection or optimization procedure, it is intuitively desirable to have the objects rank-ordered. From the range of chemometrics methods used in this work, only PROMETHEE is capable of producing such information.

Analysis of the NBS 2704 and the BSR polished data sets by PROMETHEE I using the residuals minimisation criterion referred to in the "Data treatment" section, produced partial ranking flow charts similar to that shown for the combined data in Fig. 7. For the BSR set, methods 4Bb and 12b outranked the others but they could not be compared, i.e. each method outperformed all others but each also performed differently on the six metal variables. For the NBS 2704 data, method 8C was selected ahead of methods 8B and 4A. It should be noted that these were the three NBS 2704 methods of digestion which had positive PC1 scores in the exploratory PCA of the combined data set (Fig. 5); this indicates that these three methods are similar to the BSR methods in that cluster. The selection of method 8C as the best performing method, is also consistent with our previous findings [12]. Referring to PROMETHEE II results (Table 5), it is seen that the two most preferred BSR methods have very similar ϕ values which, however, are well above the value for the next few methods (11Bb, 6Ab and 8Ab); similarly for the NBS 2704 set, method 8C had a considerably higher ϕ value than that of each of the next two methods.

Thus three methods of digestion (4Bb, 12b and 8C) stand out in their analytical performance. The single common feature is the presence of HF in their acid mixtures; also of note is the absence of HCl from both of the preferred acid mixture digests from the BSR group (Table 1). As noted previously the first three preferred methods of the NBS 2704 group appear to cluster with the BSR methods, therefore it seems reasonable to attempt to compare at least the best performing methods of the two data sets by analysing the combined set of methods. PROMETHEE I preference flow diagram (Fig. 7) shows the results of this analysis for the partial ranking of 17 of the methods. Method 4Bb outranks all others, except 12b to which it cannot be compared. In turn method 12b outranks all the methods except 4Bb and 8Ab to which it cannot be compared. Thus arguably the preferred method is 4Bb but it probably does not differ significantly from method 12b. PROMETHEE II data (Table 5) support this argument; the difference in the net flow ϕ values for these two methods is of no practical significance, but both clearly outperform methods 8Ab and 6Ab. A perusal of the acid composition for the first few preferred methods (Table 1), again indicates that the presence of HF in the acid mixture plays a major role and also that HCl may be a significant variable; all three methods without HCl in their mixture (4Bb, 11Bb and 12b) are ranked highly. This suggestion is consistent with our previous studies using PROMETHEE analysis to investigate the significance of the various conditions and microwave oven settings to method performance [12]. In that work it was shown that the ranking (digestion method performance) criterion was most closely associated with the HF and HCl criteria. Thus it is recommended that the preferred low pressure microwave method of digestion for rock or sediment analysis should use an HF and HNO_3 digest mixture and settings similar to those shown for the relevant methods in Table 1. These recommendations are in agreement with general guidelines on soil and rock digestion [31]. They are also consistent with the trend of some recent work on the dissolution of rock, soil and sediment samples by microwave digestion [2,5,32] in which HF–HNO_3 digests were successfully used.

Comments on the four chemometrics procedures

It was demonstrated that the PROMCALC software incorporating the PROMETHEE and

GAIA ranking procedures offers a powerful chemometrics approach for the investigation of multivariate data. The essential concept underlying PROMETHEE procedure assumes that the ranking information is contained in the pairwise differences of the data. This difference information is then systematically transformed into a single ranking scale. Notwithstanding the unusual, associated nomenclature, every step of this transformation may be in principle, readily illustrated using a simple data set. Once the essential information from PROMETHEE processing is available, GAIA in conjunction with the PROMETHEE II results, may be used to benefit from the display and clustering capabilities of the PCA routine. In contrast, the PCA-based procedures are difficult to illustrate simply, and moreover uncertainties often arise with the interpretation of the chemical significance of the extracted PCs. Further, with methods such as SIMCA which depend on PCA modelling, uncertainties with the quality of the model may readily occur, particularly if the commonly recommended modelling procedures are unsuccessful. These comments are not intended to discourage the use of exploratory PCA, SIMCA or FC procedures. When present together in a package such as SIRIUS, they form a powerful combination of chemometric methods. Indeed for the purposes of sample classification the SIMCA and FC methods must be preferred over PROMETHEE and GAIA, however, it is suggested that these classification procedures are most usefully applied with the benefit of results from PROMETHEE and GAIA analysis.

Conclusions

The four chemometrics methods, PCA, MDM, SIMCA and FC, used to investigate the data structure of analytical results for metals from differently microwave-digested sediment and rock materials, indicated that the four approaches provided consistent information about outliers, groupings and trends. However, only the MDM PROMETHEE procedure provided the rank order information which facilitated the selection of a suitable microwave digestion method. The suitable method finally selected was found to be consistent with previous recommendations.

REFERENCES

1 L.B. Gilman and W.G. Engelhardt, Spectroscopy, 4 (1988) 14.
2 A.D. Hewitt, At. Spectrosc., 11 (1990) 187.
3 P.J. Lamothe, P.J. Fries and J.J. Consul, Anal. Chem., 58 (1986) 1881.
4 C.G. Millward and P.D. Kluckner, J. Anal. At. Spectrom., 4 (1989) 709.
5 B. Kratochvil and S. Mamba, Can. J. Chem., 68 (1990) 360.
6 G.M. Kimber and S. Kokot, Trends Anal. Chem., 9 (1990) 203.
7 T. Noltner, P. Maisenbacher and H. Puchelt, Spectroscopy, 5 (1989) 49.
8 H. Matusiewicz and R.E. Sturgeon, Prog. Anal. Spectrosc., 12 (1989) 21.
9 R.A. Nadkarni, Anal. Chem., 56 (1984) 2233.
10 H.M. Kingston and L.B. Jassie, Anal. Chem., 58 (1986) 2534.
11 M.H. Feinberg, Analysis, 19 (1991) 47.
12 S. Kokot, G. King, H.R. Keller and D.L. Massart, Anal. Chim. Acta, 259 (1992) 267.
13 Flame Atomic Absorption Spectrometry Analytical Methods, Varian Techtron, Sunnyvale, CA, 1989.
14 E. Rothery (Ed.), Analytical methods for Zeeman graphite tube atomizers, Varian Techtron, Sunnyvale, CA, 1986.
15 G. King, personal communication, Government Chemical Laboratories, Brisbane, 1991.
16 D.L. Massart, B.G.M. Vandeginste, S.N. Deming, Y. Michotte and L. Kaufman, Chemometrics: A Textbook, Elsevier, Amsterdam, 1988.
17 S. Wold, K. Esbensen and P. Geladi, Chemometrics Intell. Lab. Syst., 2 (1987) 37.
18 A. Thielemans and D.L. Massart, Chimia, 39 (1985) 236.
19 M. Nagel, H. Horing, D. Feiler and H.-J. Dobberkau, Statistical Software Newsletter, 11 (1986) 117.
20 S. Wold, Pattern Recognition, 8 (1976) 127.
21 M.P. Derde and D.L. Massart, Chemometrics Intell. Lab. Syst., 4 (1988) 65.
22 S. Wold, Technometrics, 20 (1978) 397.
23 J.P. Brans, B. Mareschal and P. Vincke, Eur. J. Oper. Res., 24 (1986) 228.
24 B. Mareschal and J.P. Brans, Eur. J. Oper. Res., 34 (1988) 69.
25 H.R. Keller, D.L. Massart and J.P. Brans, Chemometrics Intell. Lab. Syst., 11 (1991) 175.
26 J.C. Bezdek, Pattern Recognition with Fuzzy Objective Function Algorithms, Plenum Press, New York, 1982.
27 M. Otto, Chemometrics and Intell. Lab. Syst., 4 (1988) 101.
28 SRM 2704 (Buffalo River Sediment) Certificate, National Bureau of Standards, USA.
29 O.M. Kvalheim, SIRIUS (Version 2.3), Department of Chemistry, University of Bergen.
30 J.P. Brans, PROMCALC (Version 3.1), Centre for Statistics and Operations Research, Free University of Brussels, Brussels.
31 P.G. Jeffrey, Chemical Methods of Rock Analysis, Pergamon Press, Oxford, 2nd edn., 1975, p. 22.
32 S. Nakashima, R.E. Sturgeon, S.N. Willie and S.S. Berman, Analyst, 113 (1988) 159.

Analytica Chimica Acta, 268 (1992) 95–105
Elsevier Science Publishers B.V., Amsterdam

Expert system for the voltammetric determination of trace metals

Part I. Determination of copper, zinc, cadmium, lead and indium

M. Esteban

Departament de Química Analítica, Universitat de Barcelona, Av. Diagonal 647, 08028 Barcelona (Spain)

I. Ruisánchez, M.S. Larrechi and F.X. Rius

Departament de Química, Universitat Rovira i Virgili (Tarragona), Pl. Imperial Tàrraco 1, 43005 Tarragona (Spain)

(Received 14th November 1991; revised manuscript received 15th April 1992)

Abstract

An expert system for the voltammetric determination of Cu, Zn, Cd, Pb and In was developed. The system guides the user in the choice of sample treatment, the most appropriate voltammetric procedure and the identification and determination of the trace metals. The techniques implemented are differential-pulse polarography and anodic stripping voltammetry, using mercury drop electrodes. Only well known methods are recommended, with particular attention to standard methods. For the identification and resolution of overlapping peaks (Cd and In), the system may call two external programs, written in turbo BASIC. Quantification is carried out by means of the multiple standard addition method, and the quality of the calibration graph is tested by several statistical validation tests. The tool kit for the development of the expert system KES (Knowledge Engineering System) is used. Only commercially available material was used. The system is easily portable if the shell for the development of the expert system is employed.

Keywords: Polarography; Voltammetry; Cadmium; Copper; Expert system; Indium; Lead; Trace metals; Zinc

For several trace metal determinations, versatile and powerful voltammetric procedures have been introduced in recent years. In some instances, the voltammetric approach has proved to be one of the best methods for certain important matrices (e.g., all types of water), becoming a definitive routine method of choice [1,2].

Although electroanalytical techniques are much cheaper than other techniques with similar detection limits, they are not very popular. This may be because, in some instances, a physicochemical knowledge of both the technique and the electrodic process is required. Because of the existence of instrumentation which is reliable, sensitive and commercially available, at low cost, well tested routine methods for toxic metal determinations in environmental surveillance, food control, occupational medicine, toxicology and hygiene [1] and a wide range of potential users (with insufficient electroanalytical foundations), the development of an expert system may be of great interest in order to guide the application of voltammetric methodologies. Moreover, it is well known that good voltammetric performance re-

Correspondence to: M. Esteban, Departament de Química Analítica, Universitat de Barcelona, Av. Diagonal 647, 08028-Barcelona (Spain).

quires the careful control of the several aspects involved in an electroanalytical measurement: technique, electrode, instrumental parameters, medium, etc. The acquisition of such experience requires time, the utility of expert systems thus being obvious [3,4].

Expert systems are within the domain of artificial intelligence. They use knowledge and operate according to the rules of reasoning of an expert. Such systems have already been applied in several branches of analytical chemistry, especially liquid chromatography [5], liquid–liquid extraction [6], spectrophotometry [7,8], and atomic absorption spectrometry [9,10]. However, in the electrochemical field, only an expert system for the automatic elucidation of electrode reaction mechanisms has been presented [11].

The simultaneous determination of Pb, Cd, Cu and Zn is probably the best developed voltammetric application, being useful for many types of materials, if sample treatment is appropriate. In fact, it has become very useful for routine analytical tasks, reaching the status of a standard method [12].

This paper outlines an expert system for the voltammetric determination of several trace metals, devoted here to the determination of Cd, Pb, Zn and Cu, In also being considered. It is based on the production of rules that allow knowledge to be represented by means of conditional statements of the form IF ... and ... THEN ... and ... They support the strategies to be followed by the user in order to identify and quantify voltammetrically the above-mentioned trace metals.

THE EXPERT SYSTEM

An expert system consists of three basic parts: the knowledge base, the inference engine and the user interface. The present knowledge base contains both the knowledge and the experience required for the simultaneous voltammetric determination of trace metals in different types of samples. The inference engine controls both the use and transmission of the knowledge implemented in the knowledge base. It works in a similar way to an expert, connecting information so as to give advice and drawing conclusions. Finally, the user interface allows communication between the user and the knowledge stored in the computer program; KES (Knowledge Engineering System) [13] is the tool kit used for the development of expert systems. KES provides useful means for designing an effective interactive user interface for the expert system.

THE KNOWLEDGE BASE

The aim of the present system is to provide guidance to the user along the different steps involved in a voltammetric determination: sample treatment, voltammetric procedure, identification and resolution of signals and determination. The knowledge implemented is based on well known procedures [1,12].

Sample treatment

This part contains information about the steps to be followed for obtaining the sample in the best conditions for the voltammetric measurement: aqueous medium containing a supporting electrolyte, at acidic pH and without organic matter. A flow diagram with the implemented knowledge is shown in Fig. 1.

Voltammetric procedure

In order to apply a voltammetric method, some aspects must be carefully taken into account. The choice of the technique is mainly determined by the concentration of the analyte. In this system, usual techniques such as differential-pulse polarography (DPP) and differential pulse anodic stripping voltammetry (DPASV) have been considered. The choice of the electrode, although it is also related to the concentration level to be reached, is linked to the reproducibility. Because of the well known difficulties associated with the use of solid electrodes (e.g., the achievement of reproducible electrode surfaces, which needs considerable experience), only mercury drop electrodes are recommended: the dropping mercury electrode (DME) or static mercury drop electrode (SMDE), both for DPP measurements, and the hanging mercury drop electrode (HMDE) for

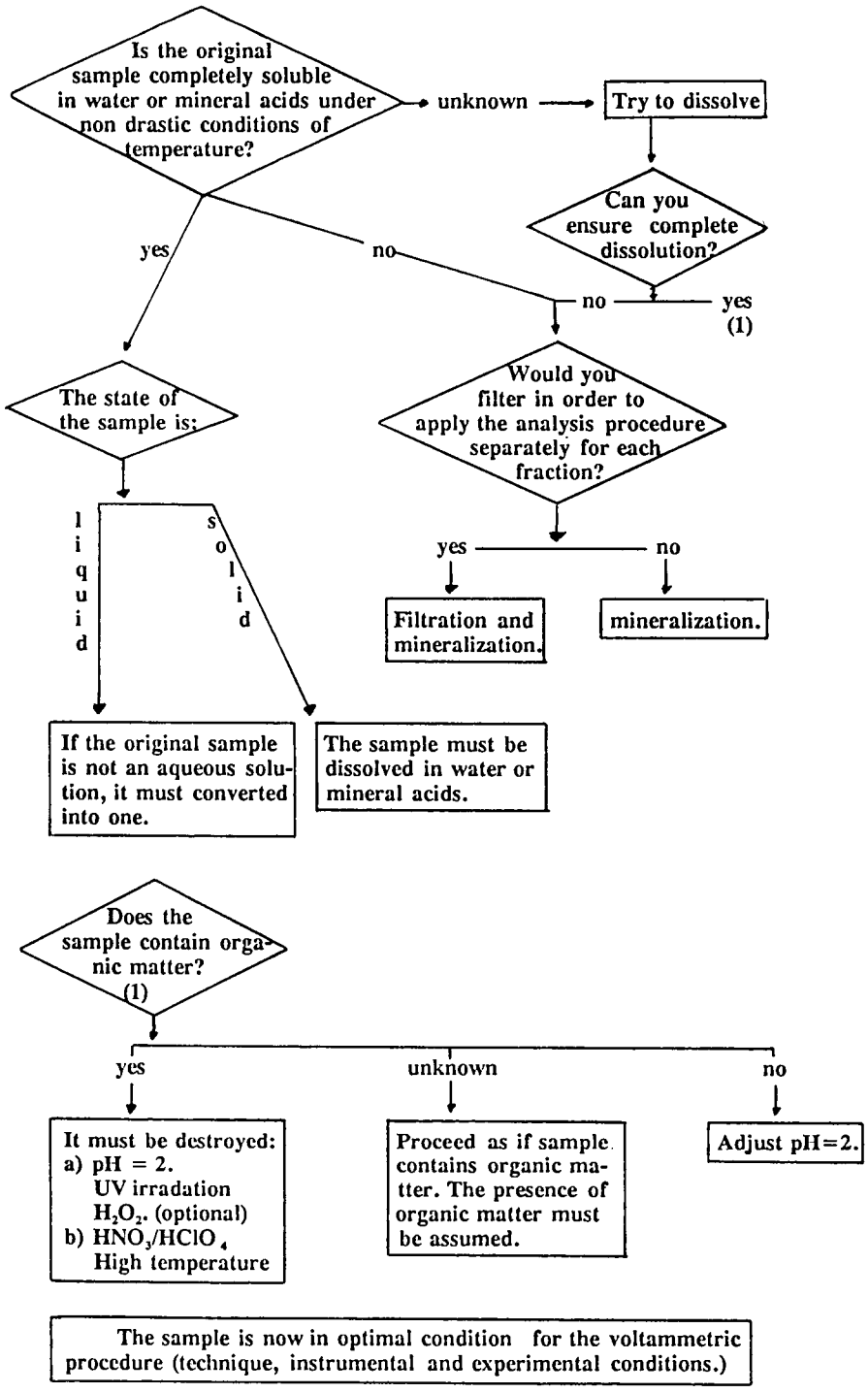

Fig. 1. Flow diagram of the knowledge base for the sample pretreatment step.

```
Attributes input.

sample: sgl

(yes, no, unknown {explain: " Try to dissolve the sample in water or mineral acids."})

{question: " Is the original sample completely soluble in water or mineral acids?"}

{explain: " The voltammetric techniques recommended must be applied to aqueous",
          "samples."}.


Attributes output.

filter: sgl

(yes {explain:"Before the voltammetric measurement, the sample should be filtered and",
              "mineralized.
              "To carry out the filtering, pass the sample through a 0.45 μm cellulose",
               "membrane. (Ref. H.W Nürnberg, Pure Appl.Chem.,54 (1982) 253.)",
              "To carry out the mineralization, treat the filtered sample (solid part)",
              "with HNO3/HClO4 (ultra pure) at high temperature. The aqueous sample",
              "(liquid part) should be treated in the same way, or irradiated with UV.",
              "After these steps, acidify to pH 2. Then the voltammetric procedure",
              "can be applied to the samples. Now the analysis of one portion of sample",
              "can begin."},
no {explain:" The sample should be mineralized; treat the filtered sample (solid part)",
             "with HNO3/HClO4 (ultra pure). To apply the voltammetric procedure,",
              "you should work with a known volume of the sample."},
absurd {explain:" "},

not necessary {explain: " "}).
```

Fig. 2. Attributes.

DPASV measurements. The rotating thin mercury film electrode (TMFE), much more sensitive [2], but much less reproducible, is not included in the expert system, because it requires much experience to apply it successfully [2].

The choice of the optimum instrumental parameters includes, for instance, drop time (for DPP), pulse magnitude (for both DPP and DPASV), pre-electrolysis and rest times and pre-electrolysis potential (for DPASV). The choice of the conditions of the medium includes pH, nature and concentration of the supporting electrolyte and absence of organic matter.

Although the presence of In is not as common as that of the other trace metals mentioned, the simultaneous determination of In and Cd is not a simple matter by means of the recommended techniques, owing to the closeness of their peak potentials. In the simultaneous presence of Cd and In, the method recommended is DPASV in a TMFE [2], which is not considered in this expert system. In these instances, the expert system proposes the determination of both cations by using an external program for overlapping peaks based on curve fitting methodology and developed in this laboratory.

Identification and resolution of the signals

Qualitative analysis of the voltammograms is based on three features: the appearance of voltammetric peaks, their characteristic potentials and the shape and width of the peaks.

```
not necessary filter:

  if    sample = yes

  then
        filter = not necessary.

  endif.
```

Fig. 3. Rules.

The expert system includes not only the values of the potentials corresponding to the reduction of each cation, but also the corresponding peak width at half-height for DPP and DPASV [14,15]. This parameter allows the detection of overlapping peaks or other secondary phenomena (adsorption processes, matrix effects, etc). Moreover, the system gives information about the possible causes of the absence of signals, or signals with unexpected potentials.

In the event of overlapping peaks, due to the simultaneous presence of Cd and In, the system may call the external program DECON for peak resolution. This program is especially recommended for DPP measurements since Gaussian-like peaks are assumed.

Determination

The quantification procedure is based on the multiple standard addition method. The system indicates the most appropriate concentration range for the calibration graph, and also proposes its validation, by means of several statistical tests. For this purpose, the system may call the external program COOKS'2 [16].

KNOWLEDGE REPRESENTATION AND INFERENCE MECHANISM

The knowledge contained in the base is presented by means of attributes and rules. Attributes represent some piece of knowledge about the domain while rules are used to link the attributes in a hierarchical manner. The information given by the end user is represented by input attributes. These, together with intermediate and goal attributes may acquire a certain distinct value during each system run (Fig. 2). About 120 rules of the type IF ... THEN ... are developed, by using the KES syntax, to build the hierarchy of the relationships between the attributes (Fig. 3).

The inference engine employs the knowledge stored in the knowledge base together with the supplementary information given by external means (end user, other programs, etc) to provide solutions. This inference works according to a well established sequence determined, in KES, by the commands of the actions section (Fig. 4). The expert system looks for the value asked for in the actions section, first by looking at the consequences of the rules in the section rules, that is, looking for intermediate and goal attributes. If no appropriate answer is obtained, the end user is asked to enter a value.

The first commands of actions are related to sample treatment; for instance, the command "obtain filter" starts the search for the value of the attribute "filter", whose information is related to the filtering procedure and mineralization of the sample (Fig. 3). The information received by the user is shown in Fig. 5.

The execution of commands 13–63 (Fig. 4) guides the user in the choice of the appropriate

```
1  message Welcome.
   ........
4  obtain filter.
   ........
13 message banner, technique, banner.
14 while status (filter) = known do
15  obtain ion_met.
    ..........
      if ion_met= Cu Zn Cd or Pb then
        obtain voltammetry1.
        if voltammetry1= yes then
          obtain technique.
        endif.
    ..........
    ..........
34  break.
35  message "Call the external program which plots the",
            "voltammograms:".
36  run register voltammogram.
37  obtain cation1.
   .........
   .........
64  if quantitative = no then
65    if split1 = yes then
       ..........
70  message "Call the external program for peak resolution",
            "(in the presence of overlapping peaks.)".
90  if quantitative = yes then
91    obtain addition.
92      while addition= yes do
          obtain sample_conc.
          message "Parameters of the calibration curve:",
                  "*******************************",
                  "slope =",SLOPE B,
                  "intercept (at y=0) =",INTER A,
                  " ".
           ........
    ..........
    endif.
  endwhile.
```

Fig. 4. Actions.

technique and in the identification of the peaks. Then, if the sentence "if ion-met = Cu, Zn, Cd o Pb then" is displayed, the expert system seeks the value of the attribute "voltammetry1" as above. Figure 6 shows a typical run for this section. It can be appreciated that, if the peaks overlap, the expert system may call DECON, the function of which is illustrated by Fig. 7, returning to the expert system.

Finally, Fig. 8 shows the procedure followed in order to obtain the calibration graph and its further validation by using the external statistical program COOKS'2. This program calculates the parameters of the calibration plot, draws the residuals plot and provides the user with the option to check the presence of influential points by means of the Cook's test [16]. In the present example, the concentration value shown in Fig. 8 results from applying the standard addition technique to the set of the first five calibration points, that is, after rejecting point 6 as it has been demonstrated statistically that it is an outlier. Finally, the analyte concentration value is given by the expert system.

The contents of the present version have been validated by checking that the system answers according to the reasoning of the human expert in all examples with known outcomes.

THE USER INTERFACE

The expert system offers the user the possibility of asking for explanations about the questions formulated and the decisions taken by the system.

Is the original sample completely soluble in water or mineral acids, under non drastic conditions of temperature and time?

1. yes
2. no
3. unknown

=? 1

The state of the sample is:

1. solid
2. liquid

=? 2

If the sample is not an aqueous sample, it must converted into one.

Does the sample contain organic matter?

1. yes
2. no
3. unknown

=? 3

Proceed as if the sample contained organic matter. Acidify the sample to pH=2 and UV irradiate it to destroy the organic matter. A Mercury arc lamp (238-265 nm, 150 or 1300W) should be used for one hour. Optionally, treat the sample with H_2O_2 ultrapure or with $HNO_3/HClO_4$ at high temperature.

The sample is now in optimal condition for voltammetric procedure (technique, instrumental and experimental conditions).

Fig. 5. Example of an interactive session with the expert system (pretreatment step).

This may be done in KES by using the instructions "explain" and "why", respectively, which are introduced by the user. The system may also be linked to external programs. There are two ways to call an external program: directly, by using the run command specified in the actions section (i.e., link with ADDA and DECON), and indirectly, by the inference engine. If an external program can provide an attribute value, the system shell treats the external program as a knowledge source and executes the program to obtain the value. When the external program finishes, the system returns to the same point in the running program.

You must work with Differential Pulse Polarography (DPP) using the Dropping Mercury Electrode (DME) or the Static Mercury Drop Electrode (SMDE).

The optimal instrumental conditions are:

E_r= Ag/AgCl or standard calomel electrode (SCE). E_w= Hg.
E_{aux}= Pt or glassy carbon.
pulse = 50 mV. (in general, between 10 and 100 mV.)
$t_{<drop>}$ = 1 s, v = 10 mV/s. t_{pulse}= 30 - 100 ms.
E_i = 0.1 V, E_f= -1.2 V.

The determination should be carried out according to the Deutsche Norm (DIN). It can be performed at pH = 2 or pH = 4.6.
a) pH=2 (0.5 ml of KCl 1M in 10 ml sample,
supporting electrolyte: $HClO_4$ or HNO_3 0.01 mol/l)
b) pH=4.6 (0.5 ml buffer KCl (1.5 M) - NaAc (0.5 M) in 10 ml of sample)

Set up the polarograph in the above mentioned conditions; the voltammogram is:

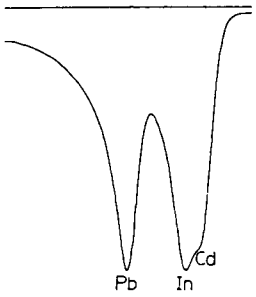

Did you observe (the presence of) different peaks in the voltammograms?
1. yes
2. no

=? 1

Following voltammetric step, the voltammograms can be analysed qualitatively, since each peak corresponds to just one cation. (Because of matrix effects and complexing agents)

Do these peaks appear at the potential values you expected?

(potential values:
E Cd(II): DPP: -0.543 V, DPASV: -0.557V.
E Cu(II): DPP: 0.06 V, DPASV: 0.05V.
E Pb(II): DPP: -0.31 V, DPASV: -0.325V.
E Zn(II): DPP: -1. V, DPASV: -1. V.

Fig. 6. Voltammetric analysis.

Peaks appear:
1. only at the potential indicated.
2. only at potential values different of those indicated.
3. some at the indicate potential values and some at different potentials too.

(Enter a number)
=? 3

When signals at potential values different of those expected are found, and the pretreatment step has been carried out correctly, those signals are not caused by complexes of other elements present in the sample or by complexes of the cations in study. For this reason, they are not taken into account.

Which of the peaks considered are observed (in the order mentioned above)?

1. first
2. second
3. third
4. fourth

(multiple answers allowed)

=? 1&3

If E (DPP) ≈ -0.31 V. or E(DPASV) ≈ -0.32 V, will be Pb^{2+}.
If E (DPP) ≈ -0.54 V. or E(DPASV) ≈ -0.55 V, will be Cd^{2+}.

From the shape of the peaks, could you say if each peak is generated by only one chemical species?
(The expert system includes the width at half-peak corresponding to the reversible reduction of a divalent cation: for DPP, W½ ≈ 58 mV, and for DPASV, W½ ≈ 44 mV.)

1. yes
2. no

=? 2

In the case of overlapping peaks, would you like to apply a curve fitting methodology?

1. yes
2. no

=? 1

Fig. 6 (continued).

SOFTWARE

In the present work, the KES 1.4 version has been implemented with an IBM PS/80. The run part of this shell is needed to execute the expert system. The different program calls that KES may execute are shown in Fig. 9. The first external program to which the expert system may be connected is ADDA. ADDA may acquire and register the data provided by the analogic polaro-

graph, which is linked to the computer through a 12-bit analogue–digital converter implemented in the polarograph. The analogue signals provided by the Metrohm Polarecord 506 are displayed on the computer screen, converted and stored (in digital form) in a communication file. The external program DECON may process this digital data in the case of the presence of overlapping peaks, by applying a curve-fitting method. DECON is called by the expert system when the user (looking at the graphic display of the voltammograms) indicates the simultaneous presence of two polarographic peaks under one signal. DECON is able to compute the area of the peaks corresponding to the individual ions present.

Finally, the external program COOKS'2 is called from the expert system for validation of the calibration graph, by means of the analysis of residuals and detection of influential points. Then, the expert system can use the parameters obtained in order to calculate the concentration of each metal ion. This is achieved by means of the usual extrapolation in the multiple standard addition method. The results are plotted on the screen.

Conclusions

The present expert system may be very useful for non-expert users in the electroanalytical field. It is based only on well tested methods, and special attention is paid to standard methods. Thus, only mercury drop electrodes are recom-

In the case of overlapping peaks, would you like to apply a curve fitting methodology?

1. yes
2. no

=? 1

For each experimental point used to plot the calibration curve, should be obtained the polarogram in the same instrumental conditions, apply a curve fitting methodology and measure the peak height.

Connexion to the external program DECON, which applies a curve fitting methodology.

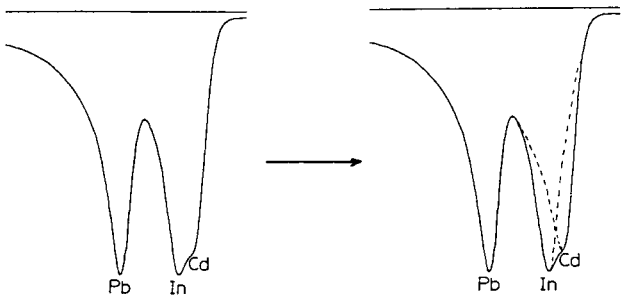

Would you like to obtain another voltammogram in which curve fitting methodology should be applied?

1. yes
2. no

=? 2

Fig. 7. Connection to DECON.

In order to carry out the quantification, the calibration curve should be obtained. The quantitative procedure is based on the multiple standard addition method, and the response signal considered is the peak height of the voltammogram. The more appropriate concentration for the calibration plot is:

* at 50% lower value given from references and
* at 150% highest value given by references.

After the calibration curve, its validation can be done by means of the analysis of residuals. For this purpose, the system calls the external program COOKS'2.

Would you like to apply these calibration and validation methodologies?
1. yes
2. no
=? 1

Which cation will be determined?
1. Zn
2. Cd
3. Pb
4. Cu
5. any other cation
=? 3

****
COMPUTER PROGRAM TO PLOT CALIBRATION LINES, THEIR RESPONSE RESIDUALS, AND TO TEST THE PRESENCE OF OUTLIERS ACCORDING TO COOK'S DISTANCE.
****

Number of points of the regression line ?? 6
(Concentrations and peak currents (response) must be given in 10^{-7} M and nA, respectively.)

Point 1: Give value of concentration? 0.00
Give value of response? 11.51
Point 2: Give value of concentration? 1
Give value of response? 36.52
Point 3: Give value of concentration? 2
Give value of response? 60.77
Point 4: Give value of concentration? 3
Give value of response? 86.36
Point 5: Give value of concentration? 4
Give value of response? 111,44
Point 6: Give value of concentration? 5
Give value of response? 126.38

Fig. 8. Connection to COOKS'2. Validation of the calibration graph.

PARAMETERS OF THE REGRESSION LINE
****

Intercept A = 13.26
Slope B = 23.56

point n°	X values	Y values	YHAT values	Residuals
1	0	11.51	13.26	-1.75
2	1	36.52	36.82	-0.30
3	2	60.77	60.38	0.39
4	3	86.36	83.94	2.42
5	4	111.44	107.50	3.90
6	5	126.38	131.10	-4.68

Sum of squared residuals = 46.27

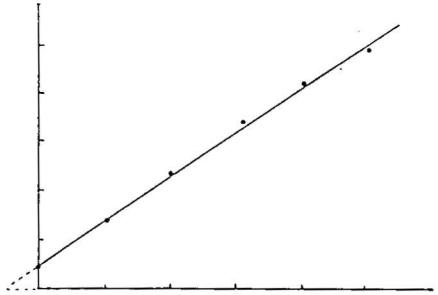

Parameters of the calibration plot, after rejecting point n°6.

slope = 24.97
intercept = 11.38

The concentration of the cation Pb <1.00>
given in mol/l, is 0.46 10^{-7}.

Which cation will be determined?
1. Zn
2. Cd
3. Pb
4. Cu
5. any other cation

=? 5

End of the expert system.

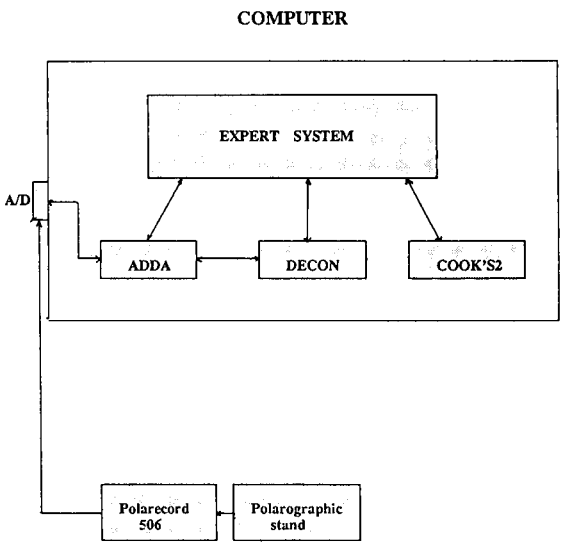

Fig. 9. External connections of the expert system.

mended, and other more sensitive, but much less reproducible electrodes (e.g., mercury film electrodes) are not taken into account. Taking into account that expert systems are tools in continuous evolution, the present version has shown its validity in the actual analysis of real samples.

This work was presented at the *II Colloquium Chemiometricum Mediterraneum*, San Miniato (Pisa), 1991. Economic support from the Spanish Ministry of Education and Science is acknowledged (CICYT projects Nos. BP90-0453 and BP90-0821).

REFERENCES

1 H.W. Nürnberg, Sci. Total Environ., 37 (1984) 9; Pure Appl. Chem., 54 (1982) 253; Anal. Chim. Acta, 164 (1984) 1.
2 T.M. Florence, Analyst, 111 (1986) 489.
3 J.W.A. Klaessens, G. Kateman and D.G.M. Vandeginste, Trends Anal. Chem., 4 (1985) 14.
4 B.A. Hohne and T.H. Pierce, in B.A. Hohne and T.H. Pierce (Eds.), Expert System Applications in Chemistry (ACS Symposium Series, Vol. 408), American Chemical Society, Washington, DC, 1989, p. 2.
5 J.A. Van Leeuwen, B.G.M. Vandeginste, G. Kateman, M. Mulholland and A. Cleland, Anal. Chim. Acta, 228 (1990) 145.
6 M. Moors and D.L. Massart, Trends Anal. Chem., 9 (1990) 164.
7 K. Janssen and P. Van Espen, Anal. Chim. Acta, 191 (1986) 169.
8 J. Smeyers-Verbeke, M.R. Detaevernier and D.L. Massart, Anal. Chim. Acta, 191 (1986) 181.
9 J. Smeyers-Verbeke, F.X. Rius, P. Vankeerberghen and D.L. Massart, submitted for publication.
10 W.R. Browett, T.A. Cox and M.J. Stillman, in B.A. Hohne and T.H. Pierce (Eds.), Expert Systems Applications in Chemistry (ACS Symposium Series, Vol. 408), American Chemical Society, Washington, DC, 1989, p. 210.
11 M. Palys, M. Bos and W.E. Van der Linden, Anal. Chim. Acta, 231 (1990) 59; 248 (1991) 429.
12 Deutsche Norm, DIN 38 406, Teil 16, March 1988.
13 KES, PS Version 2.4, Software Architecture and Engineering, Arlington, VA, 1990.
14 E.P. Parry and R.A. Osteryoung, Anal. Chem., 37 (1965) 1634.
15 G.E. Batley and T.M. Florence, J. Electroanal. Chem., 55 (1974) 23.
16 F.X. Rius, J. Smeyers-Verbeke and D.L. Massart, Trends Anal. Chem., 8 (1989) 8.

Analytica Chimica Acta, 268 (1992) 107–114
Elsevier Science Publishers B.V., Amsterdam

Expert system for the voltammetric determination of trace metals

Part II. Methods for determining nickel, cobalt and thallium at different concentration ratios

M. Esteban

Departament de Química Analítica, Universitat de Barcelona, Av. Diagonal 647, 08028 Barcelona (Spain)

I. Ruisánchez, M.S. Larrechi and F.X. Rius

Departament de Química, Universitat Rovira i Virgili (Tarragona), Pl. Imperial Tàrraco 1, 43005 Tarragona (Spain)

(Received 16th December 1991)

Abstract

An expert system for the voltammetric determination of Cu, Zn, Cd, Pb, In, Ni, Co and Tl was developed with special attention to methods for determining Ni, Co and Tl at different concentration ratios. The system guides the user in the choice of sample treatment, the most appropriate voltammetric procedure and the identification and determination of trace metals. The techniques implemented are differential-pulse polarography, anodic stripping voltammetry and adsorptive stripping voltammetry, using mercury drop electrodes. Only well known methods are recommended, with particular attention to standard methods. For the identification and resolution of overlapping peaks, the system may be used in conjunction with two external programs, written in turbo BASIC. Quantification is carried out by means of the multiple standard addition method, and the quality of the calibration graph is tested by several statistical tests performed by another external program. The expert system is developed using KES (Knowledge Engineering System).

Keywords: Polarography; Voltammetry; Cobalt; Expert system; Nickel; Thallium; Trace metals

In recent years, versatile, reliable and inexpensive electrochemical instrumentation has been developed, and a new generation of microprocessor-based apparatus has become available commercially. Moreover, some workers have described modifications in classical analogue polarographic instruments in order to attach them to mini- or microcomputers [1]. Parallel to these efforts, powerful voltammetric procedures have been introduced for a number of toxic metals, especially Cd, Pb, Cu and Zn, in different materials, with particular attention to environmental samples [2–5].

Nickel, cobalt and thallium are toxic metals and their determination is of great interest in environmental surveillance, quality control in food and occupational medicine, toxicology and hygiene.

Polarography has not been widely used for the determination of Ni and Co because of the irreversibility of the electrodic processes at the dropping mercury electrode (DME). However, a very

Correspondence to: M. Esteban, Departament de Química Analítica, Universitat de Barcelona, Av. Diagonal 647, 08028-Barcelona (Spain).

efficient method for their determination has been proposed, which is based on the accumulation of Ni(II) and Co(II) at a hanging mercury drop electrode (HMDE) at an appropriate potential by using dimethylglyoxime (DMG) [6]. This general scheme of adsorptive stripping voltammetry [7] has been widely described for the simultaneous measurement of Ni and Co by different experimental approaches and techniques [8]. Polarographic determinations of Tl have been described [9], but determinations are usually performed by stripping voltammetry, using an HMDE, in EDTA–acetate buffer [10,11].

In this paper an expert system is described for the determination of Pb, Cd, Cu, Zn, In, Ni, Co and Tl by voltammetric techniques. The system is an enhancement and improvement of a previously described expert system for the determination of Pb, Cu, Cd, Zn and In [12]. The system guides the user according to well tested voltammetric procedures, and suggests alternative procedures when the standard methods are not applicable.

THE EXPERT SYSTEM

The expert shell KES (Knowledge Engineering System) [13] has been used to develop the present system. The global architecture of the expert system is as described in Part I [12], but with an enhancement in size, because of the wider possibilities considered here.

The knowledge base implemented deals with sample treatment, voltammetric procedure identification and resolution of signals and determination. The knowledge base devoted to sample treatment is the same as previously described (summarized in Fig. 1 of Part I), as the main requirements needed for all the voltammetric methods taken into account are the same, independent of the trace metal considered.

The knowledge base has been enlarged to include data on Ni, Co and Tl. In all instances, only mercury drop electrodes (DME, SMDE and HMDE) have been considered. The methods for determining Ni and Co in the presence of DMG [6] and Tl in the presence of EDTA [10,11] have proved to be the most sensitive and suitable for the routine analysis of different types of material, achieving the status of standard methods [14]. The standard method for determining Ni and Co was developed, in fact, for the determination of Ni, and it has some limitations for the determination of Co, the best known being the presence of large excesses of Ni and/or Zn [15,16]. In such cases, alternatives have been proposed [4,8,14,15], the choice of method is not so obvious and some experience is required. Therefore, the expert system has been designed in virtue of the concentration of the analyte in comparison with the quantification limits reported for each method, and the Ni/Co and/or Zn/Co concentration ratios, in order to take advantage of the resolution of each method.

For the determination of Ni and Co, the expert system considers four possibilities, corresponding to well tested methods. Two of the methods, referred to as "option a" [13] and "option b" [4], are based on adsorptive stripping voltammetry (AdSV), but they are performed under different conditions of the aqueous medium.

```
if ion_met = Ni or Co then
   message banner, trace, banner.
   obtain method.
   message "Set up the polarograph according to the conditions mentioned;",
           "call the external program, which plots the voltammogram:".
   run register voltammogram.
   if peak1 = yes then
      obtain voltammetry2.
      message banner.
      display attach explain of value of voltammetry2.
      message banner.
      obtain quantitative.
   else
      message banner, ldd, banner.
      message end.
      stop.
   endif.
.....
break.
endif.

if ion_met = Tl then
   message banner, trace, banner.
   obtain method.
   message "Set up the polarograph according to the conditions mentioned;",
           "Call the external program which plots the voltammogram:",
   run register voltammogram.
   if peak1 = yes then
      display attach explain of conc3.
      obtain quantitative.
   else
      message banner, ldd, banner.
      message end.
      stop.
   endif.
.....
```

Fig. 1. Actions.

However, their usefulness is very similar: simultaneous determination of Ni and Co in the absence of (large) excesses of Ni or Zn. When this condition is not met, these methods are not recommended [8,14,15]. "Option c" allows the simultaneous determination of Ni and Co by AdSV, when Ni is in large excess, by using nioxime (instead of DMG used in option a) in HEPES buffer at pH 7.6 [14]. The last alternative considered is "option d", which was developed for determining Co in the presence of large excesses of Ni and Zn, and is a polarographic determination based on adsorption–catalytic effects of Co in the presence of dioxime and nitrite [16].

For the determination of Tl, a much rarer trace metal than Ni or Co, the knowledge base is built according to the standard method [13], which is a stripping voltammetric method, in EDTA–acetate buffer medium.

Identification of the signals appearing in the voltammograms follows the same pattern as in the first system [12], based on the values of the peak potentials. Moreover, the presence of anomalous features is tested by means of the values of the peak width at half-height [17,18]. In the case of overlapping peaks, mainly due to the simultaneous presence of Cd and In, the system may call the external program DECON.

The quantification procedure is based on multiple standard addition. The system indicates the most appropriate concentration range for the calibration graph, and also proposes the validation of the calibration graph by means of several statistical tests. For this purpose, the system may call the external program ULC which can perform an analysis of residuals, calculate the regression coefficients and the most common statistical parameters of the calibration process, and carry out tests on slope and/or intercept or detection of influential points [19].

In tests with known answers, the system provides recommendations according to the rules of reasoning of an expert; as a consequence, the contents of the present system have been validated.

KNOWLEDGE REPRESENTATION AND INFERENCE MECHANISM

This part of the system controls both the use and transmission of knowledge implemented in

Do you know the approximate metal-ion concentration?
1. yes
2. no

=? 1

Do you know both the approximate concentration of Ni and/or Co and the concentration ratios [Ni]/[Co] and/or [Zn]/[Co] in the sample? Choice:

1. If [Ni],[Co] > 1.0E-11 M and [Ni]/[Co] and/or [Zn]/[Co] is low.
2. If [Ni],[Co] > 1.0E-11 M and [Ni]/[Co] and/or [Zn]/[Co] is high.
3. If you are interested only in the determination of Co, and [Co] is > 3.0 E-10 M.

Note:
The choice of the method depends on the concentration levels. The methods corresponding to options 1 and 2 are based on the formation of complexes with DMG or Nioxime, respectively, and their adsorption at the hanging mercury drop electrode. For more information enter the command "explain".

(Enter a number)
=? 1

Fig. 2. Example of an interactive session with the expert system (choice of technique).

The procedures indicated in reference 13 (Option a) or in reference 4 (Option b) can be followed.

Option a (ref. 13):

The medium conditions, in the absence of great excesses of Ni and/or Co, are the following:
An aqueous solution containing 1×10^{-4} M of DMG and at pH 9.3, obtained by means of the addition of ammonia buffer NH_3/NH_4Cl 0.1-1 M (0.1 M is recommended at the lowest Ni and/or Co concentrations).

Option b (ref. 4):

The medium conditions are as follows:
An aqueous solution containing 1×10^{-4} M of DMG and at pH 8.3, obtained by means of the addition of boric acid/sodium hydroxide buffer 1M.

Fig. 3. Example of advice provided by the expert system.

The instrumental parameters of both options (a and b) are:

E <preelectrolysis> = - 0.7 V (vs SCE).
t <preelectrolysis> = 2 - 10 min.
(Recommendation: For relatively high concentrations, [Ni],[Co] > 50 μg/l (50ppb), dilute the sample in order to achieve the optimal conditions. Then,
t<pe> ≈2min.,if 1μg/l (1ppb) < [Ni], [Co] < 50μg/l (50ppb)
t<pe> =5min., if [Ni], [Co] ≈ 1 μg/l (1ppb)
t<pe> ≈10min.,if 5ng/l < [Ni], [Co] < 1μg/l)

t<rest> =20 s, v<scan rate> = 10 - 20 mV/s, E= 50 mV (in general inside the range 10 - 100 mV.)
tp = 30 - 100 ms.

If you are interested in references, enter: display attach Valenta of kb; the same applies to norm DIN and Liverpool.

Set up the polarograph according to the conditions mentioned, the voltammogram is:

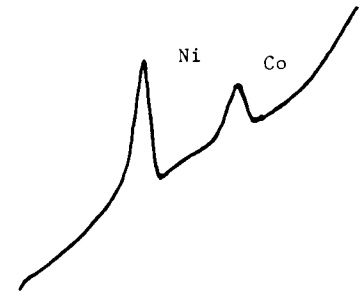

Fig. 4. Determination of Ni and Co.

the knowledge base. Attributes and rules represent the knowledge base and are used in the way previously described [12]. In the following we shall refer only to the determination of Ni, Co and Tl. References to the determination of Pb, Cd, Cu and Zn were described in detail elsewhere [12].

Figure 1, which corresponds to the actions section of the expert system (for more details see Part I [12]), contains the commands, written according to KES orthography rules, which transmit the knowledge base implemented in the expert system to the user. If the condition "if ion-met = Ni or Co then" is met, by means of the command "obtain method" the expert system advises the user on the most appropriate voltammetric technique. With this aim, the first question appearing in Fig. 2 is concerned with the user's knowledge of the approximate concentration of Ni or/and Co. After an affirmative answer, all the possibili-

(Enter a number)
=? 2

You should use Differential Pulse Adsorptive Stripping Voltammetry (DPAdSV), using the Hanging Mercury Drop Electrode (HMDE). (Method of Donat-Bruland.)

The medium conditions are:

Buffer HEPES [N- (2-hydroxyethyl)- piperazine- N'- 2- ethanesulphonic acid], at a concentration of 0.03 M, (pH ≈7.6) containing 1.E-4 M Nioxime [Cyclohexane-1,2-dione dioxime].

The instrumental parameters are:

E<preelectrolysis> = -0.6V, t<preelectrolysis> = 5 - 30 min.
t<rest> = 30 s, v<scan rate> = 10 - 20 mV/s.
E = 50 mV (10 - 100 mV.), tp = 30 - 100 ms.

If you are interested in references, enter: display attach Donat of kb.

(Enter a number)
=? 3

You should use Differential Pulse Polarography (DPP), using the Dropping Mercury Electrode (DME) or the Static Mercury Drop Electrode (SMDE). (Method of Bobrowski.)

The medium conditions are:

An aqueous solution at pH ≈8, by using ammonium buffer NH_3-NH_4Cl 0.1 M, containing 1.E-4 M Nioxime [Cyclohexane-1,2-dione dioxime], and 0.5 M $NaNO_2$.

The instrumental parameters are:

t<drop> = 1 - 2 s, E = 10 - 100 mV, v<scan rate> = 10 - 20 mV/s.
E<initial> = -1 V, E<end> = -1.3 V vs. SCE.
(vs. Ag/AgCl shifted 0.042 V.)
tp = 30 - 100 ms.

If you are interested in references, enter: display attach Bobrowski of kb.

Fig. 5. Voltammetric analysis.

ties considered appear on the screen (also included in Fig. 2). Possibility 1 involves the options a and b mentioned in the knowledge base. Possibilities 2 and 3 are referred to options c and d, respectively.

When the user selects possibility 1, Fig. 3 appears on the screen, detailing the medium conditions associated to option a (method: [13]) and option b (method: [4]). The next step is illustrated in Fig. 4, where the instrumental parameters (identical for both options) are shown.

When the user selects possibilities 2 or 3 in Fig. 2, the methods of Donat and Bruland (option c) [15] or Bobrowski (option d) [16], respectively,

Set up the polarograph according to the conditions mentioned; the voltammogram is:

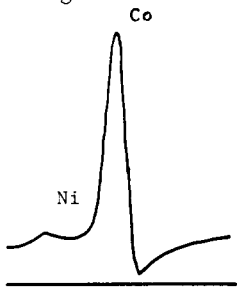

Did you observe different peaks in the voltammogram?

1. yes
2. no

=? 1

At what potential values do the peaks appear? (Potential value (vs. Ag/AgCl) working with):

DPAdSV
Option a (pH=9.3) : 1) ≈-0.95V 2) ≈-1.1V
Option b (pH=8.3) : 1) ≈-0.95V 2) ≈-1.1V
Option c (Donat-Bruland): 1) ≈-0.87V 2) ≈-0.98V
DPP Option d (Bobrowski): 2) ≈-1.18V

1. first
2. second

(multiple answers allowed)
=? 1&2

If E(DPAdSV) ≈ -1.1V or E(DPAdSV) ≈ -0.98V or E(DPP) ≈ -1.18V, the peak will correspond to Co(II).
If E(DPAdSV) ≈ -0.95V or E(DPAdSV) ≈ -0.87V, the peak will correspond to Ni(II).

From the shape of the peaks, can you state that each peak corresponds to only one chemical species?
(The expert system includes the width at half-peak corresponding to the reversible reduction of a divalent cation. For DPP, $W_{1/2} \approx 58$ mV and for DPASV, $W_{1/2} \approx 44$ mV)

1. yes
2. no

=?

Fig. 6. Identification of the voltammetric peaks.

are recommended. Figure 5 details the medium conditions and the instrumental parameters of these methods.

For the case of unknown approximate concentrations of Ni or/and Co (negative answer to the first question in Fig. 2), the expert system leads the user to the more usual methods, options a and b (Fig. 3). Only in the case of unsuccessful performances of these methods is the user directed to options c and d.

For all the options used, the polarographic signals are identified from the information shown in Fig. 6. Finally, if the user is interested in determining Tl, a standard method is recommended [14]. The information given by the system is summarized in Fig. 7.

Conclusions

The present expert system may be very useful for non-expert users in the electroanalytical field, especially for the determination of Ni and Co in samples with large excess of Ni and/or Zn. It represents an improvement over a previously described system, and it is also based in well tested methods, with particular attention to standard methods.

Which of the following cationshave to be determined?
1. Cu Zn Cd or Pb
2. Ni or Co
3. Tl
4. others

=? 3

We are now in the field of trace analysis; in this type of analysis the detection and quantification limits should be determined for the working conditions of each laboratory. The values recommended in this expert system are only a guide (and correspond to values given in the references). As a consequence, in each particular case, the detection limit should be obtained from the blank under the particular working conditions.

Do you know the approximate metal-ion concentration?
1. yes
2. no

=? 2

You should use Differential Pulse Polarography (DPP), using the Dropping Mercury Electrode (DME) or the Static Mercury Drop Electrode (SMDE). (Method of Bobrowski.)

The medium conditions are:

An aqueous sample free of organic matter, at pH 4.6 (by addition of 0.5 ml buffer solution KCl (1.5 M) - NaAcO (0.5 M) and containing 1 ml of EDTA 0.2 M (in order to complex the Pb^{2+}).

The instrumental parameters are:

E_r = Ag/AgCl or Standard Calomel Electrode. Ew = Hg.
E_{aux} = Pt or glassy carbon .
pulse= 20 - 50 mV, v= 2 - 10 mV/s.
$E_{<initial>}$ = -0.1 V, $E_{<end>}$ = -0.8 V.

Fig. 7. Determination of Tl.

This work was presented at the *II Colloquium Chemiometricum Mediterraneum*, San Miniato (Pisa), 1991. Economic support from the Spanish Ministry of Education and Science is acknowledged (CICYT projects Nos. BP90-0453 and BP90-0821).

REFERENCES

1 W. Petersen, Anal. Chim. Acta, 248 (1991) 77.
2 H.W. Nürnberg, Sci. Total Environ., 37 (1984) 9.
3 T.M. Florence, Analyst, 111 (1986) 489.
4 The Determination of Trace Metals in Marine and Other Waters by Voltammetry or AAS, HMSO, London, 1988.
5 P. Ostapczuk, P. Valenta, H. Rützel and H.W. Nürnberg, Sci. Total Environ., 60 (1987) 1.
6 B. Pihlar, P. Valenta and H.W. Nürnberg, Fresenius' Z. Anal. Chem., 307 (1981) 337.
7 J. Wang, Stripping Analysis. Principles, Instrumentation and Applications, VCH, Deerfield Beach, FL, 1985.
8 C. Locatelli, F. Fagioli and T. Garai, Anal. Chem., 60 (1991) 1409.
9 E. Jacobsen and G. Kalland, Anal. Chim. Acta, 29 (1963) 215.
10 J.E. Bonelli, H.E. Taylor and R.K. Skogerboe, Anal. Chim. Acta, 118 (1980) 243.
11 V. Gemmer-Colos, I. Kiehnast, J. Trenner and R. Neeb, Fresenius' Z., Anal. Chem., 306 (1981) 144.
12 M. Esteban, I. Ruisánchez, M.S. Larrechi and F.X. Rius, Anal. Chim. Acta, 268 (1992) 95.
13 KES, PS Version 2.4, Software Architecture and Engineering, Arlington, VA, 1990.
14 Deutsche Norm, DIN 38 406, Teil 16, March 1988.
15 J.R. Donat and K.W. Bruland, Anal. Chem., 60 (1988) 240.
16 A. Bobrowski, Anal. Chem., 61 (1989) 2178.
17 E.P. Parry and R.A. Osteryoung, Anal. Chem., 37 (1965) 1634.
18 G.E. Batley and T.M. Florence, J. Electroanal. Chem., 55 (1974) 23.
19 R. Boqué, F.X. Rius and D.L. Massart, submitted for publication.

Analytica Chimica Acta, 268 (1992) 115–122
Elsevier Science Publishers B.V., Amsterdam

Multivariate correction of chemical interferences in hydride generation atomic absorption spectrometry

Günter Henrion, René Henrion, Ralph Hebisch and Birgit Boeden

Institute of Analytical Chemistry, Humboldt University Berlin, Hessische Str. 1–2, D-O-1040 Berlin (Germany)

(Received 9th December 1991)

Abstract

In hydride generation atomic absorption spectrometry, chemical interferences among hydride-forming elements lead to systematic errors in the determination of concentrations. Using the system of Se, Sb and As as an example of simultaneously occurring elements, it is shown how to remove the systematic underestimations by the use of multi-component calibration. The advantage of this approach relies on the multivariate treatment of mutual interferences. For the given problem, application of multiple linear regression turns out to be equivalent to partial least squares. Estimation of the standard error of prediction confirms the temporal stability of the model. Further, in contrast to the prediction of concentrations, an "inverse" model is established in order to attempt a description of interferences.

Keywords: Atomic absorption spectrometry; Antimony; Arsenic; Hydride generation; Multivariate analysis; Selenium

The determination of hydride-forming elements plays an important role in analytical chemistry. The main reason is their high ecotoxicity at very low concentration levels. The method of choice for the determination of elements such as As, Sb and Se (which are subject of this paper) is hydride generation atomic absorption spectrometry (HGAAS). Hydride generation may be realized in batch and in continuous-flow modes. The main advantage of the hydride generation technique is good preconcentration, chemical separation of the analyte from potential matrix interferences and very efficient introduction of the analyte into the atomizer [1]. On the other hand, many interferences exist. A first systematic report on intererences of 48 elements was given by Smith [2]. He found that the most serious interferences are caused by many transition metals and the other hydride-forming elements. The latter give rise to numerous problems, because in many samples of geological [3,4] and biological [5,6] origin or in environmental studies [7,8] these elements occur jointly.

Many investigations have been carried out to explain and to overcome such cross-interferences of hydride-forming elements. During the step of hydride generation it is generally not possible to separate the hydride of the analyte from those of potential interferents. As a consequence, interferences in liquid and gaseous phases have to be taken account of. Hulanicki et al. [9] used a twin-channel flow system to characterize both of these types of interferences. Dittrich and Mandry [10–12] suggested the formation of interelement compounds (e.g., AsSb) in the liquid phase and also in the gaseous phase. Their explanations were based on spectroscopic measurements of such species and thermodynamic calculations.

Correspondence to: G. Henrion, Institute of Analytical Chemistry, Humboldt University Berlin, Hessische Str. 1–2, D-O-1040 Berlin (Germany).

Welz and Melcher [13] used addition of copper ions to avoid the interference of selenium during the determination of arsenic. They found that this interference depends only on the concentration of the interfering element in the solution and not on the analyte-to-interferent ratio. Castillo and co-workers [14,15] investigated interferences in different types of atomizers. More theoretical treatments of interferences were given by Dedina [16,17], who described different types of interferences in detail.

The shortcoming of these investigations is that they considered only one interferent beneath the analyte. In practice, especially for environmental analyses (e.g., sea water and coal fly ash), these samples are much more complex. The present investigations represent a first attempt to take into account the disturbing influence of more than one interferent in a sample.

EXPERIMENTAL

Apparatus

For measurements in the batch mode an AAS 30 atomic absorption spectrometer (Jenoptik, Jena) equipped with a hydride generation system and an electrically heated quartz tube atomizer was used. All elements were determined using hollow-cathode lamps (Narva, Berlin). The operating parameters and the instrument settings were chosen according to the manufacturer's recommendations and are listed in Table 1. The settings for purge gas flow-rate and carrier gas flow-rate were 600 and 300 ml min^{-1}, respectively. Auto-zero of the instrument was realized during the first 2.5 s of the reaction phase. For all elements the time-integrated absorbance over 25 s was determined.

TABLE 1

Working conditions in the batch mode

Parameter	Se	Sb	As
Wavelength (nm)	196.0	217.6	193.7
Current of hollow-cathode lamp (mA)	6	7	8
Slit width (mm)	0.6	0.6	0.5
Cuvette temperature (°C)	780	900	900
Purge phase 1 (s)	15	5	15
Reaction phase (s)	14	14	14
Purge phase 2 (s)	30	40	30

The measurements in the continuous-flow mode were carried out using a Perkin-Elmer Model 300 atomic absorption spectrometer equipped with a laboratory-built quartz tube atomizer according to Hulanicki et al. [9]. The flow system was used in combination with a peristaltic pump and a gas–liquid separator. The temperature of the atomizer was kept constant at 900°C. The pumping rates for sodium tetrahydroborate solution (0.5%) and hydrochloric acid (2 mol l^{-1}) were 2.9 and 8.5 ml min^{-1}, respectively. The argon carrier gas flow-rate was 20 l h^{-1}. The auto-zero time for all measurements was 10 s and the corresponding integration time was 30 s.

Reagents

All reagents were of analytical-reagent grade. Hydrochloric acid (Laborchemie, Apolda, Germany) was cleaned by sub-boiling distillation. Sodium tetrahydroborate solutions were prepared by dissolving the powdered form (Merck) in deionized water and stabilized with 1% (w/v) sodium hydroxide. These solutions were filtered before use and stored in a refrigerator. For stock standard solutions Titrisol concentrates (Merck) were used, which were prepared according to the manufacturers recommendations. The working solutions were prepared immediately before the measurements by diluting the standards with hydrochloric acid. The concentrations of As, Sb and Se were chosen in the same range, so it was possible to determine the content of all these three elements in the same sample without any dilution. Another aspect kept in mind was that the concentrations of these elements cover a range around the limits of water quality for human use [18].

MULTI-COMPONENT CALIBRATION

The mentioned interferences lead to a superposition of ordinary measurement error (random)

by a systematic deviation. In the present Se, Sb, As system one observes systematic underestimations of true concentrations. Subsequently it will be described how to obtain a computational correction of this effect by multi-component calibration. Traditionally such a correction is performed by means of single-element considerations. This, however, does not take account of the complexity of a system of interfering elements. Therefore, it is suggested that the problem is treated as one of multi-component calibration which has proved superior to classical univariate calibration.

The underlying statistical methods, such as multiple linear, principal components, latent root, partial least-squares regression or canonical correlation analysis, have been extensively described in the statistical (e.g. [19]) and chemometric (e.g., [20]) literature. In typical applications of multi-component calibration a set of element concentrations is related to a set of spectral absorbances, and the former is to be predicted by the latter. By doing so, spectral interferences can be handled (examples in AAS were given by Baxter and co-workers [21,22]). In the present situation concentrations of elements determined by simple calibration were used as the predicting variables while true concentrations of the same elements are to be predicted. In contrast to spectral data sets, this is a completely different situation from both the computational and statistical points of view (the set of predictors is usually much larger in the case of spectral data and it is also more seriously affected by the multi-collinearity problem). Concerning statistical methods, considerations are restricted to classical multiple linear regression (MLR) and partial least squares (PLS).

Results of batch mode

In order to establish the effect of chemical interferences in the Se, Sb, As system, a set of training data was established according to a factorial design: 64 synthetic samples were prepared with amounts of Se, Sb and As independently varying between the four levels 25, 50, 75 and 100 ng. Each calibration sample was measured twice. Results of measurements were fixed as amounts (in ng) rather than intensities of signals, in order to keep them stable for future investigations. Finally, two data matrices, with 128 rows and 3 columns (elements) each, were obtained: $\boldsymbol{X}^{\mathrm{meas}}$ (resulting from measurements) and $\boldsymbol{X}^{\mathrm{true}}$ (resulting from known concentrations according to the described factorial design). Note that, formally, each row in $\boldsymbol{X}^{\mathrm{true}}$ occurs twice in correspondence with repeated measurements in $\boldsymbol{X}^{\mathrm{meas}}$. Now, MLR and PLS relate both matrices by means of certain model equations. Using these models it is possible to predict true (but then unknown) concentrations of Se, Sb and As in test samples from the corresponding measured values (which are affected by chemical interferences). Before doing so one ought to validate the obtained models by means of samples with known true element concentrations but which did not participate in the model building phase. This was done in the present example by splitting both data matrices into two parts in a canonical way, exploiting the fact that each sample was endowed with two parallel determinations. The first determinations served for modelling, whereas the second were considered as test samples to which the model had to be applied. Because for these (artificial) test samples true concentrations were also known, one can sum the deviations between predicted (by the

TABLE 2

Standard errors of measurements and predicted amounts compared with true amounts for 64 samples not included in the model building phase (values in ng for batch mode and $\mu g\ l^{-1}$ for continuous-flow mode)

Method	Batch mode			Continuous-flow mode		
	Se	Sb	As	Se	Sb	As
Measurements	6.40	4.82	9.47	1.20	0.97	3.56
Simple linear regression	2.98	2.17	5.15	0.71	0.69	2.18
MLR (optimum subset)	2.44	1.79	2.49	0.68	0.65	1.72
PLS (6 variables)	2.40	1.82	2.53	0.67	0.66	1.79
PLS (3 variables)	2.56	1.82	3.17	0.67	0.65	1.74

model) and true amounts to yield an estimation of the standard error of prediction (*SEP*) according to

$$SEP = \left(\sum_{i=1}^{64} \delta_i^2 / 64 \right)^{\frac{1}{2}} \quad (1)$$

where δ_i refers to the difference between true concentration on the one hand and the measured or predicted concentration on the other of the ith sample which did not participate in the model building phase.

The results are summarized in Table 2 and Fig. 1. Figure 1 illustrates well an increasing underestimation in measurements due to chemical interferences. This is most notable for As, where the error of measurement (random + systematic) reaches about 10 ng as an average over the considered range. For Sb the influence of the remaining two elements seems less remarkable. The simplest computational approach of correction would consist in simple linear regression, e.g., predicting true concentrations of Se exclusively by measured concentrations of Se, thereby ignoring the contribution of the remaining elements. This would correspond to choosing an optimum coefficient in order to shift the cloud of points in Fig. 1 towards the bisecting line. In fact, this simple approach is able to reduce markedly the standard error of prediction with improvements of about 50% compared with pure measurements in the present example. Nevertheless, simple linear regression does not consider mutual influences of different elements. Therefore, in the multivariate approach, the true concentrations of Se, Sb and As were considered to depend on the measured concentrations of the following single-element and cross-element terms: Se, Sb, As, Se · Sb, Se · As and Sb · As. Table 2 confirms that there is still a relevant gain in reducing the error of prediction by multivariate methods. First, this is true for As owing to the strong influence of both Se and Sb. The MLR results were obtained after reducing by stepwise selection the total set of six predictors to an optimum subset. For PLS calculations the so-called PLS mode 2 was used, i.e., the total set of three element concentrations is predicted by a single model.

It is interesting that MLR and PLS estimations do not differ significantly, in contrast to applications where whole spectra are used for predic-

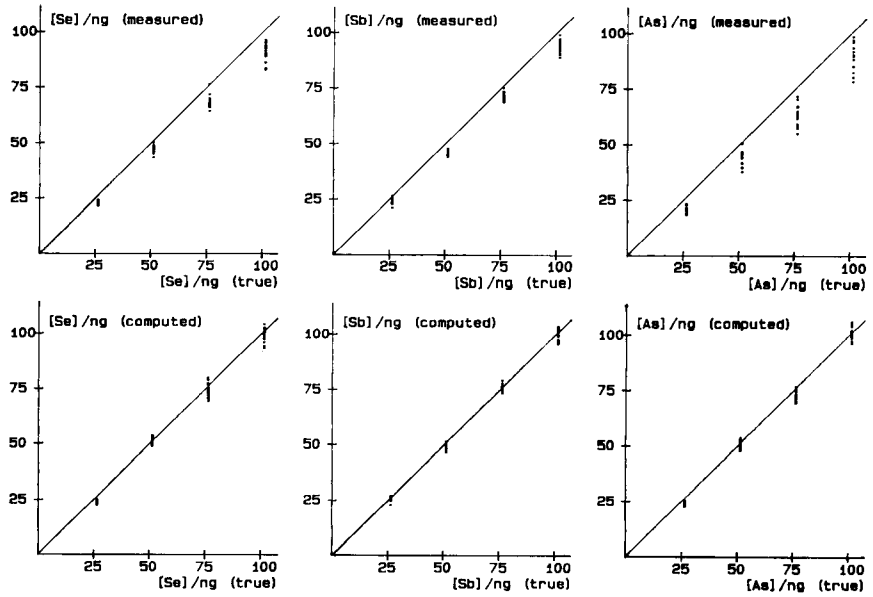

Fig. 1. Illustration of the error of prediction for measured and computed amounts in the batch mode (compare Table 2).

tion. The explanation is simple: in the present example, the predicting matrix X^{meas} (extended by columns corresponding to cross-terms) arises from the matrix X^{true}. All variables of the latter matrix are, of course, uncorrelated due to the orthogonal factorial design. This orthogonality, however, is only slightly perturbed in X^{meas} although absolute values are strongly distorted by chemical interferences compared with the design matrix. Therefore, all predicting variables remain in moderate correlation and, consequently, the multi-collinearity problem has only subordinate importance here. If only the three original variables (Se, Sb, As) are used as predictors for PLS and cross-terms are omitted, then the error increases for elements being strongly subjected to interferences. Quadratic terms turned out not to be significant in any case. Figure 1 illustrates how the systematic deviations of measured from true concentrations are removed by the multivariate approach (here MLR results). Apart from this, it is easily recognized that the cloud of points is not merely shifted towards the bisecting line (like, e.g., by simple linear regression) but, additionally, the dispersion around this line is considerably reduced.

Results of continuous-flow mode

In addition to the batch mode, the continuous-flow mode was investigated as an alternative technique. The methodological environment was the same as described for the batch mode, except that now in the factorial design the concentrations of Se, Sb, As varied between the four levels 10, 20, 30 and 40 $\mu g\ l^{-1}$. The results are given in Table 2 and Fig. 2. Again, interferences are greatest for As and the improvement by computational correction is similar (although slightly weaker) to that in the batch mode. In contrast to the batch mode, the influence of cross-terms seems to vanish. Perhaps this is due to another underlying mechanism of interferences.

Stability investigations

In order to affirm the improvements obtained so far, investigations of stability were made. Here, stability refers to temporal changes and to reduction of factorial design. Considerations are re-

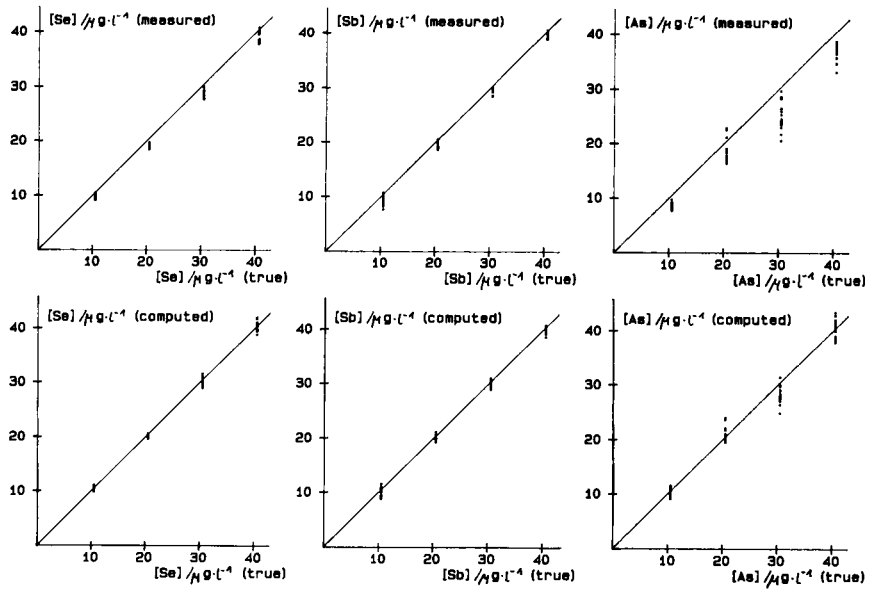

Fig. 2. Illustration of the error of prediction for measured and computed concentrations in the continuous-flow mode (compare Table 2).

TABLE 3

Errors of prediction for 20 additional test samples in batch mode

Method	Error (ng)		
	Se	Sb	As
MLR (optimum subset)	2.54	1.61	3.28
PLS (6 variables)	2.56	1.58	3.28
MLR (reduced design)	2.83	1.65	3.50

stricted to the batch mode. Because, so far, measurements for model building and the test phase were made at the same time, 20 additional test samples were prepared several weeks later in order to check whether the model remains stable in relation to instrumental outputs. Further, the concentrations of test samples were uniformly distributed over the relevant range. The *SEP* was computed again according to Eqn. 1 but now with 64 replaced by 20. The results are given in Table 3 and Fig. 3. Comparison with the batch mode results in Table 2 shows good agreement. Consequently, it seems possible to restrict the time-consuming modelling phase to a single investigation (with respect to the given system of elements and the given instrumental conditions). Then, using the established model, future test objects may be analysed without repetition of model building. The other problem of stability arises from the cost of preparing large numbers of samples for the factorial design. This becomes relevant when the system of considered elements is extended, e.g., by including Bi, Te, Sn, etc., in the analysis. As the number of samples to be prepared for a full orthogonal factorial design at k levels for n elements is k^n, one is forced to restrict the number of levels with increasing n. Then, however, the established model may become unstable. To obtain an impression of this effect in the present example, a model was additionally used which was derived from the original one by deleting all combinations where one of the four levels, namely 75 ng, appeared. Then, only 27 samples remained for model building. Predictions of the 20 test sample concentrations from the reduced factorial design now become slightly worse but still are much better than measurements. Hence restricting to three levels in the given situation is justified if the expenditure on sample preparation seems too high.

Description of interferences

Until now, statistical modelling was used for predicting true concentrations from measured

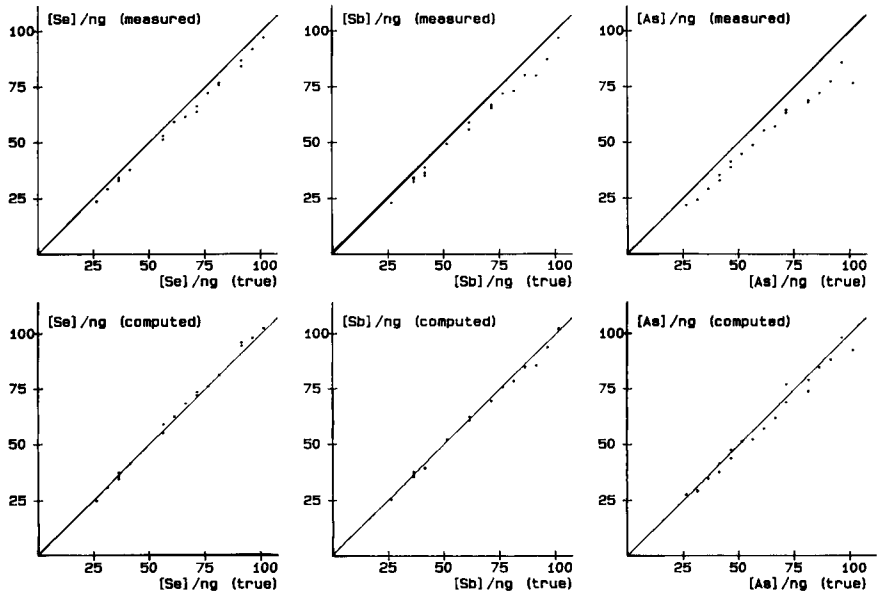

Fig. 3. Illustration of the error of prediction in the batch mode for 20 additional test samples (compare Table 3).

values, i.e., the direction of modelling was $X^{meas} \rightarrow X^{true}$. If, in contrast, one wishes to describe interferences and, perhaps, to find a chemical mechanism, then the reverse direction $X^{true} \rightarrow X^{meas}$ has to be modelled, as the measured concentrations are the logical result of chemical interferences the degree of which depends on the true element concentrations. Similar, but much more detailed, studies were undertaken by Kościelniak and Parczewski for the K, Na, Sr [23], Fe, Na and Ca, Sr [24] and Ca, Ti [25] systems. Concerning this subject, we restrict ourselves to indicating the model equations without deriving hypotheses about the chemical mechanism which would require much more sophisticated investigations. Nevertheless, it is possible to get an impression of the structure of interferences. Table 4 summarizes the regression coefficients, c_i, of linear models of the type

$$\mathrm{Se}^{meas}(\mathrm{Sb}^{meas}, \mathrm{As}^{meas}) = c_1[\mathrm{Se}] + c_2[\mathrm{Sb}] + c_3[\mathrm{As}] + c_4[\mathrm{Se}][\mathrm{Sb}] + c_5[\mathrm{Se}][\mathrm{As}] + c_6[\mathrm{Sb}][\mathrm{As}]$$

for the description of interferences in batch and continuous-flow modes. Non-significant terms are deleted. As to be expected, in a first approximation the measured concentrations are in one-to-one correspondence with the true concentrations (regression coefficients nearly 1). Apart from these trivial contributions there are contributions of other terms relating these to chemical interferences. As all of the non-trivial contributions have a negative sign, one can observe a uniform underestimation by measurements. To make contributions of cross-terms and single-element terms comparable, average values for the true concentrations (expressions in brackets) taken over the total factorial design were inserted. The average single-element concentration in the batch mode, for instance, was (25 + 50 + 75 + 100)/4 ng = 62.5 ng, whereas for cross-products of concentrations the average was 3906.25 ng. Then, regression coefficients multiplied by average concentrations give the average contributions of non-trivial terms denoted in parentheses.

Now, it is immediately verified that Se/As interferences dominate the whole system. One observes that the influence of this pair in the determination of As is even higher than in the determination of Se. There is no clear explanation why the dominance of cross-terms over single-element terms changes from the batch to the continuous-flow mode. It may be caused by different chemical mechanisms (cf., [9]), but also by

TABLE 4

Regression coefficients for the description of interferences, with values in parentheses indicating average contributions related to the corresponding factorial design

Parameter	Batch mode					
	[Se]	[Sb]	[As]	[Se]·[Sb]	[Se]·[As]	[Sb]·[As]
Se^{meas}	0.96				-9×10^{-4} (3.5 ng)	
Sb^{meas}	−0.03 (1.9 ng)	0.96				-3×10^{-4} (1.2 ng)
As^{meas}			1.04		-2×10^{-3} (7.8 ng)	-4×10^{-4} (1.6 ng)
	Continuous-flow mode					
Se^{meas}	0.99			-6×10^{-4} (0.4 $\mu g\,l^{-1}$)		
Sb^{meas}	−0.02 (0.5 $\mu g\,l^{-1}$)	1.01	−0.02 (0.5 $\mu g\,l^{-1}$)			
As^{meas}	−0.11 (2.8 $\mu g\,l^{-1}$)		0.91			

a too small sample size, which perhaps makes it uncertain to decide whether a functional dependence is of the type $A = f(A, B, C)$ or of the type $A = f(A, B \cdot C)$. In fact, using a reduced factorial design, similar to stability investigations in multi-component calibration, confirms that the stability of the set of significant terms is more seriously affected by sample size than goodness of prediction.

Conclusion

The investigated Se, Sb, As system is dominated by Se/As interferences. Multi-component calibration, using any accepted method of multivariate regression, is an efficient approach for the computational correction of systematic errors in measurements. Goodness of prediction is stable over time, thus allowing an extensive factorial design to be established once and only once and, subsequently, to use the obtained model for routine analyses. A generalization to more complex systems, such as Se, Sb, As, Bi, Te, Sn, is straightforward from the methodological point of view, but care has to be taken with an appropriate size of factorial design.

The authors thank Professor Dr. A. Hulanicki and his group at Warsaw University for the possibility of using their device for continuous-flow measurements and thank the Fonds der Chemischen Industrie for financial support.

REFERENCES

1 T. Nakahara, Prog. Anal. At. Spectrosc., 6 (1983) 163.
2 A.E. Smith, Analyst, 100 (1975) 300.
3 A. Meyer, C. Hofer, G. Tölg, S. Raptisand G. Knapp, Fresenius' Z. Anal. Chem., 296 (1979) 337.
4 J. Agterdenbos, J.T. Van Elteren, D. Bax and J.P. Ter Heege, Spectrochim. Acta, Part B, 41 (1986) 303.
5 M. Fleischer and K.H. Schaller, in B. Welz (Ed.), 4. Colloquium Atomspektrometrische Spurenanalytik, Bodenseewerk Perkin-Elmer, Überlingen, 1987, p. 577.
6 M. Verlinden and H. Deelstra, Fresenius' Z. Anal. Chem., 296 (1979) 253.
7 J.W. Hershey, T.S. Oostdyk and P.N. Keliher, J. Assoc. Off. Anal. Chem., 71 (1988) 1090.
8 R.E. Sturgeon, K.W.M. Siu, S.N. Willie and S.S. Berman, Analyst, 114 (1989) 1393.
9 A. Hulanicki, E. Bulska and M. Wałcerz, Fresenius' Z. Anal. Chem., 332 (1988) 176.
10 K. Dittrich and R. Mandry, Analyst, 111 (1986) 269.
11 K. Dittrich and R. Mandry, Analyst, 111 (1986) 276.
12 K. Dittrich and R. Mandry, Wiss. Z. Karl-Marx-Univ. Leipzig, Math.-Naturwiss. Reihe, 35 (1986) 82.
13 B. Welz and M. Melcher, Anal. Chim. Acta, 131 (1981) 17.
14 J.R. Castillo, J.M. Mir and I. Perez, Microchem. J., 39 (1989) 119.
15 J.R. Castillo, J.M. Mir and M.T. Gomez, Microchem. J., 39 (1989) 213.
16 J. Dedina, Prog. Anal. Spectrosc., 11 (1988) 251.
17 J. Dedina, Anal. Chem., 54 (1982) 2097.
18 Directives of the Council of the European Community on Water Quality for Human Use, Amtsblatt der EG, Nr. L 229/11, EEC, Brussels, 1980.
19 R.F. Gunst and R.L. Mason, Regression Analysis and its Applications, Dekker, New York, 1980.
20 H. Martens and T. Næs, Multivariate Calibration, Wiley, New York, 1990.
21 D.C. Baxter and J. Öhman, Spectrochim. Acta, Part B, 45 (1990) 481.
22 D.C. Baxter, W. Frech and I. Berglund, J. Anal. At. Spectrom., 6 (1991) 109.
23 A. Parczewski and P. Kościelniak, Fresenius' Z. Anal. Chem., 297 (1979) 148.
24 P. Kościelniak and A. Parczewski, Anal. Chim. Acta, 165 (1984) 297.
25 P. Kościelniak and A. Parczewski, Anal. Chim. Acta, 177 (1985) 197.

Analytica Chimica Acta, 268 (1992) 123–134
Elsevier Science Publishers B.V., Amsterdam

Optimization of calibration data with the dynamic genetic algorithm

Tong-Hua Li

Department of Chemistry, Tongji University, Shanghai 200092 (China)

C.B. Lucasius and G. Kateman

Laboratory for Analytical Chemistry, University of Nijmegen, Toernooiveld, 6525 ED Nijmegen (Netherlands)

(Received 3rd January 1992)

Abstract

Genetic algorithms constitute a set of powerful search heuristics. A modified genetic algorithm was used to optimize calibration data sets. In order to construct an ideal genetic procedure, the diversity in a population is crucial. The idea proposed is to estimate the diversities along two directions, namely the diversity between the chromosomes in a population and the diversity between the alleles in all chromosomes. The newly defined diversity functions are able to describe the procedure of a genetic algorithm in detail and can be used as a feedback for dynamic control of the process in an almost ideal way. The optimization results show that for both short and long runs the dynamic genetic algorithm is superior to the "classical" genetic algorithms and that after optimization not only can the data sets be compacted and refined but also the predictive ability of the calibration model can be improved.

Keywords: Optimization methods; Calibration; Dynamic control; Genetic algorithms; Wavelength selection

Genetic algorithms (GAs) are based on the simulation of natural selection, genetics and evolution and have been intensively studied and applied in recent years [1–10]. Much of the interest in genetic algorithms is ascribed to the fact that genetic algorithms belong to the class of efficient domain-independent search strategies that are usually superior in performance to traditional methods without the need to incorporate highly domain-specific knowledge. Several applicatons of genetic algorithms in machine learning, adaptive systems and optimization also show that genetic algorithms are more powerful search heuristics in noisy environments (an environment is defined by a given problem) where the space usually is large, discontinuous, complex and poorly understood. Recently, genetic algorithms were introduced into chemometrics by Lucasius and Kateman [11–15]. They devoted much attention to the applications of genetic algorithms in this discipline, and clearly pointed out that chemometrics is a fertile area for the application of genetic algorithms.

In this work, a modified genetic algorithm was employed in a practical chemical problem. Consider a calibration data set that is the response measured by an advanced chemical instrument and usually is a multivariate, multi-dimensional and multi-sample set. Our purpose is to develop an optimum approach that can automatically select variables, diagnose outliers, retrench redundant data and build a calibration model that has powerful predictive capabilities and is robust in noisy environments. This means that the method

Correspondence to: Tong-Hua Li, Department of Chemistry, Tongji University, Shanghai 200092 (China).

should construct a subset (subspace) that contains the same calibration information as the original set except for part of the experimental and manual errors. In general, this is a procedure of compacting and refining data sets. Because a few erroneous data will drastically influence the reliability of the results, any intelligent system, e.g., an intelligent instrument or an expert system, should be provided with this recognition capability.

This optimization problem has attracted attention for a long time. It is well known that the selection of variables (e.g., wavelength) can reduce the calibration residuals [15,16] and avoid the spectral areas where no information is contained (essentially baseline or drift). Diagnosing outliers has been an active topic recently [17,18] and it is of benefit for building a calibration model [19]. Recently, a new method, simulated annealing, was used as global optimization method with wavelength selection for UV spectrophotometry [20].

However, these traditional methods (except for the simulated annealing algorithm) generally work for one-dimensional cases and usually need highly domain-dependent knowledge. The complexity makes the traditional methods useless when a high-dimensional optimization problem is involved. Therefore, those methods which are domain-independent, called weak methods, are considered in this field.

Apart from discussing the aforementioned analytical optimization problem, in this paper much attention is paid to genetic algorithms themselves and some important improvements. According to the ideas of analysis of variance, new diversity functions are proposed and defined to describe the genetic process. In addition, the defined functions are used as a feedback to control efficiently the GA's process in an ideal way.

The principles of genetic algorithms are presented in the next section, followed by the diversity functions, their definitions and properties, and then the results and a discussion, including the description of a GA procedure: an ideal GA procedure, dynamic control and the optimized results of near-infrared reflectance (NIR) data and liquid chromatographic–diode-array detection (LC–DAD) data.

GENETIC ALGORITHMS

Genetic algorithms are adaptive generate-and-test procedures derived from the principles of natural population genetics. There are numerous variants of GAs, and this section describes one of the most common. Because most chemists are not familiar with this field, we shall first discuss the GA procedure briefly. The main idea behind genetic algorithms is simple. Figure 1 shows the skeleton of a genetic algorithm.

During iteration t, the genetic algorithm keeps a population $P(t)$ which consists of a number of competing candidate solutions in which better performing individuals have a higher probability of surviving and generating later generations. The wealth of information in the individuals is saved and propagated in a highly parallel fashion. This intrinsic parallelism, for which Holland [1] laid the mathematical foundations, has the capability of making structural changes over time, discovering better and better individuals and/or improving the consistency of internal knowledge.

The architecture of a genetic algorithm can be divided into five components: representation, initiation, evaluation, genetic operations and genetic parameters.

First, a genetic algorithm requires each candidate solution to be represented as a fixed-length string, or "chromosome". The chromosome, analogous to natural chromosomes, consists of "genes" for which usually a binary alphabet {0,1} is used. In general, each gene on this abstract

```
genetic algorithm()
{
  t=0;
  initialize population P(0);
  evaluate P(0);
  while ( termination conditions )
    {
        t=t+1;
        select P(t) from P(t-1);
        recombine P(t);
        evaluate P(t);
    }
}
```

Fig. 1. The skeleton of a genetic algorithm.

chromosome is a group of bits. Both theoretical and empirical results have shown that a bitstring notation is a powerful representation to encode a wide variety of information that is not necessarily bound to a restricted domain. Other representations are available, although they have not been intensively studied. In the present context, we use a pseudo-high-dimensional chromosome to represent a candidate subset. The chromosome is divided into several segments according to the number of dimensions in the calibration problem. Each segment represents a sampling manner in one dimension; {0,1} expresses a selection, that is, if the ith gene of a segment is "1", the ith column (or row) is selected to construct a subset which is a candidate for the solution. The length of the whole chromosome has the fixed value m; n chromosomes construct a population. In this way the population may be regarded as a matrix with n rows and m columns. The sampling strategy is optimized and the global or near-global optimum subset is expected to be found at the end of the evolution process.

The second component is the method of creating an initial population. For practical reasons, a random initial population is frequently used. In the present analytical application, special knowledge is available to put into the initial population. For instance, some special wavelengths can be chosen in every subset of the initial population in order to gain a higher sensitivity. Hence in this population, some alleles (columns in the population matrix) always take 1 s. This should be done carefully, however, as genetic algorithms are notoriously opportunistic and may rapidly converge to a local optimum if the population contains a few chromosomes that are far superior to the remainder of the population [21].

The next component is called evaluation or fitness. The evaluation function plays the role of the environment. It provides a measure of the subset's fitness for the optimization problem. It governs the extent to which chromosomes can or cannot survive in a population and influence the next generation. The evaluation usually is expensive. Typically it requires more than several hundred samples before genetic algorithms have sufficient information to bias strongly subsequent samples into successful subspaces [3]. The highest price to be paid for searching a large space is the calculation of evaluation functions. In the present context, the evaluation function is PRESS (predictive residual error sum of squares) of cross-validation. For a sampled subset, a powerful calibration method, the modified principal component regression, is used to decompose the competitive subsets. Because this method exploits both calibration and predictive measured data to build its model, only one decomposition is needed for every sampling. The price therefore is evidently reduced. After decomposition, cross-validation is used, i.e., each time the "leave-on-out" method is used for predicting the left sample. This is repeated until every sample has been left out once and only once. PRESS is an average over all prediction residuals of squares in a subset.

Another component, the most important in GAs, is the following set of variation operators: the crossover operator, the mutation operator and the inversion operator. The chief among these operators is crossover, through which the selected parents can pass their genetic material to their offspring. Figure 2 illustrates the way in which the crossover operator works. When two parents are selected, two breakpoints i and j are created at random, where $0 < j$, $j < m$. Two new offspring members are generated by exchanging the par-

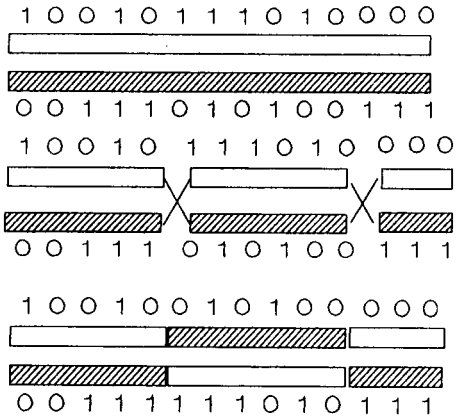

Fig. 2. The crossover operation. Two parent chromosomes exchange part of their genetic material and two offspring have new constructions.

ents' segments and both contain part of the genetic material of their parents. Crossover is an important operator in GAs, despite the fact that it is unable to create new information that does not exist in the parent structures.

The way in which one can "discover" new or retrieve lost information is by using the mutation operator. Mutation randomly changes the genes in a chromosome according to the mutation probability. For example, in a randomly chosen chromosome a position is selected at random; if this gene is 0, it mutates to 1, and vice versa. In the present context only crossover and mutation are used; the inversion operator was not used in this study.

The last component, the genetic parameters, includes the size of a population, the probability of crossover, the probability of mutation, the number of generations, etc. It is recognized that when a genetic algorithm is used to optimize a practical problem, the setting parameters themselves must usually also be optimized with regard to convergence speed. Although the optimization of genetic setting parameters has been intensively studied [4,22], there is still a great freedom of choice for these parameters, and varying these parameters in run-time can improve the performance of GAs [21]. In the present context, we shall introduce some new parameters that enable the genetic procedure to be performed more efficiently.

DIVERSITY FUNCTIONS

Although genetic algorithms have been applied successfully to optimization problems in gas pipeline control [23], semiconductor layout [24] and the design of computer networks [25], there are still several performance issues that are not very clear. It is our feeling that there is still much to learn about how to implement GAs efficiently with respect to time.

The first issue is an inherent trade-off between exploitation and exploration which has been discussed in many publications [26,27]. GAs could be thought of as search strategies between the random search and the hill-climbing strategies. For the random search strategy, historical knowledge about estimates of the optimum solution is ignored and every region is sampled blindly. Usually it is intolerably inefficient. For the hill-climbing strategy, the best-so-far is exploited to limit the search space, other latent opportunities being ignored. It is sensitive to pointing to an incorrect direction when the problem is complex.

A genetic algorithm takes a balance between exploiting what already works best and exploring possibilities that might eventually evolve into something even better. However, in practice, the optimum balance cannot be achieved automatically. It is not clear whether the balance is optimum and how to control it as well as possible.

The second issue is premature convergence, i.e., the search becomes trapped in a local optimum before the global optimum is found. In this situation, the crossover operator becomes less effective because some loci are fixed on alleles and the search space is reduced. At the same time, lower mutation rates can hardly help to prevent the search from becoming trapped in local optima, whereas higher mutation rates will disrupt the proliferation of high-performance alleles in addition to poor ones. A robust search strategy should anticipate the premature convergence and effectively avoid it. In general, this is a balance between a broad search and a sufficient refinement.

In order to gain a deep insight into the issues mentioned above, some tools or functions to monitor a genetic process and, if possible, to control this process are needed. These tools should be domain-independent. There are several functions that have been proposed to describe the GA behaviour. In earlier work by DeJong [22], the allele loss was used as one of the criteria to choose the setting parameters. Mauldin [28] proposed the minimum Hamming distance to enforce the needed diversity to avoid premature convergence. He defined a uniqueness value that is an allowed distance between any offspring and all existing chromosomes in the population. Whenever a new individual was generated and it contained an existing structure, the alleles were randomly changed in the offspring until the required distance was achieved. Grefenstette [21]

measured the population entropy for his travelling salesman problem. The population entropy is a good measure, that is, as the population converges, the entropy approaches zero. However, his definition of entropy makes it suitable only for his particular problem. Baker [29] observed that rapid convergence often occurs after an individual or a group of individuals has passed a large number of offspring to the next generation. He and Booker [30] measured the percentage involvement, i.e., the percentage of the current population producing offspring. In this way they could anticipate rapid convergence and had a chance to prevent it.

All of these efforts have in common that they want to make an ideal genetic algorithm. The key to an ideal genetic algorithm is to maintain a high degree of diversity within a population. Population diversity is crucial to a GA's ability to continue the fruitful exploration of the search space. In contrast to other GA researchers, we think that the diversity should contain two contexts, one being the diversity between the chromosomes in a population and the other the diversity between the alleles in all chromosomes. The former is concerned with the efficiency of genetic operators and the latter mainly expresses the state of convergence.

For these reasons, we propose new diversity functions that can describe the behaviour of a genetic algorithm and can be used to control the genetic process to work in an ideal manner. The ideal of these diversity functions originates from chemometrics, and is called ANOVA (analysis of variance).

Again, consider a population at time t as a matrix, in which a row expresses a chromosome and a column in an allele. The statistical analysis is carried out along two directions, rows and columns. Then the diversity functions, named the "between chromosome" diversity (BC) and the "between allele" diversity (BA), are defined as follows:

$$BC = \left(\sum_i S_i^2/m - S^2/nm \right)/(n-1) \quad (1)$$

$$BA = \left(\sum_j S_j^2/n - S^2/nm \right)/(m-1) \quad (2)$$

where S is the sum of genes "1" in a population, S_i expresses the sum over a row, i is the row index, S_j expresses the sum over a column and j is the column index.

As the genes are members of a binary alphabet here, the diversity functions have some important properties (the proof of these properties is presented in the Appendix), as follows.

The diversity functions are indifferent to mutual exchange of two chromosomes in a population, i.e., the diversity functions are independent of the permutations of the chromosomes.

If a population is homogeneous in either 0 or 1, the diversity functions are zero. This implies that there is no information in this population when the diversity functions all are zero.

When all the chromosomes in a population are identical, the BC function is zero and the BA function holds a constant value that is dependent on how many genes "1" are in a chromosome. Hence, if BC is low, convergence is expected to be achieved.

On crossover, the BA function is unchanged. In other words, BA is independent of the crossover operator.

If a population "loses" a chromosome, i.e., all the genes in this chromosome are zero, the maximum value of BC is m/n. Moreover, if k chromosomes are lost, the maximum value of BC is $mk(n-k)/n(n-1)$. Because this expression is limited, the BC function is always less than m/n.

When a population "loses" an allele, i.e., if a gene "0" occupies the same position on all chromosomes, the maximum value of BA is n/m. Moreover, when p alleles are lost, the maximum value of BA is $np(m-p)/m(m-1)$.

The diversity functions are independent of the problem as long as the representation is binary. They are able to describe comprehensively a genetic process. We shall use them to describe a genetic process.

RESULTS AND DISCUSSION

Description of genetic processes

Let us consider a key loop of a genetic algorithm which is illustrated in Fig. 3. This loop is

slightly different from common genetic algorithms. In addition to the crossover probability P_c and the mutation probability P_m, two new parameters, P_d and P_r, are added into this loop.

P_d is a duplication parameter. Duplication or multiple duplication can improve the performance of the process. There are several reasons for using P_d: the best-so-far or a group of them should survive in the next generation, so there is less risk of losing a better structure; when degeneracy or near degeneracy exists in problem space, multiple duplication can find most solutions [11]; and when the number of duplications, P_d, is large, it can prevent an individual from generating a large number of offspring members in the next generation. Consequently, the performance of the population is effectively improved. Figure 4 illustrates the relationship between P_d and the population performance, where the population performance is defined as the sum of the reciprocals of the evaluation functions (since in our problem lower variances correspond to better solutions, this definition gives the better individuals higher weights); other parameters are $P_c = 0.1$, $P_m = 0.01$, $P_r = 3$. Clearly, a higher P_d indicates a higher population performance.

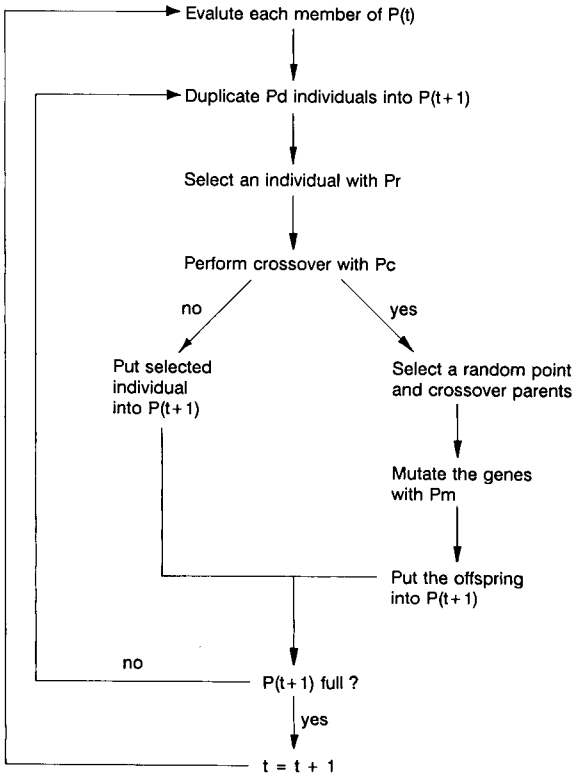

Fig. 3. A key loop of the dynamic genetic algorithm. The parameters P_r, P_c and P_m are defined in the text. An ideal GA will be formed by dynamically by varying these parameters according to ANOVA.

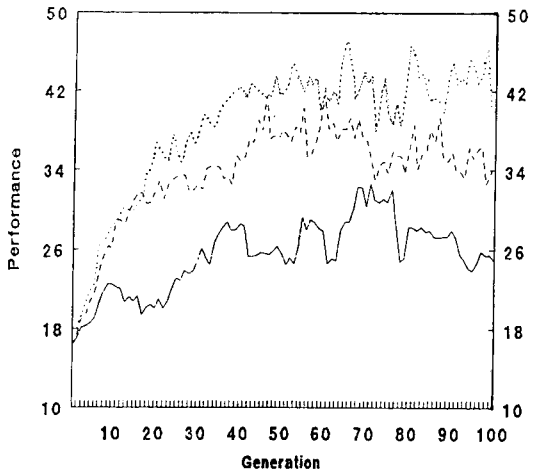

Fig. 4. Influence of the duplication function (P_d) on performance. The population performances of the first 100 generations are illustrated with different P_d: (solid line, $P_d = 2$; dashed line, $P_d = 6$; dotted line, $P_d = 10$), with $P_c = 0.1$, $P_m = 0.001$, $P_r = 3$. The higher is P_r, the better is the performance.

P_r is a selective or mating parameter. In most applications, a Gauss weighed probability is assigned to every individual according to its evaluation. In order to study the effects of different mating fashions, we construct a schedule as follows. After evaluation of each member of $P(t)$, the individuals are sorted according to their evaluations (according to property "*a*", the diversity functions are unaffected), then each half part is assigned a different selection probability. P_r is the ratio of the two probabilities. When $P_r = 1$, i.e., completely random selection, every individual has an equal opportunity of being selected as a parent. When P_r is very large, the under-average-performing individuals have almost no opportunity of being selected. Figure 5 shows that the *BC* and *BA* functions are both affected by P_r values, where $P_c = 0.6$, $P_m = 0.001$, $P_d = 2$. Varia-

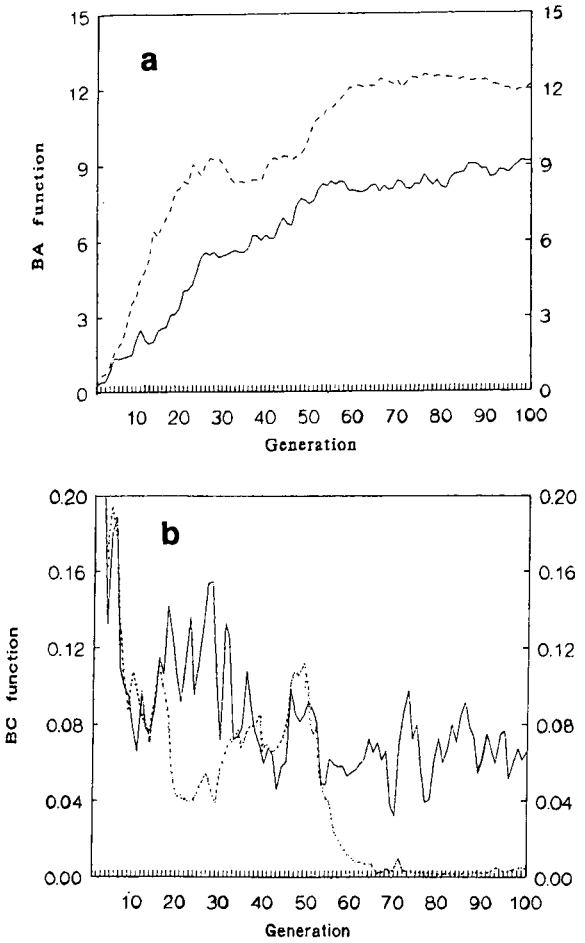

Fig. 5. Relationship between ANOVA and P_r. *BA* and *BC* functions of the first 100 generations with different P_r: (solid lines, $P_r = 1$; dashed lines, $P_r = 3$): (a) *BA* function vs. P_r; (b) *BC* function vs. P_r; $P_c = 0.6$, $P_m = 0.001$, $P_d = 2$.

tion of P_r can affect the exploitation of what is known so far.

The P_c and P_m parameters are defined as usual. They are the most important parameters in a genetic process. Their effects can be described by *BC* and *BA*, respectively. In Fig. 6, where $P_m = 0$, $P_d = 2$, $P_r = 2$, the *BC* value clearly reflects the behaviour of different P_c values (property "*d*", *BA* is unaffected). When P_c is low, the diversity between the chromosomes disappears rapidly. The genetic operators become ineffective. In contrast, high P_c values enable the search to continue for a relatively long time before convergence. In most practical applications, a value, 0.6, is frequently used. Clearly, this is not the best way of setting parameters. It has been shown that a significant improvement can be gained by varying P_c [21]. We shall vary P_c in a different way (see below).

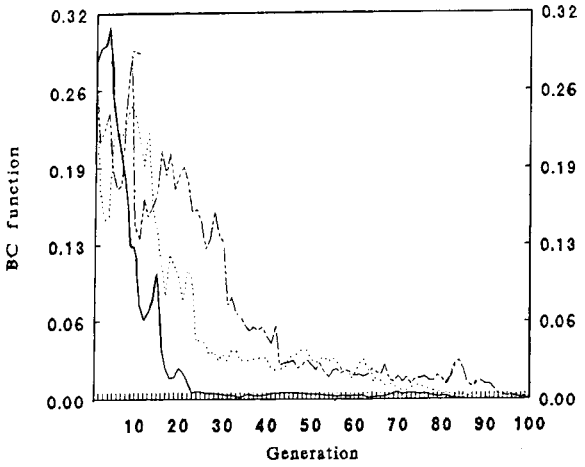

Fig. 6. Influence of crossover probability (P_c) on *BC* function. *BC* function of the first 100 generations with different P_c (solid line $P_c = 0.2$; dotted line, $P_c = 0.6$, dashed line, $P_c = 1.0$), with $P_m = 0$, $P_d = 2$, $P_r = 2$.

Similar results can be found in Fig. 7, where $P_c = 0.2$, $P_d = 2$, $P_r = 2$. *BA* describes the be-

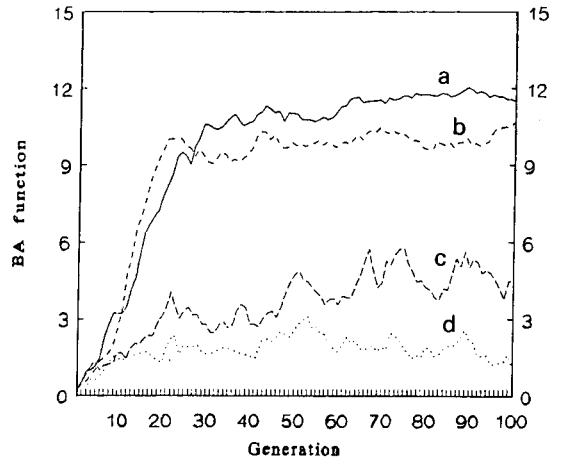

Fig. 7. Influence of mutation probability (P_m) on *BA* function. *BA* function of the first 100 generations with with different P_m (a, $P_m = 0.001$; b, $P_m = 0.01$; c, $P_m = 0.1$; d, $P_m = 0.2$) with $P_c = 0.2$, $P_d = 2$, $P_r = 2$.

haviour for different P_m values. When P_m is low, there is an evidently rapid convergence taking place (property "*c*"). Usually, this indicates a premature convergence. On the other hand, when P_m is high, *BA* varies around a relatively low value, and no convergence would be expected to be achieved in this situation. This is the reason why most GAs use a lower P_m (usually $P_m = 0.001$). However, in this instance, there is great risk of convergence to local optimum points such as illustrated in Fig. 7.

In summary, the variances in a population can be expressed by the diversity functions. They are useful for describing a genetic procedure and the effects of the genetic setting parameters. As the efficiency and the convergence are the main problems in a genetic algorithm, we shall focus our attention on the construction of the optimum balance between them.

Ideal genetic algorithm

So far we have discussed genetic algorithms, new diversity functions and a genetic procedure. Now we propose a dynamic genetic algorithm that can approximate an ideal genetic procedure.

An ideal genetic procedure is an approach such that the balance between exploitation and exploration can be automatically adjusted and the genetic operators will be most efficient. It is an approach such that both a broad search through the problem space and a local refinement are given sufficient consideration. It is also an approach such that high performance and convergence are reached simultaneously within a limited CPU time.

A GA's strategy can be described by the diversity functions. Figure 8 shows the different behaviours of the *BC* and *BA* functions with different strategies in a limited evolution time. Strategy I quickly converges before it does a broad search. In this situation, the premature converegence is frequently expected to take place, and this strategy often finds a local optimum instead of the global optimum. In contrast, strategy III does too much random searching to converge, i.e., there is a great risk of losing better structures of the solution and it is usually inefficient. Strategy II is considered as an ideal genetic procedure. It keeps

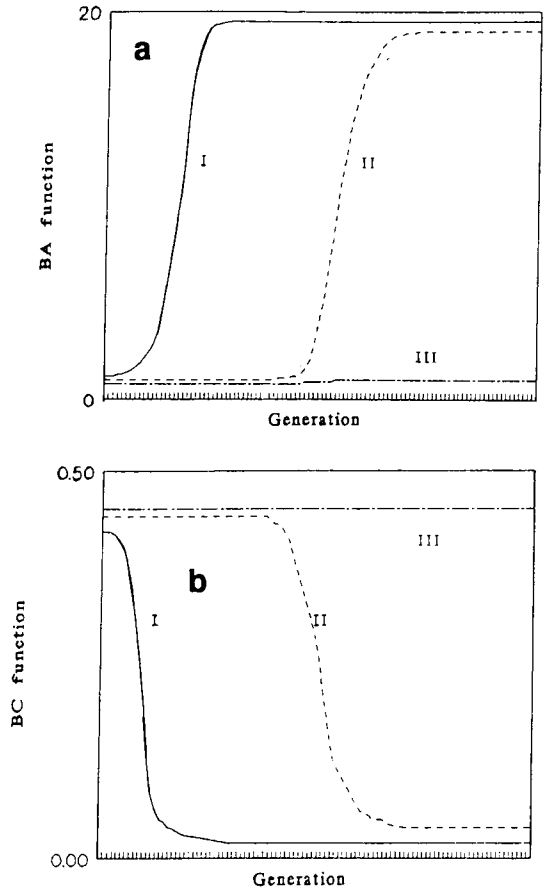

Fig. 8. An ideal genetic procedure. Strategy I, quick convergence; strategy II, an ideal genetic procedure; strategy III, random search.

a high diversity in the search stage and has enough refinement to converge to a global or near-global solution. This strategy can be implemented by a dynamic genetic algorithm.

To construct a dynamic genetic algorithm, the whole procedure is divided into three stages: initiation, search and refinement. In the initial stage, the values of the diversity functions are dependent on the initial conditions of a genetic algorithm, so the diversity functions' behaviour is unpredictable. The parameters are kept at their initial values in this stage. The time of the initial stage is one tenth of the whole generation.

In the search stage, the main parameters are designed to vary to guarantee a broad search and efficient exploitation. For this purpose the *BC* function should be held at a higher level and the *BA* function at a lower level (properties *c*, *e* and *f*). If the *BC* value is less than a minimum critical limit $BC_{min}(m/n)$, the crossover probability is adjusted upwards slightly. If the *BC* value is larger than a maximum critical limit, $BC_{max}(m/n)$, the crossover probability is forced downwards slightly. The allowed range of the crossover probability is from 0.2 to 1. The lower limit of crossover guarantees that the genetic operators are not completely ineffective. Meanwhile, the *BA* value is held in the range from $BA_{min}(n/m)$ to $BA_{max}(n/m)$. According to the *BA* value, the mutation probability should be varied from 0.001 to 0.2 to have sufficient alleles in a population and in order to avoid premature convergence, i.e., when *BA* is higher P_m is adjusted upwards slightly and vice versa. In this stage, P_d and P_r are held at low values. The search stage is designed as the main part of the genetic procedure, e.g., half of the generation time.

In the last stage, refinement, the balance is designed toward exploitation and the search is forced in the local regions where there are higher probabilities of finding the optimum solutions. In this stage the changes of the parameters are fixed by a linear annealing schedule. The mutation probability decreases from the current value to the minimum value (0.001). P_d and P_r are linearly increased to their maxima ($P_d = 10$, $P_r = 5$). Only the crossover probability P_c is held at a constant value (0.6) in order for the refinement to be carried out efficiently. The experiments show that the behaviour of a dynamic genetic algorithm is near strategy II.

Optimized results

In this section we empirically explore the effect of the dynamic genetic algorithm discussed in the last section and present the optimized results of two calibration data sets.

Near-infrared reflectance spectroscopic data. Recently, near-infrared analysis has frequently been used for calibration by multiple linear regression and principal component regression. However, outliers cause much trouble in many chemical applications. The outlier diagnostics for regression are important both for the predictive ability and for interpretation [8]. We recognize that the diagnosis of outliers and the optimization of variables in fact are based on the same concepts, as both methods are based on an accuracy and precision model that can be constructed by an optimized subset instead of all experimental data.

A genetic algorithm is designed for optimizing published [8] near-infrared reflectance data. The data used here consist of 28 samples and 19 variables (wavelengths); the experimental measurements of the samples are percentages of protein. The size of the population is 50 and the length of a chromosome is 47 (28 + 19) bits.

When diagnosing outliers by GAs, there is a restriction on the selection of the number of samples, i.e., a minimum number of samples has to be limited. This is because our evaluation function is PRESS, borrowed from cross-validation, for which the value is dependent on the number of samples. Here, we let the minimum number of samples be ten.

A dynamic genetic algorithm (DGA) and a traditional genetic algorithm (TGA) are programmed for comparison. In order to compare their behaviours within an acceptable CPU time, the run time is limited to 30 s for short runs and to 300 s for long runs on a mainframe computer (NAS9600) in C language. Table 1 shows a comparison of DGA and TGA in the short-run mode for ten repeats where each time a different random seed is used. The initial parameters are $P_d = 2$, $P_r = 2$, $P_c = 0.6$ and $P_m = 0.001$. For DGA, BC_{min} is 0.2, BC_{max} is 0.4, BA_{min} is 2 and BA_{max} is 5. P_c and P_m are varied in the search stage. In this stage, they are observed to increase simultaneously. P_c frequently reaches the maximum value, i.e., 1, and P_m is ca. 0.1. The diversities are kept at relatively higher levels. Except for the fourth and ninth runs, both the best-so-far and the population performances of DGA are better than those of TGA.

Table 2 shows the results of the long-run mode. For this mode the behaviours of both DGA and TGA are improved. For TGA, two experiments

TABLE 1

Comparison of TGA and DGA in the short-run mode.

No.	TGA		DGA	
	Best-so-far performance	Population performance	Best-so-far performance	Population performance
1	2.0004	49.325	1.5911	60.971
2	1.8875	48.065	1.6341	56.662
3	1.6906	57.702	1.6732	59.642
4	1.2176	72.095	1.3855	63.486
5	2.0284	48.711	1.7830	54.951
6	1.5326	64.463	1.4797	61.206
7	1.7713	50.136	1.2846	76.018
8	2.2255	43.036	1.4970	64.085
9	1.6522	56.628	2.0290	46.639
10	1.2548	77.953	1.1951	80.922
Mean	1.7161	56.811	1.5552	62.458
Variance	0.1155	3.805	0.0815	3.297

are carried out with different P_m values. When $P_m = 0.001$, the population performance is higher, implying that the search converges but to a local optimum (the best-so-far is the highest). When $P_m = 0.1$, a better best-so-far is found, but convergence is not reached. It is evident that DGA is superior in both the best-so-far and overall performance.

In the NIR data, there are three manual outliers which were diagnosed by Näes [8] with a two-step method that is fairly complex. In fact, there are also some data that contain more experimental errors than other data. We hold that the optimization must be carried out for samples and wavelengths simultaneously, regardless of manual or experimental errors. In other words, a 28×19 matrix, in which some data carry the same useful information and some data contain considerable manual and experimental errors, is redundant for one component (protein) prediction. Our purpose is to find an optimized subset that is expected to contain the same useful information and smaller errors compared with the original.

In our experiment, the number of variables (wavelengths) and the number of samples are optimized as 8 and 10, respectively. Therefore, a compact calibration subset, 10×8 matrix, is obtained by means of minimization of PRESS. Consequently, the three manual outliers and some inaccurate samples are out of the subset. The PRESS of the optimized subset is near 0.01 when the number of principal components reaches three. It is considerably lower than the value of 1.20 for the original set and the value of 0.04 for the set of 25 samples without three manual outliers.

LC–DAD data. Liquid chromatography coupled with diode-array detection generates a two-dimensional response dependent on time and wavelength. At each wavelength there is a chromatogram and at each time there is a spectrum. Simultaneously optimizing high-dimensional analytical data is an important issue in chemometrics. Although several powerful calibration methods claim that they are able to handle high-dimensional data sets without the need for pretreatment, higher precision can be obtained by the optimized combination of a subset of the original one [20]. An experiment is programmed for demonstration of such improvement.

The LC–DAD data used here result from the measurement of a two-component mixture, anthracene and phenanthrene. They consist of 46 spectra and 40 wavelengths. Six samples are calibration standards and five samples are predictions. For comparison, the optimization is for wavelengths and spectra (i.e., six samples are the calibration standard). The predictive abilities of before and after optimization are shown in Table 3.

After optimization, 13 spectra and 20 wavelengths are selected to combine a calibration subset. From Table 3 it is seen that the average rates of recovery of before and after optimization are nearly the same. The variances are significantly different [$F_{9,9}(0.05) = 3.137$] by means of statistics ($5.29 > 3.137$). It is evident that after optimiza-

TABLE 2

Comparison of TGA and DGA in the long-run mode

Performance	TGA		DGA
	$P_m = 0.001$	$P_m = 0.1$	
Best-so-far performance	1.2734	1.2564	1.0853
Population performance	61.628	25.431	88.974

TABLE 3

Predictive abilities before and after optimization

Sample No.	Real value	Before optimization		After optimization	
		Calculation	Recovery (%)	Calculation	Recovery (%)
1	6.46	6.52	100.93	6.37	98.61
	1.63	1.58	96.93	1.57	96.32
2	5.38	5.41	100.56	5.27	97.96
	2.72	2.71	99.63	2.67	98.16
3	1.62	1.50	92.59	1.62	100.00
	6.54	6.65	101.68	6.55	100.15
4	2.69	2.67	99.26	2.67	99.26
	5.45	5.47	100.37	5.42	99.45
5	4.04	4.07	100.74	3.87	98.28
	4.09	4.06	99.27	4.07	99.51
Mean			99.20		98.77
Variance [a]			0.887		0.385

[a] F-test $= 0.887^2/0.385^2 = 5.29$.

tion the predictive ability of the calibration model is enhanced.

Conclusions

Genetic algorithms have been applied to a simple chemometrics problem. The diversity functions introduced have the power to describe the internal process of genetic algorithms and controlling it. The designed dynamic genetic algorithm significantly improves the behaviour of the GA process within a limited evolution time. Using GAs, it is possible to optimize calibration data sets and enhance the predictive ability of a calibration model successfully.

However, the application of GAs is a young field, and there are abundant opportunities for both theoretical and practical studies from which there is still much to be learned. Also, the power of GAs should be tested on higher level problems such as adaptive systems or the task of optimizing an executable code.

The Netherlands Government is thanked for providing financial support to enable Dr. T.-H. Li to do research in the Laboratory for Analytical Chemistry at the University of Nijmegen for 6 months. Professor Näes is thanked for his kindness in allowing the authors to use his NIR data. C.B. Lucasius acknowledges the financial support of the Dutch Foundation for Chemical Research (SON), the Dutch Foundation for Informatics Research (SION), and the Dutch Organization for Scientific Research (NWO), Grant 700-344-007. The reviewers are thanked for their critical comments and useful suggestions.

APPENDIX

Analysis of variance (ANOVA) is a powerful statistical technique which can be used to separate and estimate the different causes of variation [21]. Here it is exploited to estimate the diversities in a population. According to the definition of between-sample estimation, our between-chromosome diversity function is

$$BC = m \sum_i (S_i - S)^2/(n-1) \tag{3}$$

where m is the length of a chromosome, S_i is a chromosome mean of genes and S is a total mean. Equation 3 can be rewritten as

$$\begin{aligned} BC &= m \sum_i (S_i/m - S/nm)^2/(n-1) \\ &= \sum_i (S_i^2 - 2S_iS/n - S^2/n^2)/m(n-1) \\ &= \left(\sum_i S_i^2/m - S^2/nm \right)/(n-1) \end{aligned} \tag{4}$$

This is Eqn. 1 in the main text.

The proof of the properties of the diversity function is as follows.

Properties a and d are easily understood.

Property b: let all genes be 1 in a population, i.e., $S_i = m$, $S = nm$, then

$$\begin{aligned} BC &= (nm^2/m - n^2m^2/nm)/(n-1) \\ &= (nm - nm)/(n-1) = 0 \end{aligned} \tag{5}$$

Property c: let each chromosome contain q alleles, i.e., $S_i = q$, S-nq, $S_j = n$, then

$$\begin{aligned} BC &= (nq^2/m - n^2q^2/nm)/(n-1) \\ &= 0 \end{aligned} \tag{6}$$

$$\begin{aligned} BA &= (qn^2/n - n^2q^2/nm)/(m-1) \\ &= (qn - q^2n/m)/(m-1) \end{aligned} \tag{7}$$

When $q = m/2$, BA reaches the maximum, $nm/4(m-1)$.

Property e: assume a population "loses" k chromosomes and the others are full with gene 1 (in this case the diversity is maximum), then

$$S_i = m,\ S = (n-k)m.$$

$$BC = \left[(n-k)m^2/m - (n-k)^2m^2/nm\right] /(n-1)$$
$$= mk(n-k)/n(n-1) \quad (8)$$

Property f: this is similar to e.

REFERENCES

1 J.H. Holland, Adaptation in Natural and Artificial Systems, University of Michigan Press, Ann Arbor, MI, 1975.
2 L. Davis and M. Steenstrup, in L. Davis (Ed.), Genetic Algorithms and Simulated Annealing, Pitman, London, 1987, pp. 1–11.
3 K. DeJong, Machine Learning, 3 (1988) 121.
4 J.J. Grefenstette, IEEE Trans. Syst. Man Cybern., SMC-16 (1986) 122.
5 J.J. Grefenstette (Ed.), Proceedings of the First International Conference on Genetic Algorithms, Lawrence Erlbaum, Hillsdale, NJ, 1985.
6 J.J. Grefenstette (Ed.), Proceedings of the Second International Conference on Genetic Algorithms, Lawrence Erlbaum, Hillsdale, NJ, 1987.
7 J.D. Schaffer (Ed.), Proceedings of the Third International Conference on Genetic Algorithms, Morgan–Kaufmann, San Mateo, CA, 1989.
8 R.K. Belew and L.B. Booker (Eds.), Proceedings of the Fourth International Conference on Genetic Algorithms, Morgan–Kaufmann, San Mateo, CA, 1991.
9 L. Davis (Ed.), Handbook of Genetic Algorithms, Van Nostrand Reinhold, New York, NY, 1991.
10 D.E. Goldberg, Genetic Algorithms in Search, Optimization, and Machine Learning, Addison-Wesley, Reading, MA, 1989.
11 Ref. 7, p. 170.
12 C.B. Lucasius, L.M.C. Buydens and G. Kateman, Self-Organizing Systems in Analytical Chemistry, in M. Grasserbauer, J.K.F. Huber and W. Wegscheider (Eds.), Euro-Analysis VII, ASAC (Austrian Society for Analytical Chemistry), Vienna, 1990, p. C2.5.L2.
13 C.B. Lucasius, M.J.J. Blommers, L.M.C. Buydens and G. Kateman, in L. Davis (Ed.), A Genetic Algorithm for Conformational Analysis of DNA, Handbook of Genetic Algorithms, Van Nostrand Reinhold, New York, NY, 1991, Ch. 18, p. 251.
14 C.B. Lucasius, S. Werten, A.H.J.M. van Aert, G. Kateman and M.J.J. Blommers, in H.-P. Schwefel and R. Männer (Eds.), Conformational Analysis of DNA using Genetic Algorithms, Proceedings of the First Workshop on Parallel Problem Solving from Nature, Springer-Verlag, Berlin, 1991, p. 90.
15 C.B. Lucasius and G. Kateman, Trends Anal. Chem., 10 (1991) 254.
16 I.Y. Bershtein, Fresenius' Z. Anal. Chem., 332 (1988) 332.
17 S.C. Rutan and P.W. Carr, Anal. Chim. Acta, 215 (1988) 131.
18 T. Näes, Chemometr. Intell. Lab. Syst., 5 (1989) 155.
19 W. Lindberg, J. Ohman and S. Wold, Anal. Chem., 58 (1986) 299.
20 J.H. Kalivas, N. Roberts and M. Sutter, Anal. Chem., 61 (1989) 2024.
21 J.J. Grefenstette, in L. Davis (Ed.), Genetic Algorithms and Simulated Annealing, 1987, pp. 42–60.
22 K.A. DeJong, PhD Thesis, University of Michigan, Ann Arbor, MI, 1975.
23 D.E. Goldberg, PhD Thesis, University of Michigan, Ann Arbor, MI, 1983.
24 J. Kim and J. McDermott, in Proceedings of the National Conference on Artificial Intelligence, 1983, pp. 197–201.
25 L. Davis and S. Coombs, in J.J. Grefenstette (Ed.), Proceedings of the Second International Conference on Genetic Algorithms, Lawrence Erlbaum, Hillsdale, NJ, 1987, p. 252.
26 L.B. Booker, D.E. Goldberg and J.H. Holland, Classifier Systems and Genetic Algorithms, Technical Report No. 8, University of Michigan, Ann Arbor, MI, 1987.
27 J.M. Fitzpatrick and J.J. Grefenstette, Machine Learning, 3 (1988) 101.
28 M.L. Mauldin, in Proceedings of the National Conference on Artificial Intelligence, Morgan–Kaufmann, San Mateo, CA, 1984, p. 247.
29 J.E. Baker, in J.J. Grefenstette (Ed.), Adaptive Selection Methods for Genetic Algorithms, Proceedings of the First International Conference on Genetic Algorithms, Lawrence Erlbaum, Hillsdale, NJ, 1985, p. 101.
30 L. Booker, Machine Learning, 3 (1988) 61.
31 J.C. Miller and J.N. Miller, Statistics for Analytical Chemistry, Wiley, New York, 1984.

Analytica Chimica Acta, 268 (1992) 135–144
Elsevier Science Publishers B.V., Amsterdam

UVDECODE: An algorithm for direct extraction and analysis of environmental polycyclic aromatic hydrocarbons with derivative UV spectrophotometry

Jorge Ares

Aluar Alumino Argentino, Department of Environmental Research, Casilla 52, 9120 Puerto Madryn (Argentina)

(Received 14th January 1992; revised manuscript received 4th April 1992)

Abstract

A method for the analysis of polycyclic aromatic hydrocarbons (PAHs) contained in complex environmental samples such as airborne particulate matter is presented, which is based on computations with *n*-successive derivative UV spectra. The algorithm can be applied to a direct extract of the sample with a single solvent such as cyclohexane. The UV spectrum of a sample (220–400 nm) is used to build a vector containing its 2nd–5th derivatives. This is multiple regressed against similar vectors containing the corresponding derivatives of the unit molar UV spectra of the target PAHs, and several noise signals built by multiplication of the analyte spectrum with several random noise vectors. The PAHs which are positively selected in this step are used for a second multiple regressive filter fitting all possible candidates into a single Beer's law model. A third filter, based on sensitivity analysis, selects the best significant components of the sample system. The present version of the algorithm has been tested with extracts of standard mixtures and extracts of SRM 1649 Urban Dust Organics (National Bureau of Standards). The results obtained are comparable in accuracy and precision to those obtained by chromatographic or direct extraction techniques. A considerable simplification of the extraction procedure and reduction of analysis costs and time are attained, which makes it a valuable tool as a secondary standard method for routine monitoring and systematic surveillance. The algorithm is coded in FORTRAN Microsoft for use in DOS 4.0 or higher AP personal computers.

Keywords: UV–Visible spectrophotometry; Derivative spectroscopy; Extraction; Multivariate analysis; Polycyclic aromatic hydrocarbons

The use of computer-enhanced spectroscopic techniques for the analysis of environmental polycyclic aromatic hydrocarbons (PAHs) is appealing because it would imply an important simplification in this field. The usual troublesome separation procedures needed to perform gas (GC) or liquid chromatography (LC) would be obviated and replaced with a single liquid–liquid extraction and subsequent determination of the UV spectrum, which can be obtained in a few minutes by means of diode-array instruments.

The UV signals of organic compounds have long been used for analytical purposes. Published collections of spectra (e.g., [1]) in different solvents allow the comparison of single species signals and the selection of adequate characteristic bands. Solvent effects can result in band displacement [2]. The UV spectra of PAHs in a given solvent are multivariate characteristic signals proportional to their concentration. Even very similar compounds which normally pose problems in analytical techniques of separation based on

Correspondence to: J. Ares, Aluar Alumino Argentino, Department of Environmental Research, Casilla 52, 9120 Puerto Madryn (Argentina).

TABLE 1

Acronyms and sources of polycyclic aromatic hydrocarbons (PAHs) used

PAH	Acronym	Source [a]
Acenaphthene	ANe	ChS, Su
Acenaphthylene	ANy	ChS, Su
Anthanthrene	Ath	Ana
Anthracene	An	ChS, Su
Benz[*a*]anthracene	BaA	ChS, Su
Benzo[*a*]pyrene	BaP	ChS, Su
Benzo[*b*]fluoranthene	BbF	ChS, Su
Benzo[*e*]pyrene	BeP	Sig
Benzo[*ghi*]perylene	BgP	ChS, Su
Benzo[*k*]fluoranthene	BkF	ChS, Su
β-naphthylamine	bNa	Sig
Crysene	Cy	ChS, Su
Coronene	Co	Ald
Dibenzo[*a*,*h*]anthracene	DahA	ChS, Su
Fluoranthene	Flt	ChS, Su
Fluorene	Fle	ChS, Su
Indeno[1,2,3-*cd*]pyrene	IcdP	ChS, Su
Naphthalene	Nt	ChS, Su
Pyrene	Py	ChS, Su

[a] Ald = Aldrich (Milwaukee, WI); Ana (Analabs, North Haven, CT; ChS = Chem Service, (West Chester, PA); Sig = Sigma (St. Louis, MO); Su = Supelco 4-8743 S610M standard mixture, Supelco (Bellefonte, PA).

molecular size or weight, such as the pairs BbF–BkF or BaP–BeP (see Table 1 for PAH acronyms), do have distinctly different UV spectra (Fig. 1).

In a mixture of several PAHs and other organic species, shape components and the amounts of their partial contributions are not evident, although Beer's law is expected to describe additive effects. A complex UV spectrum of a sample containing several PAHs in a matrix of other UV absorbers is in principle of little analytical value unless it can be adequately filtered to separate the individual contributors to the overall absorbance. When a single component is to be sorted out from a complex matrix of highly absorbing matter, it is usually convenient to utilize not the primitive UV spectrum, but a high-order derivative of it [3].

Multiple regression techniques, factor decomposition [4], principal component analysis [5], regression on principal components [6] and linear programming [7] have been indicated as suitable approaches for multivariate calibration of spectral data. In the application of multivariate techniques, a useful procedure consists in solving some system of simultaneous equations which satisfy Beer's law and contain a function of the unit molar absorbances of the target analytes known to be in the mixture. This happens in an analysis of a known standard mixture, and can be referred to as the "transparent" case. If it is just a hypothesis that the mixture contains certain components (the "blind" case), the inclusion of spectra of these substances in the data set might produce biased results when they are not in fact present in the sample. A preliminary test must first be carried out to see if a spectrum of a certain candidate lies in the space defined by the data for the mixtures. If a component is a true

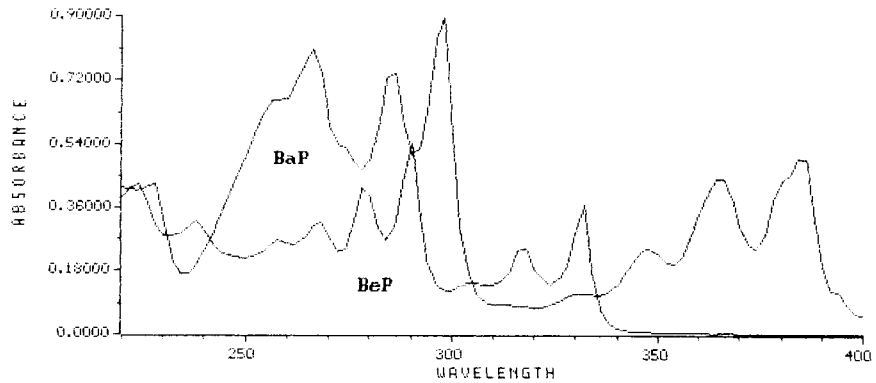

Fig. 1. PAH isomers which usually pose difficulties in separative chromatography have different UV spectra in the range 220–400 nm.

part of the mixture, it will coincide with the space. If it is not present at all, it will be orthogonal to the mixture space, in the statistical sense [4]. The problem of selecting a reasonable set of candidates for components of a mixture has been addressed [8,9] by means of similarity techniques and factor analysis. Both of these have been shown to be limited when the number of components is greater than five.

The objective of this study was to develop a set of mathematical filters which would allow the quantification of the concentrations of different UV absorbers in a mixture of naturally occurring organic compounds. The exclusion of false-positive results was addressed by adding several equations containing random noise to the equation systems and performing a sensitivity analysis by deleting/including one compound at a time in the multivariate calibration system.

EXPERIMENTAL

Algorithm principle

The UV spectrum of a mixture of organic compounds that is known to contain a target PAH in an unknown amount can be formulated as

$$A(i) = aA(i,t) + A(i,r) \quad (1)$$

where $A(i,t)$ is the unit molar absorbance at wavelength i of the target t and $A(i,r)$ is the absorbance of the remaining unknown compounds r. If $A(i,r)$ could be established, then a would express the concentration of the target. In a mixture of UV absorbers, an approximation to $A(i,r)$ can be built by summing several white noise signals centred around the primitive spectrum:

$$A(i) = aA(i,t) + b(n)N(n,i) \quad (2)$$

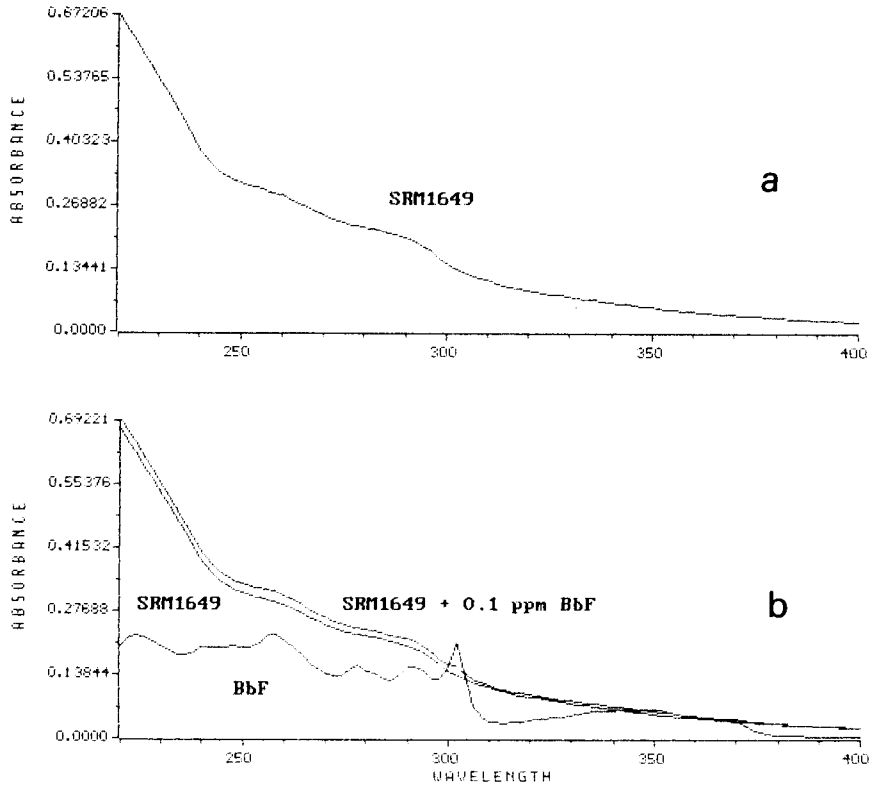

Fig. 2. (a) UV spectrum of SRM 1649 (cyclohexane extract) and (b) after addition of 0.1 μg ml^{-1} of BbF, the spectrum of which is also shown.

where

$$N(n,i) = W(n,i) \times A(i) \quad (3)$$

$W(n,i)$ being a random term. Equation 2 can be fitted to the analyte UV spectrum by usual regression techniques, since no colinearity is expected to occur among terms or with the target PAH spectrum. Equations 2 and 3 also apply when the primitive absorbances $A(i)$ are replaced with their n-order derivatives, which is convenient for removing most of the interfering matrix effects usually present in environmental samples [3].

The procedure is illustrated in Fig. 2, where the UV spectrum of a cyclohexane extract of a sample of urban dust (NBS Standard Reference Material SRM (1649) is shown together with the spectrum resulting after addition of 0.1 μg ml^{-1} BbF. In order to extract from the sample spectrum the contribution of BbF, a multiple regression model is solved which contains the unit molar spectrum of BbF and several white noise terms as in Eqn. 2. Some of the resulting noise spectra are shown in Fig. 3. The selection of white noise is not unique and in principle various combinations would yield similar results. Random noise signals can be generated in some of the usual ways (e.g., [10]).

A positive identification of a target PAH is defined when the significance of a in Eqn. 2 is high in relation to that of all bs of noise terms. A test for this is dividing the t value of the coefficient a by the sum of all t values of the noise in the regression model of Eqn. 2. Additions of BbF are completely recovered in the model estimate, and the ratio of the t values quantifying the

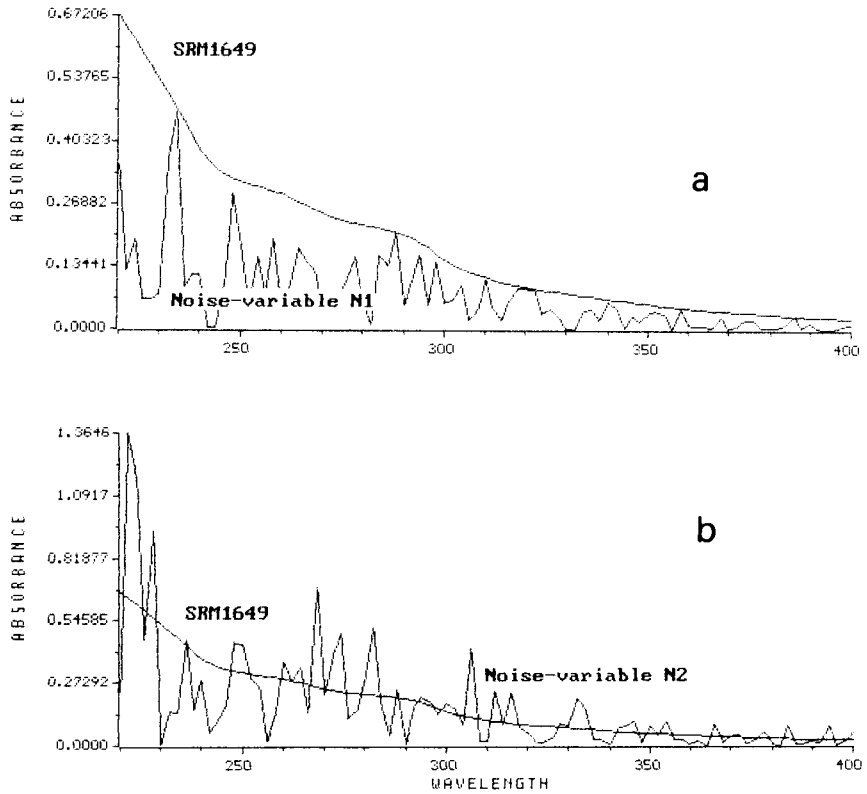

Fig. 3. UV spectrum of SRM 1649 (cyclohexane extract) and the resulting spectra after multiplication by two random noise signals: (a) normally distributed random noise, range 0.0–1.0; (b) exponentially distributed random noise.

significance of the target and the noise increase linearly from 0.7 to 1.1 as the concentration of BbF in the extract increases by 0.01 μg ml^{-1}.

A second filter is then applied by fitting all positive identifications in a single additive model:

$$A(i) = a(1)A(i,1) + a(2)A(i,2) + a(3)A(i,3) + \ldots + b(1)N(1,i) + b(2)N(2,i) + b(3)N(2,i)\ldots \quad (4)$$

where $a(n)$ represents the concentrations of the n targets. In a third step, the model in Eqn. 4 is successively calculated omitting a single target component at a time and retaining those estimates which are not modified by the inclusion of other components. At the end, a single Beer's law model is calculated containing only the components which have passed the sensitivity test.

Standards and instrumentation

Table 1 lists the PAHs used in this study and their sources. Also, cold and Sohxlet extracts with or without ultrasonic pretreatment were obtained from NBS Standard Reference Material SRM 1649 Urban Dust Organics, which was used as a source of a complex environmental matrix containing PAHs and many other UV absorbers. A standard mixture containing sixteen PAHs (Supelco 4-8743 S610M) was also used for calibration purposes.

All UV spectra were obtained with an HP 8452 UV–visible (single-beam, deuterium source) diode-array spectrophotometer (Hewlett-Packard). The unit was coupled to an HP Vectra 286/12 with math coprocessor. Operation was in the general scanning mode, with a SINTORGAN chromatography-grade cyclohexane blank, at intervals of 2 nm, in the range 220–400 nm with a 15-s integration time. The vector of 91

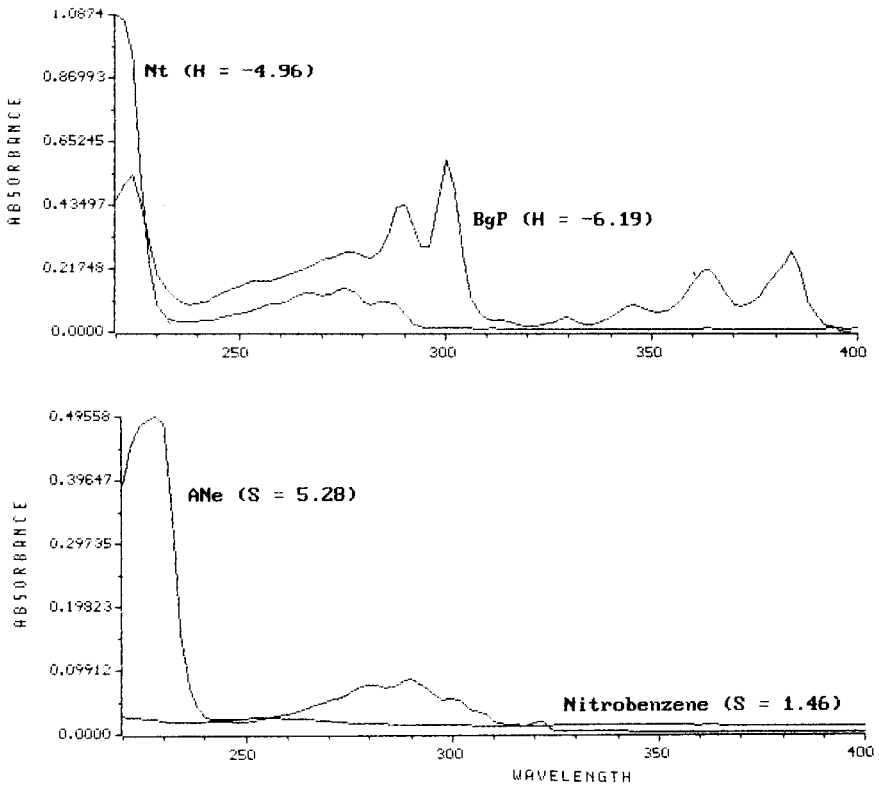

Fig. 4. Examples of UV spectra of PAHs with different H and S values. Nitrobenzene is included as an example of a "flat" spectrum not suitable for the analysis described here.

TABLE 2

Fractional composition of Supelco 4-8743 S610M PAH standard mixture

PAH	Fraction	PAH	Fraction
ANe	0.172	ANy	0.344
Flt	0.034	An	0.017
Nt	0.172	BgP	0.034
BaA	0.017	Fle	0.034
BaP	0.017	Phe	0.017
BbF	0.034	DahA	0.034
BkF	0.017	IcdP	0.017
Cy	0.017	Py	0.017

absorbance values was magnetically stored up to the seventh significant digit. Most PAHs yield 1 μg ml^{-1} concentration UV spectra in the 220–400 range which satisfy the following criteria:

$$S = A(i) > 4.00 \quad (5)$$

$$-H > 5.0 \quad (6)$$

where H is the spectrum entropy value [11]:

$$H = \sum a(i) \log_2 a(i) \quad (7)$$

for

$$a(i) = A(i) / \sum A(i) (i = 1, \ldots, 91) \quad (8)$$

which quantifies the amount of information contained in it (bits). Spectra with numerous distinct peaks have small H values, whereas "flat" spectra are characterized by higher H values. Figure 4 shows some examples of PAH spectra with their corresponding S and H values. Nitrobenzene is presented as an example of a "flat" UV spectrum which is not suitable for the purposes described here.

The files were used within the MS-DOS 4.0 environment and processed with ad hoc developed FORTRAN Microsoft programs (UVDECODE system), which use the 2nd–5th derivatives of the UV spectrum. The multiple regression algorithm is based on a method described by Ostle [12] and performs a computation of the single and pairwise regression coefficients in the usual way [13–15]. The computations needed to solve for one sample take about 7 min. The complete analysis of one sample including a cold cyclohexane extraction takes about 15 min.

RESULTS AND DISCUSSION

Determination of individual PAH concentrations in complex mixtures

All targets known, "transparent" case. This type of analysis occurs during calibration steps, when a standard of known qualitative and quantitative

TABLE 3

Relative mass compositions of thirteen mixtures of fourteen PAHs in a study of multiple calibration [a]

PAH	Mixture												
	1	2	3	4	5	6	7	8	9	10	11	12	13
BaP	0.120	0.100	0.080	0.070	0.067	0.065	0.063	0.049	0.044	0.042	0.041	0.038	0.028
BeP	0.880	0.750	0.610	0.570	0.500	0.480	0.478	0.368	0.334	0.314	0.310	0.289	0.216
Nt		0.150	0.120	0.110	0.100	0.090	0.095	0.074	0.066	0.063	0.062	0.057	0.043
BgP			0.170	0.160	0.140	0.135	0.130	0.100	0.093	0.087	0.086	0.083	0.060
Cy				0.070	0.067	0.065	0.063	0.049	0.044	0.042	0.041	0.038	0.028
Py					0.110	0.113	0.111	0.086	0.078	0.073	0.070	0.067	0.050
An						0.037	0.037	0.028	0.026	0.024	0.024	0.022	0.017
Fle							0.015	0.012	0.011	0.010	0.010	0.009	0.007
DahA								0.230	0.208	0.195	0.190	0.180	0.134
Flt									0.092	0.087	0.086	0.080	0.060
BaA										0.059	0.058	0.054	0.040
Phe											0.013	0.013	0.009
ANe												0.067	0.050
Co													0.252

[a] The target lists (×8 PAHs) contained five PAHs which were not present in the mixtures: bNA, BbF, BkF, IcdP and ANy.

composition is screened for all its components. Table 2 describes the fractional composition of the Supelco 4-8743 S610M standard, which was diluted to obtain extract PAH concentration in the range 0.001–1.5 μg ml^{-1}.

All sixteen PAHs were positively identified in all the dilutions. An overall estimate of the prediction error (PE) was computed as

$$PE = \mathrm{Abs}(E - O)/O \quad (9)$$

where E is the expected value according to the dilution performed and O is the observed analytical value. The attained PE was 0.05 and it was confirmed that Beer's law holds reasonably for this family of compounds at the explored concentration range.

Targets unknown: the "blind" case. An experiment was designed to explore the usual analytical situation where an unknown sample is searched for the existence of PAHs where presence in the mixture or not is not known. Table 3 describes the relative concentrations of thirteen mixtures containing fourteen PAHs which were searched with four different target lists containing eight PAHs selected from the mentioned fourteen and five other intentional false positives as listed. Figure 5 shows the fitting line of expected/observed values and the prediction error in the range of concentrations 0.03 to 1.05 μg ml^{-1}.

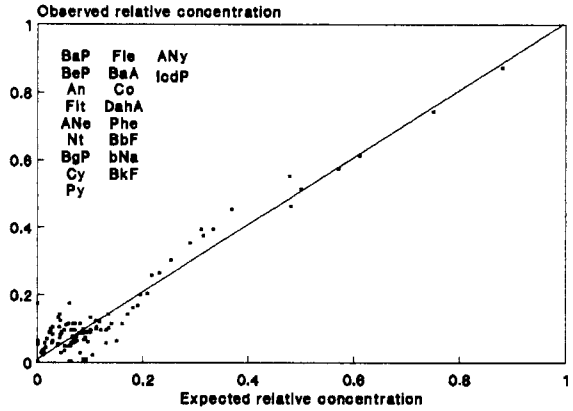

Fig. 5. Results of the analysis of PAH mixtures in Table 3 using "blind" target lists with false-positive and false-negative compound occurrences. $PE = 0.208$. Concentration range: 0.03–1.05 μg ml^{-1}.

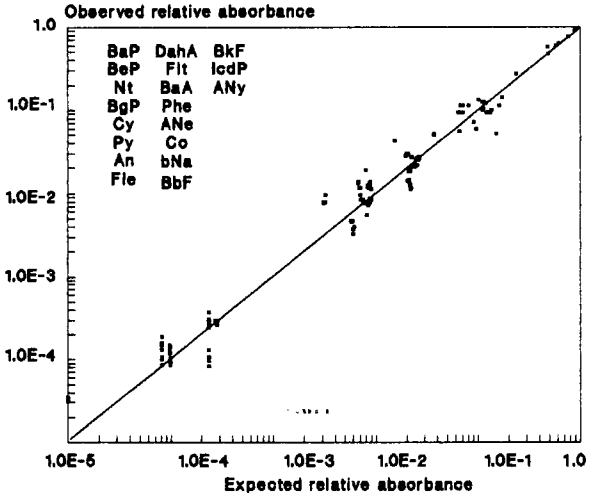

Fig. 6. Results of the analysis of PAH mixtures in Table 3 after dilution and addition to an extract of SRM 1649 in order to generate a low range of relative absorbances in a complex matrix.

It is of interest to explore the range of prediction errors that can be achieved when the relative UV absorbance of the PAHs is a small fraction of the overall sample absorbance. With this aim, the mixtures in Table 3 were diluted and added to an extract of SRM 1649 in a range that generated relative PAH absorbances from 0.00001 to 1.0. This range was chosen on the grounds that extracts of ambient dust like SRM 1649 yield relative PAH absorbances in a range that is seldom below 0.001. Figure 6 shows the results of this experiment. As expected, the prediction error increases at lower relative absorbances, reaching a value of 0.6 at a relative absorbance of 0.00001. This is considered adequate for most analytical purposes at this very low range of absorbances and corresponding analyte concentrations.

Separation of similar isomers occurring in complex matrices: BbF–BkF in SRM 1649

The separation of these isomers poses problems in most chromatographic techniques used in environmental analysis. They have not been certified in SRM 1649 because various methods of analysis yielded very different concentrations. None of them was found by the reported GC

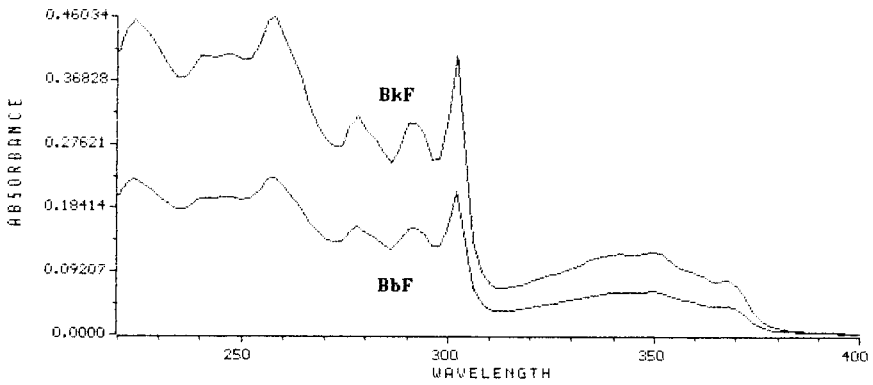

Fig. 7. UV spectra of BbF and BkF.

method, and only BkF was found by one of the reported LC methods. Both were reported by the third LC method (BbF, 6.2 μg g^{-1}; BkF, 2.1 μg g^{-1}). Elsaid et al. [16], working with a direct extraction with Shpolskii solvents, only reported values for BkF.

The two isomers have similar UV spectra (Fig. 7), which indicated the convenience of extending the use of UVDECODE to a standard addition mode, where the SRM 1649 extract was spiked with increasing amounts of BbF and BkF alternately. Spiking of any of the isomers produces a

TABLE 4

Results in (μg g^{-1} in dust) for five certified PAHs in SRM 1649 obtained with UVDECODE and various extraction procedures

No.	BaP	BgP	Flt	BaA	IcdP	Extraction method
1		8.4	10.7			Benzene–cyclohexane 48 h, 2 solvent changes
2		2.1	16.5	2.3		Benzene–cyclohexane 48 h, 3 solvent changes
3	3.4			2.9		Benzene–cyclohexane 63 h, 4 solvent changes
4	4.7	6.7		1.3		Benzene–cyclohexane 63 h, 5 solvent changes
5	2.0	3.0			0.2	Cyclohexane, cold, 10 min
6	2.0	2.9		2.3	0.3	Cyclohexane, cold, 10 min
7	1.9	2.7		0.3	0.1	Cyclohexane, cold, 10 min
8	1.8	2.6		0.4	0.2	Cyclohexane, cold, 10 min
9	3.2	3.7	2.9	2.2		Cyclohexane, cold + ultrasonic pretreatment, 10 min
10	2.2	2.3	1.8	1.8		Cyclohexane, hot, 2 h
11	3.5	4.0		2.3		Cyclohexane, hot, 5 h
12	6.6		2.3	0.4		Cyclohexane, hot, 15 h
13	11.3	15.3				Cyclohexane, hot, 15 h
14	9.5	15.5				Cyclohexane, hot, 24 h
n	12	12	5	10	4	
Av.	4.3	5.7	6.8	1.6	0.2	
Range	1.9 –	2.1 –	1.8 –	0.3 –	0.1 –	
	11.3	15.5	16.5	2.9	0.3	
Other reported results on SRM 1649						
[16]	3.2	6.3	–	2.8	–	
[17]	2.9	4.5	7.0	2.6	3.3	
[18]	2.6	3.9	7.0	2.8	–	

linear complete recovery of the target isomer but the estimates of both isomers are also highly correlated. By solving the system of linear equations describing the recovery trends, the concentration of each isomer at the null concentration point of the other can be estimated. This yields a concentration of BbF of 5.8 $\mu g\ g^{-1}$ (0.00066 $\mu g\ ml^{-1}$ in the extract) and (slightly lower than) 0.0 $\mu g\ g^{-1}$ for BkF, which is in good agreement with one of the estimates reported in the SRM 1649 certificate [17]. The operation of UVDECODE in a standard addition mode takes about 7 min more per spiking step, which is still a very convenient alternative for such a difficult analytical problem. The procedure appears robust enough to handle a larger number of similar isomers, which requires increasing the number of equations to be solved.

PAHs in environmental samples: certified values in SRM 1649 Urban Dust standard

SRM 1649 was extracted in a number of different ways including benzene–cyclohexane solvent changes, different extraction temperatures and duration of the extraction cycle with cyclohexane with an without ultrasonic pretreatment. Table 4 shows the results obtained. It is observed that most of the extraction techniques used allow the identification of most of the certified PAHs in a range that is comparable to that obtained with the extraction procedures used by other workers quoted in the standard certificate and elsewhere. The most efficient method is extraction with cold cyclohexane under ultrasonication, because it achieves a reasonable yield in a minimum time. IcdP is underestimated with respect to the certified value, which also holds for the other methods listed at the bottom of Table 4 ([16–18]). Depending on which extract is selected, it is possible to replicate almost exactly the certified NBS values for most of the compounds. It seems more illustrative, however, to show the ranges and average values obtained with the various alternatives.

Conclusions

Estimates of the partial concentrations of organic compounds having UV absorption spectra with entropy values lower than −5 (91 bands equally spaced from 220 to 400 nm) in mixtures of complex environmental samples can be obtained from the analysis of a single-step cyclohexane extract of the material. The UVDECODE algorithm filters and decodes to concentration values the partial UV signals from a set of target compounds even if some or most of the targets are not present in the analyte. Other unknown UV absorbents not considered in the target set but present in the analyte do not significantly interfere in the estimates. The simplicity of the direct extraction and the minimization of possible losses which are common to pre-chromatographic separation steps indicate that UVDECODE is a convenient method for the determination of environmental PAHs; there is no theoretical limitation to the use of this algorithm for the analysis of other organic compounds, provided that their UV absorption spectrum would convey a minimum amount of information, as indicated by its entropy value.

M. Pachetti is thanked for performing some of the extractions of SRM 1649.

REFERENCES

1 H.H. Perkampus, I. Sandeman and C.J. Timmons, Documentation of Molecular Spectroscopy, UV Atlas of Organic Compounds, Vol. V, Plenum, New York, 1971.
2 F. Dorr, in H.H. Perkampus and H. Fisher (Eds.) UV Atlas of Organic Compounds, Plenum, New York, 1971, Sect. E.
3 I. Doll, M. Knochen and C. Altesor, Analyst, 116 (1991) 69.
4 W. Winding, Chem. Int. Lab. Syst., 5 (1988) 201.
5 P. Geladi, Chem. Int. Lab. Syst., 5 (1989) 209.
6 T. Naes and H. Martens, in H. Meuzelaar and T. Isenhour (Eds.), Computer Enhanced Analytical Spectroscopy, Plenum, New York, 1987, Chap. 6.
7 J. Ares, Anal. Chim. Acta, 187 (1986) 195.
8 M. Otto and W. Wegscheider, Anal. Chem., 57 (1985) 63.
9 E.R. Malinowsky and D.G. Howery, Factor Analysis in Chemistry, Wiley-Interscience, New York, 1980.
10 M.G. Kendall and A. Stuart, The Advanced Theory of Statistics, Vol. 1, Griffin, New York, 4th edn., 1977.
11 G. Korn, Mathematical Handbook for Scientists and Engineers, McGraw-Hill, New York, 1968, p. 613.
12 B. Ostle, Statistics in Research, Iowa State College Press, Ames, IA, 1954, Chap. 4.

13 A. Ralston and H.J. Wolf, Mathematical Methods for Digital Computers, Wiley, New York, 1962, Chap. 7.
14 IBM System 360/Scientific Subroutine Package, GH20-0205-4, IBM, White Plains, NY, 1970.
15 N.R. Draper and H. Smith, Applied Regression Analysis, Wiley, New York, 1966.
16 A.E. Elsaid, A.P. D'Silva, V.A. Fassel and R.L.M. Dobson, Anal. Chem., 59 (1987) 971.
17 Certificate of Analysis, Standard Reference Material 1649, National Bureau of Standards, Washington, DC, 1982.
18 S.A. Wise, W.J. Bonnet and W.E. May, in A. Bjorset and A. Dennis (Eds.), Polynuclear Aromatic Hydrocarbons: Chemistry and Biological Effects, Batelle Press, Columbus, OH, 1976, p. 791.

Analytica Chimica Acta, 268 (1992) 145–151
Elsevier Science Publishers B.V., Amsterdam

Analytical potential of the interaction between triiodide ion and hexadecylpyridinium chloride micelles in an aqueous medium

M[a]. Loreto Lunar, Soledad Rubio and Dolores Pérez-Bendito

Department of Analytical Chemistry, Faculty of Sciences, University of Córdoba, 14004-Córdoba (Spain)

(Received 10th December 1991; revised manuscript received 21st April 1992)

Abstract

The association between triiodide ion and hexadecylpyridinium chloride (cetylpyridinium chloride; CPC) micelles is discussed. The formation of the I_3^-–CPC system under given conditions results in a bathochromic shift from 350 nm (absorption wavelength of the I_3^- complex) to 500 nm (maximum absorption wavelength of the I_3^-–CPC association) in addition to a substantial increase in the absorptivity and stability constant of the triiodide complex. The interaction between I_3^- and aqueous CPC micelles was studied in depth. This novel association may be of great help in improving the photometric monitoring of reactions involving the I_2–I^- pair and hence in increasing the sensitivity and selectivity of their determinations.

Keywords: UV–Visible spectrophotometry; Cetylpyridinium chloride; Hexadecylpyridinium chloride; Iodide; Micellar media; Triiodide

Micellar systems have been successfully utilized to improve existing analytical methods. Features such as sensitivity and selectivity can be greatly enhanced by implementing reactions in micellar media [1–4]. One major asset of micelles that has been widely used in this respect is their ability to increase the stability constants of complexes with respect to those corresponding to aqueous media [1]. This is a result of an increase in the local concentration of reagents in the micellar pseudo-phase that increases the apparent equilibrium formation constant of the complex. In this context, the interaction between triiodide ion and *N*-alkyltrimethylammonium halides as cationic surfactants has been studied to some extent [5,6]; the apparent equilibrium formation constant of triiodide was found to be 50 times higher in the presence of dodecyltrimethylammonium chloride (DTAC) [6] or hexadecyltrimethylammonium bromide (cetyltrimethylammonium bromide, CTAB) [5]. The increase in the maximum absorbance observed at 360 nm on addition of CTAB to a solution containing iodine and potassium iodide provided a sensitive direct method for the determination of micromolar concentrations of iodine with no liquid–liquid extraction [5]. These micelles cause only a slight bathochromic shift (about 8 nm) in the peak position of the triiodide ion so *N*-alkyltrimethylammonium halide cationic surfactants do not enhance the spectral selectivity to the extent required for monitoring triiodide ion. Because iodine is a frequent subject of biomedical and environmental studies and also a reaction product that is frequently monitored by photometric tech-

Correspondence to: D. Pérez-Bendito, Department of Analytical Chemistry, Faculty of Sciences, University of Córdoba, 14004-Córdoba (Spain).

nique in order to determine a variety of substances, the development of improved methods for the determination of trace amounts of this halogen is essential.

While investigating the effect of various cationic micelles on the spectral features of triiodide ion, it was found that the position of the triiodide peak was shifted to ca. 500–530 nm, depending on the experimental conditions used, and the molar absorptivity of ion was significantly increased by the presence of hexadecylpyridinium chloride (cetylpyridinium chloride; CPC) at concentrations slightly higher than its critical micellar concentration (c.m.c., 1.2×10^{-4}). These two effects may allow one to overcome completely or at least minimize the selectivity and sensitivity problems confronting many of the original photometric procedures involving aqueous media for monitoring iodine. It should be noted that the features of the I_3^-–CPC system change when CPC is added at a concentration about 50–times higher than its c.m.c. to a triiodide complex solution; under these conditions, the effect on the absorbance and spectral parameters of triiodide ion is similar to that exerted by *N*-alkyltrimethylammonium halide micelles, yet the stability constant of triiodide ion in CPC micelles is larger.

In this work the interaction between triiodide ion and CPC micelles and its potential analytical significance were studied. The origin of the difference between the effect of CPC on the spectral features of triiodide ion and those of other cationic surfactants (DTAC, CTAB, DTAB), each of which has a similar non-polar tail and a different polar head group, is also of great theoretical interest.

EXPERIMENTAL

Apparatus and reagents

Spectrophotometric measurements were performed on a Hitachi U-2000 spectrophotometer fitted with 1-cm path-length cells. The spectrophotometer cell compartment was thermostated by circulating water through it, by using a Neslab RTE bath with a temperature stability of ± 0.1°C.

All reagents were of analytical-reagent grade and were used as received. Doubly distilled water was used throughout. The iodine concentration of the stock solutions was determined with sodium thiosulphate that had been standarized with potassium iodate using 2% starch as indicator. All glass flasks used for iodine solutions were wrapped in aluminium foil to exclude light in order to prevent photochemical reactions. CPC was purchased from Serva.

Spectrophotometric studies

The effect of different parameters potentially influencing the I_3^-–CPC association was studied by changing them in turn while keeping all others constant. The apparent formation constant of the triiodide ion in a mixed solution of I_2, NaI and CPC was determined spectrophotometrically at 360 or 500 nm, depending on the CPC concentration used, through the absorbance changes at these wavelengths with varying NaI concentration at constant concentrations of I_2 and CPC. The apparent formation constants were determined by using the mole ratio method [7].

Experimental conditions for triiodide monitoring in a CPC medium

Maximum signal intensity and stability with time of the I_3–CPC association were obtained with iodine concentrations between 1×10^{-7} and 1×10^{-5} M and NaI concentrations between 1×10^{-4} and 5×10^{-4} M. The pH of the solution was kept between 2 and 10 and the temperature did not exceed at 20°C. The CPC concentrations were between 2×10^{-4} and 6×10^{-4} M. The maximum absorbance at 500 nm was obtained within a few seconds to a few minutes, depending on the reactant concentrations used.

RESULTS AND DISCUSSION

Iodine molecules interact strongly with CPC ions to yield a complex that is sparingly soluble in water but is readily soluble in CPC micelles. Although the occurrence of a precipitate at CPC concentrations below its c.m.c. hinders the recording of a reliable absorption spectrum for

I_2, the absorption peak shifts gradually from 460 to 360 nm on increasing the CPC concentration. At higher CPC concentrations above the c.m.c., the complex is redissolved and the peak remains at 360 nm. As the absorption spectrum of iodine is known to depend significantly on the polarity of the surrounding medium, the marked hypsochromic shift in the peak position in the CPC micellar solution compared with that obtained in water could be due to solubilization of the iodine molecules in the hydrophilic surface region of the CPC micelle [6], inasmuch as bathochromic shifts are observed when I_2 is dissolved in hydrophobic media [8]. On the other hand, iodide ion has been reported to bind strongly to the positively charged micelles of CPC, which allows the potentiometric titration of iodide by using a graphite-coated sensor [9].

Spectral study of the I_3^-–CPC association at CPC concentrations about 50–timers its c.m.c.

Addition of sodium iodide to solutions containing iodine dissolved in CPC micelles resulted in a gradual increase in the absorbance but in no shift of the peak at 360 nm (Fig. 1). This change can reasonably be ascribed to the formation of triiodide ion. However, as the peak location is red shifted by 8 nm in the CPC solution compared with that in water [10], triiodide ion can also be assumed to be dissolved in the surface region of the CPC micelle. The local concentrations of iodine and iodide in the micellar pseudo-phase should increase the apparent equilibrium formation constant of I_3^-. This constant was determined by adding 7×10^{-3} M CPC to solutions containing 4.06×10^{-5} M I_2 and iodide concentrations between 0 and 4×10^{-4} M and measuring the absorbance of these solutions at 360 nm. The mole ratio method was used to calculate the value of the constant and it was found to be 4×10^5 mol^{-1} l at 20°C. As this constant is 10^3 mol^{-1} l at 10°C and 730 mol^{-1} l at 25°C in aqueous media [6], the addition of CPC increases the apparent equilibrium formation constant of I_3^- by a factor of ca. 400. Therefore, the increase in the analytical concentration of I_3^- produced by the surfactant provides a sensitive, direct method for the determination of about 1×10^{-7} M concentrations of I_2.

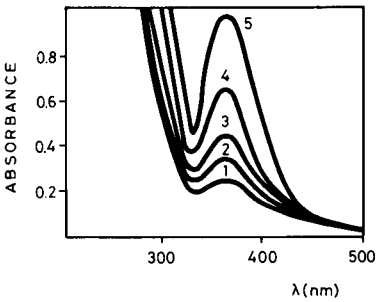

Fig. 1. Effect of sodium iodide concentration on the absorption spectrum of solutions containing 4.06×10^{-5} M I_2 and 7×10^{-3} M CPC. Iodide concentration: (1) 0; (2) 1.06×10^{-5}; (3) 2.06×10^{-5}; (4) 4.06×10^{-5}; (5) 8.01×10^{-5} M.

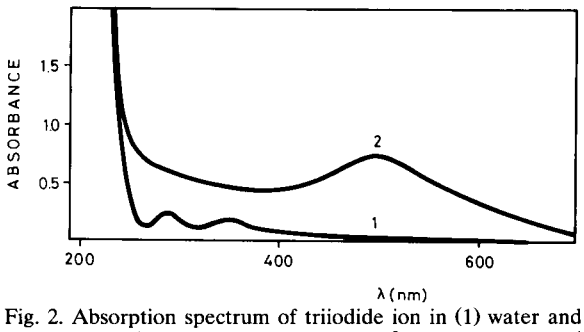

Fig. 2. Absorption spectrum of triiodide ion in (1) water and (2) 1.05×10^{-4} M CPC. $[I_2] = 4.06 \times 10^{-5}$ M; $[I^-] = 3 \times 10^{-4}$ M.

Spectral study of the I_3^-–CPC association at CPC concentrations just above its c.m.c.

The spectral features of the I_3^-–CPC association change dramatically at CPC concentrations below about 7×10^{-4} M: the characteristic bands of I_3^- in water are shifted to about 500–530 nm, depending on various experimental factors, and a marked increase in the absorbance maximum is observed (Fig. 2). No bathochromic shift of the iodine peak in the absence of iodide was detected at CPC concentrations below ca. 7×10^{-4} M, but only insolubilization of iodine owing to the formation of the aforementioned iodine– CPC complex. The formation rate and stability with time of the I_3^-–CPC association depend on the experimental conditions used. Instability arises from the gradual insolubilization of the I_3^-–CPC associa-

tion, yet the association is stable enough under certain experimental conditions to permit reproducible analytical results. Because of the singular features of this I_3^-–cationic micelle interaction and because this surfactant at concentrations lower than 7×10^{-4} M can enhance both the sensitivity and selectivity in the photometric monitoring of iodine, the effects of variables influencing the formation rate, maximum absorbance, peak position, stability, etc., of the I_3^-–CPC association were studied in order to obtain an idea of its analytical potential and to shed some light on the interaction mechanism involved.

Variables affecting the I_3^-–CPC system at CPC concentrations just above its c.m.c.

The different variables affecting this system were changed individually in turn. The CPC concentration used was found to be essential to determine the features of the I_3^-–CPC association. Figure 3A shows the absorbance maximum obtained as a function of the CPC concentration. A break point appears at 1.4×10^{-4} M CPC,

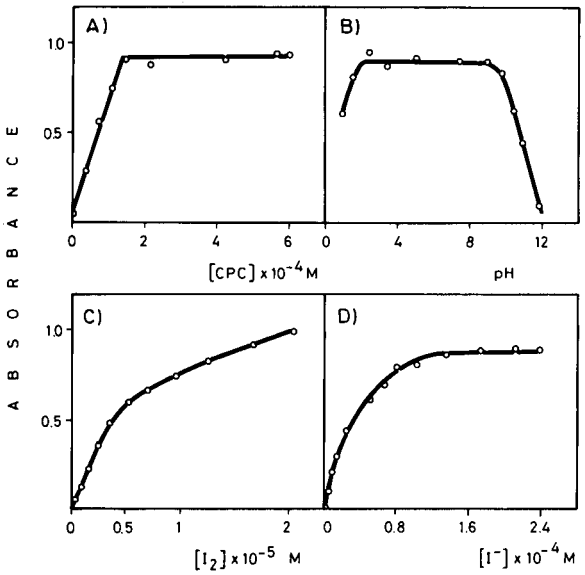

Fig. 3. Influence of (A) CPC concentration, (B) pH, (C) iodine concentration and (D) iodide concentration on the absorbance at 500 nm of the I_3^-–CPC association. $[I_2] = 2.07 \times 10^{-5}$ M (A, B and D); $[I^-] = 1.32 \times 10^{-4}$ M (A and B) and 4.62×10^{-3} M (C); [CPC] = 1.82×10^{-4} M (B) and 1.05×10^{-5} M (C and D).

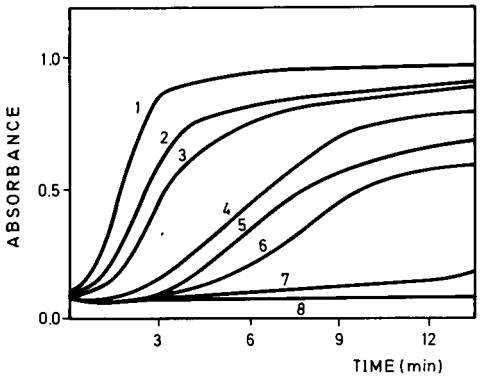

Fig. 4. Effect CPC concentration on the kinetics of formation of the I_3^-–CPC association. $[I^-] = 1.32 \times 10^{-4}$ M; $[I_2] = 2.07 \times 10^{-5}$ M. CPC concentration: (1) 8.4×10^{-4}; (2) 9.8×10^{-4}; (3) 1.05×10^{-3}; (4) 1.12×10^{-3}; (5) 1.26×10^{-3}; (6) 1.4×10^{-3}; (7) 1.96×10^{-3}; (8) 2.8×10^{-3} M.

above which the absorbance obtained remained constant throughout the range examined. The formation of the I_3^-–CPC association was virtually instantaneous between 4×10^{-5} and 6×10^{-4} M CPC. Higher surfactant concentrations (ca. 1×10^{-3} M) gave rise to an induction period, the length of which increased with increase in the CPC concentration. Figure 4 shows the variation of the induction period as a function of CPC concentration. At a CPC concentration of ca. 5×10^{-3} M the bathochromic shift disappeared and the I_3^-–CPC association showed the spectral features reflected in Fig. 1. The stability of this association varied as a function of CPC concentration. Thus, the maximum absorbance was decreased by 55% and 1.2% 30 min after reactants were mixed for 7×10^{-5} and 6×10^{-4} M CPC, respectively.

Figure 3B shows the dependence of the maximum absorbance of the I_3^-–CPC system on pH. The association rapidly decomposes below pH 2. Thus, at pH 1.9, the absorbance maximum decreases by 15% after 1 h. In an aqueous medium, the fraction of overall iodine present as I_2 decreases sharply in the pH range 6–10 as a result of I_2 being replaced with I^- and IO_3^- [11]. The hydrolysis of I_3^- proceeds very slowly at pH 5–6 in an aqueous medium, but rapidly above pH 6.4. CPC considerably delays the hydrolysis of I_2, which is only significant above a pH of ca. 9 (Fig.

3B). The position of the I_3^-–CPC peak does not change in the pH range examined.

The influence of the iodine concentration on the absorbance at 500 nm is shown in Fig. 3C. Concentrations of iodine as low as 1×10^{-7} M can be determined with no liquid–liquid extraction. No changes in the spectral features of the I_3^-–CPC association with the iodine concentration were observed.

The iodide concentration used has a critical influence on the features of the I_3^-–CPC association. Such a concentration must be at least three times the iodine concentration to cause a bathochromic shift in the I_3^- spectrum, which increases as the iodide concentration increases. Thus, the peak position remains unchanged at 500 nm up to about 5×10^{-4} M and then changes up to about 530 nm for an iodide concentration of 6.5×10^{-3} M. Figure 3D shows the dependence on the iodide concentration of the absorbance of the I_3^-–CPC association at 500 nm. Maximum absorbance was obtained above ca. 1.3×10^{-4} M iodide. Because iodide ion yields an insoluble salt with CPC, an excess of this ion should be avoided in order to prevent precipitation. The stability with time and the formation rate of the I_3^-–CPC association were maximum above ca. 1×10^{-4} M iodide.

Increased temperature had an adverse effect on the absorbance at 500 nm of the I_3^-–CPC association, although the extent was smaller than that to which the I_3^-–starch complex was affected and remained virtually constant between 10 and 20°C (Table 1). The temperature did not affect the rate of the formation of the I_3^- ion, which was instantaneous up to about 25°C. The absorbance of the I_3^-–CPC association was always greater than that of the I_3^-–starch complex at every temperature examined.

Organic solvents such as ethanol and non-ionic surfactants destroyed the I_3^-–CPC association.

This study of variables provided a wide enough range of experimental conditions for monitoring triiodide ion in CPC micellar media.

TABLE 1

Maximum absorbance of the triiodide ion in different media at different temperatures [a]

Temperature (°C)	Medium		
	Water (λ = 350 nm)	CPC (λ = 500 nm)	Starch (λ = 586 nm)
2	0.107	0.587	0.406
10	0.102	0.483	0.337
15	0.095	0.477	0.223
20	0.089	0.473	0.110
25	0.086	0.341	0.101
35	0.074	0.177	0.094
45	0.075	0.131	0.092

[a] $[I_2] = 2.07 \times 10^{-5}$ M; $[I^-] = 1.32 \times 10^{-4}$ M; [CPC] = 1.8×10^{-4} M; [starch] = 0.06%.

Action of CPC on the triiodide ion at surfactant concentrations just above its c.m.c.

Some experiments were done in order to shed some light on the action of CPC on the triiodide ion at surfactant concentrations lower than ca. 7×10^{-4} M. The apparent equilibrium constant for the formation of triiodide ion was determined by adding 1.05×10^{-4} M CPC to solutions containing 2.07×10^{-5} M I_2 and iodide concentrations between 0 and 2.5×10^{-4} M. Absorbance data at 500 nm for these solutions were used to calculate the value of the constant by the mole ratio method. It was found to be $(5.4 \pm 0.2) \times 10^4$ mol^{-1} l at 20°C, i.e., about 50-times that in water. Therefore, concentrations of iodine of about 1×10^{-7} M can be determined with no liquid–liquid extraction.

Because of the different action of CPC compared with other cationic surfactants with similar non-polar tails (DTAB, CTAB, DTAB), it was checked whether the polar head group was the sole agent responsible for the bathochromic shift. A pyridinium salt (pyridinium trifluoroacetate) at concentrations similar to and higher than those at which CPC causes the bathochromic shift was added to triiodide solutions. Experiments were made over the temperature range 2–25°C. No changes in the spectral features of the triiodide ion were observed at any time. Therefore, the presence of micelles is essential to alter the spectral features of the triiodide ion.

As the absorption spectrum of iodine is known to depend significantly on the polarity of the surrounding medium and it yields absorption bands with peaks at 500–530 nm in hydrophobic

media such as hexane, it can be reasonably assumed that the iodine molecules in micellar solutions of CPC at surfactant concentrations between ca. 4×10^{-5} and 6×10^{-4} M are dissolved in the hydrocarbon core. However, there is no solid evidence to support this hypothesis, so further experiments must be made in this respect. Major issues to be elucidated are the role of the iodide ion, which is essential to produce the effects observed, and the region where I_2 and I^- are dissolved in the micelles.

Analytical potential of the I_3^-–CPC association

Despite the poor spectral features of the I_3^- complex in aqueous media (maximum absorbance at 350 nm and low absorptivity) and its relatively low stability constant, photometric monitoring of this complex is part of number of analytical methods.

Both the bathochromic shift of the maximum absorbance of the triiodide ion from 350 to 500 nm and the increased absorptivity provided by the CPC micellar medium can be used to enhance the selectivity and sensitivity of analytical methods involving the I_2–I^- system. The frequency with which iodine is determined directly in a wide variety of samples (environmental, food, biochemical, etc.) requires an enhanced photometric procedure for its determination at the micromolar level that does not need extraction and so that no organic solvent needs to be used. Compared with starch solutions, CPC solutions are more stable as they are insensitive to microorganisms. Also, CPC solutions can be prepared with accurately known concentrations. In order to compare the analytical features of the I_3^-–CPC system with those of the I_3^-–starch system the optimum starch content was first determined by keeping the pH at 5.3 and the I_2 and I^- concentrations constant at 1×10^{-5} and 1.6×10^{-4} M, respectively, changing the starch content between 0 and 0.2% and measuring the absorbance at 586 nm. The signal was found to increase with increasing starch content between 0 and 0.08%, above which it remained unaltered, at least up to 0.2%. Therefore a 0.1% starch content was chosen optimum.

The calibration graph for the determination of I_2 in the presence of starch consists of two portions, the first of which has a very gentle slope between 0 and 8×10^{-6} M. The sensitivity of the calibration graph obtained in the same I_2 concentration range in the presence of CPC was higher by about one order of magnitude. Table 2 summarizes the analytical figures of merit of the two methods for the determination of I_2. The detection limit obtained by using CPC instead of starch was higher by one order of magnitude. The instrumental noise and drift were $\pm 1 \times 10^{-3}$ absorbance and within $\pm 1 \times 10^{-3}$ absorbance h^{-1} at 500 nm, respectively.

The use of the I_3^-–CPC association in various types of reactions was examined and the preliminary results obtained are discussed below.

Use of the I_3^-–CPC association in the determination of hydroperoxides. Hydroperoxides such as H_2O_2 and organic hydroperoxides (cumene and *tert*-butyl hydroperoxide and hydroperoxoli-

TABLE 2

Quantitative performance of the I_3^-–CPC and I_3^-–starch methods [a]

Parameter	I_3^-–CPC system	I_3^-–starch system	
Linear range (M)	$(0.1–11) \times 10^{-6}$	$(3.0–7.5) \times 10^{-6}$	$(7.54–40) \times 10^{-6}$
Slope ± S.D. (absorbance mol^{-1} l)	$(3.89 \pm 0.008) \times 10^4$	$(4.3 \pm 0.9) \times 10^3$	$(2.27 \pm 0.03) \times 10^4$
Intercept ± S.D. (absorbance)	$(0.7 \pm 0.4) \times 10^{-2}$	$(-1.7 \pm 5.7) \times 10^{-3}$	$(-1.44 \pm 0.08) \times 10^{-1}$
r [b]	0.999	0.96	0.999
Standard error of the estimate (absorbance)	0.0085	0.0050	0.0070
Detection limit (M)	4.0×10^{-8}	8.8×10^{-7}	
R.S.D. (%) [c]	3.0 [d]	6.8 [d]	3.5 [c]

[a] $[I^-] = 1.6 \times 10^{-4}$ M; [CPC] = 2×10^{-4} M; [starch] = 0.1%. [b] Correlation coefficient, $n = 6$. [c] $n = 11$, for [d] 5×10^{-6} and [e] 18×10^{-6} M I_2.

noleate) are substrates of interest for different types of samples, e.g., serum [12], hydrocarbons [13], oils [14], the determination of which is usually carried out by conventional photometric iodimetric methods. Detection limits for H_2O_2, cumene hydroperoxide, *tert*-butyl hydroperoxide and hydroperoxolinoleate of ca. 3×10^{-7} M were obtained by adding CPC to the reaction mixture, which is significantly lower than those afforded by the conventional iodimetric method, which is the most generally applicable procedure for the determination of micro amounts of hydroperoxides (detection limits about 1×10^{-6} M [15]). The precision obtained by using small sample volumes was fairly good and minimum pretreatment of hydrocarbons and oil samples was required.

Effect of the I_3^-–CPC association on the metal-catalysed I^-–H_2O_2 system. The enhanced sensitivity and selectivity provided by CPC can be exploited for the determination of catalysts that accelerate the conversion of excess of iodide into I_3^- by H_2O_2, such as in the determination of Mo(VI) in plants, which often requires the removal of interferents (e.g., by ion exchange) because the reaction is interfered with a number of species [16]. In addition to increasing the sensitivity to Mo(VI), the use of CPC resulted in significantly increased selectivity [e.g., iron(III) was tolerated at concentrations 20 times that of molybdenum].

Effect of the I_3^-–CPC association on the I_2–azide system. The reaction between iodine and azide is induced by sulphur-containing organic and inorganic substances that accelerate it. This effect has been widely used for the determination of many sulphur compounds (drugs, pesticides, amino acids, etc.). Studies still in progress have shown so far that conventional kinetic procedures can be considerably improved by using the CPC micellar medium. For example, it is possible to determine amounts of thiuram disulphides about 25 times lower than with an earlier method [17].

A detailed study of each of the above-mentioned systems is in progress in order to provide a more precise appraisal of the significance of the I_3^-–CPC association in the context of analytical chemistry. Its application can be extended to classical methods such as volumetric titrations (CPC can be used as a chemical indicator instead of starch for end-point detection) and in qualitative analyses for iodine and, in general, in quantitative analyses involving the iodine–iodide system as analyte or reagent.

The authors gratefully acknowledge financial support from the CICyT.

REFERENCES

1 W.L. Hinze, in K.L. Mittal (Ed.), Solution Chemistry of Surfactants, Vol. 1, Plenum, New York, 1979, p. 79.
2 L.J. Cline Love, J.G. Harbata and J.G. Dorsey, Anal Chem., 56 (1984) 1132A.
3 E. Pelizzetti and E. Pramauro, Anal. Chim. Acta, 169 (1985) 1.
4 W.L. Hinze, H.N. Singh, Y. Baba and N.G. Harvey, Trends Anal. Chem., 3 (1984) 193.
5 M. Cuccovia and H. Chaimovich, Anal. Chem., 54 (1982) 789.
6 K. Hayakawa, M. Kanda and I. Satake, Bull. Chem. Soc. Jpn., 52 (1979) 3171.
7 D.A. Skoog and D.M. West, Principles of Instrumental Analysis, Holt, Rinehart and Winston, New York, 1979, p. 105.
8 F.H. Getman, J. Am. Chem. Soc., 50 (1928) 2883.
9 W.S. Selig, Fresenius' Z. Anal. Chem., 330 (1988) 127.
10 A.D. Awtrey and R.E. Connick, J. Am. Chem. Soc., 73 (1951) 1842.
11 D.A. Palmer and M.H. Lietzke, Radiochim. Acta, 31 (1982) 37.
12 M. El-Saadani, H. Esterbauer, M. El-Sayed, M. Goher, A.Y. Nassar and G. Jürgens, J. Lipid Res., 30 (1989) 627.
13 H. Pobiner, Anal. Chem., 33 (1961) 1423.
14 W. Horwitz (Ed.) Official Methods of Analysis of the Association of Official Analytical Chemists, AOAC, Washington, DC, 1975, p. 489.
15 E. Azaz, M. Donbrow and R. Hamburger, Analyst, 98 (1973) 663.
16 L.C.R. Pessenda, A.O. Jacintho and E.A.G. Zagatto, Anal. Chim. Acta, 214 (1988) 239.
17 Z. Kurzawa, K. Janowicz and J. Kurzawa, Anal. Chim. Acta, 243 (1991) 201.

Analytica Chimica Acta, 268 (1992) 153–157
Elsevier Science Publishers B.V., Amsterdam

Determination of active components in insecticide formulations by derivative ultraviolet spectrophotometry

J.A. Jimena García, J. Giménez Plaza and J.M. Cano Pavón

Department of Analytical Chemistry, Faculty of Sciences, University of Málaga, E-29071 Málaga (Spain)

(Received 2nd January 1992; revised manuscript received 8th May 1992)

Abstract

A rapid second-derivative ultraviolet spectrophotometric method for the resolution of mixtures of two components in commercially available insecticide formulations that cannot be resolved by conventional spectrophotometry was developed and applied to the analysis of mixtures of piperonyl butoxide with neopynamine, permethrin and fenitrothion, with satisfactory results.

Keywords: UV–Visible spectrophotometry; Derivative spectroscopy; Fenitrothion; Insecticides; Neopynamine; Permethrin; Piperonyl butoxide

A variety of methods are available for the determination of pesticide residues, few of which, however, are concerned with the direct assay of commercial formulations. Such formulations usually contain their active components in an inert solvent. Determining the concentration in the inert solvent requires the use of a rapid procedure that is normally employed for quality control tests on the formulations.

Most of the methods developed so far for the analysis of commercially available pesticide formulations are either gas chromatographic [1–3] or liquid chromatographic methods [4,5]. Ultraviolet–visible spectrophotometry has also been used for this purpose, viz., in the resolution of fenitrothion–parathion-methyl mixtures [6]; however, the applicability of this technique in this area is hindered by serious spectral band overlap.

In this work, derivative UV spectrophotometry was used for the analysis of formulations containing binary mixtures of piperonyl butoxide with permethrin, neopynamine and fenitrothion, the first of which has a synergic effect on the action of the others. The derivative technique is particularly useful for obtaining qualitative and quantitative information on spectra consisting of poorly resolved bands and has so far been chiefly applied in pharmaceutical analysis and clinical chemistry [7].

Correspondence to: J.M. Cano Pavón, Department of Analytical Chemistry, Faculty of Sciences, University of Málaga, E-29071 Málaga (Spain).

EXPERIMENTAL

Apparatus

Spectra were recorded on a Shimadzu UV-240 spectrophotometer furnished with an OPI-2 derivative module and quartz and glass cuvettes of 1.0-cm path length. A Shimadzu LC-6A liquid chromatograph with a LiChrosorb RP-8 (Merck) column was used.

Reagents

The reagents included individual solutions and binary mixtures of piperonyl butoxide with per-

methrin, neopynamine and fenitrothion at different concentrations in hexane and ethanol.

Procedures

The procedure used to assay the mixtures depended on the components involved.

Resolution of piperonyl butoxide–fenitrothion mixtures in ethanol. Spectrophotometric measurements were made between the maximum (peak) and minimum (valley) of the second-derivative spectrum of the mixture, viz., between 280 and 300 nm for piperonyl butoxide and between 220 and 230 nm for fenitrothion. A calibration graph was previously constructed for each component from solutions of known concentrations. If the concentration of piperonyl butoxide is higher than that of fenitrothion, a solution of the former at the same concentration as in the sample is prepared on the basis of the calibration graph corresponding to the band at 280–300 nm. This new solution is used as a blank in order to determine the fenitrothion concentration so as to resolve the overlapped bands. The concentration of piperonyl butoxide should between 2.0×10^{-5} and 1.4×10^{-4} M and that of fenitrothion between 2.0×10^{-5} and 1.2×10^{-4} M.

Resolution of piperonyl butoxide–permethrin mixtures in hexane. Measurements were made between the maximum (peak) and minimum (valley) of the second-derivative spectrum over the wavelength range 280–300 nm and yielded the concentration of piperonyl butoxide. Another set of measurements over the range 200–210 nm provided the overall concentration of the two components, from which that of permethrin was calculated by difference. When the concentration of

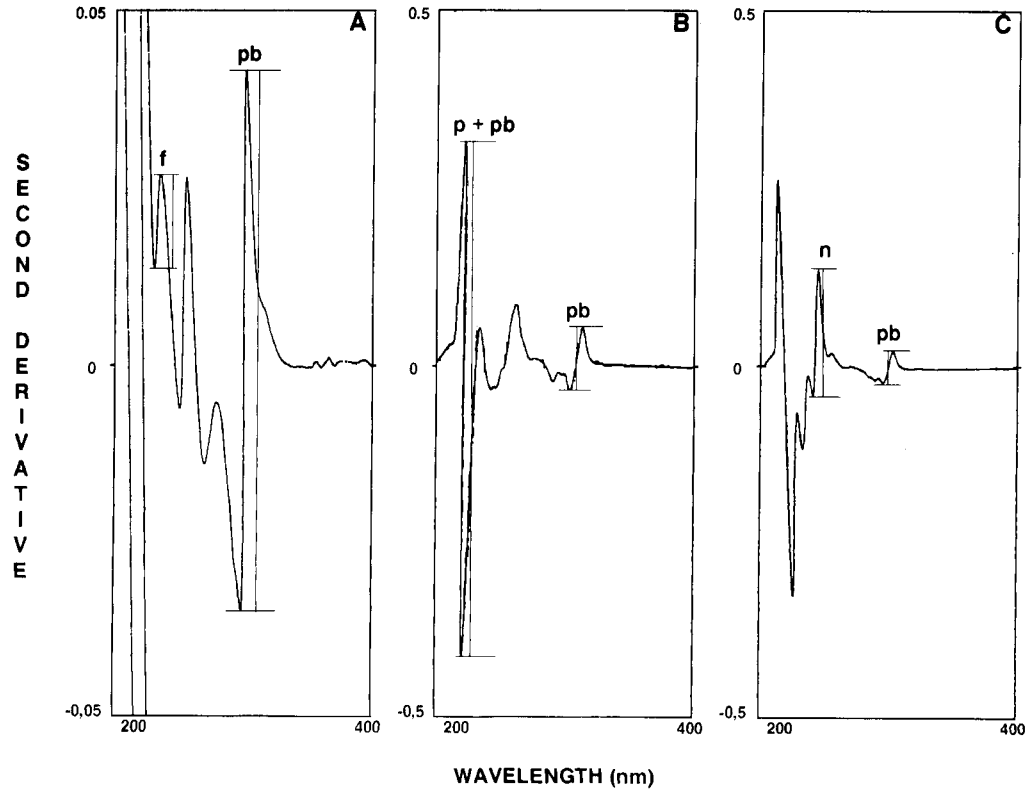

Fig. 1. Second derivative UV spectra of the insecticide mixtures assayed. (A) Fenitrothion (f, 1.2×10^{-4} M) and piperonyl butoxide (pb, 8.0×10^{-5} M). (B) Permethrin (p, 6.0×10^{-5} M) and piperonyl butoxide (pb, 8.0×10^{-5}). (C) Neopynamine (n, 8.0×10^{-5} M) and piperonyl butoxide (pb, 4.0×10^{-5} M).

TABLE 1

Figures of merit of the calibration graphs

Insecticide	Solvent	Calibration equation [a]	Wavelength range (nm)	Correlation coefficient	Derivative signal range (DSR)	R.S.D. (%) ($n = 7$)
Piperonyl butoxide	Ethanol	$h = 13.48C - 1.734$	280–300	0.999	0.05	1.106
	Hexane	$h = 10.17C - 22.700$	200–210	0.996	0.10	–
		$h = 7.63C - 1.830$	280–300	0.999	0.10	1.423
Fenitrothion	Ethanol	$h = 5.10C - 38.500$	220–320	1.000	0.05	0.678
		$h = 3.34C + 0.560$ [b]		0.999	0.10	3.140
Permethrin	Hexane	$h = 14.90C - 6.000$	200–210	0.998	0.50	1.940
Neopynamine	Hexane	$h = 3.40C - 0.680$	230–240	0.998	0.50	3.060

[a] h = Read-out distance (mm); C = concentration ($M \times 10^5$). [b] This equation applies when the concentration of piperonyl butoxide is higher than that of fenitrothion.

piperonyl butoxide is higher than that of permethrin, a solution of the former at the same concentration as in the sample is also prepared as in the previous instance, and is subsequently employed to determine permethrin. The concentrations of piperonyl butoxide and permethrin should

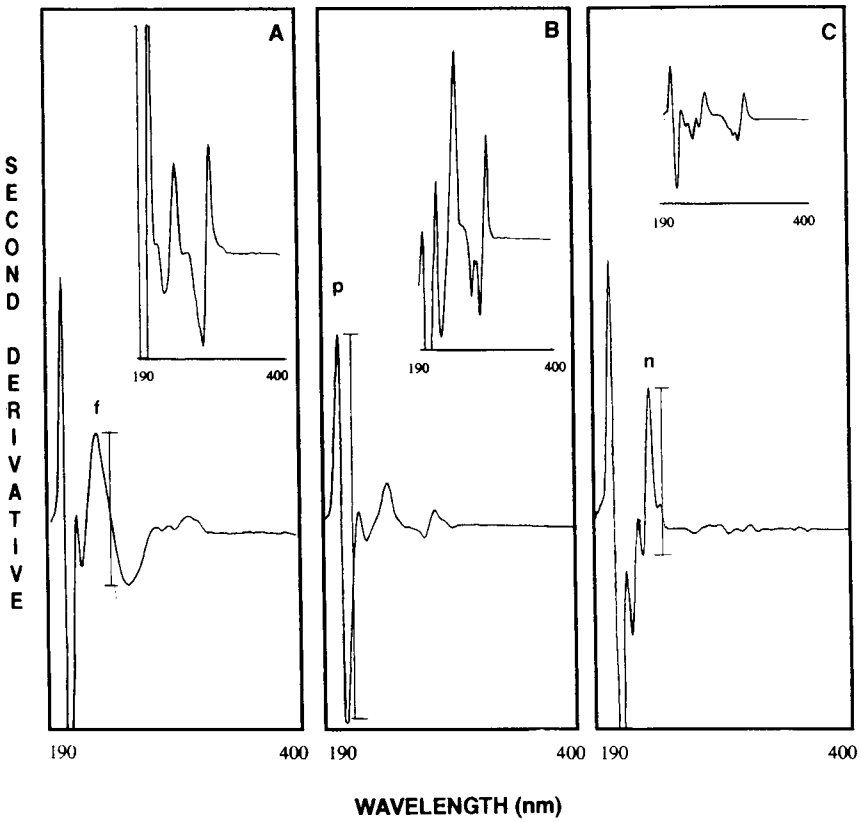

Fig. 2. Second-derivative UV spectra of the commercial formulations assayed. (A) Fenitrothion (f, 8.0×10^{-5} M) and piperonyl butoxide (1.0×10^{-4} M). (B) Permethrin (p, 7.0×10^{-5} M) and piperonyl butoxide (1.0×10^{-4} M). (C) Neopynamine (n, 2.0×10^{-5} M) and piperonyl butoxide (1.0×10^{-4} M). Top, second-derivative UV spectra of the insecticide mixtures; bottom, second-derivative UV spectra of the secondary component.

TABLE 2

Resolution of mixtures of piperonyl butoxide (PB) and fenitrothion (F)

Added (10^{-5} M)		Found (10^{-5} M)		$(h)_{PB}$ [a] (mm)	$(h)_F$ [b] (mm)
PB	F	PB	F		
8.0	10.0	8.3	10.3	110	14
8.0	12.0	8.6	11.7	114	21
8.0	14.0	8.5	13.4	113	30
8.0	16.0	8.6	16.3	114	45

[a] Wavelength range = 280–300 nm; DSR = ±0.05. [b] Wavelength range = 220–230 nm; DSR = ±0.05.

TABLE 3

Resolution of mixtures of piperonyl butoxide (PB) and permethrin (P)

Added (10^{-5} M)		Found (10^{-5} M)		$(h)_{PB}$ [a] (mm)	$(h)_P$ [b] (mm)
PB	P	PB	P		
4.0	2.0	4.0	2.3	32	31
6.0	6.0	5.9	6.3	47	96
8.0	6.0	7.8	6.4	61	100
10.0	8.0	10.1	7.9	79	128

[a] Wavelength range = 280–300 nm; DSR = ±0.1. [b] Wavelength range = 200–210 nm; DSR = ±0.5.

lie in the ranges 2.0×10^{-5}–2.0×10^{-4} M and 2.0×10^{-5}–8×10^{-5} M, respectively.

Resolution of piperonyl butoxide–neopynamine mixtures. Measurements were made between the maximum and minimum of the second-derivative spectrum over the wavelength ranges 280–300 and 230–240 nm for piperonyl butoxide and neopynamine, respectively. If the concentration of piperonyl butoxide is higher than that of neopynamine, a solution of the former at the same concentration as in the sample is prepared, and is employed to determine neopynamine. The concentrations of piperonyl butoxide and neopynamine should lie in the ranges 2.0×10^{-5}–1.2×10^{-4} and 1.0×10^{-5}–1.0×10^{-4}M, respectively.

RESULTS AND DISCUSSION

Binary mixtures of piperonyl butoxide with neopynamine, permethrin and fenitrothion, which are commonplace in commercially available insecticide formulations, cannot be assayed directly by UV–visible spectrophotometry owing to extensive spectral overlap of the absorption bands of these compounds. However, their second-derivative spectra do allow complete or at least partial resolution of the mixtures. The piperonyl butoxide–fenitrothion mixture in ethanol yields a sig-

TABLE 4

Resolution of mixtures of piperonyl butoxide (PB) and neopynamine (N)

Added (10^{-5} M)		Found (10^{-5} M)		$(h)_{PB}$ [a] (mm)	$(h)_N$ [b] (mm)
PB	N	PB	N		
4.0	8.0	3.9	8.1	32	27
6.0	10.0	6.0	9.9	48	33
8.0	6.0	8.4	6.4	66	21
10.0	10.0	9.0	10.5	77	35

[a] Wavelength range = 280–300 nm; DSR = ±0.1. [b] Wavelength range = 230–240 nm; DSR = ±0.5.

TABLE 5

Analysis of commercial formulations by second-derivative UV spectrophotometry (D) and liquid chromatography (LC) [a]

Formulation No.	Piperonyl butoxide			Neopynamine			Permethrin			Fenitrothion		
	Stated concentration (10^{-5} M)	Found (10^{-5} M)		Stated concentration (10^{-5} M)	Found (10^{-5} M)		Stated concentration (10^{-5} M)	Found (10^{-5} M)		Stated concentration (10^{-5} M)	Found (10^{-5} M)	
		D	LC		D	LC		D	LC		D	LC
1	10.0	10.5	9.6	2.0	2.2	2.2	–	–	–	–	–	–
2	10.0	9.0	10.2	–	–	–	7.0	6.2	6.9	–	–	–
3	10.0	10.5	10.4	–	–	–	–	–	–	8.0	8.2	8.3

[a] The values are based on repetitive measurements on seven samples.

nal between 280 nm (minimum) and 300 nm (maximum), the intensity of which is proportional to the concentration of the former component (Fig. 1A). The mixture yields another signal between 220 nm (minimum) and 230 nm (maximum) that increases linearly with increasing fenitrothion concentration.

The piperonyl butoxide–permethrin mixture in hexane provides no signal exclusive to permethrin (Fig. 1B). Hence piperonyl butoxide is determined as in the previous mixture, while the overall concentration of the components is obtained from the signal appearing between 200 nm (minimum) and 210 nm (maximum), the intensity of which is dependent on the concentration of both. Finally, the concentration of permethrin is obtained by difference.

With regard to the piperonyl butoxide–neopynamine mixture in hexane, the former component is determined as in the previous two instances, while the latter is determined from the signal obtained between 230 nm (minimum) and 240 nm (maximum), the intensity of which depends exclusively and linearly on the concentration of this component (Fig. 1C). Hence the two components can be determined independently.

Table 1 lists the figures of merit of the calibration graphs run for the four components assayed.

The procedure was applied to the resolution of various binary mixtures of the four insecticides at different concentrations. As can be seen from Tables 2–4, the results obtained were satisfactory. The assays are reasonably fast, which is of special importance for the quality control of commercially available formulations.

Finally, if the concentration of piperonyl butoxide is higher than that of the other insecticides contained in the formulation, band overlap is even more extensive, which hinders the determination of the second insecticide considerably. Piperonyl butoxide is present as a major compound in some commercially available formulations. In this instance, the use of a blank solution containing the same concentration as the sample, which is previously calculated from the calibration graph for this component corresponding to the signal at 280–300 nm, reduces the spectral interferences to a significant extent.

The proposed methods were validated by applying them to the analysis of various commercially available formulations (Fig. 2); the results obtained were compared with others found by using liquid chromatography with acetonitrile–water (3 + 2) as the mobile phase at a flow-rate of 1.2 ml min^{-1} and spectrophotometric detection. The results are summarized in Table 5.

REFERENCES

1 S. Lorusso, A. di Muccio, M. Boccacci and G. Notarangelo, Rass. Chim., 35 (1983) 117.
2 D.J. Sura, R.H. Simon and F. Beyerlein, J. Chromatogr., 314 (1984) 117.
3 D. Wei, G. Zhang, X. Ma and Y. Yi, Sepu, 5 (1987) 323.
4 R.L. Pérez, J. Assoc. Off. Anal. Chem., 66 (1983) 789.
5 U. Nehmer and N. Dimov, J. Chromatogr., 288 (1984) 227.
6 C.S.P. Sastry and D. Vijaya, Acta Cienc. Indica, Ser. Chem., 12 (1986) 138.
7 F. Sánchez Rojas, C. Bosch and J.M. Cano Pavón, Talanta, 35 (1988) 753.

Analytica Chimica Acta, 268 (1992) 159–162
Elsevier Science Publishers B.V., Amsterdam

Indirect determination of arginine by graphite furnace atomic absorption spectrometry after preconcentration on a Nafion chemically modified tungsten coil

Litong Jin, Hui Zhu, Tongmin Xu, Wei Tong, Weiliang Zhou and Yuzhi Fang

Department of Chemistry, East China Normal University, 3663 Zhong Shan Road (N), Shanghai 200062 (China)

(Received 26th September 1991; revised manuscript received 2nd March 1992)

Abstract

A method for the indirect determination of arginine by graphite furnace atomic absorption spectrometry after preconcentration on a Nafion chemically modified tungsten coil is described. The mechanism is discussed. In HCl solution (pH 3.5), the exchange competition between protonated arginine and Cu^{2+} on the Nafion film causes a decrease in the amount of Cu^{2+} binding to the Nafion film, resulting in a decrease in the absorption signal of Cu^{2+} being measured. A linear relationship between the decrease in absorbance and the concentration of arginine is obtained in the range 3.1×10^{-8}–2.5×10^{-7} mol l^{-1}. The relative standard deviation for ten parallel determinations is 2.3%. The detection limit is 1.3×10^{-8} mol l^{-1}. The results for the content of arginine determined in cephradine injection are satisfactory.

Keywords: Atomic absorption spectrometry; Arginine; Preconcentration

About 70 elements can be determined directly by atomic absorption spectrometry (AAS). However, indirect AAS must be used to determine non-metallic elements, organic compounds, pharmaceuticals and certain metallic elements that are difficult to atomize. Xu et al. [1] have reviewed the application of indirect AAS in analytical chemistry. The operation of conventional indirect AAS is often complicated because separation and concentration processes such as extraction and filtration have to be used to eliminate certain excess reactants, products and matrices after several chemical reactions, and this can lead to losses of certain species to be measured. In this work, a method involving a chemically modified tungsten coil combined with graphite furnace AAS (GFAAS) was developed. Without chemical reactions and complicated separations, arginine, which cannot be measured directly, competes with a metal ion that can be detected directly in the ion exchange on the Nafion film. This method of indirect AAS is simple, sensitive, and easy to operate. The determination of arginine by this method gave satisfactory results.

Arginine, a fundamental protein component, is a basic amino acid with a guanidino group. It is used in the clinic treatment of liver coma. Conventional determination methods for arginine include liquid chromatography [2], fluorimetry [3] and chemiluminecence methods [4]. The method of indirect determination of arginine with a chemically modified tungsten coil and GFAAS has not been reported previously.

Correspondence to: Litong Jin, Department of Chemistry, East China Normal University, 3663 Zhong Shan Road (N), Shanghai 200062 (China).

EXPERIMENTAL

Apparatus and reagents

A Hitachi Model 180-80 polarized Zeeman-effect atomic absorption spectrometer was used. pH measurements were made with an Orien Model 211 digital pH meter. A 0.05% Nafion solution in methanol was prepared by diluting an appropriate amount of 5% Nafion 117 (DuPont) with methanol.

Other reagents were of analytical-reagent grade. Doubly distilled, deionized water was used throughout.

Construction of Nafion-modified tungsten coil

A piece of 0.5-mm tungsten wire was coiled tightly into a 3-mm disc, leaving a 2.5-cm length for connection to the holder [5]. A 10-μl volume of 0.05% methanolic Nafion solution was transferred onto the tungsten coil with a micro syringe. The coil was then placed under an IR lamp for 1.5 min to evaporate the solvent.

General procedure

Immerse the Nafion–tungsten coil in HCl (pH 3.5) containing an appropriate amount of Cu^{2+} and start magnetic stirrer and timer. After 3 min, transfer the tungsten coil into doubly distilled water for cleaning, then dry it with filter-paper and place it in the graphite cup. Start the atomization procedure and measure the absorbance under the following conditions: wavelength, 324.8 nm; Cu lamp current, 7.5 mA; bandpass, 1.3 nm; sheathing gas (argon) flow-rate, 200 ml min^{-1}; drying temperature, 80–120°C for 10 s; ashing temperature, 600°C for 10 s; atomization temperature, 2700°C for 7 s; and cleaning temperature, 2800°C for 3 s.

Add an appropriate amount of arginine to the solution of Cu^{2+}. Repeat the above procedure and record the absorbance. The decrease in absorbance observed is directly proportional to the concentration of arginine added in the range 3.1×10^{-8}–2.5×10^{-7} mol l^{-1}.

RESULTS AND DISCUSSION

Mechanism

When Cu^{2+} is added to HCl (pH 3.5), it will be exchanged on the Nafion film:

$$2\,-(SO_3Na)_{film} + Cu^{2+} \rightleftharpoons -[(SO_3)_2Cu]_{film} + 2Na^+$$

When arginine is added to this acidic solution, it is protonated:

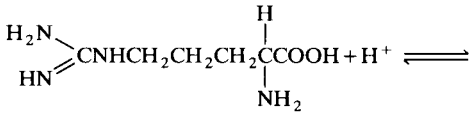

(A)

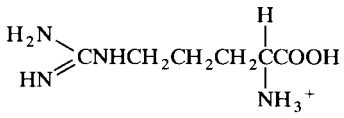

(B)

The protonated arginine will compete with Cu^{2+} in ion exchange on the Nafion film:

$$-(SO_3Na)_{film} + B^+ \rightleftharpoons -(SO_3B)_{film} + Na^+$$

This competition process will reduce the amount of Cu^{2+} binding to the Nafion film, which results in a decrease in the absorption signal. This decrease in absorption signal increases linearly with the amount of arginine added.

Selection of measurement conditions

Acidity. The decrease in the Cu absorption signal caused by the exchange competition of arginine varies with the pH of the solution because the pH value affects the degree of protonation of arginine. There is a marked decrease in absorption signal in pH 3.5 HCl where the degree of protonation of arginine is complete. Therefore, HCl of pH 3.5 is recommended.

Preconcentration time. As expected, the preconcentration time will also affect the exchange of Cu^{2+} and protonated arginine on the Nafion film. Figure 1 shows the effect of preconcentration time on the absorption signal. Fig. 1a shows the change in the absorption signal of 2.0×10^{-6} mol l^{-1} Cu^{2+} with preconcentration time, and

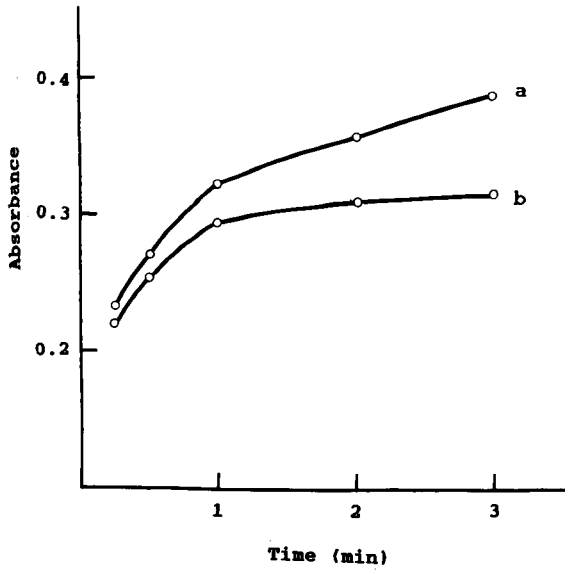

Fig. 1. Effects of preconcentration time on absorbance. HCl, pH 3.5; 0.05% Nafion solution, 10 μl. (a) 2.0×10^{-6} mol l^{-1} Cu^{2+}; (b) 2.0×10^{-6} mol l^{-1} $Cu^{2+}+1.3\times10^{-7}$ mol l^{-1} arginine.

Fig. 1b represents the effect of preconcentration time on the absorption signals of the same amount of Cu^{2+} but containing 1.3×10^{-7} mol l^{-1} arginine. Both curves tend to increase with increasing preconcentration time. The exchange equilibrium of Cu^{2+} and protonated arginine is reached after 3 min of preconcentration. In this work, a 3-min preconcentration time was adopted.

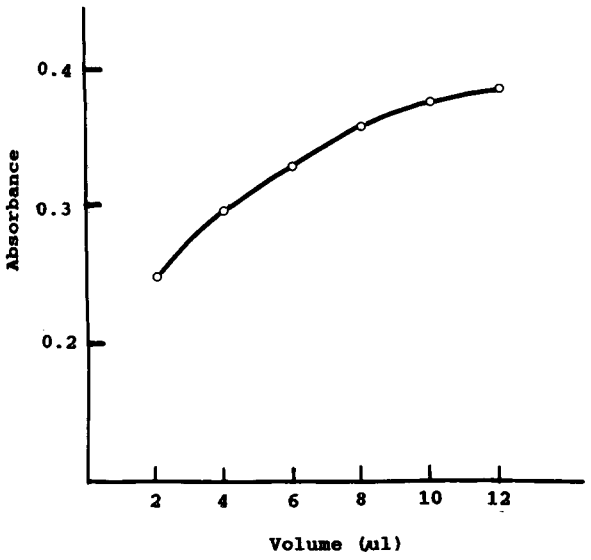

Fig. 2. Effect of the volume of 0.05% Nafion solution added on absorbance. HCl, pH 3.5; preconcentration time, 3 min.

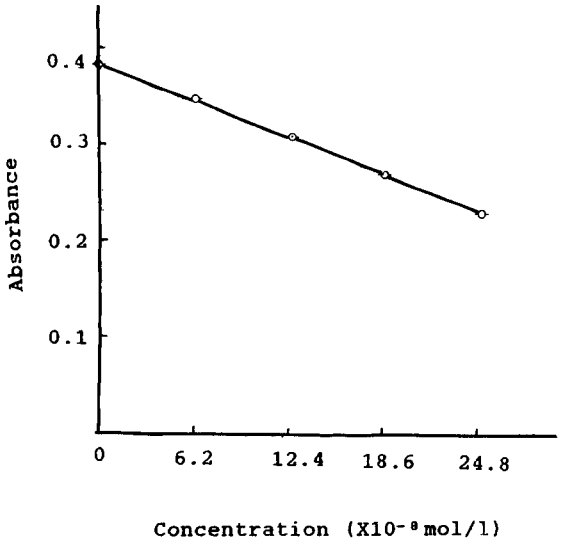

Fig. 3. Calibration graph. HCl, pH 3.5; preconcentration time, 3 min; volume of 0.05% Nafion solution, 10 μl.

Amount of Nafion. The amount of Cu^{2+} exchanged on the Nafion film can be affected by the amount of Nafion used to modified the tungsten coil. In pH 3.5 HCl containing 2.0×10^{-6} mol l^{-1} Cu^{2+}, the measured absorption signals increase with increasing volume of Nafion solution used to modify the tungsten coil and reaches a plateau above 10 μl of Nafion solution. Therefore, 10 μl of Nafion solution were used to modify the tungsten coil.

Calibration, precision and detection limit

Under the above recommended conditions, a linear relationship between the decrease in absorbance and the concentration of arginine was obtained in the range 3.1×10^{-8}–2.5×10^{-7} mol l^{-1}. The relative standard deviation for ten parallel determinations of 1.3×10^{-7} mol l^{-1} of arginine at 2.0×10^{-6} mol l^{-1} of Cu^{2+} was 2.3%. The detection limit was 1.3×10^{-8} mol l^{-1}.

TABLE 1

Results of analyses of pharmaceutical samples

Sample	Amount of arginine added (10^{-8} mol l^{-1})	Amount of arginine found (10^{-8} mol l^{-1})	Recovery (%)	Content of arginine in sample (%)
Cephradine injection 1	0	4.3	102.3	31.6
	4.4	8.8		
Cephradine injection 2	0	4.4	95.5	31.0
	4.4	8.6		
Arginine injection	0	5.2	97.7	102.0
	4.4	9.5		

Interferences

The determination of 1.3×10^{-7} mol l^{-1} of arginine at 2.0×10^{-6} mol l^{-1} of Cu^{2+}, was not affected by the presence of 3.1×10^{-5} mol l^{-1} of tartaric acid, 1.5×10^{-5} mol l^{-1} of ammonium oxalate, urea, glucose, salicylic acid, citric acid, D-tyrosine and thiourea or 2.0×10^{-6} mol l^{-1} of cephradine.

Sample analysis

Cephradine injection contains a certain amount of arginine. The contents of arginine in cephradine injection and arginine injection were measured according to the recommended procedure. The results are given in Table 1.

This work was supported by a grant from the Laboratory of Electroanalytical Chemistry, Changchun Institute of Applied Chemistry, Academia Sinica.

REFERENCES

1 T. Xu, B. Xu and Y. Fang, Huaxue Shijie, 6 (1985) 235.
2 G.G. Hughes, S. Frutiger and C. Fonck, J. Chromatogr., 389 (1987) 327.
3 M. Toshiki, K. Megumi and K. Michiya, Bunseki Kagaku, 30 (1981) 765.
4 H. Tadashi, T. Motohiro, E. Takashi and I. Masakatsu, Chem. Lett., 3 (1985) 341.
5 B. Xu, T. Xu, M. Shen and Y. Fang, Talanta, 32 (1985) 1016.

Analytica Chimica Acta, 268 (1992) 163–169
Elsevier Science Publishers B.V., Amsterdam

Comportement de mélanges d'acides aminés et de peptides vis-à-vis du cuivre(II)

Application à l'analyse d'hydrolysats de caséine

E. Lati, C. Dauphin et M. Hamon

Laboratoire de Chimie Analytique, Faculté des Sciences Pharmaceutiques et Biologiques de Paris Sud, F 92 290 Chatenay Malabry (France)

M. Silvestre

Faculdade de Farmacia da UFMG Departamento de Alimentos, Av. Oligario Maciel 2360 30 180 Belo Horizonte (Brésil)

(Received 18th April 1992)

Abstract

(*Behaviour of mixtures of amino acids and small peptides with copper(II). Application to the analysis of caseine proteolysates.*) The object of the present study was to specify the behaviour of some mixtures of amino acids and peptides during titration by a solution of copper sulphate in an alkaline solution (potentiometric indication with copper electrode) and the results obtained with caseine proteolysates. The precision and reproducibility of these assays are satisfactory. A negative influence of the degree of polymerization of the peptides on the ion metallic consumption permits an estimate of the polymerization degree of proteolysates.

Résumé

Le présent mémoire, après avoir précisé le comportement en mélange d'acides aminés et de peptides, lors du dosage par une solution titrée de sulfate de cuivre en solution aqueuse alcaline (indication potentiométrique à électrode de cuivre), expose les résultats obtenus, dans les mêmes conditions sur des hydrolysats de caséine. La précision et la reproductibilité de ces dosages sont satisfaisantes. Une influence négative du degré de polymérisation des peptides sur la consommation d'ion métallique permet une évaluation du degré d'hydrolyse de ces protéolysats.

Keywords: Titrimetry; Amino acids; Copper; Peptides

Dans de précédentes études [1,2] nous avons pu montrer que le potentiel pris par une électrode de cuivre, placée dans une solution d'acides aminés en milieu aqueux alcalin (pH voisin de 10), dans laquelle est introduite une solution de sulfate de cuivre titrée, présente une brusque variation, lorsque le volume ajouté correspond à un rapport de 2 ions cuivriques pour 3 acides aminés. Cette stoechiométrie est différente de celle observée pour certaines solutions pures d'acides aminés et nous a conduit à envisager la formation de complexes mixtes incluant différents acides aminés.

Nous avons pu conforter cette hypothèse depuis lors. En effet, il est possible d'observer

Correspondence to: M. Hamon, Laboratoire de Chimie Analytique, Faculté des Sciences Pharmaceutiques et Biologiques de Paris Sud, 5 rue Jean-Baptiste Clément, F 92 290 Chatenay Malabry (France).

une grande différence de solubilité des complexes cuivriques obtenus en partant d'acides aminés en mélange ou en solution pure. A titre d'exemple, dans les conditions expérimentales utilisées lors du dosage de la leucine ou de la tyrosine, il se produit une précipitation quasi totale du complexe, alors que pour des mélanges comportant la totalité des acides aminés physiologiques, le milieu reste limpide même en présence d'un excès de cuivre(II).

Nous avons montré dans un travail récent [3] qu'il était possible de réaliser d'une manière analogue le dosage de dipeptides, tripeptides et tétrapeptides. Les dérivés de la glycine réagissent selon un rapport de 4 ions cuivriques pour trois molécules. Cependant des influences opposées conduisent pour d'autres peptides à une consommation en cuivre(II) légèrement inférieure ou supérieure selon les cas, soit en fonction de l'existence d'un groupement fonctionnel supplémentaire, soit également en raison du caractère donneur ou accepteur d'électrons des substances [4–6].

Toutefois le point primordial de cette étude a été la constatation de l'existence d'un rapport molaire cuivre/peptide pratiquement constant, quelque soit le nombre d'acides aminés (deux, trois ou quatre) constituant le peptide.

Il résulte de ce fait que la même quantité d'ions cuivriques réagit avec des masses de plus en plus grandes de peptides et que, par conséquent, la consommation de cuivre(II), rapportée à un chainon acide aminé, décroît rapidement avec l'augmentation du degré de polymérisation.

Il peut donc être envisagé d'apprécier l'importance de la taille des peptides d'un mélange à l'aide d'un tel dosage cuprimétrique.

Ceci nous a conduit à étendre cette étude à l'évaluation du degré d'hydrolyse de protéolysats de caséine qui est le but du présent mémoire.

PARTIE EXPÉRIMENTALE

Appareillage

Il est constitué d'un Ensemble Titrimat Tacussel, comportant un tiroir de titrage, (type TAT_6), une électroburette, un enregistreur potentiométrique (type EPL_3) et une unité Derivol permettant le tracé des courbes différentielles $dE/dV = f(V)$. L'électrode de mesure est constituée par un fil de cuivre (diamètre 1 à 2 mm); l'électrode de référence est une électrode au calomel.

Réactifs

Solution titrée de sulfate de cuivre 0,1 mol l^{-1}: sulfate de cuivre anhydre 15,96 g ou sulfate de cuivre pentahydraté 24,96 g; eau distillée quantité suffisante pour (qsp), 1000 ml.

Étalonnage de la solution de sulfate de cuivre. Dans un erlenmeyer de 100 ml introduire: solution de sulfate de cuivre, 2 ml; tampon acéto-acétique pH 5, 10 ml; eau distillée environ, 50 ml.

Porter à l'ébullition, ajouter quelques milligrammes d'indicateur 2-pyridyl 1-azo 2-naphtol (PAN) et titrer par une solution d'EDTA 0,05 mol l^{-1} jusqu'au virage du violet au jaune.

Solution de borate de sodium à pH 10: acide borique, 6,2 g; chlorure de potassium, 4,46 g; eau distillée, 1000 ml.

Ajouter après dissolution: solution d'hydroxyde de sodium 0,1 mol l^{-1}, 880 ml; eau distillée qsp, 2000 ml.

Acides aminés et peptides: glycine; glycyl–glycine; glycyl–méthionine; glycyl–phénylalanine; glycyl–sérine; glycyl–thréonine; glycyl–glycyl–glycine; tétraglycine (produits standard, Sigma, Saint Louis MO, USA).

Caséine et hydrolysats de caséine. Mixture d'acides aminés (A): L-alanine 3,4 g (38,16 mmol), acide-L-aspartique 9,6 g (72,12 mmol), acide-L-glutamique 22,5 g (153 mmol), L-cystéine 7,7 g (32,0 mmol), L-histidine 4,3 g (27,7 mmol), L-proline 6,1 g (53,0 mmol), L-phénylalanine 3,8 g (23,0 mmol), L-tyrosine 9,3 g (50,8 mmol), L-sérine 9,2 g (87.5 mmol), L-thréonine 4,2 g (32,6 mmol), L-arginine 5,5 g (31,6 mmol), L-lysine (chlorhydrate) 3,6 g (19,7 mmol), L-tryptophane 1,5 g (7,3 mmol), L-méthionine 2,3 g (15,40 mmol), glycine 7,7 g (102,6 mmol) (concentration en mmol pour 100 g = 742; Teneur en azote α-aminé = 10,61 g.

Mode opératoire

Mélange de peptides. Introduire dans un bécher, une prise d'essai exactement pesée, correspondant à environ 0,5 mmol de peptide. Ajouter 50

ml d'eau, puis 40 ml de solution de borate de sodium à pH 10. Titrer par la solution de sulfate de cuivre en présence du système d'électrodes indiqué précédemment. Déterminer le point d'équivalence par l'enregistrement de la courbe dérivée.

Mélange d'acides aminés et de peptides. Introduire dans un bécher 0,4 g de mixture A d'acides aminés, en présence, soit de diglycine, de di et triglycine, ou de di et tétraglycine, soit enfin des trois peptides (la masse totale étant maintenue à 1 g). Ajouter 50 ml d'eau puis continuer comme pour le mélange de peptides.

Caséine, hydrolysats de caséine. Introduire dans un bécher 0,4 g (hydrolysat pur ou en mélange avec des acides aminés) ou 0,8 g (caséinate de potassium). Ajouter 50 ml d'eau pure.

ÉTUDE DES PARAMÈTRES ANALYTIQUES

Cas d'un mélange de peptides

Répétabilité. L'étude de la répétabilité a été menée sur un mélange équimolaire de di et triglycine. La moyenne obtenue sur dix dosages est de 98,0% avec un écart type de 0,60 et un coefficient de variation de 0,61.

Reproductibilité. La moyenne obtenue sur dix dosages est de 97,9% avec un écart type de 0,63 et un coefficient de variation de 0,64.

Cas d'un mélange à parties égales (m / m) de mixture (A) d'acides aminés et de diglycine

Répétabilité. Sur dix dosages correspondant chacun à une prise d'essai d'environ 1 g, la moyenne obtenue est de 7,07 mmol g^{-1} avec un écart type de 0,76% et un coefficient de variation de 0,77%.

Reproductibilité. Les dosages sont effectués sur dix prises d'essai voisines, de 1 g de mélange, la moyenne obtenue est de 7,03 mmol g^{-1} avec un écart type de 0,76% et un coefficient de variation de 0,77%.

Cas d'un hydrolysat de caséine

Répétabilité. Sur dix dosages correspondant chacun à une prise d'essai d'environ 0,4 g, la moyenne obtenue est de 1,73 mmol g^{-1} avec un écart type de 0,70% et un coefficient de variation de 0,40%.

Reproductibilité. La moyenne obtenue sur dix prises d'essai différentes voisines de 0,4 g est de

TABLEAU 1

Mélanges de dipeptides et de polymères de glycine

Mélange	Pourcentage		Consommation en Cu(II) (mol mol^{-1})		± Ecart type ($n = 10$)	%
	mmol	g	Théorique	Expérimentale		
Glycylthréonine,	50	57	1,395	1,385	±0,002	−0,71
glycylglycine	50	43				
Glycylglycine,	50	39	1,245	1,260	±0,006	+1,2
glycylméthionine	50	61				
Glycylméthionine,	50	54	1,330	1,335	±0,002	+0,38
glycylthréonine	50	46				
Glycylglycine,	35	26				
glycylsérine,	35	33	1,313	1,306	±0,020	−0,53
glycylphénylalanine	30	41				
Diglycine,	50	41	1,315	1,29	±0,010	−1,90
triglycine	50	59				
Diglycine,	75	68	1,315	1,31	±0,008	−0,38
triglycine	25	32				

1,72 mmol g^{-1} avec un écart type de 2,30% et un coefficient de variation de 1,4%.

RÉSULTATS ET DISCUSSION

Absence d'influence de la nature des peptides

Étude de mélanges de dipeptides. Compte tenu de l'observation précédemment citée, de la formation vraisemblable de complexes mixtes à partir de mélanges d'acides aminés, nous avons tout d'abord déterminé si un tel phénomène pouvait être observé avec les dipeptides.

Pour ce faire, 4 mélanges ont été étudiés pour lesquels la somme des consommations théoriques de cuivre(II), calculée à partir des résultats obtenus en solution pure, a été comparée à la consommation expérimentale.

Les peptides constituant ces mélanges ont été choisis de manière à contenir la glycine liée à d'autres acides aminés dont les consommations en cuivre sont différentes en solution pure. Ainsi, la glycyl–glycine étant considérée comme référence, la glycyl–méthionine donne un complexe plus pauvre en cuivre. Le comportement de la glycyl–sérine est très voisin de celui de la glycyl–glycine, alors que celui de la glycyl–phénylalanine et surtout de la glycyl–thréonine conduit à une consommation plus élevée en cuivre (II) [3].

Les proportions des 5 peptides ont été calculées en moles et sont indiquées ainsi que les résultats obtenus dans le Tableau 1.

Il est aisé de constater qu'il existe une bonne coïncidence entre les résultats théoriques et expérimentaux puisque leur variation est de l'ordre de 1%.

Nous pouvons donc en conclure que chaque peptide se comporte comme s'il était seul.

Étude de mélanges de diglycine et triglycine. Devant les résultats précédents l'étude concernant l'influence du degré de polymérisation a été réalisée sur deux mélanges de diglycine et de triglycine.

Un mélange à 50% (mole-à-mole) donne une consommation expérimentale de 98,1% de la théorie. Un mélange de 75% de diglycine et 25% de triglycine donne 99,6% (Tableau 1).

Ici encore, il est possible de considérer qu'il n'y a pas d'influence notable de comportement induite par le mélange.

TABLEAU 2

Comparaison des consommation théorique et expérimentale de mélanges de glycine et de ses polymères

Mélange	Pourcentage		Consommation		± Ecart type ($n = 10$)	%
	mmol	g	Théorique	Expérimentale		
Glycine,	50	36,3				
diglycine	50	63,7	0,96	0,93	0,012	−3
Glycine,	40	23,8				
diglycine,	30	31,3	1,03	0,94	0,013	−8,7
triglycine	30	44,9				
Glycine,	86,9	70				
triglycine	7,4	15	0,69	0,61	0,008	−11,5
tétraglycine	5,7	15				
Glycine,	73,9	50				
triglycine,	14,7	25	0,78	0,67	0,012	−14
tétraglycine	11,4	25				
Glycine,	65,6	40				
triglycine,	19,4	30	0,84	0,71	0,008	−15,5
tétraglycine	15	30				

Comportement de mélanges d'acides aminés et de peptides

Influence de la polymérisation: mélanges de glycine et de ses polymères. Nous avons effectué le dosage de mélanges de glycine et de 3 polymères (diglycine, triglycine et tétraglycine).

Ces polymères qui, à l'état isolé, consomment tous environ 1,30 mol mol^{-1} de cuivre, semblent donner des complexes d'autant moins stables que la polymérisation est plus grande. Cette hypothèse est confirmée par les résultats expérimentaux obtenus avec différents mélanges (Tableau 2).

En effet, si pour le mélange équimolaire de glycine et de son dipeptide la valeur mesurée ne présente qu'un léger déficit (3%) par rapport à la somme des consommations théoriques de chaque constituant, l'addition du tripeptide entraine un déficit plus important (8,7%) par rapport à la valeur théorique. Ce déficit est encore plus net dans le cas d'un mélange de glycine et de tétrapeptide.

Dans ce dernier cas, au fur et à mesure que la proportion de glycine diminue, le résultat expérimental s'éloigne de plus en plus de la théorie calculée.

Mélanges contenant l'ensemble des acides aminés et un ou plusieurs polymères de la glycine. L'addition à 0,4 g d'un mélange usuel (mixture A) d'acides aminés en poudre, soit de diglycine, soit de di et triglycine, soit de di et tétraglycine, soit enfin des trois peptides (la masse totale du mélange étant maintenue à 1 g) permet d'étudier l'influence éventuelle d'un mélange d'acides aminés sur le comportement de ces polymères vis à vis du cuivre (II). Les résultats sont donnés dans le Tableau 3.

Ici encore, la diminution de fixation des ions cuivriques en fonction du degré de polymérisation est nette. En effet, si la consommation de cuivre par mole du mélange contenant des quantités égales de dipeptide et de la mixture d'acides aminés, diminue d'environ 3,5%, on note une baisse supplémentaire de 5% lors de l'intervention du tripeptide. Le remplacement du tripeptide par le tétrapeptide entraine une diminution de consommation encore plus nette (18%) qui reste identique dans le cas de l'addition de masses égales des trois peptides.

Un calcul mathématique (à partir d'un système de quatre équations) a permis d'estimer la consommation de chacun des composants de ces mélanges.

Les résultats calculés à partir des différents mélanges précédents exprimés en mol mol^{-1} de Cu^{2+} ne peuvent être considérés que comme des valeurs approximatives.

Ils sont de l'ordre de $0,65 \pm 0,10$ mol mol^{-1} pour les acides aminés, de $1,26 \pm 0,05$ pour la

TABLEAU 3

Consommation de Cu(II) en mmol pour une masse égale à un gramme de mélange de peptides et d'acides aminés

Mélange	Pourcentage en masse	Quantité en mmol	Consommation de Cu(II) en mmol
Mixture A,	50	3,57	7,07
diglycine	50	3,79	
Mixture A,	40	2,86	
diglycine,	30	2,27	6,72
triglycine	30	1,58	
Mixture A,	40	2,86	
diglycine,	30	2,27	5,80
tétraglycine	30	1,22	
Mixture A,	40	2,86	
diglycine,	20	1,51	5,86
triglycine,	20	1,05	
tétraglycine	20	0,81	

diglycine, de 1,14 ± 0,05 pour la triglycine et de 0,97 ± 0,08 pour le tétrapeptide.

Il en résulte que les consommations correspondant aux acides aminés et au dipeptide sont voisines de celles observées dans le cas de solutions ne contenant qu'un seul type de molécules. En revanche la baisse est importante dans le cas de la triglycine et surtout de la tétraglycine.

Cette diminution de consommation de cuivre(II) par ces deux dernières molécules lorsqu'elles sont introduites dans des mélanges peut conduire à l'hypothèse que les complexes avec des tri et tétraglycine seraient moins stables que les autres. Ceci pourrait être relié à la compétition de plusieurs groupements amide pour former une liaison semipolaire dans le cas de ces polypeptides [7–10].

Cette diminution de consommation de cuivre(II), déjà nette lorsqu'elle est exprimée par rapport à une mole de peptide, l'est encore davantage si elle est envisagée par rapport à un chainon acide aminé.

Dans ces conditions, 3 moles d'acides aminés consomment 2 moles de cuivre(II), et 3 moles de diglycine en consomment deux fois plus. La consommation par molécule d'acide aminé, libre ou sous forme de dipeptide est donc sensiblement identique.

En revanche, celle du tripeptide n'est plus que 2 moles de cuivre pour 5 chainons (soit environ 60% des précédentes) et celle de la tétraglycine de 1 mole de cuivre pour 4 chainons soit environ 40% de la consommation déterminée pour un dipeptide.

Dosage du caséinate de potassium et d'hydrolysats de caséine purs ou en mélange avec des acides aminés

Ces études préliminaires nous ont incités à développer le dosage cuprimétrique d'hydrolysats de protéines. En effet, au vu des précédents résultats, il est possible d'espérer différencier ces préparations selon leur teneur, non seulement en acides aminés, mais surtout en peptides, et ce, en fonction de la taille de ceux ci.

Les résultats expérimentaux obtenus sont reportés dans le Tableau 4.

Comme cela était prévisible, la protéine native consomme déjà une certaine quantité d'ions cuivriques. Cette consommation croît avec l'hydrolyse parallèlement à l'évolution du rapport azote α-aminé/azote total.

Mais l'intérêt de la méthode cuprimétrique apparait surtout dans le cas d'addition d'acides aminés à un produit peu hydrolysé.

Un mélange de l'hydrolysat 1 et de la mixture A d'acides aminés réalisé de manière à obtenir une valeur de l'azote α-aminé (6,3%) relativement voisine de celle de l'hydrolysat 2 (5,8%) conduit à une consommation de cuivre(II) de 311 mmol pour 100 g au lieu de 213 mmol pour l'hydrolysat 2.

La simple comparaison de ces valeurs montre que le dosage cuprimétrique permet une diffé-

TABLEAU 4

Dosage cuprimétrique du caséinate de potassium et d'hydrolysats de caséine

Produit analysé	Azote α-aminé g/100 g (n = 10)	Rapport N aminé/ N total	Consommation de cuivre (mmol Cu(II)/ 100 g de produit) (n = 10)
Caséinate de potassium			52,7 ± 1,23
Hydrolysat 1	3,84 ± 0,23	0,27	160 ± 1,58
Hydrolysat 2	5,82 ± 0,19	0,42	213 ± 2,55
Mixture A	10,50 ± 0,41	0,82	480 ± 2,65
45% mixture A 55% hydrolysat 1	6,28 ± 0,32	0,47	311 ± 2,45

renciation plus précise de ces deux types de préparations que la classique détermination de l'azote α-aminé dont les résultats dépendent en outre des conditions opératoires utilisées.

Conclusion

L'étude que nous avons réalisée permet de constater tout d'abord l'absence d'interférence entre les différents peptides lors de leur dosage en mélange.

En revanche, le comportement de mélanges d'acides aminés d'une part et de di-, tri-, et tétrapeptides conduit à observer une diminution très nette de consommation de cuivre(II) pour une même masse d'échantillon en fonction du degré de polymérisation des peptides.

Ces observations préalables nous ont conduit à réaliser des dosages cuprimétriques de caséine et d'hydrolysats de cette protéine.

Les valeurs obtenues montrent une évolution parallèle à celle observée dans le cas précédent. En effet, la consommation de cuivre augmente avec l'importance de l'hydrolyse, de manière analogue à la classique détermination de l'azote α aminé.

Cependant les résultats obtenus avec la méthode cuprimétrique proposée sont plus précis et plus reproductibles que ceux issus du titrage acidimétrique en présence de formaldéhyde.

En outre, la méthode cuprimétrique présente une nette supériorité lorsqu'il s'agit de différencier un hydrolysat homogène, d'un mélange d'acides aminés libres et d'un produit moins hydrolysé.

BIBLIOGRAPHIE

1 E. Lati, C. Dauphin et M. Hamon, Ann. Pharm. Fr., 47 (1989) 344.
2 E. Lati, C. Dauphin et M. Hamon, Ann. Pharm. Fr., 49 (1991) 24.
3 E. Lati, C. Dauphin et M. Hamon, Anal. Chim. Acta, 254 (1991) 89.
4 R. Driver et W.R. Walber, Aust. J. Chem., 21 (1968) 671.
5 Y. Kimitto, S. Hideto, O. Yonejiro et O. Shuji, Tetrahedron Lett., 21 (1980) 2649.
6 I. Sovago, F. Etelba et A. Gergely, J. Chem. Soc., Dalton Trans., 11 (1982) 2159.
7 K. Nakamoto et P.Y. McCarthy, Spectroscopy and Structure of Metal Chelate Compounds, Wiley, New York, 1968.
8 H. Dobbie et W.O. Kermack, Biochem. J., 59 (1955) 546.
9 S.T. Glastone et E. Hammel, J. Am. Chem. Soc., 63 (1941) 243.
10 H.C. Freeman, J.C. Schoone et J.G. Sime, Acta Crystallogr., 18 (1965) 381.

Analytica Chimica Acta, 268 (1992) 171–176
Elsevier Science Publishers B.V., Amsterdam

Rapid enthalpimetric method for the determination of thiol compounds in petroleum oils

L.S. Bark and Sumardi

Department of Chemistry, University of Salford, Salford M5 4WT (UK)

(Received 18th March 1992)

Abstract

A rapid method is proposed for the determination of thiol sulphur in petroleum oil fractions. The thiol is reacted with phenylmercury(II) acetate in a kerosene medium. By adjusting the sensitivity of the system the heat changes are usable over a wide range of concentrations of the analyte (from 0–10 to 50–100 mM thiol) in the oil.

Keywords: Thermometric methods; Enthalpimetry; Petroleum, Sulphur compounds; Thiols

The sulphur present in crude oils occurs as numerous types of organic sulphur compounds in addition to hydrogen sulphide and elemental sulphur [1]. The concentration of the sulphur compounds usually varies with the molecular weight or boiling range of the fraction of petroleum being investigated. There are only a few low-molecular-weight sulphur compounds in petroleum spirit, but as the molecular weight of a given crude increases, the concentration of sulphur compounds increases. In many oils the heavier fractions contain sufficient sulphur to account for at least one atom per molecule. Although some molecular types containing two sulphur atoms have been identified, most sulphur compounds in petroleum contain only one atom of sulphur and therefore these heavier fractions actually contain elemental sulphur. There are reports of compounds containing both sulphur and nitrogen [2]. Alkanethiols with both normal and branched alkyl groups and with the thiol group in a primary, secondary or tertiary position have been isolated. Aromatic thiols have not been isolated from petroleum oils. Alkyl sulphides and some cyclic sulphides having four or five carbon atoms in the ring have been found, but no dialkyl sulphides have been found. Thiophenes and related compounds have also been found in oils. Approximately 50 thiols have been identified in crude oils [3,4].

Generally, thiols occur for the most part in light petroleum fractions and sulphides and thiophenes are confined to middle and higher petroleum fractions. The thiols, because of their volatility, along with hydrogen sulphide, accumulate mostly in the gasoline fractions of the petroleum and are of great concern to the refiner because of their undesirable odours, poor combustion characteristics and the corrosive nature of their combustion products. The most predominant are *n*-alkane-2-thiols such as butane-2-thiol. Alkane-1-thiols are relatively minor constituents of the entire thiol concentrate.

Although the methods used for analyses for thiols have been reviewed several times and an estimated 500 papers have been published in the last 25 years, apart from the report of a method in which alkanethiols were titrated in the pres-

Correspondence to: L.S. Bark, Department of Chemistry, University of Salford, Salford M5 4WT (UK).

ence of carboxylic acids and phenols by a two-titration procedure utilizing acrylonitrile polymerization and acetone dimerization as indicator reactions [5], there have been few reports of the use of thermometric and enthalpimetric methods used and none which utilize the advantages of these techniques for the assay of industrial samples containing thiols.

Thiols react with mercury(II) salts to form mercaptides which are more stable and less dissociated than the corresponding silver mercaptides [6], and for these reasons they have been widely used in the titrimetric determination of thiols. Several mercury compounds have been proposed for the precipitation and subsequent determination of thiols, but it was considered that doubts must be expressed about the uniform stoichiometry of the reactions of some inorganic mercury reagents in that one or two thiol groups could react with the mercury ligand. This ambiguity is removed by using organomercury compounds containing only one available mercury valency. A relatively large number (ca. 15) of reviews have been published concerned with the applications of organic mercury compounds in the determination of thiols in various materials.

Several organomercury compounds were investigated in preliminary studies. Several practical parameters had to be considered, including the cost of the reagents per determination and their solubility in organic solvents, and also potential health hazards for any industrial use. Consideration of the various characteristics (general availability, solubility in organic solvents, especially hydrocarbons) of mercury(II) compounds combined with considerations of the problems of miscibility of the solutions of the reagents with industrial samples, indicated that it would be best to have a potential reagent that dissolves in kerosene or some similar industrial material and that also has a good heat of reaction with a thiol group or a sulphide moiety. Of the various commercially available materials, although the sodium salt of *p*-chloromercury(II) benzoate is recommended for the determination of thiol groups [7], it is expensive, and of the other available reagents soluble in organic hydrocarbon solvents which are stable under the normal storage conditions envisaged for routine work, it was concluded that only phenylmercury(II) acetate was feasible.

Phenylmercury(II) acetate is readily obtainable in a state of high purity and has been recommended as a standard in the determination of mercury [8]. It has been used industrially as a fungicide and bactericide. It is more soluble in benzene, alcohols and acetic acid than in water and does not decompose until heated to about 150°C. It was therefore selected as the reagent for this investigation.

EXPERIMENTAL AND RESULTS

Apparatus

The electronic circuitry and the injection apparatus used for direct injection enthalpimetric (DIE) techniques has been described previously [9].

Reagents and solvents

Kerosene. Commercially available kerosene in the UK is coloured with an organic dyestuff for legislative reasons. In separate preliminary experiments to study the possible effects of the colour and any other impurities in commercial kerosene, experiments were done with (i) commercial kerosene, (ii) kerosene that had been shaken with an equal volume of silver nitrate solution (1% w/v), washed with water and dried by filtering through a cellulose plug (this treatment is to remove any thiols and hydrogen sulphide), and (iii) a "purified" kerosene.

To remove all types of sulphur compounds, and any oxygen and nitrogen compounds, a sample of kerosene was shaken with one tenth of its volume of concentrated sulphuric acid for ca. 10 min. The process was repeated 2–3 times. The remaining oil was washed with water. The separated oil was then stirred with activated charcoal to decolorize the kerosene. The kerosene was then dried by filtration through a cellulose plug.

Isopropanol. GPR-trade isopropanol was purified by shaking with silver nitrate crystals (5 g l^{-1}) and kept in direct sunlight for 2 h. The liquid was distilled twice and the second distillate was collected in an amber-coloured bottle and nitro-

gen was bubbled through the liquid at a brisk rate for 30 min before the bottle was sealed.

Various other solvents, such as chloroform, 1,4-dioxane, hexane and benzene were purified by distillation. The fractions boiling within 2–5°C of the literature values of the boiling points were collected. Light petroleum (b.p. 60–80°C) was used as received.

Ammonium dithizonate indicator. Dithizone (5 mg) was dissolved in ammonia solution (sp. gr. 0.880, 5 ml) and purified ethanol (50 ml) was added (the ethanol had been purified using the same procedure as for the purification of isopropanol).

Thiols. The following thiols were obtained from various commercial suppliers: *n*-butanethiol (not less than 97% purity), *sec*-butanethiol (not less than 97% purity), *tert*-butanethiol (not less than 98% purity), *n*-heptanethiol (not less than 95% purity) and *tert*-heptanethiol (isomeric mixture). Thiol solutions in purified kerosene were standardized by titration with silver nitrate solution using ammonium dithizonate indicator [10].

Sulphides and related substances. GPR-grade sodium sulphide, diethyl sulphide, diphenyl sulphide, thiophene and sulphur were used as received.

Preliminary studies

Preliminary studies to ascertain the best solvent for phenylmercury(II) acetate were made. Solutions of *n*-butanethiol dissolved in benzene and in "purified" kerosene were titrated with phenylmercury(II) acetate dissolved in various solvents: 1,4-dioxane, ethanol, butanol, isobutanol, some ketones, esters and pyridine, in which phenylmercury(II) acetate is readily soluble.

TABLE 1

Results for the titration of *n*-butanethiol

Amount of thiol (mmol)	0.0184	0.0368	0.0552	0.0736	0.0920
Heat pulse [a] (mm)	21	46	64	84	106

[a] Corrected for blank reading which was −6 mm. Each result is the mean of three measurements.

Using benzene as the solvent, in many instances the heat change during the titration was found to be small compared with the heat of mixing of the solvent and benzene. It was noted that 1,4-dioxane has a relatively small heat of mixing with benzene and it dissolves phenylmercury(II) acetate up to a concentration of about 0.5 M. The optimum system found by trial and error was 1,4-dioxane–hexane (1 + 1, v/v), which produced a zero heat change when mixed with either 1,4-dioxane–light petroleum (1 + 1, v/v) or 1,4-dixoane–kerosene (1 + 1, v/v).

Using kerosene as the solvent and mixing a kerosene sample containing the thiol with an equal volume of 1,4-dioxane, the thiol can be titrated with phenylmercury(II) acetate solution in 1,4-dioxane–hexane (1 + 1, v/v) with a small heat of mixing of the solvents. 1,4-Dioxane–hexane (1 + 1, v/v) readily dissolves phenylmercury(II) acetate up to a concentration of 0.13 M.

Construction of calibration graph using n-butanethiol as the analyte

Integral volumes of *n*-butanethiol solution in purified kerosene were diluted to a fixed volume with kerosene and an equal volume of 1,4-dioxane was added. Aliquots of each mixture were then used as the samples. After thermal equilibrium had been established, a fixed volume (nominally 2 ml) of phenylmercury(II) acetate solution [0.13 M in 1,4-dioxane–hexane (1 + 1, v/v] was injected into the analyte sample. The heat pulse was recorded. The results are given in Table 1.

The sensitivity of the bridge and recorder system could be increased by least tenfold before the noise level became unacceptable for routine work. It was found to be advisable to cover the vessel with an insulated cover to minimize evaporation of the solvent.

Effects of different kerosenes as the solvent

Known volumes (0.4–2 ml) of *n*-butanethiol solution (0.02 M) in purified kerosene were added to each of the three different kerosene samples. The volume was made up to 10 ml with the corresponding kerosene before being diluted with 1,4-dioxene (10 ml) and then "titrated" (using the

TABLE 2

Calibration results for *n*-butanethiol dissolved in various kerosene samples

Sample [a]	Heat pulse (mm) [b]					
	Amount of thiol (mmol)					Blank
	0.02	0.04	0.06	0.08	0.10	
1	30	58	86	117	144	−6
2	30	58	87	116	144	−12
3	30	59	87	118	146	−11

[a] Sample 1 = commercial (blue) kerosene; sample 2 = kerosene treated with silver nitrate; sample 3 = "purified" kerosene. [b] Heat pulses corrected for blank in appropriate solvent.

DIE technique) with phenylmercury(II) acetate solution. The results are given in Table 2.

Although the results show that commercial kerosene does not contain any impurities that react either with the mercury reagent or with any part of the reagent solution, to avoid any possible difficulties in interpretation of research results, only purified kerosene was used in the subsequent investigations to ascertain if a procedure for routine determinations was feasible.

Interferences

The possible interference effects of sulphur-containing substances which normally occur in petroleum were studied. The effect was estimated from the amount of *n*-butanethiol found (in kerosene) by titration before and after a potential interferent had been added. A calibration graph was used to determine the amount of "thiol" present in the sample. The results are given in Table 3. Hydrogen sulphide interfered at all concentrations tested (i.e., at least down to 0.001 mmol); The nitrogen compounds tested, i.e., pyridine (1.0 mmol), quinoline (0.5 mmol) and diphenylamine (0.5 mmol) and the oxygen compounds oleic acid (0.3 mmol), cyclohexanol (0.6 mmol) and acetophenone (0.5 mmol) gave no response. Phenols (phenol, individual cresols and xylenols and mixtures of phenol cresols and xylenols to a total of 2.0 mmol equivalent of phenol) gave a response $> 10\%$ of that for a blank determination.

Repeatibility of titrations

Twenty titrations were done with 0.07 mmol of *n*-butanethiol with the sensitivity of the recorder and the bridge at a median value. The recorder and bridge were adjusted to give a reading of 100 units for the initial amount. The average value recorded was 99.7 and the relative standard deviation was 1.10%.

Effects of different thiols

Butanethiols. The effects of different amounts (0–0.1 mmol) of the three butanethiols were investigated by dissolving each thiol in purified kerosene and titrating with phenylmercury(II) acetate. The slopes of all the calibration graphs relating the amount of thiol to the heat pulse obtained were within 2% of the mean.

TABLE 3

Effect of other compounds on the determination of *n*-butanethiol

Compound added	Amount (mmol)	Amount of thiol (mmol)	
		Actual	Found
Sulphur	2 mg(0.06)	0.0	0.0
Diethyl disulphide	0.20	0.0	0.0
	1.00	0.0	0.0
Diphenyl disulphide	1.00	0.0	0.0
	1.00	0.105	0.105
Ethyl sulphide	0.05	0.0	0.001
	0.05	0.105	0.15
	0.10	0.0	0.002
	2.0	0.0	0.002
	2.0	0.015	0.0156
	4.0	0.0	0.002
	4.0	0.015	0.0151
Mixture of:			
diphenyl disulphide	0.7		
diethyl disulphide	1.0	0.070	0.072
ethyl sulphide	1.0		
Thiophene	1.0	0.015	0.015

Heptanethiols. Different amounts of *n*- and *tert*-heptanethiol were investigated as above. The heat pulse obtained for *n*-heptanethiol was ca. 10% higher than that obtained from *tert*-heptanethiol over the range 0.01–1.0 mmol and ca. 5% higher than the pulses obtained with the butanethiols.

As weight concentration of thiols in crude oils has been reported [11] to be ca. 0.004% for the butanethiols and less than 0.00001% for heptanethiols, this means that in practice any variation in the type of thiol in the actual sample has no significant effect the value obtained, assuming that the thiol is regarded as being "butanethiols" and reported as "thiol sulphur".

Possible interferences in commercially available oils

The thiol sulphur content of a series of commercially available heavy lubricating oils was determined by using 10-ml aliquots of the oil diluted with an equal volume of commercial kerosene. To a second series of aliquots were added known amounts of *n*-butanethiol in kerosene and the amounts of thiol sulphur in these spiked samples were determined using the procedure outlined for the preparation of the calibration graph. In no instance did the amount of thiol found vary by more than 3% from that added. It is concluded that any additives in the commercial samples have no effect on the method.

Proposed method

The sample for titration must be sufficiently mobile to allow easy stirring and a ready transfer of any heat change to the temperature probe. The procedure used before the titrant is injected depends on the viscosity of the original sample, as follows.

For viscous samples, transfer an amount of the sample into a tared beaker. Weigh the beaker and contents. Add known amounts of kerosene and stir until the mixture is mobile.

For samples which are mobile, dilute an aliquot of the sample with an equal volume of kerosene and stir well to achieve homogeneity.

For all mobile titration samples, transfer an aliquot (20 ml) of the mixture into the thermostated reaction vessel. Insert the temperature sensor and switch on the electronic bridge and recording system. When temperature equilibrium has been established (the thermal trace is parallel to the time axis), inject a fixed volume (nominally 2 ml) of phenylmercury(II) acetate solution (nominally 0.15 M in 1,4-dioxane–hexane (1 + 1, v/v)). Record the heat pulse.

Using a previously prepared calibration graph, calculate the amount of thiol sulphur present in the titration sample and thence in the original sample.

Range of the proposed method

By a suitable choice of recorder and operational amplifiers in the bridge system, and using a reaction vessel which is thermostated to within 1°C of the established temperature (i.e., the temperature at which calibration was carried out), it is possible to adjust the overall sensitivity of the apparatus in decadic intervals to give linear calibration graphs for ranges of concentration of 0–10 to 50–100 mmol of thiol sulphur per litre of oil.

Routine operations

For routine work it has been found that disposable polyethylene beakers and stirring with a vertical paddle stirrer enables a rapid and inexpensive analysis to be made. The stirrer and thermometric probe are easily cleaned by dipping them in clean kerosene and stirring for ca. 30 s. For quality control purposes, it is possible to replace the recorder with a suitable digital voltmeter and shunt adjusted to give a reading of, say, 100 units for the standard sample. Thus any value obtained using a routine sample can be directly compared with the standard.

DISCUSSION

The use of phenyl mercury(II) acetate to react with the sulphydryl groups of thiols and hydrogen sulphide gives sufficient heat of reaction for this to be used in the enthalpimetric determination of the sulphur compounds. The use of a low thermal capacity organic solvent system enhances the

temperature changes and with suitable precautions it is possible to determine the thiol sulphur in oils over an industrially acceptable range of concentrations.

Although the system is calibrated using *n*-butanethiol, the different effects of other thiols present in the system may be ignored and all the thiol reported as "thiol sulphur". Whilst compounds such as ethyl sulphide have an effect, as 0.1 mmol of ethyl sulphide gives no more effect than 0.002 mmol of *n*-butanethiol, and the relative amounts of the sulphides in oil fractions investigated are reported to be much lower than the amounts of thiols encountered, any interference is virtually zero.

Many industrial samples are highly coloured and the higher molecular weight fraction oils may contain large amounts of materials that are infrared absorbing over a very wide range of wavelengths. Some of the lighter fractions used as lubricants may contain additives and also very highly dispersed graphite. Such samples cannot readily be assayed by infrared methods. The fact that the samples are non-conductors of electricity requires procedures that involve electrometric methods of any kind to have conducting electrolytes added to the non-polar sample in sufficient amounts to cause relatively large dilution factors. Chromatographic methods often require preseparation of the thiols before injection on to the chromatographic column and, because of the easily oxidizable nature of the analytes, this may lead to errors.

Virtually the only restriction on the method is that of viscosity, because it is essential to have a titration sample that can be stirred thoroughly and rapidly with a simple laboratory stirrer, so the use of kerosene as the solvent is very advantageous when the original sample is highly viscous. As indicated in the proposed method, viscous samples are readily assayed by simply weighing an amount of the sample in the beaker, adding a known volume of kerosene and stirring until a homogeneous and mobile mixture is obtained. Using an aliquot of this as the titration sample in the usual way allows the concentration of the thiol in the original viscous sample to be calculated. The advantage of the enthalpimetric technique with regard to the range of concentrations that can be determined simply by adjusting the sensitivity of the electronic and recording systems is also an advantage in smaller laboratories, where the number of routine sample of one particular concentration range is not large enough to warrant dedicating an instrument to that range.

The ease and speed of operation and the low cost of enthalpimetric methods have been discussed previously [12] and there is no doubt that these, combined with the range and scope of the proposed method, make it of potential value to the industrial oil analyst.

REFERENCES

1 Kirk-Othmer Encyclopedia of Chemical Technology, Vol. 14, Interscience, New York, 2nd edn., 1967, p. 850.
2 J.S. Ball, Proc. Am. Pet. Inst., 42, Sect. VIII (1962) 27.
3 G.D. Galpern, Int. J. Sulfur Chem. (B) 6 (1971) 117.
4 R.C. Arnold, P.J. Launer and A.P. Lien, Anal. Chem., 24 (1952) 1741.
5 E.J. Greenhow and L.H. Loo, Analyst, 99 (1974) 360.
6 W. Stricks and I.M. Kolthoff, J. Am. Chem. Soc., 75 (1953) 5673.
7 P.D. Boyer, J. Am. Chem. Soc., 76 (1954) 4332.
8 Reference Substances for Use in Organic Microanalysis, Analytical Methods Committee, Analyst, 87 (1962) 304.
9 L.S. Bark and L. Kershaw, J. Thermal Anal., 18 (1980) 371.
10 R.K. Kunkel, J.E. Buckley and G. Gorin, Anal. Chem., 31 (1959) 1098.
11 C.J. Thompson, H.J. Coleman, H.T. Rall and H.M. Smith, Anal. Chem., 27 (1955) 175.
12 L.S. Bark and N. Hadipranoto, J. Thermal Anal., 37 (1991) 183.

Analytica Chimica Acta, 268 (1992) 177–183
Elsevier Science Publishers B.V., Amsterdam

Coprecipitation with aluminium hydroxide and x-ray fluorescence determination of trace metals in water

Mohamed A.H. Eltayeb [1] and René E. Van Grieken

Department of Chemistry, University of Antwerp (UIA), Universiteitsplein 1, B-2610 Antwerp-Wilrijk (Belgium)

(Received 12th March 1992; revised manuscript received 1st May 1992)

Abstract

Coprecipitation of trace elements on aluminium hydroxide was combined with energy-dispersive x-ray fluorescence for the analysis of environmental water. The parameters for the preconcentration method were studied. The optimum procedure involves addition of 1 mg of the carrier, at pH 7.3, to a 200-ml water sample. The pH was adjusted by addition of ammonia solution. Quantitative recoveries were obtained for Ti(IV), Cr(III), As(V), Pb(II) and Th(IV). The precision was 4–6% and the detection limits were in the range 0.2–0.8 $\mu g\ l^{-1}$.

Keywords: Sample preparation; X-ray fluorescence spectrometry; Coprecipitation; Preconcentration; Trace metals; Waters

Coprecipitation offers a simple and highly efficient method for the preconcentration of trace elements in solution. It is used extensively for the enrichment of trace elements from fresh, sea and waste waters. Widely used collector precipitates include $Fe(OH)_3$ [1,2] and $Al(OH)_3$ [3].

Coprecipitation with $Al(OH)_3$ as a collector followed by filtration of the precipitate on a Nuclepore membrane filter and direct multi-element analysis of the loaded membrane seems particularly attractive in x-ray fluorescence (XRF), as the high adsorption efficiency of $Al(OH)_3$ allows the use of small amounts of Al carrier, resulting in a thin-film specimen producing a relatively low x-ray scattering background. As $Al(OH)_3$ is a light element matrix, the characteristic x-rays from the elements to be determined will not suffer from significant matrix absorption. Except at higher pH levels, the usually abundant alkali and alkaline earth metal ions are not expected to coprecipitate significantly as their hydroxides are fairly soluble. All these conditions favour a straightforward thin target preparation.

However, coprecipitation with $Al(OH)_3$ has not been used in combination with multi-element XRF. Only Stewart and Brooksbank [3] used a carrier of $Fe(OH)_3$ and $Al(OH)_3$ and Y as an internal standard for the XRF determination of uranium in water.

In this work, studies were made of the preconcentration from waters of traces of Ti(IV), Cr(III), Mn(II), Co(II), Ni(II), Cu(II), Zn(II), As(V), Se(IV), Pb(II), Th(IV) and U(VI) with $Al(OH)_3$ followed by filtration of the precipitate on a Nuclepore membrane filter and subsequent analysis of the loaded membrane by energy-dispersive x-ray fluorescence (EDXRF). Lake water was used as a matrix throughout the study.

Correspondence to: R.E. Van Grieken, Department of Chemistry, University of Antwerp (UIA), Universiteitsplein 1, B-2610 Antwerp-Wilrijk (Belgium).

[1] On leave from Sudan Atomic Energy Commission, National Council for Research, Khartoum, Sudan.

EXPERIMENTAL

Equipment and x-ray fluorescence measurements

The EDXRF instrument was a Tracor X-ray (Mountain View, CA) TX 5000 unit, which is a micro-computer-based EDXRF spectrometer with a rhodium target tube operated at 15, 25 and 40 kV for the determination of elements with low, medium and high atomic number, respectively. A 0.127-mm aluminium filter and 0.05- and 0.127-mm rhodium filters were used to remove the Rh-L lines and to reduce the background spectra for 15-, 25- and 40-kV excitation, respectively. The unit included a ten-position automatic sample changer and a 30 mm^2 Si(Li) detector with a resolution of 155 eV at 5.9 keV. The unit is interfaced to and controlled by an IBM PC/AT

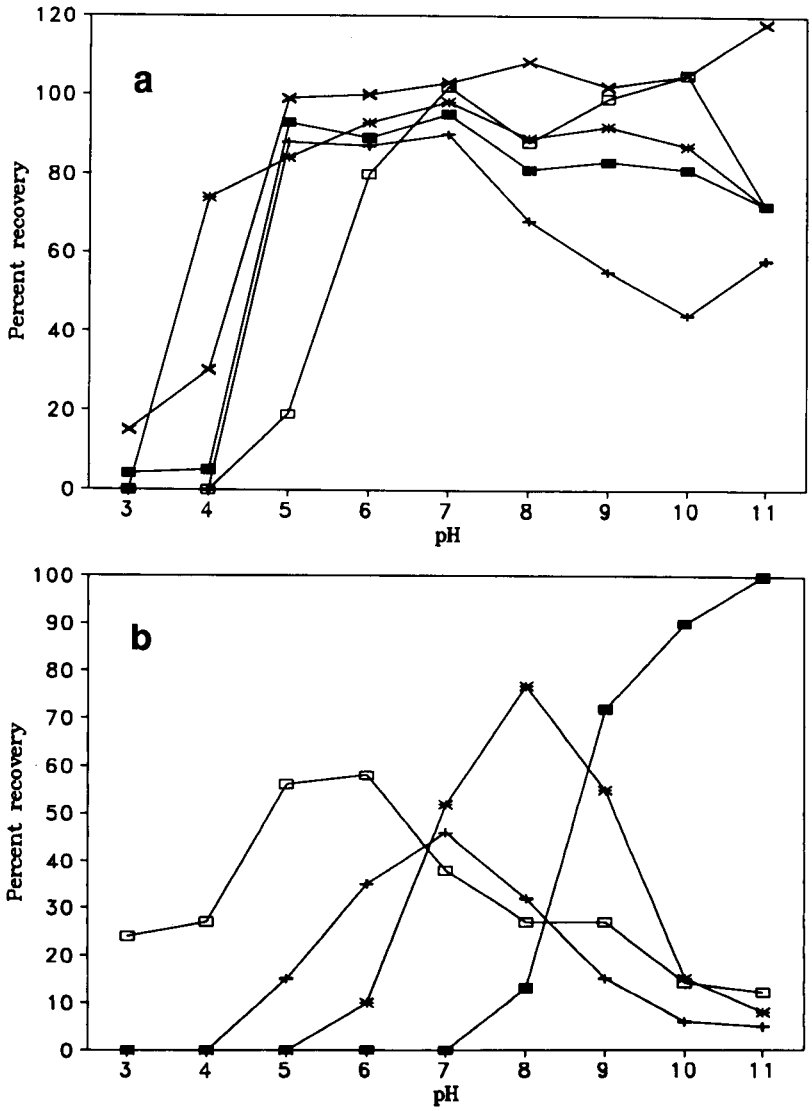

Fig. 1. Influence of pH on the recovery (5-μg trace element spikes; 200-ml sample volume; 1 mg Al carrier). (a) ■ = Ti; + = As; * = Cr; □ = Pb; × = Th. (b) ■ = Mn; + = Cu; * = Zn; □ = U.

computer. For the purpose of calibration of the spectrometer, a series of single-element thin-film standards, obtained from Micromatter (Seattle, WA) was used. The net intensities of the characteristic peaks in the spectrum were evaluated by means of a non-linear least-squares fitting program [4].

Reagents

All the reagents were of analytical-reagent grade and doubly distilled water was used throughout. Working solutions of the elements studied were prepared by appropriate dilutions of stock solutions of 1000 mg l^{-1} of each element. The carrier solution was prepared by dissolving the appropriate weight of $Al(NO_3)_3 \cdot 9H_2O$ (UCB) in water to give a concentration of 10 mg Al ml^{-1}. This solution was acidified and stored until it was needed. A 25% ammonia stock solution (Merck) stored in a polythene container was used.

Water collection

Water for the optimization and evaluation experiments was collected from a lake near the University of Antwerp (UIA). The water was then immediately filtered through a Whatman type 541 filter-paper, acidified to pH 2 and stored in a precleaned polythene jar until it was used.

Procedure

For optimizing the parameters of the preconcentration procedure, 200 ml of the acidified water were spiked with the desired concentration of each of the studied trace elements. The carrier solution was added, then the solution was stirred for about 10 min to ensure equilibration between the various ions. During stirring, the pH of the solution was raised by the addition of concentrated ammonia solution and finally adjusted to the required value with dilute ammonia solution. The final volume was about 205 ml. This solution was allowed to stand for about 1 h and then filtered through a Nuclepore membrane filter of 0.4 μm pore-size and 47 mm diameter, retained in a Gelman filtration apparatus. The precipitate was washed with methanol and the precipitate-loaded membrane, containing the precipitate over 11.0 cm^2 surface area, was stretched on a Teflon ring and weighed with another Teflon ring so as to prevent curling of the membrane on drying on 70°C for about 1 h. Thin-film samples were thus obtained, which were present directly to the EDXRF unit.

RESULTS AND DISCUSSION

pH dependence

Samples of 200 ml were spiked with 1 mg of aluminium carrier and 5-μg amounts of the elements under study and the pH was adjusted from 3 to 11 by the addition of aqueous ammonia solution [NaOH was not used because soluble sodium aluminate ($NaAlO_2$) would be formed]. The results are shown in Fig. 1. The recoveries of Co(II) and Ni(II) appeared to be below 1% in all instances and that of Se(IV) below 22%.

For all the elements included in Fig. 1, the recovery increases with increasing pH to reach a maximum at ca. pH 7, where $Al(OH)_3$ has its isoelectric point (lowest solubility). An exception is Mn, with a maximum recovery at pH 11. Further, Fig. 1 shows a slight decrease in recovery at higher pH. The ions studied show different degrees of recovery. Co(II), Ni(II), Cu(II) and Zn(II) are not quantitatively recovered because they form soluble complexes with ammonia. As a general rule, adsorbability increases with decreasing solubility of the adsorbed compound. The elemental recoveries on $Al(OH)_3$ are in the corresponding order: $< 1\%$ for Co(II) and Ni(II) and 46 and 52% for Cu(II) and Zn(II), respectively. Hence, the amine complexes formed by these ions in the water matrix might have solubilities in the order Co(II) > Ni(II) > Cu(II) > Zn(II).

Ti(IV), Cr(III), Pb(II) and Th(IV) ions show quantitative recoveries at pH 7. These ions can be precipitated with ammonia as their hydroxides. The collection starts at pH 3–4. Th(IV) is collected quantitatively at pH 5. The recovery decreases for Ti(IV) and Cr(III) at pH > 7, possibly because the carrier is more soluble at high pH values and, also, excess of ammonia is known to dissolve $Cr(OH)_3$ [5]. For Pb(II) and Th(IV), no such decrease is observed, hence it seems that

hydroxide precipitation alone is sufficient to bring about quantitative recoveries of these elements. Traces of Cr(III), Pb(II) and Th(IV) had been reported to be collected quantitatively as their hydroxides with ammonia precipitation and $La(OH)_3$, $Al(OH)_3$ and $Fe(OH)_3$ as collector [6–9]. As $Al(OH)_3$ starts to precipitate at pH 4.1, Ti(IV) at pH 2 and Th(IV) at pH 3.5 [10], the precipitation observed for these ions at pH 3–4 can be explained by pure hydroxide precipitation. However, the hydroxides of Cr(III) and Pb(II) start to precipitate at pH 5.3 and 5.6, respectively [10], but still in this experiment these metal ions formed precipitates at pH 3–4. This can be explained by local precipitation by the concentrated ammonia solution and the formation of kinetically stabilized materials, although ammonia was added while the solution was being stirred. As(V) is collected up to ca. 90% at pH 5 where the precipitation of $Al(OH)_3$ is almost completed [5]; up to pH 7 the recovery of this element remains constant and thereafter it decreases sharply. It is clear that coprecipitation is the sole process by which this element is collected, i.e., no precipitation is involved. Traces of As were reported to be quantitatively coprecipitated on $Fe(OH)_3$ [11] as iron(III) arsenate. It is also possible that the As here is present as aluminium arsenate.

The precipitation of Mn(II) as MnO_2 starts at pH 8 and is complete at pH 11. The oxidation to MnO_2 is affected by dissolved oxygen [12].

Although U(VI) has been precipitated by ammonia as the sparingly soluble diuranate, $(NH_4)_2U_2O_7$, and $Al(OH)_3$ has been used as a collector [8], in the present study U(VI) showed a maximum recovery of 58% at pH 6. U(VI) forms a soluble carbonate complex when sodium carbonate is present in the solution [5]. The formation of this soluble complex prevents the complete precipitation of ammonium diuranate salt. This is probably the reason for the poor recovery of U(VI) in this study.

At pH > 10.5, $Al(OH)_3$ will dissolve, hence precipitates present above this pH must be due to precipitates formed at lower pH values, that is, in a process of slow dissolution.

At pH > 11 the precipitate peels off, possibly because at such high pH the alkaline earth metal also coprecipitated owing to the presence of hydrogen-carbonate formed by CO_2 dissolved in the water. Hence it was impossible to perform further experiments.

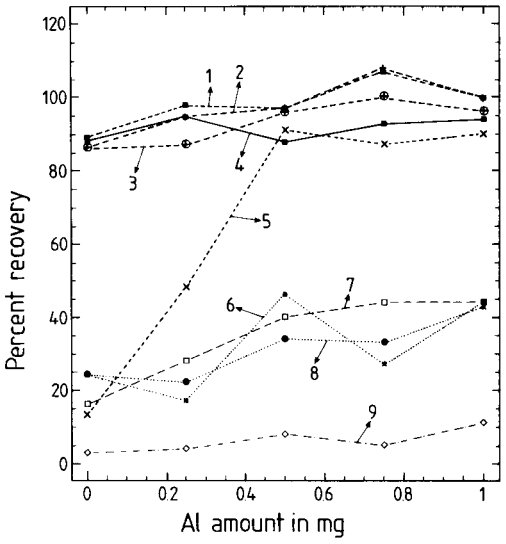

Fig. 2. Influence of the amount of Al carrier on the recovery (5-μg trace element spikes; 200-ml sample volume; pH 7.3). 1 = Pb; 2 = Th; 3 = Cr; 4 = Ti; 5 = As; 6 = U; 7 = Zn; 8 = Cu; 9 = Se.

A pH of 7.3 was chosen as the optimum pH and all further experiments were carried out accordingly.

Dependence on initial aluminium concentration

The experiments were performed with 200-ml samples spiked with 5 μg of the elements under study and with Al carrier amounts of 0, 250, 500, 750 and 1000 μg. The results are shown in Fig. 2.

As can be seen, even without the addition of the carrier, only by adjusting the pH to 7.3 with ammonia are more than 85% of Ti(IV), Cr(III), Pb(II) and Th(IV) precipitated as their hydroxides. Luke [13] established the conditions for the determination of many trace elements by hydroxide precipitation. However, in the absence of the carrier, the filtration process is extremely time consuming and it takes 3 h to filter off a volume of 200 ml, whereas after addition of the carrier the filtration process requires about 15 min. The recoveries increase with increasing amount of the

carrier added, reaching 100% for Ti(IV), Cr(III), Pb(II) and Th(IV) with 250 μg of Al. The effect of the added carrier on the recovery of As(V) is very clear: without carrier, only 13% is recovered and a maximum recovery of 87% is reached with 1 mg of Al.

The recoveries of Cu(II), Zn(II), Se(IV) and U(VI) increase to some extent with increasing amount of carrier, but it was not possible to use larger amounts of Al because then the precipitate tends to flake on drying. This increase in the recoveries of the elements studied is expected as the three processes of carrier precipitation, namely surface adsorption, ion-exchange and occlusion, are expected to increase with increase in the amount of Al added. An amount of 1 mg of Al was adopted in subsequent work.

Effect of the concentration of the trace elements studied

Samples spiked with the elements under study in the concentration range 0.5–1400 μg^{-1} l were treated as described under Experimental. The recoveries of Co(II) and Ni(II) were $< 1\%$ and for Se(IV) $< 15\%$ in all experiments. All other results are shown in Table 1.

As can be seen, the apparent recoveries are slightly affected, at both the low and high concentration ends, by the concentration of the specific element. The deviations in the lower concentration range are probably due to poor statistics and inaccurate correction for the concentrations of these elements in the lake water sample (blank) to which no addition was made, i.e., experimental error. It is also possible that the organic constituents in the lake water matrix can affect the results at such low concentration levels. The deviation at the high end can be explained by the coprecipitation capacity of the carrier surface being exceeded and by x-ray absorption effects.

These recovery data indicate that the method can conveniently be used for the determination of Ti(IV), Cr(III), Pb(II) and Th(IV) in the range 10–800 $\mu g\ l^{-1}$. The linear range for As is from 10 to 200 $\mu g\ l^{-1}$. For environmental water with lower concentrations, the elimination of organic constituents (such as by wet digestion with acids) prior to the preconcentration step seems to be necessary. The average recovery together with the standard deviation is indicated for each element for the concentration range 10–800 $\mu g\ l^{-1}$ in the bottom row of Table 1. Ti(IV), Cr(III), As(V),

TABLE 1

Influence of trace element concentration on the recovery (200-ml sample volume; 1 mg Al carrier; pH 7.3)

Trace element concentration ($\mu g\ l^{-1}$)	Recovery (%) [a]							
	Ti	Cr	Cu	Zn	As	Pb	Th	U
0.5	55	56	–	–	–	–	–	–
5.0	63	96	45	38	70	115	93	89
10	95	93	43	43	80	114	102	37
25 [a]	96	99	39	50	83	99	96	47
50	98	96	46	46	84	104	98	44
100	95	98	50	54	98	102	109	44
200	91	96	46	43	84	91	99	44
400	93	92	43	29	77	90	99	53
600	87	87	41	12	65	90	91	60
800	85	87	50	20	66	93	94	70
1000	75	77	46	17	53	84	82	55
1400	78	79	57	20	59	87	92	55
Average [b] ± S.D.	93 ± 5	94 ± 5	45 ± 4	38 ± 16	86 ± 7	98 ± 9	99 ± 5	50 ± 11

[a] Data are averages of nine measurements for the 25 $\mu g\ l^{-1}$ concentration and single measurement results for other concentrations. [b] The average is calculated for the concentration range 10–800 $\mu g\ l^{-1}$ except for As(V), where the range 10–200 $\mu g\ l^{-1}$ was used.

TABLE 2

Influence of sample matrix on the recovery (5-μg trace element spikes; 200-ml sample volume; 1 mg carrier; pH 7.3)

Element	Recovery ± standard deviation per measurement (%)		
	Doubly distilled water [a]	Tap water [a]	Lake water [b]
Ti	94 ± 5	96 ± 4	96 ± 4
Cr	95 ± 4	95 ± 3	99 ± 6
Cu	84 ± 32	95 ± 8	39 ± 7
Zn	90 ± 6	103 ± 5	50 ± 6
As	84 ± 8	72 ± 4	83 ± 5
Pb	103 ± 1	100 ± 2	99 ± 5
Th	80 ± 16	98 ± 1	96 ± 5
U	85 ± 11	40 ± 2	47 ± 17

[a] Average from three measurements. [b] Average from nine measurements.

Pb(II) and Th(IV) show acceptable recoveries and standard deviations.

Dependence on matrix composition

In order to evaluate the effect of the matrix composition, experiments were done on 200-ml samples of doubly distilled water, tap water, sea water and lake water, which were spiked with 5 μg of each of the metals studied. The recoveries of Co(II) and Ni(II) were below 25% and those of Se(IV) were below 15%. The other results are shown in Table 2.

All the ions listed show a recovery above 80% in doubly distilled water. In the tap water low recoveries are seen for As(V) and U(VI), whereas in the lake water Cu(II), Zn(II) and U(VI) are poorly recovered. These poor recoveries are possibly due to the presence of organic molecules in the environmental waters. Results for sea water are not shown because, owing to the high abundance of alkaline earth metals, the precipitate flaked on drying and no measurements were possible. These experiments show the need for careful study of the recovery of the preconcentration method in the actual matrix to which it will be applied rather than, as often happens, testing the method in a doubly distilled water matrix and assuming that the same recoveries will be obtained in other matrices.

Precision

The overall precision of the method was evaluated by analysing five samples of 200 ml each of lake water spiked with 5 μg of each of the metal ions studied. The results are given in the last column of Table 2.

For Ti(IV), Cr(III), As(V), Pb(II) and Th(IV) ions, the relative standard deviations are 4, 6, 5, 5 and 5%, respectively. The precision of the method for these ions can also be estimated from the standard deviations in Table 1. From these data, it can be concluded that the method is adequate for the determination of Ti(IV), Cr(III), As(V), Pb(II) and Th(IV), but for low concentrations the organic constituents should be removed before the preconcentration step can be applied. However, care should be taken to optimize the parameters of the preconcentration step for each matrix to be studied. Also, for the ions with low recoveries, the precision of the method is good for specific conditions; with the exception of U(VI), they all show a relative standard deviation below 7%.

Enrichment factor and detection limit

For the optimized conditions, the enrichment factor, F, was calculated from the equation

$$F = (Q_T/Q_M)(Q_{0M}/Q_{0T})$$

where Q_{0T}, Q_T and Q_{0M}, Q_M are the amounts of the trace element and the matrix before and after the preconcentration step, respectively [14]. An enrichment factor of 15000 was obtained for Ti(IV), Cr(III), As(V), Pb(II) and Th(VI). This is comparable to most other preconcentration techniques. The detection limits of the method under optimized conditions were calculated using the 3σ criterion for a 1000-s live measuring time. In the absence of contamination, the method has a detection limit between 0.2 and 0.8 $\mu g\, l^{-1}$ for Ti, Cr, As, Pb and Th.

M.A.H.E. acknowledges a research fellowship from the International Atomic Energy Agency. Part of this work was supported by the Belgian Ministry of Science Policy under grant 84-89/69.

REFERENCES

1 R. Chakravorty and R. Van Grieken, Int. J. Environ. Anal. Chem., 11 (1982) 67.
2 V. Hudnik, S. Gomiscek and B. Gorenc, Anal. Chim. Acta, 98 (1978) 39.
3 J.H. Stewart, Jr., and R.D. Brooksbank, Nucl. Instrum. Methods, 193 (1982) 315.
4 P. Van Espen, H. Nullens and F. Adams, Nucl. Instrum. Methods, 142 (1977) 243.
5 L. Erdey, Gravimetric Analysis, Pergamon, Oxford, 1st English edn., 1965.
6 L. Chuecas and J.P. Riley, Anal. Chim. Acta, 35 (1966) 240.
7 D.L. Fuhrman and G.W. Latimer, Talanta, 14 (1967) 1199.
8 T. Kiriyama and R. Kuroda, Anal. Chim. Acta, 71 (1974) 375.
9 Z. Marczenko and K. Kasiura, Chem. Anal. (Warsaw), 9 (1964) 87.
10 E.S. Amis, J.F. Coetzee, P.J. Elving, H. Freiser, J.A. Goldman, J.G. Hanna, A.E. Nielsen and A.M. Schwartz, Treatise on Analytical Chemistry, Part 1, Theory and Practice, Wiley, New York, 1978.
11 Z. Marczenko and M. Mosjki, Chem. Anal. (Warsaw), 14 (1969) 495.
12 Z. Marczenko, Separation and Spectrophotometric Determination of Elements, Horwood, Chichester, 1986.
13 C.L. Luke, Anal. Chim. Acta, 41 (1968) 237.
14 A. Mizuike, Enrichment Techniques for Inorganic Trace Analysis, Springer, Berlin, Heidelberg, New York, 1983.

Analytica Chimica Acta, 268 (1992) 185–188
Elsevier Science Publishers B.V., Amsterdam

Investigations in bioanalytical chemistry

Part II. Differential-pulse adsorption voltammetry of bilirubin

Wenrui Jin and Xin Zhao

Department of Chemistry, Shandong University, Jinan 250100, Shandong (China)

Chen Ding, Funing Wang and Zuquan Gao

Department of Biology, Shandong University, Jinan 250100, Shandong (China)

(Received 8th October 1991; revised manuscript received 21st April 1992)

Abstract

The electrochemical behaviour of bilirubin in Tris–HCl buffer solution at a hanging mercury drop electrode was investigated. The adsorption phenomena were observed by differential-pulse adsorption voltammetry (DPAV). In 0.01 mol l^{-1} Tris–1.2×10^{-3} mol l^{-1} HCl buffer, the detection limit and the linear range of bilirubin were 2×10^{-10} and 1×10^{-9}–4×10^{-7} mol l^{-1} by DPAV, respectively. The influences of light and oxygen on bilirubin were also studied. The method was applied to samples of refined bilirubin.

Keywords: Polarography; Voltammetry; Bilirubin

The determination of bilirubin in human serum is of great importance in the diagnosis and treatment of diseases of infants and adults, notably neonatal kerniderus obstructive and necrotic liver diseases. Of the methods for the detection of bilirubin, usually spectrophotometry is used in clinical laboratories [1–3]. Electrochemical studies of bilirubin are scarce. D.c. polarography [4–7], linear-sweep voltammetry [8,9], controlled-potential coulometry [9], differential-pulse polarography [10] and differential-pulse voltammetry [11] have been used for investigation of bilirubin. The sensitivity of these methods is usually ca. 10^{-5} mol l^{-1}. A previous paper [12] reported on the anodic differential-pulse voltammetry of bilirubin at a glassy carbon electrode in $Na_2B_4O_7$–KH_2PO_4 buffer solution. The limit of detection is 3.3×10^{-9} mol l^{-1}. However, the accuracy of the method, with a relative standard deviation of $\pm 20\%$, is not satisfactory.

Adsorption voltammetry is a recently developed method suitable for trace analyses of inorganic ions, organic compounds and biological materials [13,14]. The adsorption voltammetry of many inorganic ions and its theory have been reported by us. Wang et al. [15] studied the differential-pulse adsorption voltammetry of bilirubin on a hanging mercury drop electrode (HMDE). In sodium acetate solution (pH 8.2) with a preconcentration time of 15 min, the detection limit is 5×10^{-10} mol l^{-1} of bilirubin.

This paper describes cathodic differential-pulse adsorption voltammetry for the determination of trace and ultra-trace amounts of bilirubin. The method relies on the effective interfacial accumu-

Correspondence to: Wenrui Jin, Department of Chemistry, Shandong University, Jinan 250100, Shandong (China).

lation of bilirubin on an HMDE. In 0.01 mol l^{-1} Tris–1.2 × 10^{-3} mol l^{-1} HCl (pH 1.3) solution, with a preconcentration time of only 5 min the detection limit is 2 × 10^{-10} mol l^{-1}. The method can be applied to the investigation of the effect of light and oxygen on the stability of bilirubin in dilute solutions and to the determination of the purity of samples of bilirubin.

EXPERIMENTAL

Apparatus

A PAR 384-A polarographic analyser coupled with a Model RE 0082 digital plotter was used in connection with a cell, using potentiostatic control of the electrode potential by means of a three-electrode system, which consisted of a PAR 303 static mercury electrode (HMDE mode) as the working electrode, a platinum plate as the counter electrode and an Ag/AgCl electrode as the reference electrode. In the preconcentration step, the solution was stirred with a PTFE-coated stirring bar, rotated by a PAR 305 magnetic stirrer.

Reagents and solutions

Analytical-reagent grade chemicals were used and all solutions were prepared with doubly distilled water. A 2 × 10^{-4} mol l^{-1} stock solution of bilirubin was prepared by dissolving an appropriate amount of bilirubin (99%) in dimethylformamide (DMF) and standard solutions were obtained by diluting the stock solution with ethanol. A 0.1 mol l^{-1} Tris solution was prepared by dissolving an appropriate amount of Tris in water in a 500-ml volumetric flask, then a 1 × 10^{-2} mol l^{-1} Tris–1.2 × 10^{-3} mol l^{-1} HCl buffer solution (pH 1.3) was prepared.

Procedure

The supporting electrolyte was 0.01 mol l^{-1} Tris–1.2 × 10^{-3} mol l^{-1} HCl (pH 1.3). The solution was deaerated for 8 min with pure nitrogen. Measurements were made after a preconcentration step in which the solution was usually stirred for a certain time, t_a, and a preconcentration potential, E_a, was applied. After a rest period, t_r, the cathodic differential-pulse voltammogram was recorded by scanning the potential in the negative direction with a scan rate of 5 mV 50 mV s^{-1} and a pulse amplitude of 100 mV. Each measurement was performed on a fresh drop. All potentials were measured against the Ag/AgCl electrode.

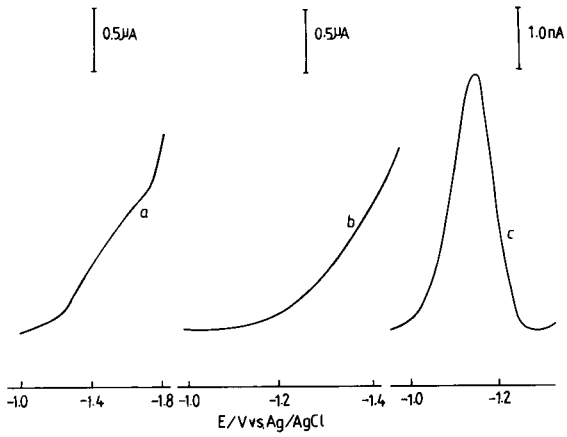

Fig. 1. Cathodic adsorption voltammograms of bilirubin. (a) Linear-sweep voltammogram: 1 × 10^{-4} mol l^{-1} bilirubin, E_a = −0.95 V, t_a = 120 s, t_r = 30 s, v = 100 mV s^{-1}. (b) Normal-pulse polarogram: 1 × 10^{-4} mol l^{-1} bilirubin, ΔE = 50 mV, v = 5 mV s^{-1}. (c) Differential-pulse adsorption voltammogram: 4 × 10^{-8} mol l^{-1} bilirubin, E_a = −0.90 V, t_a = 120 s, t_r = 15 s, ΔE = 50 mV, v = 5 mV s^{-1}.

RESULTS AND DISCUSSION

Adsorptive voltammetric characteristics of bilirubin

The cathodic voltammograms and polarogram of bilirubin for different methods are shown in Fig. 1. No peak appears on the linear-sweep voltammogram when the concentration of bilirubin changes from 1 × 10^{-8} to 1 × 10^{-4} mol l^{-1} (Fig. 1a). Also on the normal-pulse polarogram for 1 × 10^{-8}–1 × 10^{-4} mol l^{-1} bilirubin no peak appears (Fig. 1b). This shows that bilirubin cannot be tested by means of linear-sweep voltammetry and normal-pulse polarography. The differential-pulse adsorption voltammogram of bilirubin is shown in Fig. 1c. A reduction peak appears at a potential of −1.13 V when the concentration of the bilirubin is 4 × 10^{-8} mol l^{-1}. The peak

current is 6.76 nA and the peak half-width is 120 mV. The results show that bilirubin can be detected by means of differential-pulse adsorption voltammetry (DPAV).

The differential-pulse voltammograms of the reduction of bilirubin at different preconcentration times, t_a, and the dependence of the peak current of the reduction of bilirubin on the preconcentration time are shown in Fig. 2. The peak current, i_p, increases when t_a increases from 0 to 90 s. For 4×10^{-8} mol l^{-1} bilirubin, when $t_a \geqslant 90$ s, i_p remains constant which suggests that the electrode surface is saturated.

Optimum experimental conditions

The concentration ratio of HCl to Tris affects the peak current. When the concentration ratio of HCl to Tris is 0.11–0.13, the peak current is maximum. Therefore, a concentration ratio of HCl to Tris of 0.12 was adopted in subsequent experiments. It was found that the optimum concentration of the supporting electrolyte was 0.01 mol l^{-1} Tris –1.2×10^{-3} mol l^{-1} HCl (pH 1.3).

The dependence of the peak current of the reduction of bilirubin on the preconcentration potential, E_a, is shown in Fig. 3. A much higher peak current can be obtained when E_a is ca.

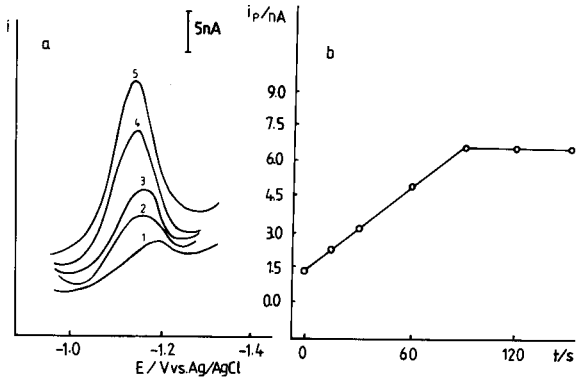

Fig. 2. (a) Differential-pulse voltammograms of reduction of adsorbed bilirubin at different preconcentration times: t_a = (1) 0; (2) 15; (3) 30; (4) 60 and (5) 90 s. (b) Dependence of peak current of reduction of bilirubin on the preconcentration time. 0.01 mol l^{-1} Tris–1.2×10^{-3} mol l^{-1} HCl, 4.0×10^{-8} mol l^{-1} bilirubin, $E_a = -0.90$ V, $t_r = 15$ s, $\Delta E = 50$ mV, $v = 5$ mV s^{-1}.

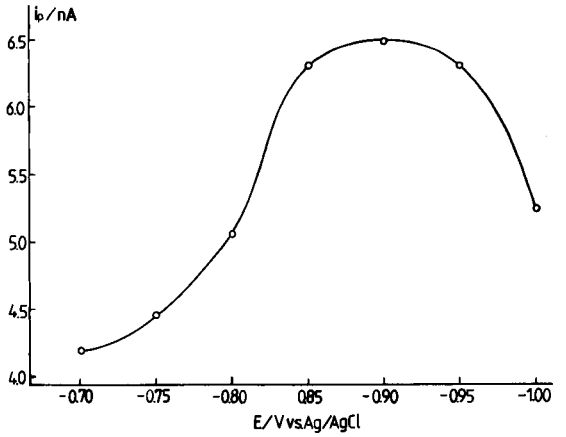

Fig. 3. Dependence of the peak current of reduction of bilirubin on the preconcentration potential. $t_a = 90$ s; other conditons as in Fig. 2.

–0.90 V, so this value was adopted in subsequent experiments.

Application

Under optimum conditions, it was found experimentally that the relationship between the peak current and the concentration of bilirubin is linear in the range 1×10^{-9}–4×10^{-7} mol l^{-1}. The detection limit is 2×10^{-10} mol l^{-1} of bilirubin for a preconcentration time of 300 s. The relative standard deviation calculated from ten successive measurements of 4×10^{-8} mol l^{-1}

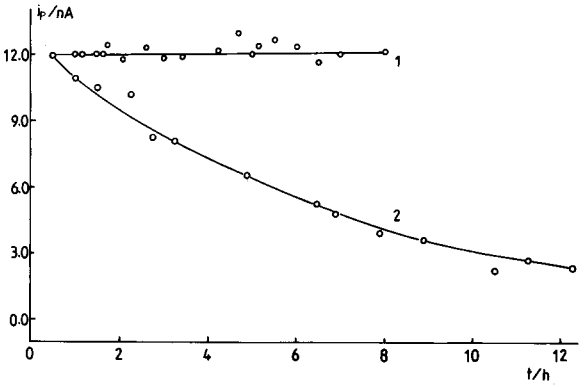

Fig. 4. Influences of light and oxygen on the stability of bilirubin 1×10^{-7} mol l^{-1} bilirubin, $t_a = 120$ s; other conditions as in Fig. 2. (1) Exposed to nitrogen atmosphere and light; (2) exposed to light and air.

TABLE 1

Results for determination of bilirubin in 0.01 mol l^{-1} Tris–1.2×10^{-3} mol l^{-1} HCl and recoveries of bilirubin

Sample No.	Content determined by spectrophotometry (%)	Content determined by DPAV (%)	Concentration determined in solution (10^{-8} mol l^{-1})	Concentration of bilirubin added (10^{-8} mol l^{-1})	Concentration of bilirubin found (10^{-8} mol l^{-1})	Recovery (%)
1	56.8	55.9	2.6	2.0	4.7	105
			2.6	2.0	4.6	100
2	55.6	55.4	3.6	2.0	5.5	95
			3.6	2.0	5.6	100

bilirubin is ±5.8%. The influences of light and oxygen on the stability of 1×10^{-7} mol l^{-1} bilirubin are shown in Fig. 4. The peak current did not change with time when the bilirubin solution was exposed to a nitrogen atmosphere and light (Fig. 4, curve 1), but when the solution was exposed to air and light, the peak current decreased (Fig. 4, curve 2). The results show that normal room light has hardly any effect, but the oxygen in the air plays an important role with regard to the stability of bilirubin.

Samples of bilirubin extracted from pig bile were dissolved in DMF and transferred into a 25-ml brown volumetric flask and diluted to volume with ethanol. Then 2.5 ml of sample solution were diluted to 25 ml with ethanol in a brown volumetric flask. Subsequently an appropriate amount of sample solution was taken, placed in an electrolytic cell containing 10 ml of supporting electrolyte. Bilirubin was detected by DPAV as mentioned above with two successive standard additions. The results are summarized in Table 1. The results obtained by DPAV are in accordance with those obtained by spectrophotometry. The recoveries of added bilirubin were 95–105%.

This project was supported by the National Science Foundation of China.

REFERENCES

1 N. Chaimori, R.J. Henry and O.J. Golub, Clin. Chim. Acta, 6 (1961) 1.
2 S. Meites and I.K. Hogg, Clin. Chem., 5 (1959) 470.
3 B.T. Doumas, B.W. Perry, E.A. Sasse and J.V. Straumfjord, Clin. Chem., 19 (1973) 984.
4 I. Tachi, Mem. Coll. Agric., Kyoto Imp. Univ. No. 42, Chem. Ser., No. 22 (1938) 1.
5 B. Tvaroha, Cas. Lek. Cesk., 100 (1961) 27.
6 B. Tvaroha, Collect. Czech. Chem. Commun., 26 (1961) 2271.
7 B. Tvaroha, Naturwissenschaften, 4 (1961) 99.
8 J.D. Van Norman, Anal. Chem., 45 (1973) 173.
9 J.D. Van Norman and R. Szentirmay, Anal. Chem., 46 (1974) 1456.
10 T.R. Koch and O.O. Akingbe, Clin. Chem., 27 (1981) 1295.
11 J. Saar and C. Yarnitzky, Isr. J. Chem., 23 (1983) 249.
12 W.-R. Jin, X. Zhao, C. Ding, F.-N. Wang and Z.-Q. Gao, Anal. Lett., in press.
13 J. Wang, Am. Lab., 17 (1985) 41.
14 R. Kalvoda and M. Kopanica, Pure Appl. Chem., 256 (1988) 97.
15 J. Wang, D.B. Luo and P.A. M. Farias, J. Electroanal. Chem., 185 (1985) 61.

Analytica Chimica Acta, 268 (1992) 189–193
Elsevier Science Publishers B.V., Amsterdam

BOOK REVIEWS

M. Grasserbauer and H.W. Werner (Eds.), *Analysis of Microelectronic Materials and Devices*, Wiley, Chichester, 1991 (ISBN 0-471-91713-3). xli + 934 pp. Price £110.00.

This is a monumental book containing well-written and well-edited contributions from 55 different authors, all known specialists in the various subjects treated. The editors are specialists in the field from a university (Professor Grasserbauer is at the Technical University of Vienna) and from industry (Dr. Werner was at Philips Research Laboratories in Eindhoven). The book starts with a prologue, the only chapter written by the editors themselves, in which the evolution of microelectronics and the importance of materials characterization for its development is briefly sketched. The description of the analytical methodologies used in microelectronics starts with an extensive list –more than three pages long– of the acronyms used throughout the book. The many individual chapters that follow are organised in 4 distinct sections. Each author (or group of authors) responsible for a methodology gives a survey of a specific method followed by examples showing method-specific analytical support in various steps of the processing of microelectronic materials and devices.

The first section deals with the bulk analysis of microelectronic materials with contributions on neutron and charged particle activation analysis, mass spectrometry using spark and laser excitation (with due reference to the new development: glow discharge excitation), optical emission and absorption spectrometry, infrared spectrometry and finally, as the only really method specific to the topic for microelectronics, deep level transient spectroscopy. Then follows a section on surface, interface and thin film analysis with description of methods such as X-ray photoelectron spectroscopy, micro Raman spectroscopy, laser microprobe mass spectrometry (the omission of Fourier transform mass spectrometry for organic analysis is a bit unfortunate), the various methods based on electron microscopy including scanning Auger, finally the methods based on low and high energy ion beam bombardment. Section 3 deals with structural analysis by diffraction, X-ray absorption fine structure spectroscopy and scanning tunneling spectroscopy. The revolutionary developments in materials characterization brought about by the application of synchrotron radiation is not sufficiently highlighted here. The final section is concerned with a number of methods for physical, electrical and geometrical characterization in microelectronics with contributions amongst others on ellipsometry, differential reflection spectroscopy, electron beam electron reflectance, microscopical characterization methods such as X-ray microscopy, scanning optical microscopy and scanning acoustical microscopy and finally electrical measurements based on the Hall effect, capacitance-voltage and resistivity measurements.

The last section is the only one which is rather specific for the characterization of microelectronic structures and devices. The other sections which cover over 75% of the entire text have a much broader relevance and could well be used for analysis in a number of other areas, e.g., in the broad field of materials characterization.

The presentation of the book is excellent with very clear and well chosen illustrations and readily interpretable black and white photos. The many references at the end of each chapter are properly chosen and refer to papers dating up to 1988.

The overall assessment of this book is that it makes a useful platform for everyone starting in the field of materials characterization. It will be a welcome addition to any library shelf and deserves addoption by teachers and students of the subject.

F. Adams

M. Stoeppler (Ed.), *Hazardous Metals in the Environment (Techniques and Instrumentation in Analytical Chemistry*, Vol. 12), Elsevier, Amsterdam, 1992 (ISBN 0-444-89078-5). x + 541 pp. Price US $225.50/Dfl. 395.00.

There is no better way of summarising the contents of this book than to quote from its first paragraph. "This book deals in its first part with the crucial steps of trace analytical procedures ranging from sample collection, sample pretreatment and instrumental techniques.... The second part describes the application of analytical methods for ten selected metals and metalloids ...". [Cd, Pb, Hg, As, Tl, Cr, Ni, Co, Al and Se]. The chapters are written by internationally respected experts (including several by the editor), and provide a tremendous concentration of information, much of it from each author's personal experience.

The first part, dealing with the pre-measurement steps of analyses, is a timely reminder of the extreme importance of sampling, sample storage and pre-treatment, contamination and analyte loss in trace analysis. The horror stories of analyses where these aspects were not recognised are legion, but the fact that such errors are still commonplace emphasises the need for continued tuition in this area.

The chapters on the various elements are very detailed, and deal with all aspects of the analytical process, except that individual procedures are understandably not given. Speciation receives due prominence, and aspects such as environmental mobility are discussed.

There are two interesting chapters on environmental specimen banking, one on the general subject, and one on the value of wine as a specimen bank!

This is altogether a very worthwhile book, that can be thoroughly recommended to all scientists involved in environmental analysis.

Alan Townshend

Alan Marshall and Francis R. Verdun, *Fourier Transforms in NMR, Optical and Mass Spectrometry*, Elsevier, Amsterdam, 1990 (ISBN 0-444-87360-0). xi + 433 pp. Price US$107.25/Dfl. 220.00 Hardback. Student Pack (5 Paperbacks): US$183.00/Dfl. 375.00 (not available in Canada).

The preface to this book claims that it is offered as a teaching and reference text for Fourier transform (FT) methods and is aimed at practising spectroscopists. The mathematics is said to be self-contained and great use is made of pictorial material.

As a teaching aid to both undergraduates and postgraduates as well as to practising spectroscopists it manifestly succeeds in its aims. The mathematics *is* self-contained and *understandable* unlike many texts which make the same claim. This feature of the book is helped greatly by comprehensive Appendices which deal with the basic mathematical functions required and pictorial representations of FT pairs and properties. The first Chapter introduces the concept of fundamental line shapes from the simple classical mass on a spring model. The interrelationship between various concepts such as absorption, dispersion and scattering and their origins are examined. Transient signals and the effects of damping are also considered. This chapter forms a good background for other parts of the book and especially Chapters 2 and 3 which deal with FTs of analog waveforms and digital (or discrete) waveforms, respectively. It is in Chapter 2 that the basic nuts and bolts of FT spectrometry are considered with the introduction of concepts such as FT pairs, convolution, apodisation, phase correction, cross-correlation and auto-correlation. Equally importantly Chapter 3 deals with the Nyquist sampling criterion, digital spectral resolution and dynamic range for digital waveforms.

Chapters 5 and 6 are dedicated to noise and non-FT methods for time domain to frequency domain transformations. The "noise" chapter highlights the effects of detector limited, source limited and fluctuation noise on Fourier and Hadamard transformations showing that it is possible to gain a signal-to-noise enhancement using these multiplex techniques, or in the case of source limited noise even a signal-to-noise degradation. The following Chapter considers alterna-

tive transformations such as the Laplace transformation and autoregression and outlines the conditions under which they provide superior resolution.

The remaining Chapters (7–9) are technique-specific dealing with FT ion cyclotron resonance mass spectroscopy, FT nuclear magnetic resonance spectroscopy and FT interferometry. I found these chapters the most easy to read being a practical and practising spectroscopist and I suspect that this will be true for many who purchase this book. Indeed these chapters can be read with minimal reference to the previous ones yet still provide an adequate understanding of each technique. The authors should be congratulated for this as there is appeal for the less mathematically orientated spectroscopists.

In general I think this book will be most valuable as a reference work owing to its comprehensive and clear treatment of a relatively complex subject which needed to be simplified. However for the latter reason it will also serve as an excellent text book for graduate students. It is also essential reading for spectroscopists with more than a passing interest in FT techniques.

R.D. Snook

J. Zyka, *Instrumentation in Analytical Chemistry I*, Ellis Horwood, Chichester, 1991 (ISBN 0-13-472218-3). 368 pp. Price US$90.50.

The book, the first in a series of volumes, focuses on the rapidly changing field of "Instrumentation in Analytical Chemistry", the aim of which is to update scientists, in particular analytical chemists, with the ever changing instrumentation available. While the philosophy of the editor is not in doubt the ability to convey the message, however, is far from convincing. This is due in part to the use of out-of-date literature. While the choice of literature is not often criticised it is of particular note here that of the entire cited literature less than 10% is post-1986. It is accepted that the older references can have a significant part in a historical and/or introductory context. The ability to predict new instrumental trends is most unlikely from the literature cited, with the rapidly changing scientific climate. However, after indicating a certain disapproval for the book there are some chapters of merit.

Of particular note is the chapter on "Modern Methods of Decomposition of Inorganic Substances". This is a subject that is frequently dismissed in a short paragraph in most texts. This, coupled with the limited amount of dedicated literature (textbooks and papers) makes this contribution of great interest, particularly for student use. The chapter covers decomposition of inorganic material at increased temperature and pressure, with acid vapours and fusion methods. Also noted is the chapter on analytical measurement in flowing streams which contains useful information on a range of detection systems together with their respective figures of merit.

A particularly disappointing chapter is "New Sources in Optical Emission Spectrometry" which fails to consider anything more recent than the 1970s! The discussion of the LMA-1 laser sampling device must omit ten years of research that has used Nd:YAG lasers for OES and MS. Also, no mention is made of what are currently regarded as "new" sources such as FANES, FAPES, GDs with r.f. or microwave excitation etc.

John R. Dean

Loic J. Blum and Pierre R. Coulet (Eds.), *Biosensor Principles and Applications*, Marcel Dekker, New York, 1991 (ISBN 0-8247-8546-0). x + 376 pp. Price US$125.00.

The area of chemical/biological sensors is one that has received much attention in recent years, both in the primary literature and in books. This present volume is part of a series on bioprocess technology, but covers a much wider remit, owing to the restricted number of practical applications that biosensors have found in the monitoring of biotechnological processes. The book is divided into fourteen chapters, which have been written by experts in the field, and provides a good balance between the various transducers/biological recognition systems currently being in-

vestigated for use in biosensors. The emphasis in each chapter is on the principle of measurement, the biological material used, the description of transducers, and characteristics and performance of the biosensor thus designed. As such the book has a practical approach which will be useful for those readers who are coming to the subject for the first time, as well as those who are already practitioners. As a volume in this particular series, it would have benefited from some other chapters dealing specifically with bioprocess monitoring, e.g., in fermentation processes, and in the area of signal processing/control. It can, however, be recommended for purchase by those scientists wanting a good, broad, up-to-date coverage of the field of biosensors.

Malcolm R. Smyth

H. Rotzsche, *Stationary Phases in Gas Chromatography* (*J. Chromatogr. Library*, Vol. 48), Elsevier, Amsterdam, 1991 (ISBN 0-444-98733-9). xiv + 410 pp. Price US$166.50.

Selectively separating stationary phases were very important in GC during the packed column era. With such phases, the desired separation could often be achieved in spite of poor plate numbers. As a consequence, several hundred types of selective phases were reported. These were thoroughly described in the monograph *Stationary Phases in Gas Chromatography* by Baiulescu and Ilie (Pergamon Press, Oxford, 1975). Since that time, GC has developed to a relatively mature technique. Several factors, such as the breakthrough of open tubular columns, the advent of immobilized stationary phases, the use of well-deactivated fused-silica capillaries and the appearance of refined stationary phase qualities have all contributed to the development. This recently published book may be justified in view of the extensive development of GC. It may, on the other hand, seem odd to present such a book at a time when the very high separation efficiencies that are available with non-polar open tubular GC columns have marginalized the role of selective phases. It is often considered that ca. 70% of all GC can be performed on non-polar phases, and that only five or six selective phases are included in a set of preferred phases.

The book is, to a large extent, based on material that has been published earlier in the former East Germany, and some sections are not really up to date; only 2.5% of the references are later than 1986. Selective phases for packed columns are treated extensively, and much of the information given in the book by Baiulescu is repeated. On the other hand, some areas that are important in current GC are treated quite briefly. One such area is the adsorption at the gas–liquid interface. Another area that is only briefly treated is the separation of chiral compounds on cyclodextrins and derivatives thereof. Although the GC field has matured, separation on cyclodextrins is a rapidly developing area.

The merit of this book is that the knowledge of stationary phases and separation columns that was earlier scattered throughout the literature has now been made easily accessible. The book can be recommended as a reference book for GC laboratories.

L.G. Blomberg

Horacio A. Mottola and James R. Steinmetz (Eds.), *Chemically Modified Surfaces* (Proceedings of the Fourth Symposium on Chemically Modified Surfaces, Chadds Ford, Pennsylvania, July 31–August 2, 1991), Elsevier, Amsterdam, 1992 (ISBN 0-444-89305-9). xiii + 399 pp. Price US$197.00/Dfl. 345.00.

This is a collection of 23 papers, and 6 abstracts of papers not published in full, grouped into characterisation of chemically modified surfaces (6 papers), modification of polymer surfaces (3), chemical modification of silica (5), chemical modification of membranes and films (4) and other topics (3). There is an interesting introductory paper by Mottola on chemical immobilisation in chemistry, and a plenary lecture by Drake et al. on fractal surfaces. The topics of most interest to analytical chemists concern the modification of membranes such as immobilisation of

amphiphilic membranes for use in optical and electrochemical biosensors (M. Thompson et al.), supports for high stability fibre-optic based immunosensors (Litwiler, Bright et al.) and polymer-encapsulated LC stationary phases (Engelhardt et al.). The book concludes with an index of contributing authors.

Shigeru Yamauchi (Ed.), *Chemical Sensor Technology*, Vol. 4, Kodansha, Tokyo and Elsevier, Amsterdam, 1992 (ISBN 0-444-98680-4). xvii + 270 pp. Price US$191.50/Dfl. 335.00.

This collection of 15 articles covers a wide range of modern chemical sensor developments. Four chapters deal with aspects of semiconductor gas sensors, and three others with potentiometric sensors. There are useful accounts of silicon technology for sensor fabrication, and chemical grafting to produce ISFETS and ENFETS. The remaining articles cover various types of biosensor – these with microvolume reaction chambers, piezoelectric sensors, immunosensors employing the surface photovoltage technique, non-invasive glucose monitoring in blood based on an ISFET, and biosensing odour compounds using plant leaves.

The series continues to provide up-to-date accounts of developments in a large and rapidly developing field, and is useful in providing sensor researchers with awareness in areas that are not directly within their particular remit.

G. Holland and A.N. Eaton, *Applications of Plasma Source Mass Spectrometry*, Royal Society of Chemistry, Cambridge, 1991 (ISBN 0-85186-566-6). viii + 222 pp. Price: £37.50.

This monograph contains twenty-one selected papers from the second international conference on plasma source mass spectrometry that was held at the University of Durham in September 1990. The papers are presented in readable camera-ready formats and cover a variety of topics.

There are contributions on fundamental aspects of ICP-MS, e.g., mass bias effects and ion formation and on sample introduction techniques such as laser ablation, flow injection, hydride generation and electrothermal vaporization. There are also several application based papers on, e.g., semiconductor grade reagents, drinking water, ^{99}Tc in environmental samples and whole blood. There is also one presentation on multivariate calibration techniques, which offer some promise in compensating for matrix effects; in this particular case with clinical samples.

The index is brief and the papers have not been categorized in any way but this monograph provides a useful and readable insight into recent developments in plasma source mass spectrometry.

Urs Peter Schlunegger, *Biologically Active Molecules. Identification, Characterization and Synthesis,* Springer-Verlag, Berlin, 1989 (ISBN 3-540-50919-4). viii + 252 pp. Price DM 128.00.

This is a collection of eleven papers, in camera-ready copy, presented at a seminar entitled *From Biological Activity to Structure* held at Interlaken, Switzerland, September 5–7, 1988. The invited contributions are covered by three papers on aspects of FAB by R.M. Caprioli and another by H.R. Morris, two on chemical phenomena of mushrooms and toadstools and β-methoxyacrylate antibiotics by W.S. Steglich and one on peptide defence systems by D.H. Williams. Other papers discuss lipopeptides, snake venom affinity chromatography and an ATR-IR study of biomembranes. There is no index.

PUBLICATION SCHEDULE FOR 1993

	S'92	O'92	N'92	D'92	J	F
Analytica Chimica Acta	267/1 267/2	268/1 268/2	269/1 269/2	270/1 270/2	271/1 271/2	272/1 272/2
Vibrational Spectroscopy		4/1				4/2

INFORMATION FOR AUTHORS

Manuscripts. The language of the journal is English. English linguistic improvement is provided as part of the normal editorial processing. Authors should submit three copies of the manuscript in clear double-spaced typing on one side of the paper only. *Vibrational Spectroscopy* also accepts papers in English only.

Abstract. All papers and reviews begin with an Abstract (50–250 words) which should comprise a factual account of the contents of the paper, with emphasis on new information.

Figures. Figures should be prepared in black waterproof drawing ink on drawing or tracing paper of the same size as that on which the manuscript is typed. One original (or sharp glossy print) and two photostat (or other) copies are required. Attention should be given to line thickness, lettering (which should be kept to a minimum) and spacing on axes of graphs, to ensure suitability for reduction in size on printing. Axes of a graph should be clearly labelled, along the axes, outside the graph itself. All figures should be numbered with Arabic numerals, and require descriptive legends which should be typed on a separate sheet of paper. Simple straight-line graphs are not acceptable, because they can readily be described in the text by means of an equation or a sentence. Claims of linearity should be supported by regression data that include slope, intercept, standard deviations of the slope and intercept, standard error and the number of data points; correlation coefficients are optional.

Photographs should be glossy prints and be as rich in contrast as possible; colour photographs cannot be accepted. Line diagrams are generally preferred to photographs of equipment.

Computer outputs for reproduction as figures must be good quality on blank paper, and should preferably be submitted as glossy prints.

Nomenclature, abbreviations and symbols. In general, the recommendations of the International Union of Pure and Applied Chemistry (IUPAC) should be followed, and attention should be given to the recommendations of the Analytical Chemistry Division in the journal *Pure and Applied Chemistry* (see also *IUPAC Compendium of Analytical Nomenclature, Definitive Rules*, 1987).

References. The references should be collected at the end of the paper, numbered in the order of their appearance in the text (*not* alphabetically) and typed on a separate sheet.

Reprints. Fifty reprints will be supplied free of charge. Additional reprints (minimum 100) can be ordered. An order form containing price quotations will be sent to the authors together with the proofs of their article.

Papers dealing with vibrational spectroscopy should be sent to: Dr J.G. Grasselli, 150 Greentree Road, Chagrin Falls, OH 44022, U.S.A. Telefax: (+1-216) 2473360 (Americas, Canada, Australia and New Zealand) or Dr J.H. van der Maas, Department of Analytical Molecule Spectrometry, Faculty of Chemistry, University of Utrecht, P.O. Box 80083, 3508 TB Utrecht, The Netherlands. Telefax: (+31-30) 518219 (all other countries).

0003-2670/92/$05.00

This issue is printed on acid-free paper.

PRINTED IN THE NETHERLANDS

Hyphenated Techniques in Supercritical Fluid Chromatography and Extraction

edited by **K. Jinno**, Toyohashi University of Technology, Toyohashi, Japan

Journal of Chromatography Library Volume 53

This is the first book to focus on the latest developments in hyphenated techniques using supercritical fluids. The advantages of SFC in hyphenation with various detection modes, such as, FTIR, MS, MPD and ICP and others are clearly featured throughout the book. Special attention is paid to coupling of SFE with GC or SFC.

In this edited volume, chapters are written by leading experts in the field. The book will be of interest to professionals in academia, as well as to those researchers working in an industrial environment, such as analytical instrumentation, pharmaceuticals, agriculture, food, petrochemicals and environmental.

Contents:

1992 x + 334 pages
Price: US $ 157.00/ Dfl. 275.00
ISBN 0-444-88794-6

ORDER INFORMATION
For USA and Canada
ELSEVIER SCIENCE PUBLISHERS
Judy Weislogel
P.O. Box 945
Madison Square Station,
New York, NY 10160-0757
Tel: (212) 989 5800
Fax: (212) 633 3880

In all other countries
ELSEVIER SCIENCE PUBLISHERS
P.O. Box 211
1000 AE Amsterdam
The Netherlands
Tel: (+31-20) 5803 753
Fax: (+31-20) 5803 705

ELSEVIER
SCIENCE PUBLISHERS